UNESP - Universidade Estadual Paulista
"Júlio de Mesquita Filho"
Faculdade de Odontologia de Araraquara

Ewerton Garcia de Oliveira Mima

Terapias alternativas para infecções causadas por biofilmes microbianos

Araraquara

2022

UNESP - Universidade Estadual Paulista
"Júlio de Mesquita Filho"
Faculdade de Odontologia de Araraquara

Ewerton Garcia de Oliveira Mima

Terapias alternativas para infecções causadas por biofilmes microbianos

Tese apresentada à Universidade Estadual Paulista (Unesp), Faculdade de Odontologia, Araraquara para obtenção do título de Livre-Docente em Prótese Parcial Removível

Araraquara

2022

Mima, Ewerton Garcia de Oliveira
Terapias alternativas para infecções causadas por biofilmes microbianos / Ewerton Garcia de Oliveira Mima. -- Araraquara: [s.n.], 2022
203 f.; 30 cm.

Tese (Livre-Docência em Reabilitação Oral) – Universidade Estadual Paulista, Faculdade de Odontologia

1. Biofilmes 2. Anti-infecciosos 3. Resistência microbiana a medicamentos 4. Fotoquimioterapia 5. Nanopartículas I. Título

Ficha catalográfica elaborada pela Bibliotecária Marley C. Chiusoli Montagnoli, CRB-8/5646
Universidade Estadual Paulista (Unesp), Faculdade de Odontologia, Araraquara
Diretoria Técnica de Biblioteca e Documentação

Ewerton Garcia de Oliveira Mima

Terapias alternativas para infecções causadas por biofilmes microbianos

Comissão julgadora

Tese para obtenção do grau de livre-docência em Prótese Parcial Removível

Profa. Dra. Ana Lucia Machado

Profa. Dra. Karin Hermana Neppelenbroek

Profa. Dra. Renata Cunha Matheus Rodrigues Garcia

Profa. Dra. Dalva Cruz Laganá

Profa. Dra. Ana Cláudia Pavarina

Araraquara, 20 de abril de 2022

DADOS CURRICULARES

Ewerton Garcia de Oliveira Mima

NASCIMENTO: 14 de junho de 1980 – Toledo – Paraná

FILIAÇÃO: Pedro Iwao Mima
Olivia Garcia de Oliveira Mima

1995/1997: Curso Técnico em Processamento de Dados no Colégio Técnico de Campinas (Unicamp) – COTUCA

1998/1998: Estágio no Centro de Computação da Universidade de Campinas (CCUEC, Unicamp)

1999/2002: Curso de Graduação em Odontologia na Faculdade de Odontologia de Araraquara, Universidade Estadual Paulista "Júlio de Mesquita Filho" – UNESP

2003/2005: Curso de Pós-Graduação em Reabilitação Oral, Área de Prótese, nível Mestrado na Faculdade de Odontologia de Araraquara – UNESP

2005/2009: Curso de Pós-Graduação em Reabilitação Oral, Área de Prótese, nível Doutorado na Faculdade de Odontologia de Araraquara – UNESP

2004/2008: Estágio Docência nas Disciplinas de Prótese Parcial Removível I e II na Faculdade de Odontologia de Araraquara – UNESP

2009/2011: Professor Auxiliar do Curso de Odontologia da Universidade São Francisco (USF) em Bragança Paulista

2011/2012: Pós-Doutorado no Programa de Reabilitação Oral, Área de Prótese na Faculdade de Odontologia de Araraquara – UNESP

2012/2012: Professor Colaborador do Departamento de Odontologia da Universidade Estadual de Ponta Grossa – UEPG

2013 até o presente: Professor Assistente Doutor da Faculdade de Odontologia de Araraquara – UNESP

2013 até o presente: Docente credenciado ao Programa de Pós-Graduação em Reabilitação Oral, Área de Prótese da Faculdade de Odontologia de Araraquara – UNESP

À Deus,

pelo dom e beleza da vida,
por me permitir ter sonhos e poder realizá-los,
pelas oportunidades concedidas,
pela saúde,
por guiar e iluminar meus caminhos e de minha família,
por sua proteção,
por me permitir ter fé e esperança!

Aos meus pais, Pedro e Olivia,

pelo amor incondicional a cada instante, pela educação e formação, pelo exemplo de pessoas humildes e batalhadoras, pela abdicação que eles sempre fizeram para que eu e meus irmãos pudéssemos sempre ter o melhor!
A vcs meu imenso e eterno amor, respeito e admiração!

A Eder Garcia de Oliveira Mima,

In memorian

Agradecimentos Especiais

Aos meus irmãos, Emerson e Eder (*in memorian*), por sempre caminharmos juntos, pelo companheirismo desde a infância e pelos laços familiares que nos unem;

À UNESP e à Faculdade de Odontologia de Araraquara que me concederam formação profissional e tantas oportunidades, que me abriram as portas ao mundo e que me abrigam como meu segundo lar;

À Universidade de São Francisco (USF) e à Universidade Estadual de Ponta Grossa (UEPG), que foram fundamentais para meu amadurecimento e início profissional;

À Ana Cláudia Pavarina, minha orientadora e amiga, por ter acreditado em mim, por ter me concedido grandes oportunidades, estímulos e conselhos;

Aos meus mestres Ana Cláudia Pavarina, Ana Lucia Machado, Eunice Teresinha Giampaolo e Carlos Eduardo Vergani, por serem grandes exemplos de dedicação, profissionalismo e competência, por me inspirarem e pela amizade;

À Janaína Habib Jorge, Marlise Inez Klein Furlan, Paula Aboud Barbugli, Renata Garcia Fonseca, Livia Nordi Dovigo e Paula Volpato Sanitá Dantas, pela competência e dedicação profissional, e também pela amizade, pelo respeito, pelo convívio diário lado-a-lado, tão imporantes para meu amadurecimento pessoal e alegria do dia-a-dia;

A todos meus orientados, Jeffersson, Vinicius, Yuliana, Thais, Amanda, Bruna, Ana Laura, Maria Isabella, Gabriela, Maria Carolina, Leticia Rosa, Geovana, Geisiane, Ana Cláudia, Letícia Camargo, Fernanda e João, por me concederem a oportunidade de exercer a docência de forma mais próxima e proporcionarem meu amadurecimento profissional, pelo respeito e por serem fundamentais para o desenvolvimento do nosso trabalho;

A todos os docentes e funcionários do Departamento de Materiais Odontológicos e Prótese, pelo convívio, pelo respeito, pela ajuda em nossos trabalhos;

À Direção e Vice-Direção desta Faculdade, Prof Edson Alves de Campos e Profa Patrícia Petromilli Nordi Sasso Garcia;

A todos os funcionários desta faculdade, do térreo ao sexto andar;

Aos apoios financeiros recebidos pela Pró-Reitoria de Pós-Graduação da UNESP (PAREex. Edital nº 03/2016 PROPG), pela Coordenação de Aperfeiçoamento de Pessoal de Nível Superior (CAPES AEX 2184/14-1), pelo Conselho Nacional de Desenvolvimento Científico e Tecnológico (CNPq MCTI/CNPQ/Universal processo nº 446401/2014-5) e pela Fundação de Apoio à Pesquisa do Estado de São Paulo (FAPESP processo nº 2013/23165-5, 2018/02513-9), sem as quais o desenvolvimento de todos esses trabalhos não seria possível.

A todas as pessoas que contribuíram para minha formação profissional e para realização deste trabalho.

"7Assim rezei e foi-me concedida a inteligência;
supliquei e o espírito da sabedoria veio a mim.
8Estimei-a mais que cetros e tronos
e julguei as riquezas sem valor, comparados a ela.
9Não a igualei com a pedra mais preciosa;
todo o ouro, à sua vista, é punhado de areia,
e a prata, ao seu lado, é como lodo.
10Amei-a mais que a saúde e a formosura;
preferi-a à luz,
pois seu brilho não conhece ocaso.
11Mas com ela vieram-me todos os bens;
riquezas incalculáveis, por suas mãos.
12Alegrei-me com esses bens,
pois a sabedoria os dirige,
mas ignorava ainda que ela fosse sua mãe.
13Assimilei-a lealmente e reparto sem inveja;
nem escondo suas riquezas;
14é tesouro inesgotável para os homens,
e os que a adquirem ganham a amizade de Deus,
e a ele se recomendam pelos dotes disciplinares." (Sb 7.7-14)[1]

[1] Bíblia Mensagem de Deus. São Paulo: Editora Santuário, Edições Loyola, 2002.

Mima EGO. Terapias alternativas para infecções causadas por biofilmes microbianos [tese de livre-docência]. Araraquara: Faculdade de Odontologia da UNESP; 2022.

RESUMO

As principais infecções médico-odontológicas são causadas por biofilmes microbianos, que são complexas comunidades de micro-organismos aderidos a uma superfície e envoltos por uma matriz polimérica. Essa matriz protege as células microbianas do biofilme contra agentes externos, como agentes antimicrobianos e a resposta de defesa do hospedeiro. Assim, organizados em biofilmes, os micro-organismos são mais tolerantes às terapias anti-infecciosas. Além disso, o uso de agentes antimicrobianos convencionais (antibióticos e antifúngicos) tem levado ao problemas da resistência antimicrobiana, a qual é uma ameaça mundial e um desafio atual para a área de saúde. Diante disso, torna-se necessária a pesquisa por novas modalidades terapêuticas contra biofilmes e para o combate à resistência antimicrobiana. Esta tese apresenta estudos realizados pelo grupo de pesquisa do candidato para o desenvolvimento de tratamentos contra infecções causadas por biofilmes e por cepas resistentes. Foram selecionados seis artigos científicos publicados em revistas internacionais de seletiva política editorial para compor esta tese. Os resultados desses estudos demonstraram a eficácia antibacteriana e antifúngica, inclusive contra cepas resistentes, de nanopartículas de dióxido de titânio com prata (TiO_2:Ag), da Terapia Fotodinâmica antimicrobiana (aPDT), da Terapia Sonodinâmica (SDT) e da *N*-acetilcisteína (NAC). A ação antimicrobiana foi maior em culturas planctônicas do que em biofilmes. As nanopartículas de TiO_2:Ag foram sintetizadas e caracterizadas para garantir uma produção padronizada dessas nanopartículas previamente aos ensaios antimicrobianos. Também foi desenvolvido um nanosistema de liberação de fármacos (nanopartículas poliméricas) para o encapsulamento de curcumina, fotossensibilizador (FS) hidrofóbico utilizado em aPDT, que resultou no depósito de uma patente. Observou-se ausência de efeitos adversos da utilização da aPDT mediada por essas nanopartículas de curcumina no tecido do hospedeiro quando utilizada in vivo num modelo animal de infecção fúngica oral em camundongos. Outro nanosistema utilizado como FS, nanoemulsão catiônica de ftalocianina de cloro e alumínio, demonstrou efeito fotodinâmico antimicrobiano contra um biofilme multiespécie, porém sem redução da biomassa do biofilme. A SDT, utilizada com intuito de melhorar a penetração do FS no biofilme, foi eficaz contra biofilme fúngico quando associada a aPDT. Já a NAC apresentou ação fungistática e reduziu a viabilidade, a biomassa e os componentes solúveis da matriz dos biofilmes, além de mostrar sinergismo com a caspofungina em culturas planctônicas. Em síntese, esses estudos mostram que mais esforços devem ser dirigidos no desenvolvimento de tratamentos alternativos aos antimicrobianos convencionais contra biofilmes microbianos e cepas resistentes antes da realização de ensaios clínicos.

Palavras chave: Biofilmes. Anti-infecciosos. Resistência microbiana a medicamentos. Fotoquimioterapia. Nanopartículas.

Mima EGO. Alternative therapies for infections caused by microbial biofilms [tese de livre-docência]. Araraquara: Faculdade de Odontologia da UNESP; 2022.

ABSTRACT

The main medical-dental infections are caused by microbial biofilms, which are complex communities of microorganisms attached to a surface and surrounded by a polymeric matrix. The matrix protects the microbial cells within the biofilm against external agents, such as antimicrobial agents and host defense cells. Hence, organized as biofilms, microorganisms show tolerance to anti-infective approaches. Moreover, the use of conventional antimicrobial agents (antibiotics and antifungals) has led to the problematic antimicrobial resistance, which is a global threat and a challenge to the health field. Therefore, the development of new therapeutic methods against biofilms and resistant strains are needed. This thesis shows studies carried out by the candidate's research group for the development of treatments against infections caused by biofilms and resistant strains. Six scientific articles published in international journals of selective editorial policy were selected to compose this thesis. The results of these studies demonstrated the antibacterial and antifungal efficacy of nanoparticles of titanium dioxide with silver (TiO_2:Ag), antimicrobial Photodynamic Therapy (aPDT), Sonodynamic Therapy (SDT), and N-acetylcisteyne (NAC) against microbial strains, including resistant one. The antimicrobial effect was higher for planktonic cultures than for biofilms. The TiO_2:Ag nanoparticles were synthesized and characterized to warrant a standard production of this nanoparticles before the antimicrobial assays. A drug-delivery nanosystem (polymeric nanoparticle) was also developed for the encapsulation of curcumin, a hydrophobic photosensitizer (PS) used in aPDT, and a patent was deposited. No adverse effects on the host's tissue were observed when the aPDT mediated by this curcumin-nanoparticles was evaluated in vivo in a murine model of oral fungal infection. Another nanosystem used as PS, cationic nanoemulsion of chloroalluminium phthalocyanine, showed antimicrobial photodynamic effect against a multispecies biofilm, but no reduction in the total biomass was observed. The SDT, used to improve the PS penetration into the biofilm, was effective against fungal biofilm when associated with aPDT. The NAC showed fungistatic effect and reduced the viability, biomass, and soluble components of the biofilm matrix, and also demonstrated synergism with caspofungin in planktonic cultures. In summary, these studies demonstrated that more efforts should be directed to the development of alternative therapies to the conventional antimicrobial agents against biofilms and resistant strains before clinical trials.

Keywords: Biofilms. Anti-infective agents. Drug-resistance. Photochemotherapy. Nanoparticles.

SUMÁRIO

1 INTRODUÇÃO 09

2 PROPOSIÇÃO 21

3 PUBLICAÇÕES 22
3.1 Publicação 1 23
3.2 Publicação 2 32
3.3 Publicação 3 66
3.4 Publicação 4 95
3.5 Publicação 5 104
3.6 Publicação 6 115

4 DISCUSSÃO 142

5 CONCLUSÃO 151

REFERÊNCIAS 152

ANEXO A 162

ANEXO B..... 198

APÊNDICE A..... 203

1 INTRODUÇÃO

As principais infecções odontológicas, como a cárie, a doença periodontal e a doença peri-implantar, estão associadas à biofilmes microbianos[1], que são complexas comunidades de micro-organismos aderidos a uma superfície biótica ou abiótica e envolvidos por uma matriz polimérica extracelular[2,3]. Organizados em biofilmes, os micro-organismos apresentam características fenotípicas distintas quando comparados com sua forma livre (planctônica) e maior resiliência às alterações ambientais, como maior tolerância aos antimicrobianos e às defesas do hospedeiro, o que dificulta o tratamento das infecções causadas por biofilmes[4].

A etiologia microbiana das infecções bucais já era relatada há mais de 100 anos atrás, no século XIX, por dentistas, como Riggs, Harlan e Miller, que promoveram o conceito de higiene bucal para o controle dessas doenças[1]. Já no século XX, o aumento do conhecimento do microbioma humano possibilitou uma melhor compreensão da microbiologia oral, com a identificação de espécies responsáveis pela cárie (bactérias cariogênicas) e doença periodontal (periodontopatógenos), e a substituição da "hipótese de placa não específica"[5] pela "hipótese de placa específica"[6]. No início da década de 90, surgiu a "hipótese de placa ecológica"[7], segundo a qual o desequilíbrio da comunidade microbiana bucal (disbiose) é decorrente de alterações ambientais do seu habitat, como dieta do hospedeiro, inflamação local, fluxo salivar e composição do meio, o que acarreta na transição de saúde para doença. Verificou-se então a necessidade de se avaliar a comunidade microbiana como um todo, ao invés de espécies específicas, para a compreensão da função das bactérias na saúde e na doença. Atualmente, sabe-se que os micro-organismos no biofilme comunicam-se entre si por meio de interações nutricionais, troca de material genético e sinalização por mediadores químicos ("quorum sensing")[8], além de interagir com o ambiente e o hospedeiro, o que acarreta em destruição do tecido e desenvolvimento de doença.

Apesar da grande quantidade de estudos do bacterioma oral humano[9-12] demonstrar a existência de uma diversidade de mais 700 espécies bacterianas por meio da moderna tecnologia do sequenciamento de alto rendimento do gene DNA ribossomal (16S rRNA), da bioinformática e das bases de dados do gente 16S rRNA[1], fungos também habitam e colonizam a cavidade bucal humana e interagem com as bactérias num biofilme polimicrobiano[13,14]. Dentre esses fungos, destaca-se a predominância das espécies do gênero *Candida* spp., apesar de outros gêneros/classe terem sido também reportados, como *Cladosporium*, *Aureobasidium*, Saccharomycetales, *Aspergillus*, *Fusarium* e *Cryptococcus*, compondo o micobioma oral humano[15]. Dentre as espécies de *Candida*, *Candida albicans* é a

mais prevalente, isolada como um micro-organismo comensal de 25 a 50% de pacientes saudáveis[16,17], mas também em infecções bucais, como cárie[18,19], doença periodontal[20-22] e peri-implantar[23], infecção endodôntica[24-26] e, principalmente, estomatite protética ou candidíase crônica associada ao uso de próteses dentárias[27-29]. Além da cavidade bucal, *C. albicans* também coloniza o trato gastro-intestinal[30], pele[31] e o trato genito-urinário feminino[32]. *C. albicans* é um fungo polimórfico, ou seja, tem a capacidade de alterar sua morfologia comensal de levedura (blastóporo) para forma filamentosa de hifas (sem constrições e com paredes paralelas) ou pseudo-hifas (com constrições e mais largas que as hifas), que são as morfologias patogênicas capazes de invadir o tecido epitelial do hospedeiro[33]. A invasão do epitélio pode ocorrer por dois processos diferentes: a endocitose, processo mediado pelas células epiteliais que não necessita que as hifas estejam vivas, uma vez que as células não viáveis também sofrem esse processo; e a penetração ativa, que é um processo realizado pela hifa, a qual necessita estar viável para penetrar entre as junções celulares ou entre as camadas do epitélio[34]. Adicionalmente, já foram reportadas nove diferentes morfologias de *C. albicans* relacionadas com diferentes nichos do hospedeiros e com sítios de saúde e doença, o que demonstra uma elevada plasticidade de *C. albicans* para colonizar ou infectar diferentes tecidos do hospedeiro[35].

A estomatite protética é clinicamente caracterizada por inflamação da mucosa palatina adjacente à prótese total ou parcial removível que, segundo Newton[36], pode apresentar 3 (três) graus de severidade: tipo I, caracterizado por pontos (petéquias) hiperêmicos na mucosa palatina; tipo II, com áreas inflamatórias difusas e; tipo III, com hiperplasia papilar associada à inflamação difusa. Essa condição afeta até dois terços dos usuários de próteses totais, com maior prevalência em mulheres e, na maioria das vezes, é assintomática[37]. Sua etiologia é multifatorial e associada a trauma local, uso noturno da prótese, próteses mal adaptadas, redução do fluxo salivar (xerostomia), higienização deficiente da prótese e fatores sistêmicos, como diabetes e uso prolongado de antibióticos, mas o principal fator etiológico é o biofilme microbiano formado na superfície da prótese[37-39]. Diferentemente das demais infecção odontológicas que são causadas por biofilmes bacterianos, a estomatite protética tem etiologia fúngica, sendo *C. albicans* o principal fator causal, isolado em até 90% desses pacientes[13]. Outras espécies de *Candida* também são isoladas da prótese desses pacientes, como *C. glabrata*, *C. tropicalis*, *C. krusei*, etc., e tem sido sugerido que a interação sinérgica entre essas espécies pode estar associada à severidade da patologia[14,28].

Entretanto, *Candida* spp. também é encontrada em próteses de pacientes saudáveis[40,41] e uma grande diversidade bacteriana também está presente no biofilme da prótese dentária,

como *Actinomyces*, *Streptococcus*, *Veillonella*, *Capnocytophaga* e *Neisseria*[13]. A análise do microbioma da prótese dentária demonstrou maior prevalência de *Streptococcus gordonii* e *Streptococcus sanguinis* em indivíduos saudáveis e maior frequência e quantidade de *Fusobacterium* em pacientes com estomatite protética[41]. Também foi verificada a presença de 32 filotipos bacterianos exclusivamente da microbiota de pacientes com estomatite protética, que incluíam espécies dos gêneros *Streptococcus*, *Atopobium* e *Prevotella*, enquanto que 26 filotipos, principalmente do gênero *Streptococcus*, foram encontrados somente na microbiota de indivíduos usuários de próteses saudáveis[42]. Além disso, *C. albicans* foi encontrado na microbiota dos dois grupos de pacientes, enquanto que *C. glabrata* e *C. tropicalis* foram verificados somente na microbiota do grupo de usuários de próteses saudáveis[42]. Análises de cultivos bacterianos também demonstraram menor proporção de cocos e maior proporção de anaeróbios obrigatórios nos biofilmes de próteses e de palato de pacientes com estomatite protética comparados com os isolados de pacientes saudáveis[43] e também maior quantidade de *Streptococcus* α-hemolítico, *Neisseria* e *C. albicans* em pacientes com estomatite protética em relação a pacientes saudáveis[44]. Assim, verifica-se a existência de um biofilme polimicrobiano diferenciado associado à estomatite protética, o que sugere que não apenas *Candida* spp. seja o fator etiológico da doença. Entretanto, a interação entre essas espécies tanto na saúde como nos casos de estomatite protética precisa ainda ser melhor entendida.

Candida spp. também forma biofilme na mucosa bucal juntamente com as bactérias e desenvolve infecção no tecido quando algum fator predisponente do hospedeiro está presente, como uso de antibióticos de amplo espectro, corticosteroides, radio ou quimioterapia e, principalmente, imunossupressão[39,45]. Por serem oportunistas, a debilidade do sistema imune é o principal fator predisponente para a ocorrência das infecções fúngicas, as quais tornaram-se mais frequentes e preocupantes no século XX, com a pandemia da Síndrome da Imunodeficiência Adquirida (AIDS) e o desenvolvimento da medicina com tratamentos que acarretam em imunossupressão, como a realização de transplante de órgãos, a terapia intensiva, a terapia antineoplásica e anti-inflamatória[46]. A candidíase bucal já foi, inclusive, considerada um indicador da AIDS antes do surgimento dos antirretrovirais[47], apesar de que alguns pacientes com infecção pelo HIV ainda manifestam candidíase bucal mesmo sob uso desses medicamentos[48]. Além de infecção local, *Candida* spp. também é responsável por infecções sistêmicas (candidemia) quando atinge a corrente sanguínea do paciente. Atualmente, a candidemia é uma das principais infecções nosocomiais, principalmente em pacientes imunossuprimidos internados em hospitais por longos períodos, e apresenta elevada taxa de mortalidade[49].

O tratamento das infecções por *Candida* spp. é realizado por meio de agentes antifúngicos tópicos ou sistêmicos. Atualmente, existem três classes de antifúngicos comercialmente disponíveis: polienos, azóis e equinocandinas. Os agentes polienos (nistatina e anfotericina B) foram os primeiros antifúngicos que surgiram nas décadas de 40 e 50; eles se ligam ao ergosterol da célula fúngica (substância semelhante ao colesterol das células mamíferas) e alteram a permeabilidade da membrana citoplasmática, com extravasamento de conteúdo intracelular, sendo, portanto, fungicidas. Os azóis foram introduzidos no mercado na década de 90, são divididos em duas classes, os imidazólicos (clotrimazol, cetoconazol e miconazol) e os triazólicos (fluconazol, itraconazol, voriconazol, posaconazol e isavuconazol), e o seu mecanismo de ação envolve a inibição da enzima responsável pela síntese do ergosterol, sendo, portanto, fungistáticos. Já as equinocandinas (micafungina, caspofungina e anidulafungina), disponibilizadas clinicamente nos anos 2000, inibem a síntese do β-1,3-glucano, componente da parede celular fúngica, e apresentam ação fungicida (para *Candida* spp.) ou fungistática (para *Aspergillus* spp.)[50,51]. Assim, comparado com a grande quantidade de diferentes tipos e classes de antibióticos disponíveis, o número de antifúngicos existentes atualmente é pequeno. Isso é explicado, em parte, pelo fato da célula fúngica ser eucariota, assim como a célula mamífera, e, portanto, apresenta poucos alvos distintos que possam ser utilizados sem que haja toxicidade ao hospedeiro[52].

A evolução no desenvolvimento dos antifúngicos foi decisiva para o tratamento de infecções oportunistas em pacientes imunossuprimidos e de infecções sistêmicas, principalmente com o fluconazol que superou as limitações dos agentes até então utilizados (miconazol e anfotericina B, os quais apresentavam citotoxicidade, espectro de ação mais reduzido, insolubilidade em água, baixa biodisponibilidade e não atingiam o fluido cérebro-espinhal)[52]. Entretanto, apesar dessa evolução, o desenvolvimento de resistência antifúngica e a incidência de outras espécies, como as espécies não-*albicans* de *Candida*, tornaram-se mais comuns[50,52,53]. Atualmente, a resistência antimicrobiana é um sério problema de saúde pública e, tanto uma grande preocupação, como também um grande desafio mundial[54,55]. O desenvolvimento de resistência antifúngica é associado ao uso prolongado do medicamento, imunossupressão severa e uso de azóis na agricultura[53]. Clinicamente, a resistência antifúngica corresponde à persistência ou progressão da infecção mesmo com a terapia antimicrobiana apropriada e, em termos laboratoriais, a resistência antimicrobiana é mensurada pela susceptibilidade de um determinado micro-organismo a um agente antimicrobiano, cuja concentração inibitória mínima é interpretada através de valores limiares[56-58]. Além disso, a resistência pode ser intrínseca (primária), quando o micro-

organismo apresenta reduzida susceptibilidade ao medicamento antes mesmo se ser exposto a ele, ou adquirida (secundária), que é desenvolvida após longos períodos de exposição ao agente antimicrobiano[56].

A resistência antifúngica tem sido bastante descrita para os agentes azóis, cujos mecanismos de resistência abrangem alterações genéticas envolvidas principalmente com a superexpressão de transportadores de efluxo de medicamentos, os quais transportam o agente antifúngico para fora da célula, mas também com alteração do alvo do medicamento (redução de afinidade entre o medicamento e seu alvo). Adicionalmente, respostas de estresse celular induzidas por ação do medicamento e formação de biofilme também são descritos como mecanismos de resistência aos azóis[57,58]. Apesar de serem medicamentos mais recentes, a resistência às equinocandinas também é um problema no tratamento das infecções fúngicas, e o mecanismo de ação envolve mutação do gene responsável pela codificação da proteína que sintetiza o β-1,3-glucano da parede fúngica (alvo das equinocandinas) e, diferentemente da resistência aos azóis, a superexpressão dos transportadores de efluxo na membrana fúngica não acarreta em resistência às equinocandinas[57,58]. Já a resistência aos polienos é mais rara, apesar de serem os antifúngicos mais antigos, o que é justificado pelo fato de serem fungicidas e, por apresentarem toxicidade ao hospedeiro, não serem utilizados por longos períodos[57,58]. O mecanismo de resistência aos polienos envolve redução do ergosterol na membrana fúngica, o que pode ocorrer devido a tratamento prévio com azol, com surgimento de resistência cruzada entre polienos e azóis, e também mutação nos genes responsáveis pela biossíntese do ergosterol[57,58]. A resistência cruzada, ou resistência a multi-medicamentos, ocorre não apenas entre polienos e azóis, como observada em *C. albicans*, *Candida dubliniensis* e *C. tropicalis*, mas também entre azóis e equinocandinas, verificada em *C. glabrata*, e entre as três classes de antifúngicos, como já reportado em *C. albicans*[59], o que confere uma preocupação ainda maior para a área da saúde. O desenvolvimento de resistência também está associado a emergência de outras espécies não-*albicans* de *Candida*, como *C. glabrata* e *C. krusei* em casos de candidemia[60], as quais apresentam menor susceptibilidade e resistência intrínseca aos azóis[61], e também ao surgimento de novas espécies, como *Candida auris*, que apresenta multirresistência às três classes de antifúngicos[62,63].

Além da resistência antifúngica, uma outra preocupação com *Candida* spp. que também acarreta em falha das terapias com os agentes antifúngicos é a tolerância dos biofilmes. A tolerância difere da resistência antimicrobiana, uma vez que na resistência ocorrem mutações genéticas hereditárias e é constatado aumento da concentração inibitória mínima do medicamento contra o micro-organismo, enquanto que na tolerância os micro-

organismos são capazes de sobreviver somente transitoriamente ao medicamento mesmo em concentrações acima da inibitória mínima e, adicionalmente, persistência ocorre quando uma subpopulação microbiana sobrevive com a terapia antimicrobiana[64]. A formação de biofilme em dispositivos médicos, como cateteres, é uma das causas de candidemia, cujo tratamento requer, além da administração do agente antifúngico, a remoção do cateter quando possível devido à tolerância das células[49]. A formação do biofilme de *C. albicans* envolve diferentes etapas: 1. a aderência de leveduras ao substrato (fase de aderência); 2. a formação de microcolônias e de tubos germinativos que iniciam a filamentação (fase de iniciação); 3. a expansão da biomassa do biofilme e a síntese da matriz extracelular (fase de maturação) e, por fim, 4. a dispersão de leveduras do biofilme que poderão colonizar outros sítios (fase de dispersão); e cada fase é regulada por uma série de genes responsáveis para que o biofilme prospere e se desenvolva[65]. A tolerância do biofilme está associada com o microambiente e o metabolismo celular diferenciado, com subpopulações de células latentes, de crescimento lento, e com a matriz do biofilme, que atua como uma verdadeira barreira física que protege as células microbianas de agentes externos, como agentes antimicrobianos e células de defesa do hospedeiro, sendo também responsável pela estrutura tridimensional, rigidez, integridade e coesão do biofilme[66]. A matriz do biofilme de *C. albicans* é formada por polissacarídeos, como mananas e β-glucanos, proteínas, lipídeos e DNA extracelular (eDNA) [67] e também de hexosaminas, ácido urônico e fósforo[68], apesar de que a função de cada componente ainda não é bem conhecida[67,68]. Entretanto, o polissacarídeo insolúvel β-1,3-glucano da matriz promove aprisionamento do fluconazol durante o tratamento antifúngico e acarreta em tolerância ao medicamento[69] e o os polissacarídeos da matriz formam juntos o complexo manana-glucano, que também é responsável pela tolerância do biofilme[67,70].

Diante dessas dificuldades impostas pelo biofilme e pela resistência antifúngica, a busca, o desenvolvimento e a pesquisa por novas modalidades terapêuticas ganham relevância no combate às infecções. Tais modalidades incluem o uso de nanopartículas[71,72], peptídeos[73,74], produtos naturais[75,76] e Terapia Fotodinâmica antimicrobiana[77-80]. Assim, essa obra é dividida em 6 (seis) capítulos, cada um correspondente a um artigo científico publicado em revistas internacionais de seletiva política editorial, que trazem os trabalhos desenvolvidos após o doutorado do candidato (do pós-doutorado até o ano presente) que buscaram tratamentos alternativos antimicrobianos a serem utilizados em infecções médico-odontológicas, principalmente a candidíase bucal.

O primeiro estudo[81] teve como objetivo sintetizar, caracterizar e avaliar a ação antimicrobiana de nanopartículas de dióxido de titânio com prata (TiO_2:Ag) em culturas

planctônicas e biofilmes de *C. albicans*, *C. glabrata*, *C. tropicalis* e *Staphylococcus aureus* resistente a meticilina (SARM). O TiO_2 é um material que apresenta estabilidade química, baixo custo, ausência de toxicidade e atividade fotocatalítica, ou seja, capacidade de oxidação e redução quando irradiado por luz com energia maior que seu intervalo de banda (3,2 eV)[82]. Essa propriedade fotocatalítica permite que o TiO_2 seja utilizado para despoluição ambiental (ar e água), células fotovoltaicas de energia solar e também em inativação microbiana[83]. Adicionalmente, a Ag é um material que apresenta conhecida atividade antimicrobiana e, na forma de nanopartículas, essa atividade ocorre por meio da geração de radicais livres[84]. Os resultados de caracterização demonstraram a presença de nanopartículas de Ag depositadas na superfície de TiO_2, sintetizado pelo método de tratamento hidrotermal assistido por micro-ondas, que permitiu a obtenção de microcristais primariamente na forma anatásio (forma estável do TiO_2) com tamanho médio de 112 nm. Os microcristais de TiO_2:Ag demostraram ação antimicrobiana e antibiofilme contra *Candida* spp. e SARM, com reduções de 1,54 a 2,33 $\log_{10}$ da viabilidade e de 11,91 a 35,66% da biomassa dos biofilmes. Adicionalmente, um modelo teórico de interação de elétrons entre Ag e TiO_2 foi proposto, utilizando modelos e cálculos computacionais, para formular o mecanismo de ação antimicrobiana dos microcristais. Esse trabalho foi desenvolvido em parceria com o Centro de Pesquisa para o Desenvolvimento de Materiais Funcionais, um dos Centros de Pesquisa, Inovação e Difusão (CEPID) da Fundação de Amparo à Pesquisa do Estado de São Paulo (FAPESP), coordenado pelo Prof. Dr. Elson Longo.

Os 4 (quatro) próximos capítulos abordam a Terapia Fotodinâmica antimicrobiana (aPDT, ou Inativação Fotodinâmica) para inativação de biofilmes e tratamento de candidíase bucal. Esses trabalhos, desenvolvidos em conjunto com outros professores dentro da linha de pesquisa do candidato, iniciaram-se durante o doutorado do candidato (2005 a 2009), que demonstrou a eficácia da aPDT na inativação de *C. albicans* em um modelo de candidíase bucal em camundongos[85] e também como um método de tratamento da estomatite protética[86,87]. Os trabalhos de aPDT do grupo de pesquisa do candidato são realizados em parceria com o Centro de Pesquisa em Óptica e Fotônica (CEPOF), outro CEPID da FAPESP, coordenado pelo Prof. Dr. Vanderlei Salvador Bagnato.

A Terapia Fotodinâmica é hoje uma modalidade de tratamento utilizada clinicamente para o câncer[88], apesar de ter sido inicialmente descoberta há mais de 100 anos atrás como um método antimicrobiano, quando Oscar Raab verificou a fotoinativação de *Paramecia caudatum* expostos ao cloridrato de acridina e luz visível[89]. Porém, com a descoberta da penicilina por Alexander Fleming[90] e o desenvolvimento dos antibióticos, os estudos com

aPDT ficaram latentes e passaram a ser mais explorados com a constatação da tolerância dos biofilmes e o desenvolvimento de resistência antimicrobiana. A aPDT requer a utilização de um agente químico inerte, geralmente um corante, denominado de fotossensibilizador (FS), associado a uma luz cujo comprimento de onda deve ser equivalente ao comprimento de onda de absorção do FS[89]. O FS deve ser aplicado no tecido ou células alvos durante um período de tempo, chamado de tempo de incubação ou de pré-irradiação que deve ser realizado em ambiente escuro, na ausência de luz (fotossensibilização), para então, em seguida, ser irradiado pela fonte de luz. A interação da luz com o FS, na presença de oxigênio, acarreta na produção de espécies reativas que são tóxicas e letais às células que incorporam o FS. Quando irradiado, o FS passa par um estado singleto de alta energia, porém de curto tempo (nanosegundos), o que faz com que retorne ao seu estado fundamental, com emissão de fóton ou calor, ou passe para um estado tripleto, também de alta energia e com maior tempo de vida (micro a milisengundos). Nesse estado, o FS pode, novamente, retornar ao seu estado fundamental ou reagir com moléculas vizinhas na presença do oxigênio. Quando o FS transfere elétrons para moléculas vizinhas, estas reagem com oxigênio gerando espécies reativas, como íons superóxidos, hidroxila e outros radicais livres, processo denominado de reação do Tipo I. Quando o FS reage diretamente com o oxigênio, conhecido como reação do Tipo II, ocorre a formação de oxigênio singleto, que oxida estruturas biológicas e, portanto, é citotóxico[89]. Além disso, atualmente sugere-se a reação de Tipo III, a qual ocorre na ausência de oxigênio, com formação de radicais inorgânicos tóxicos à célula alvo[91].

Uma série de FS são utilizados em aPDT, sendo os sais fenotiazínicos (azul de metileno e azul de toluidina) os mais populares, mas também a rosa bengala, estruturas tetrapirróis (porfirinas, clorinas, bacterioclorinas e ftalocianinas), produtos naturais, como hiperecina e curcumina, e também nanopartículas[92]. A curcumina (CUR) é um FS interessante por ser um produto natural extraído dos rizomas de *Curcuma longa* L. (açafrão), muito utilizado na culinária, com propriedades antioxidantes, anticâncer, anti-inflamatória e antimicrobiana[93]. Estudos do grupo de pesquisa do candidato demonstraram que a aPDT mediada pela CUR e diodos emissores de luz (LED) com comprimento de onda azul (~450 nm) foi efetiva para inativação de culturas planctônicas e biofilmes monoespécies de *Candida* spp.[94,95], SARM[96], biofilmes polimicrobianos[97] e *C. albicans* num modelo murino de candidíase bucal[98].

Entretanto, a CUR não é solúvel em água (lipossolúvel) e, por isso, necessita de solventes orgânicos para sua dissolução, como dimetilsulfóxido (DMSO), o que limita sua utilização in vivo. Além disso, a CUR tem baixa biodisponibilidade e elevada instabilidade

(degradação fotolítica e hidrolítica)[93]. Por isso, sistemas de liberação controlada de fármacos têm sido utilizados para carrear CUR, de maneira que ela possa ser utilizada in vivo e alcançar o(s) tecido(s) alvo(s). Esses sistemas incluem micelas, lipossomas, nanopartículas, ciclodextrinas, nanoemulsões, etc.[99,100] Nesse contexto, o segundo capítulo desta obra teve como objetivo encapsular CUR em nanopartículas poliméricas para serem utilizadas em aPDT[101]. Para a síntese das nanopartículas, foram utilizados ácido poli-lático como polímero e sulfato de dextrana pela técnica da nanoprecipitação, que permitiu o encapsulamento de CUR na concentração máxima de 260 μM com eficiência de 67%. Essas nanopartículas obtidas apresentaram carga negativa (aniônica) e, visando maior eficiência contra biofilme, brometo de cetiltrimetilamônio (CTAB) foi adicionado na rota final de síntese para obtenção de nanopartículas catiônicas (carga positiva). Após a síntese, o tamanho das nanopartículas foi maior que 200 nm e aumentou ao longo de 40 dias, assim como o índice de polidispersão, que mensura a distribuição do tamanho das nanopartículas em suspensão[102]. Ao longo desse período, a carga das nanopartículas também sofreu variação, tendendo à neutralidade. O encapsulamento não alterou a faixa de absorção de luz da CUR (espectro azul) e as nanopartículas com CUR demonstraram fotodegradação, assim como a CUR livre (não encapsulada). A liberação de CUR das nanopartículas foi progressiva e gradual ao longo de 48 h. Quando utilizadas na aPDT, culturas planctônicas de *C. albicans*, SARM e *Streptococus mutans* apresentaram redução de 0,78 $\log_{10}$ (*C. albicans* submetida à aPDT mediada pelas nanopartículas aniônicas) até completa inativação (todas as espécies submetidas à aPDT com CUR livre e nanopartículas catiônicas). Os biofilmes simples e polimicrobianos dessas espécies mostraram reduções de 0 (ausência de efeito) a 4,44 $\log_{10}$. Adicionalmente, imagens de microscopia confocal sugeriram menor captura do FS pelas células do biofilme polimicrobiano quando o biofilme foi lavado após a fotosensibilização e a análise de citotoxicidade demonstrou que o encapsulamento da CUR em nanopartículas aniônicas eliminou a citotoxicidade do veículo da CUR livre (DMSO a 10%). Com esse trabalho, foi depositada uma patente no Instituto Nacional da Propriedade Industrial (INPI, processo BR 10 2016 015631 9, "Processo de Obtenção de Nanopartículas Poliméricas Aniônicas e Catiônicas de Curcumina, Nanopartículas obtidas e Seus Usos", Anexo A).

Previamente à realização de um estudo clínico para avaliar a eficácia de uma nova terapia e/ou medicamento em humanos, é importante que essa avaliação seja realizada em modelos animais que mimetizem a condição patológica a ser tratada. Apesar das questões éticas envolvidas, estudos em animais permitem maior controle de variáveis envolvidas no estudo (menor viés) e realização de análises que não são possíveis de serem conduzidas em

humanos, como avaliações histopatológicas. Assim, o terceiro capítulo desta obra avaliou a aPDT mediada pela CUR em nanopartículas num modelo murino de candidíase bucal[103], no qual o período de infecção foi prolongado para que a aPDT pudesse ser utilizada em cinco sessões consecutivas, simulando uma aplicação clínica[104]. As nanopartículas de CUR foram sintetizadas e apresentaram características semelhantes às do estudo prévio[101]. Após o tratamento dos animais, foi observada redução de *C. albicans* nos grupos submetidos à aPDT mediada pela CUR livre e em nanopartículas catiônicas, com redução de 1,11 e 0,74 $\log_{10}$. As maiores reduções observadas, 1,58 e 2,57 $\log_{10}$, foram nos grupos de animais tratados com nistatina quatro vezes ao dia (sem anestesia) e uma vez ao dia sob anestesia, respectivamente, ambos tratamentos realizados durante cinco dias consecutivos, como a aPDT. A análise histopatológica mostrou invasão fúngica no epitélio e poucas células inflamatórias no tecido. Apesar da nistatina ter apresentado um melhor resultado antifúngico, a imunoexpressão de citoqueratinas 13 e 14 desses animais foi mais semelhante aos dos animais com infecção de *C. albicans*. As citoqueratinas são proteínas do citoesqueleto das células epiteliais comumente expressas em condições patológicas, como carcinomas[105]. Já os animais submetidos à aPDT mediada pela CUR livre, a imunoexpressão dessas citoqueratinas foi mais semelhante a do grupo de animais saudáveis, sugerindo que aPDT possa ter contribuído para a reorganização do citoesqueleto celular. Além disso, não foi verificado dano ao DNA das células do tecido lingual dos animais, sugerindo que os tratamentos apresentaram segurança.

O quarto capítulo desta obra teve como objetivo avaliar a aPDT mediada por outro nanosistema utilizado como FS, nanoemulsão catiônica de ftalocianina cloro-alumínio (cNE-FcClAl), associado a LED no comprimento de onda vermelho (sinal máximo em 660 nm) contra biofilme polimicrobiano formado por *S. mutans*, *C. albicans* e *C. glabrata*[106]. Ftalocianinas são FS derivados de porfirinas que necessitam de metais em sua estrutura para apresentarem um efeito fotodinâmico e, por serem hidrofóbicos[92], necessitam de solventes orgânicos ou sistemas de liberação controlada. As nanoemulsões são um tipo desses sistemas de característica bifásica (óleo/água ou água/óleo), na qual uma fase encontra-se dispersa na outra na forma de minúsculas gotas, e são estabilizadas por um agente emulsificante que também confere carga ao sistema[107]. Nesse estudo, as cNE-FcClAl foram sintetizadas pelo grupo do Centro de Nanotecnologia e Engenharia de Tecidos de Ribeirão Preto (Universidade de São Paulo, USP), sob responsabilidade do Prof. Dr. Antonio Claudio Tedesco, com o qual o grupo de pesquisa do candidato tem parceria. Esse FS já foi avaliado pelo grupo de pesquisa do candidato contra *C. albicans*[108], SARM[109] e em modelo murino de candidíase bucal[110,111]. Os resultados desse quarto estudo desta obra mostraram que, no biofilme polimicrobiano, *S.*

mutans apresentou maior susceptibilidade à aPDT (redução de 2,24 log_{10}) do que as espécies de *Candida* (redução de 1,30 a 1,39 log_{10}). O biofilme submetido à aPDT apresentou diminuição da atividade metabólica de 53,7%, porém não houve redução da biomassa total do biofilme, indicando que, apesar da aPDT ter reduzido a viabilidade microbiana, a estrutura do biofilme não foi afetada. As imagens de microscopia confocal mostraram captura do FS pelas células do biofilme.

Apesar da aPDT ser efetiva para inativar células microbianas, o biofilme reduz bastante sua eficácia, pois a matriz atua como uma barreira física para penetração do FS. Visando então uma melhor penetração do FS no biofilme, o quinto estudo desta obra[112] avaliou a Terapia Sonodinâmica (SDT), a qual segue os mesmos princípios da PDT mas, ao invés de utilizar luz para ativação do FS, aqui denominado de sonosensibilizador (SS), a SDT utiliza ultrassom, o qual permite maior penetração no tecido vivos[113]. Os mecanismos de ação da SDT, apesar de não serem completamente entendidos, envolvem: 1. Formação de microbolhas no meio líquido pela propagação do ultrassom, que oscilam em baixa ou alta amplitude e geram danos na membrana celular (cavitação acústica)[114]; 2. Formação de espécies reativas pela ativação do SS pelo ultrassom, com implosão das microbolhas que alteram pressão e temperatura do meio e, por meio de reações sonoquímicas, geram oxigêno singleto (sonólise) e emissão de luz que acarretam nas reações tipo I e II da PDT (sonoluminescência)[114]. Para a realização dessa pesquisa, inicialmente foi solicitada uma bolsa de pesquisa no exterior (BPE) à FAPESP (2015/25997-3) para iniciar uma parceria internacional com o Prof. Dr. John Francis Callan, pesquisador referência em SDT, da Universidade de Ulster, em Coleraine na Irlanda da Norte, bolsa essa que foi denegada. Com isso, numa segunda oportunidade, foi possível estabelecer essa colaboração internacional por meio do Programa de Apoio para a realização de Estágio no Exterior - PAREex- da Pró-Reitoria de Pós-Graduação (PROPG) da UNESP (edital 3/2016).

Neste estudo, a SDT foi comparada com a aPDT e ambas foram combinadas contra biofilme de *C. albicans*. Os FS utilizados foram a rosa bengala e o Photodithazine® (PDZ, derivado da clorina e6) associados à luz de LED branca e vermelha (~660 nm), respectivamente, para a aPDT. Esses mesmos FS foram utilizados como SS e, assim, associados ao ultrassom de 1 MHz de frequência para a SDT. Os resultados com culturas planctônicas demonstraram que tanto a aPDT como a SDT isoladamente reduziram o crescimento de colônias fúngicas de 4,35 log_{10} até completa irradiação. Entretanto, quando biofilmes de *C. albicans* foram avaliados, somente a associação dos tratamentos simultaneamente (aPDT + SDT) promoveu redução da viabilidade do biofilme de 1,45 a 3,39

log_{10}, ao passo que as terapias isoladas não foram efetivas. Isoladamente, a aPDT e a SDT reduziram a biomassa do biofilme de 30,9 a 53,4%, enquanto que a associação das terapias diminuiu a biomassa de 63,1 a 75,5%. A análise em microscopia óptica e confocal demonstrou redução da espessura do biofilme, menor número de células filamentosas e maior quantidade de células não viáveis após a terapia combinada.

O desenvolvimento de novos medicamentos antimicrobianos requer um elevado custo e longo tempo até esses estarem diponibilizados comercialmente para a população. Assim, o estudo de novas aplicações de medicamentos já existentes em outra finalidade distinta de sua indicação original, conhecida como reposicionamento de medicamentos (*drug repurposing*), é uma estratégia interessante para redução de custos e tempo[115]. Tem sido relatado que a N-acetilcisteína (NAC), um medicamento mucolítico utilizado para doenças respiratórias[116], apresenta ação antibiofilme contra micro-organismos patogênicas, com redução da matriz polimérica[117,118]. Nesse contexto, o sexto estudo[119] desta obra avaliou a ação da NAC em biofilmes fúngicos de *C. albicans* suscpetível e resistente a fluconazol.

Os resultados demonstraram ação fungistática da NAC, com concentração inibitória mínima (CIM) de 25 mg/mL para ambas as cepas. Concentrações maiores que a CIM reduziram a viabilidade em até 2,77 log_{10} e a biomassa em até 88% de biofilmes pré-formados e de biofilmes em formação. Porém, concentração menor que a CIM apresentou um efeito oposto: aumento da viabilidade fúngica em até 0,73 log_{10}. Adicionalmente, a NAC reduziu componentes solúveis da matriz do biofilme de ambas as cepas (polissacarídeos em até 2.696,15 μg/mL, eDNA em 1.008,73 ηg/μL, além de proteínas do matriz da cepa susceptível em 95,62 μg/mL) e mostrou sinergismo com o antifúngico caspofungina em até 115% somente em culturas planctônicas de ambas as cepas.

2 PROPOSIÇÃO

Os seis trabalhos que compõem esta obra e apresentados a seguir foram publicados pelo candidato após o doutorado em revistas científicas internacionais e abordam estratégias alternativas aos antifúngicos para o tratamento de biofilmes microbianos, especialmente os de *C. albicans*, visando o tratamento de infecções, inclusive as causadas por cepas resistentes.

3 PUBLICAÇÕES

Publicação 1: *Antimicrobial activity of TiO_2:Ag nanocrystalline heterostructures: Experimental and theoretical insights*. Artigo publicado no periódico **Chemical Physics**, 2015; 459: 87–95.

Publicação 2: *Encapsulation of curcumin in polymeric nanoparticles for antimicrobial Photodynamic Therapy*. Artigo publicado no periódico **PLoS One**, 2017; 12(11): e0187418.

Publicação 3: *Antimicrobial Photodynamic Therapy mediated by curcumin-loaded polymeric nanoparticles in a murine model of oral candidiasis*. Artigo publicado no periódico **Molecules**, 2018; 23(8). pii: E2075.

Publicação 4: *Effect of chloroaluminium phthalocyanine in cationic nanoemulsion on photoinactivation of multispecies biofilm*. Artigo publicado no periódico **Photodiagnosis and Photodynamic Therapy**, 2018; 24: 212-219.

Publicação 5: *Antimicrobial sonodynamic and photodynamic therapies against Candida albicans*. Artigo publicado no periódico **Biofouling**, 2018; 34(4): 357-367.

Publicação 6: *Fungistatic action of N-Acetylcysteine on Candida albicans biofilms and its interaction with antifungal agents*. Artigo publicado no periódico **Microorganism**, 2020; 8, 980.

3.1 Publicação 1·

Chemical Physics 459 (2015) 87–95

Contents lists available at ScienceDirect

Chemical Physics

journal homepage: www.elsevier.com/locate/chemphys

Antimicrobial activity of TiO_2:Ag nanocrystalline heterostructures: Experimental and theoretical insights

Rafaela S. André [a], Camila A. Zamperini [b], Ewerton G. Mima [c], Valéria M. Longo [d,*], Anderson R. Albuquerque [e,f], Júlio R. Sambrano [e], Ana L. Machado [c], Carlos E. Vergani [c], Antonio C. Hernandes [d], José A. Varela [b], Elson Longo [b]

[a] UFSCar – Universidade Federal de São Carlos, Department of Chemistry, 13565-905 São Carlos, SP, Brazil
[b] UNESP – Universidade Estadual Paulista, Instituto de Química, 14801-907 Araraquara, SP, Brazil
[c] UNESP – Universidade Estadual Paulista, Escola de Odontologia de Araraquara, Departamento de Materias Odontológicos e Próteses Dentárias, 14801-903 Araraquara, SP, Brazil
[d] USP – Universidade de São Paulo, Instituto de Física de São Carlos, 13560-970 São Carlos, SP, Brazil
[e] UNESP – Universidade Estadual Paulista, Grupo de Modelagem e Simulação Molecular, P.O. Box 477, CEP 17033-360 Bauru, SP, Brazil
[f] Instituto Federal de Educação, Ciência e Tecnologia do Sertão Pernambucano, IFSetão-PE, 56400-000 Floresta, PE, Brazil

ARTICLE INFO

Article history:
Received 13 February 2015
In final form 17 July 2015
Available online 29 July 2015

Keywords:
Antimicrobial activity
TiO_2:Ag
Nano crystalline
DFT

ABSTRACT

We report the synthesis and characterization of silver-decorated titanium dioxide (TiO_2:Ag) nanoparticles, as well as a discussion of their antimicrobial activity. This material was synthesized by microwave-assisted hydrothermal treatment and characterized by complementary techniques. The minimum inhibitory concentration and minimum bactericidal/fungicidal concentration of TiO_2:Ag nanoparticles against planktonic and biofilm-forming strains of methicillin-resistant *Staphylococcus aureus*, *Candida* species (spp.) and the total biofilm mass were determined. The basis of the biological activity of TiO_2:Ag was investigated by electronic analysis of the material using theoretical quantum chemical calculations. In the proposed mechanism of action, the impregnated semiconductor donates electrons to the forbidden band gaps in the metal, generating point defects, with partially located electrons and holes at the surface, initiating a radical process involving the solvent and biological target. Our results suggest that this TiO_2:Ag nanomaterial has potential for use in the development of new therapeutic agents.

© 2015 Elsevier B.V. All rights reserved.

1. Introduction

Nanocrystalline titanium dioxide (nc-TiO_2) is a modern photoactive material with a wide range of possible applications, such as in solar cells, self-cleaning fibers, pollutant removal [1], sunscreen [2], water splitting, and as an antifungal agent via photokilling [3–7]. Desirable characteristics exhibited by nc-TiO_2 include stability, nontoxicity, chemical inertness, low cost, as well as antimicrobial activity. TiO_2 nanoparticles can be designed in crystalline form, with the rutile and anatase phases being the most stable. To improve its antimicrobial properties, modifications of TiO_2 have been proposed, such as the addition of noble metal dopants [8].

Silver (Ag) is the most extensively studied nanoparticle used for microbial inactivation, and its antimicrobial efficacy has been attributed to the release of ions and/or production of reactive oxygen species (ROS) [9]. When TiO_2 is modified by Ag addition, the Ag can also contribute to antimicrobial activity, by interacting with either proteins in the bacterial cell membrane or intracellular elements such as DNA, leading to cell death [10].

The yeast, *Candida albicans*, an opportunistic commensal of humans, can cause infections when favorable alterations occur in the local or systemic environment, such as with the use of dentures or immunosuppressive agents. Infections caused by *C. albicans* range from superficial, mucosal infections to systemic, life-threatening diseases. Although *C. albicans* is the most prevalent and virulent species, other species from this genus have also been isolated from candidal infections, such as *C. glabrata* and *C. tropicalis* [11]. The increasing prevalence of infections caused by non-albicans *Candida* spp. is significant, as these infections may be intrinsically resistant to antifungal agents, with mortality rates similar to that observed for *C. albicans* infection [12].

Overuse and misuse of antibiotics have led to the emergence of multidrug-resistant bacterial strains. Methicillin-resistant *Staphylococcus aureus* (MRSA) is a major human pathogen, often causing nosocomial infections. Recently, the emergence of community-associated MRSA has also been a matter of serious concern because it

* Corresponding author.
E-mail address: valeria.longo@liec.ufscar.br (V.M. Longo).

http://dx.doi.org/10.1016/j.chemphys.2015.07.020
0301-0104/© 2015 Elsevier B.V. All rights reserved.

· Artigo nas normas do periódico *Chemical Physics*.

can cause widespread and/or severe disease in an otherwise healthy population [13]. The ability of MRSA to grow on host surfaces and biomaterials used in indwelling medical devices is an important virulence factor frequently associated with chronic/recurrent infections. Therefore, there is an urgent need to develop new antibacterial agents. Nanomaterials offer an attractive alternative to antimicrobial agents and have drawn considerable research interest in the biological field.

The development of heterostructured nanomaterials with novel capacities for recombination of electrons and holes in the band gap is considered a good approach to combating microbial resistance. Although several approaches have been reported for combining nanomaterials, there is a need to optimize the resultant structure as well as its microstructure. In this context, hydrothermal treatment assisted by microwave irradiation (HTMW) is a safe, eco-friendly, and reproducible method, which is widely used for synthesizing various nanomaterials [14].

Biofilms are structured communities of microbial cells attached to a surface enclosed in a self-produced, complex, biopolymer matrix. Cells in biofilms are phenotypically distinct from their planktonic forms, and exhibit increased resistance to antimicrobial drugs and host defense mechanisms [15]. Although biofilm formation is the most common mode of microbial survival in a natural ecosystem, to the best of our knowledge, there are no reported studies to date evaluating the effect of TiO_2 nanoparticles decorated with Ag (TiO_2:Ag), obtained by HTMW, on *Candida* spp. and MRSA biofilms.

Therefore, the goals of this study were to synthesize TiO_2:Ag by using HTMW and to assess the antimicrobial activity of this nanomaterial against *Candida* spp. and MRSA. Due to difficulties in assigning correct electronic responses at atomistic resolution, the key factor governing the antifungal activity of nc-TiO_2 is still unclear. Fortunately, first-principle simulations can fundamentally extend our understanding of electronic properties at atomic-scale resolution. Therefore, to complement experimental data, the bulk of the anatase and metallic Ag in TiO_2:Ag was evaluated by first-principle calculations. In light of these results, an antifungal mechanism, involving the formation of ROS, was formulated.

2. Experimental section

2.1. Preparation and characterization of TiO_2:Ag

To obtain nanoparticles of TiO_2, titanium isopropoxide ($Ti[OCH(CH_3)_2]_4$) with 97% purity, sourced from Alfa Aesar, was used as a precursor of titanium (Ti) in isopropanol. A solution of the Ti in isopropanol was prepared to a final concentration of 0.0025 M Ti, and hydrolysis was performed with an excess of H_2O:Ti of 500:1. The solution was maintained under constant agitation in an ice bath. The white colloid was placed in a sealed 100-mL Teflon autoclave and HTMW was applied by using 2.45-GHz microwave radiation at 800-W power. The sample was heated at 140 °C for 16 min, resulting in a white precipitate; then, the autoclave was naturally cooled to room temperature. The product was washed until the pH reached 7 and dried in an oven at 100 °C. For Ag impregnation, the TiO_2 obtained was suspended in distilled water (9 wt% solid loading), and the pH was adjusted to 5 with HNO_3. While the solution was constantly stirred at 60 °C, 5 mL of $AgNO_3$ (1.4×10^{-2} M) and NaOH were added to raise the pH to 9, resulting in a brown precipitate [16]. The precipitate was washed until the pH reached 7, and then dried in an oven. An aqueous solution of the resultant TiO_2:Ag (2000 mg L^{-1}) was prepared for microbiological testing.

TiO_2:Ag nanostructures were characterized by X-ray diffraction (XRD), carried out on the as-prepared sample using a Rigaku DMax 2500PC diffractometer at 40 kV and 150 mA with Cu-Kα radiation, a graphite monochromator, and a rotary anode, as well as by high-resolution transmission electron microscopy (HRTEM); Tecnai G2TF20, FEI. Morphological and size characterization were performed by field-emission gun scanning electron microscopy (FEG-SEM; Supra 35-VP, Carl Zeiss). Raman spectra at room temperature were obtained using a Horiba Jobin–Yvon Raman LabRAM microspectrometer with 514 nm as the excitation wavelength, through an Olympus TM BX41 microscope. The Cary 5G spectrometer was used to measure ultraviolet–visible (UV–vis) absorption in order to calculate the energy of the band gap. To better understand the characterization of TiO_2:Ag, the short-range order of pure TiO_2 was investigated by Fourier transform (FT)-Raman analysis and UV–vis absorption.

2.2. Procedure for determining antimicrobial activity

To determine the antimicrobial effect of the TiO_2:Ag solution synthesized, the minimum inhibitory concentration (MIC) of planktonic cells and the minimum bactericidal concentration (MBC)/fungicidal concentration (MFC) of planktonic cells and also biofilm-forming cells (MBCb/MFCb) were determined using a broth microdilution assay, as described by the Clinical and Laboratory Standards Institute [17,18] (documents M7-A7 and M27-A3), with some modifications. Standard strains of MRSA, *C. albicans*, *C. glabrata*, and *C. tropicalis* from the American Type Culture Collection (ATCC 33591, ATCC 90028, ATCC 2001, and ATCC 4563, respectively) were used. In all subsequent procedures, unless otherwise specified, tryptic soy broth (Acumedia Manufacturers, Inc.) and RPMI-1640 medium (Sigma–Aldrich) were used for MRSA and *Candida* spp., respectively. The solid media used were mannitol salt agar (Acumedia Manufacturers, Inc.) for MRSA and Sabouraud dextrose agar (Acumedia Manufacturers Inc.) containing 5 μg mL^{-1} gentamicin for *Candida* spp. To prepare the inoculum, *Candida* spp. and MRSA were individually streaked onto agar medium and incubated for 48 h at 37 °C. One loopful of each culture was individually transferred to 10 mL of broth and incubated overnight at 37 °C in an orbital shaker set at 75 rpm. The microbial cells were then harvested by centrifugation at 4000× *g* for 5 min, washed twice with phosphate-buffered saline (PBS; pH 7.2), and resuspended in their respective media.

The MIC and MBC/MFC were determined by incubating MRSA and *Candida* spp., individually, in 96-well microtiter plates for 24 h at 37 °C, while being exposed to serial two-fold dilutions of TiO_2:Ag solution (from 1000 mg L^{-1} to 15.62 mg L^{-1}) in their respective media. Inoculated broth without TiO_2:Ag solution was used as the positive control and uninoculated broth was used as the negative control. The MIC was defined as the lowest concentration of TiO_2:Ag at which no microbial growth was detected by visual inspection. To establish the MBC/MFC, 10-μL aliquots from each well were inoculated in duplicate onto agar plates. After 48 h of incubation at 37 °C, the number of colony-forming units per milliliter (CFU mL^{-1}) was counted and the $\log_{10}$(CFU mL^{-1}) value was calculated. The MBC/MFC was defined as the lowest concentration of TiO_2:Ag solution resulting in no detectable growth.

To determine the MBCb/MFCb and the total biomass of mature 48-h biofilms, the colonies were quantified (CFU mL^{-1}) and the absorbance of the crystal violet stain was determined. Spectrophotometrically standardized cell suspensions (MRSA: 1×10^7 - cells mL^{-1}; *Candida* spp.: 1×10^6 cells mL^{-1}) were placed into each well of 96-well microtiter plates and incubated for 90 min at 37 °C in an orbital shaker set at 75 rpm; this was the cell-adhesion phase. The wells were then washed twice with 200 μL of PBS to remove non-adherent cells and filled with 200 μL of the broth medium, and the plates were incubated again (37 °C, 75 rpm, 48 h). The broth medium was replaced with 100 μL of fresh

medium after 24 h. Following biofilm formation (48 h), the medium was aspirated, and non-adherent cells were removed by washing twice with 200 μL of PBS. Broth medium (200 μL) containing various concentrations (from 1000 mg L^{-1} to 15.62 mg L^{-1}) of TiO_2:Ag was added to the biofilms, followed by incubation for 24 h. To determine the MBCb/MFCb, the biofilms were scraped out of the wells and suspended in 1000 μL of PBS with vigorous vortex mixing for 1 min. For the contents of each well, 10-fold dilutions were prepared, and 10-μL aliquots of these were inoculated in duplicate on agar plates. After 48 h of incubation at 37 °C, the CFU mL^{-1} value was determined and the $\log_{10}$(CFU mL^{-1}) value was calculated. For the determination of total biomass, biofilms were fixed with methanol and stained with 1% crystal violet solution for 5 min. The stain bound to the biofilm was dissolved in 33% acetic acid solution and the optical density was measured at 570 nm using a spectrophotometer (Thermo Plate TP-Reader). For experiments involving both planktonic and biofilm-forming cells, cells incubated in broth medium without TiO_2:Ag were used as the positive control, while plain broth medium (without cells or TiO_2:Ag) was used as the negative control. All experiments were performed in triplicate on three independent occasions. Data obtained from CFU mL^{-1} and total biomass quantifications were statistically assayed by analysis of variance and Tukey's post hoc test at 5% significance.

3. Computational method and models

To determine the electronic effects of the metal/oxide heterostructure on biological activity, we conducted a computational simulation of anatase-phase TiO_2 and Ag by using a periodic approach of density functional theory. The anatase phase of TiO_2 has a tetragonal structure belonging to the $I4_1/amd$ space group, defined by two lattice parameters (a = 3.78 Å and c = 9.51 Å), and one internal coordinate, u = 0.208. The Ag unit cell is a cubic hexoctahedron (Fm_3m space group), composed of a single non-equivalent atom with the lattice parameters $a = b = c$ = 4.04 Å. We have previously studied this system and used this computational methodology for several conditions, including surfaces [19,20], point defects [21], and bulk disorder [22].

Besides the separated computational simulation for metal and oxides be sufficient to explain the electronic band alignment for extended systems [23–25], we presented also a more realistic structural model for nano heterostructure. This model was built by supporting a neutral [Ag_4] cluster on the periodic 2 × 2 (1 0 1) TiO_2 surface supercell (the most stable titanium dioxide surface) [20] with one oxygen vacancy at the topmost O atom. The computational study of metal clusters on a supporting oxide surface presents a large number of almost degenerated isomers. The number of possible stable configurations with several cluster size to find the global minimum is not a trivial task, so is outside of the scope and aim of the present work. Small clusters are useful models to access the most important properties related to metal/support interaction. So, the present model does possible to clarify the electron transfer and charge accumulation around the clusters and include all point defects discussed here. Theoretical models with increasing amount of supported Ag atoms will converge the electronic properties toward the separated systems. So, the proposed $[Ag]_4/TiO_{2-x}$ model is the minimum one to explain the main features of this material.

All simulations were carried out using the CRYSTAL14 [26] computer code with the HSE06 Heyd–Scuseria–Ernzerhof exchange–correlation functional [27]. CRYSTAL uses a Gaussian-type basis set to represent crystalline orbitals as a linear combination of Bloch functions defined in terms of local functions (atomic orbitals). The atomic centers were treated using the all-electron Gaussian-type basis set (s/sp/d): Ti 6/6621/31, O 6/31/1, and Ag 6333/53211/531. Diagonalization of the Fock matrix was performed using the Monkhorst–Pack grid with 16 k-points for Ag and 30 k-points for TiO_2. The accuracy of the Coulomb and exchange series was controlled by a set of five thresholds (10^{-8}, 10^{-8}, 10^{-8}, 10^{-8}, and 10^{-18}).

The atomic positions of all atoms in all models were fully relaxed until the largest component of the ionic forces was $<3 \times 10^{-4}$ eV/Å. The electronic structure, density of states (DOS) and band structure were analyzed using the Properties14 module in CRYSTAL, employing the same k-points sampling as the diagonalization of the Fock matrix for optimization of the data.

4. Results and discussion

TiO_2 and TiO_2:Ag samples were characterized with respect to their long-range order from XRD patterns. As shown in Fig. 1, samples of both TiO_2 and TiO_2:Ag were indexed as the anatase phase of TiO_2 with tetragonal structure (powder diffraction file [PDF] number 21-1272). Diffraction peaks related to secondary phases were detected and indexed as metallic Ag (Ag; PDF number 65-2871), in addition to the primary anatase phase of TiO_2, in the TiO_2:Ag sample.

These results show the anatase phase of the nanomaterial has broad peaks; these are an indication of the structural disorder of the nanomaterial [24], which is a consequence of the synthesis method. HTMW is an economical and quick method to obtain crystalline structures. Several highly crystalline materials with nanoassembled morphology have previously been obtained using this method of synthesis [28,29]. The results of Rietveld analysis of well-ordered nanoparticles, formed with the assistance of HTMW, highlight the changes in their intermediate-range order, which generate freezing distortion of the angles between the clusters constituents of crystalline structure [28,30]. These distortions and tilts are important in the formation of hole–electron pairs and their final recombination in semiconductors [24,31]. In particular, in TiO_2:Ag, there is a surface modification attributed to the misalignment between the TiO_2 and metallic Ag phases. X-rays interact with several planes of the material, and, consequently, the diffraction pattern is typical of bulk analysis, resulting from various diffraction planes. In the case of our as-prepared sample, TiO_2 recovered by metallic Ag, long-range analysis detected modifications identified by metallic Ag peaks on the TiO_2 surface.

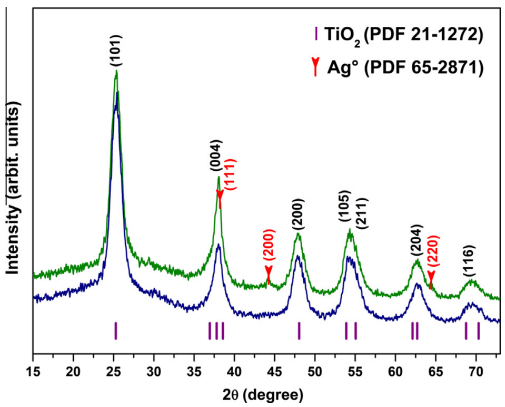


Fig. 1. X-ray diffraction patterns of TiO_2 (anatase phase; PDF number 21-1272) and TiO_2:Ag.

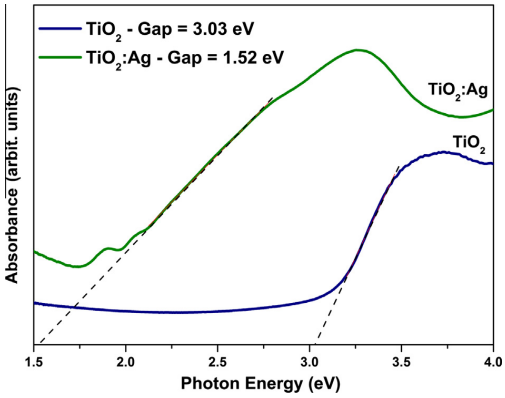


Fig. 2. UV–visible absorption spectra for TiO_2 and TiO_2:Ag samples.

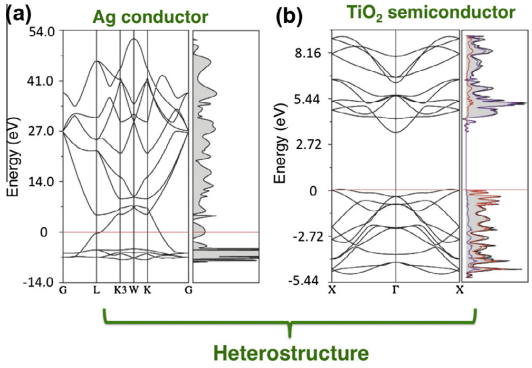


Fig. 3. Band structure and projected density of states. (a) Ag and (b) TiO_2; the TiO_2:Ag heterostructure.

The experimental spectral dependence of absorbance of the sample prepared by the co-precipitation method and HTMW is depicted in Fig. 2.

The optical energy band gap is related to absorbance and photon energy through the following equation, previously described by Wood and Tauc [32]:

$$h\upsilon\alpha \propto (h\upsilon - E_g^{opt})^2$$

where α is the absorbance, h is the Planck constant, v is the frequency, and E_g^{opt} denotes the optical band gap.

The optical band gap values for TiO_2 and TiO_2:Ag samples were 3.03 and 1.52 eV, respectively. The exponential optical absorption edge, and hence the optical band gap, is controlled by the degree of structural order/disorder of the TiO_2 or TiO_2:Ag lattice, interface, and surface.

The decrease in the band gap can be directly related to the increase in defects in the TiO_2 lattice. In this study, the modification of the TiO_2 lattice induced by Ag recovery raised the intermediary levels within the band-gap region, thus reducing the measured optical band gap. Increased disorder is linked to deep defects within the band gap and increased order is associated with shallow defects that readily disappear if total order is achieved.

The tail of the absorbance spectrum trace observed for TiO_2:Ag samples indicates the presence of several new states; hence, localized electronic levels in the forbidden band gap are probably introduced by the presence of metallic Ag [33]. The drastic reduction in the band gap of TiO_2:Ag could occur by virtue of a plasmonic effect of Ag on the surface, the presence of this new structure on the surface creating new localized levels in the band gap, or, most probably, both. In plasmonics, metal nanostructures can serve as antennae to convert light into localized electric fields or as waveguides to route light to desired locations with nanometer precision [34]. With a tight control over the nanostructures in terms of size and shape, light can be effectively manipulated and controlled with unprecedented accuracy [35]. Of all metals, Ag has played the most important role in the development of plasmonics, and its unique properties make it well suited for most next-generation plasmonic technologies. The plasmonic surface is unique, in that it can use nanostructures of different sizes (from tens to hundreds of nanometers), thus bridging the gap between the micrometer and nanometer levels.

These results indicate that the heterostructure formed with TiO_2 and Ag increased the formation of deep states in the band gap, leading to electron sharing between TiO_2 and Ag (semiconductor/metal). Theoretical models are very useful in rendering an interesting perception of the effects of diverse structural modifications to the electronic structure, and consequently the band gap, of a material. This is useful in the present case for improved understanding of the overall process.

Fig. 3 depicts the band structure and projected DOS of TiO_2 and Ag; we can observe how the electronic structures of TiO_2 and of Ag are aligned, and observe the atomic-level interaction between TiO_2 and Ag in the heterostructure. This is a useful way to represent interfaces and was previously used by our group to model the bulk/surface structure of TiO_2 [24] and a Ag_2WO_4:Ag heterostructure [25].

The calculated indirect band gap, between the X-point in the valence band and the Γ-point in the conduction band (CB) of the irreducible Brillouin zone, for the anatase phase was 3.51 eV. As expected, the band structure of the Ag phase had a characteristic metallic profile. The TiO_2 and Ag phases each showed a local far-field interaction in their band gap, which probably facilitated hybridization between the TiO_2 and metallic Ag band gaps, and resulted in a total reduction of 1.51 eV for the experimentally measured total band gap.

The FEG-SEM micrograph shows that TiO_2:Ag structures have an apparent homogenous and spherical morphology (Fig. 4a and b), with an agglomerate and polydisperse nature.

As can be seen in Fig. 4, the random aggregation process between the small spherical TiO_2:Ag nanoparticles resulted in a shapeless grain morphology. The HTMW route for synthesizing nanoparticles, the focus of a rapidly developing area of research, has been shown to be efficient in the processing of several complex oxides [36]. Bilecka and Niederberger [37] have published an overview of microwave-assisted liquid-phase routes for the preparation of inorganic nanomaterials. When synthesizing nanoparticles from a solution (or a gas phase), the growth of an individual nanostructure following the nucleation process occurs by two primary mechanisms: aggregation and coarsening. Crystal growth by aggregation may occur via a range of mechanisms, including interaction between randomly oriented particles (coalescence) or highly oriented particles (oriented attachment). Coalescence is defined as aggregation of two nanoparticles of roughly equal size, with no molecular exchange between them [38]. The oriented attachment mechanism is based on the assumption that nanoparticles dispersed in a liquid medium possess a very high degree of freedom for rotational and translational motion, when coalescence does not take place; in fact, crystal growth occurs by means of oriented collisions/rotation and is called non-classical crystallization [39]. In the present study, the morphology of the TiO_2:Ag nanopar-

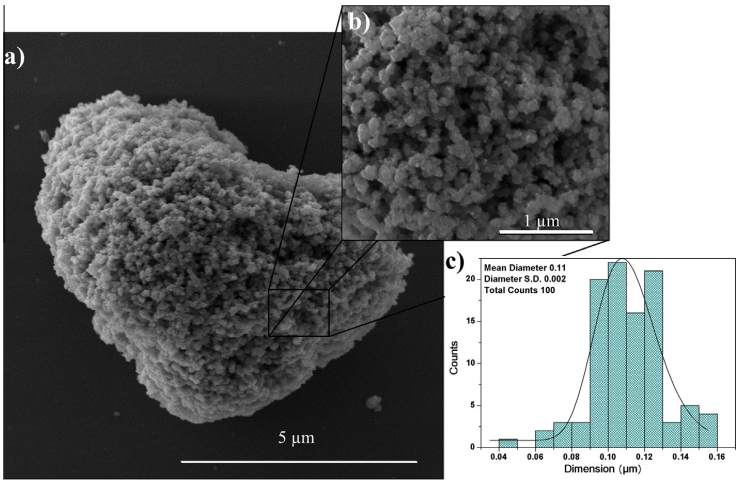


Fig. 4. (a) FEG-SEM micrograph of TiO_2:Ag nanoparticles; (b) magnified view of the FEG-SEM micrograph; (c) size-distribution histogram indicating the mean sizes for a total of 100 nanoparticles.

ticle seems to result from the aggregation mechanism. The facility and low-temperature requirements for the synthesis of TiO_2:Ag nanoparticles were attributed to the rapid rate of the reaction and direct microwave coupling with a water rotational barrier, which allowed uniform heating of the solution at start-up [40]. Compared with the usual methods, HTMW has the advantages of shortening the reaction time and producing products with a small particle size, narrow particle-size distribution, and high purity. However, the exact nature of the interaction of microwaves with reactants during particle synthesis is somewhat unclear and speculative, although the interaction of dielectric materials, liquids, or solids, with microwaves leads to a phenomenon commonly known as dielectric heating. However, its aforementioned characteristics qualify HTMW as a typical bottom-up process. The average nanocrystal particle-size distribution was estimated from FEG-SEM micrographs by analysis of 100 particles with a mean diameter of 112 nm (Fig. 2c), using the ImageJ software [41].

HRTEM micrographic analysis (Fig. 5) showed spherical nanoparticles homogeneously distributed on the TiO_2 surface. These nanoparticles, with diameters of <10 nm, were identified as metallic Ag with an interplanar distance of 2.37 Å, which corresponded to the (1 1 1) plane of Ag, according to the XRD pattern (PDF 65-2871; see Fig. 3). This result confirms the presence of Ag on the TiO_2 surface, showing the impregnation of TiO_2 with metallic Ag to form a heterostructure. Observation of the HRTEM image (Fig. 5, inset) confirms that the TiO_2:Ag nanoparticles were formed by interactions between randomly oriented TiO_2 and Ag particles, namely, coalescence (see Fig. 6).

The short-range order of TiO_2 and TiO_2:Ag samples was investigated by FT-Raman analysis. All Raman modes observed for the TiO_2 sample were attributed to the anatase phase, with peaks centered at 149, 200, 402, 518, and 642 cm^{-1} being related to the five Raman-active modes with the symmetries $E_{g(1)}$, $E_{g(2)}$, $B_{1g(3)}$, $A_{1g(4)}$, and $E_{g(3)}$, respectively [24,42]. As recently reported from theoretical calculations, 518 cm^{-1} corresponds to a B_{1g} Raman-active mode [21].

The TiO_2:Ag Raman spectra showed a shift in the frequency of Raman-active modes that can be attributed to the local disorder

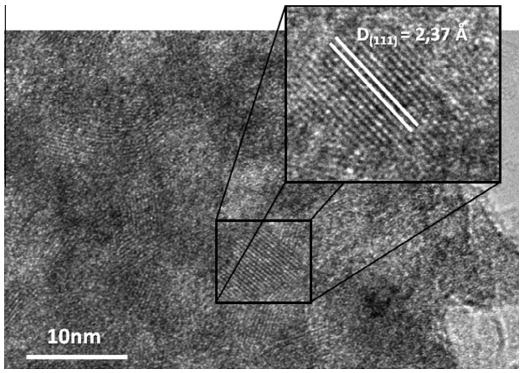


Fig. 5. High-resolution transmission electron microscopy image of a TiO_2 nanosphere with Ag impregnation. The interplanar distance of 2.37 Å corresponds to the (1 1 1) plane of Ag (inset).

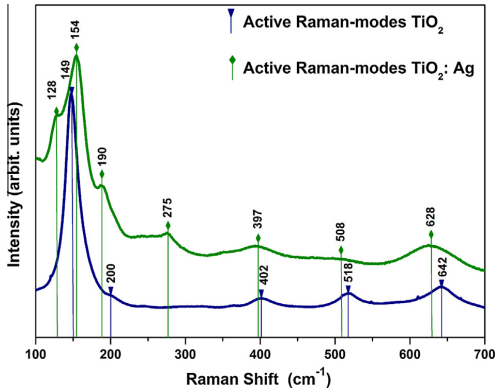


Fig. 6. Fourier transform-Raman spectra for TiO_2 and TiO_2:Ag, as recorded at room temperature.

caused by the addition of Ag on the surface of TiO_2. In addition, the TiO_2:Ag sample presented two uncharacteristic anatase Raman-active modes at 128 and 275 cm^{-1}. These Raman modes are very close to those presented by the brookite phase of TiO_2 [43,44]. The appearance of the latter phase could be due to a compressive stress on the first few layers of TiO_2 molecules that packs the surface atoms closely because of the presence of Ag on the surface. This compressive force could be responsible for an induced phase-transformation from the anatase to brookite phase of TiO_2. The long-range XRD analysis of TiO_2:Ag did not detect the brookite phase of TiO_2, probably because of its low content.

Additional evidence of a compressive force at the TiO_2:Ag heterostructure surface is the $E_{g(1)}$ (154 cm^{-1}) and $E_{g(2)}$ (190 cm^{-1}) inelastic modes that demonstrate a blue shift and red shift, respectively, when compared with the TiO_2 sample. A pressure effect induced by the surrounding particles and interface stress in lead titanate ($PbTiO_3$) nanocrystals was successfully used to induce a frequency shift of the soft mode at 89 cm^{-1} [45,46]. Saviot et al. [46] reported experimental and theoretical results showing that $E_{g(1)}$ and $E_{g(2)}$ frequencies for bulk anatase under hydrostatic pressure cannot be degenerate, and an anti-crossing pattern must exist. In other words, when the anatase phase was submitted to a pressure of <7 GPa, the intensity of the $E_{g(1)}$ frequency showed a blue shift, and that of $E_{g(2)}$ a red shift. This anti-crossing behavior is rather well reproduced in the calculations reported by Albuquerque et al. [19].

The MIC values obtained for TiO_2:Ag against the planktonic strains of *C. albicans*, *C. glabrata*, and *C. tropicalis* were 62.5, 15.0, and 31.25 mg L^{-1}, respectively, showing that *C. glabrata* was the most susceptible species, while *C. albicans* was the most resistant. Other studies also found that the MIC values for both Ag and gold nanoparticles differed for different *Candida* spp., as well as between clinical isolates and reference strains [47,48]. Despite different levels of susceptibility, TiO_2:Ag nanoparticles were able to inhibit the growth of three *Candida* spp. In a previous study, microbiological tests showed that the exposure of *C. albicans* to anatase TiO_2 nanoparticles did not completely inhibit its growth (only a 30% reduction was reported) [24]; these findings confirm one of the advantages of using TiO_2 and Ag in association. Additionally, at concentrations of >250 mg L^{-1} TiO_2:Ag, the $\log_{10}$(CFU mL^{-1}) value was zero for *C. glabrata* (MFC = 250 mg L^{-1}), indicating that the TiO_2:Ag nanoparticles were able to kill *C. glabrata* planktonic cells. Although no MFC value was obtained for the other two *Candida* spp., there were significant reductions in the $\log_{10}$(CFU/mL) values for *C. albicans* and *C. tropicalis* treated with TiO_2:Ag at concentrations of >125 and 31.25 mg L^{-1}, respectively (Fig. 7). Although the MIC values of Ag nanoparticles obtained in other studies [49,50] were lower than those obtained in the present study, it is important to highlight that a hybrid nanomaterial was used in this case. Another study also evaluated a hybrid nanomaterial, Ag-decorated hydroxyapatite (HA@Ag), and reported MIC and MFC values of 62.5 and 250 mg L^{-1}, respectively, for *C. albicans*, similar to the values obtained in the present study [16]. Combining nanoparticles reduces the concentration of each individual nanoparticle. Therefore, during Ag impregnation of TiO_2 in the present study, 7×10^{-5} mol $AgNO_3$ could achieve an Ag/Ti ratio of 0.06 in the resultant TiO_2:Ag. Reduced concentration of Ag is of interest, as it may decrease both the cost of manufacturing and the cytotoxicity to host cells, in addition to preventing microbial resistance.

Antimicrobial tests using planktonic MRSA cells yielded MIC and MBC values of 500 and 1000 mg L^{-1} TiO_2:Ag, respectively, indicating bacteriostatic and bactericidal effects. These results are partly in agreement with those reported by Kowal et al. [51], who obtained MICs for MRSA cells, but not for *C. albicans*, when amorphous states of Ag-doped Ti were used without UV irradiation. However, inhibition of cell growth was not observed when non-irradiated Ag-doped crystalline anatase was evaluated. This was attributed to an increase in the size of the Ag particles and their reduced content at the crystal surface. The size and shape of nanoparticles, the nature of support materials, and the components of nanocomposites may influence the antimicrobial activity of nanomaterials. Smaller particles can interact more efficiently with the bacterial surface and penetrate into the cell [52]. Potara et al. [9] suggested that an increased uptake rate of smaller particles could also increase the intracellular release of Ag ions, which might add to the antimicrobial effect. In the present study, the size of the Ag nanoparticles decorating the TiO_2 surface was very small (<10 nm), which may have contributed to the antibacterial effect against the methicillin-resistant strain of *S. aureus*.

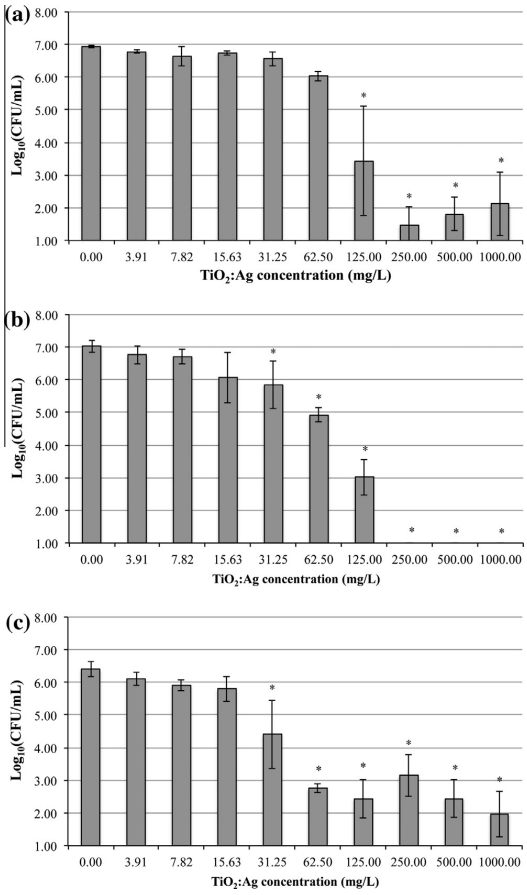


Fig. 7. Mean values of $\log_{10}$(CFU mL^{-1}) of (a) *Candida albicans*, (b) *C. glabrata*, and (c) *C. tropicalis*) planktonic cells after incubation with serial two-fold dilutions of TiO_2:Ag (μg mL^{-1}) in RPMI-1640 medium. Error bars represent standard deviation. *: Significantly different from 0 (control), 15.62, 31.25, 62.5, 125, and 250 μg mL^{-1}.

When biofilms were cultivated, no MFCb was obtained for any of the *Candida* spp. studied, i.e., no concentration of TiO_2:Ag was found to completely inhibit the growth of *C. albicans*, *C. glabrata*, or *C. tropicalis*. Nonetheless, significant reductions, of 2.11, 1.54, and 1.64 $\log_{10}$(CFU mL^{-1}), were observed for treatment of *C. albicans*, *C. glabrata*, and *C. tropicalis* biofilms, respectively, with 1000 mg L^{-1} TiO_2:Ag (data not shown). Similarly, for MRSA, no MBCb was obtained for TiO_2:Ag, i.e., no concentration of TiO_2:Ag

was found to completely inhibit growth of MRSA biofilms. However, the mean $\log_{10}$(CFU mL^{-1}) values of MRSA biofilms obtained at 500 and 1000 mg L^{-1} TiO_2:Ag were significantly lower ($P < 0.05$) compared with those of the control culture, with reductions of 2.33 and 1.81 $\log_{10}$(CFU mL^{-1}), respectively (data not shown). As expected, the antimicrobial activity of the TiO_2:Ag nanoparticles against biofilm-forming cells was lower than that against planktonic cultures. This result is in agreement with that reported by Zamperini al. [16], who also observed that reduction of $\log_{10}$(CFU mL^{-1}) values of *C. albicans* biofilms was only achieved with HA@Ag at 1000 mg L^{-1}. Resistance to Ag nanoparticles exhibited by biofilm cells has been demonstrated in recent studies [23]. Even when Ag nanoparticles were combined with nystatin or chlorhexidine, only a synergic or additive effect was observed for biofilms of *C. albicans* and *C. glabrata*, without complete biofilm eradication by any Ag/drug combination. Among other factors, the presence of extracellular polymeric matrix among biofilm-forming cells probably impairs the diffusion of metal nanoparticles and, consequently, inhibits direct contact between them and the cells present in the deeper layers of the biofilm. Other factors that have been associated with the drug resistance exhibited by biofilm cells include lower growth rate, heterogeneity, gene expression related to drug resistance, and the presence of persistent cells [10].

Crystal violet staining also demonstrated a significant reduction ($P < 0.05$) in the total biomass (lower absorbance values) of *Candida* spp. and MRSA biofilms treated with 1,000 mg L^{-1} TiO_2:Ag. Reductions of 35.66%, 20.70%, and 19.51% for *C. albicans*, *C. glabrata*, and *C. tropicalis*, respectively, and 11.91% for MRSA, were observed (data not shown); these results are in agreement with those obtained from the viability assay (CFU mL^{-1}). Previous studies also demonstrated a reduction of the biofilm biomass of *Candida* spp. treated with HA@Ag [16] and Ag nanoparticles [10]. However, few studies have evaluated the antimicrobial effect of nanoparticles against MRSA biofilms. A recent investigation showed that treatment with Ag-conjugated, superparamagnetic iron oxide nanoparticles at a concentration of 1 mg mL^{-1} resulted in a 30% reduction of the MRSA biofilm biomass, as evaluated by crystal violet staining [53]. A decrease in biofilm biomass indicated that TiO_2:Ag nanoparticles can disrupt biofilms. This is an important finding, because when a biofilm is dispersed and cells become detached, the susceptibility of cells to antimicrobial agents is higher than that of cells within an intact biofilm.

To understand the role of the metal:oxide interaction, we analyzed the electronic structure and Fermi level of both Ag and TiO_2. Fig. 8 shows the comparative DOSs of Ag and TiO_2.

As shown in Fig. 8, Ag shows several electronic states in the region of the TiO_2 band gap. When Ag was used to decorate TiO_2, in the TiO_2:Ag heterostructure obtained in the present study, the metal may have filled some electronic bands of the semiconductor, decreasing the band gap of the system. As a result, the metal may inject electrons into the TiO_2, creating holes on the TiO_2 surface.

Fig. 9 shows the TIO_2:Ag heterostructure model, $[Ag]_4/TiO_{2-x}$ with the electronic spin density isosurface, located around the metal clusters. It is also showed the band structure and the projected DOS. In this case its clear that the intermediary levels are attributed for the absorbed $[Ag_4]$ cluster. It is expected that the number of ney levels in the gap increases with the cluster size. For nanostructured materials, discrete levels with high Fermi level and high strained clusters are more reactive than extended surfaces.

We can observe that this model are consistent with the previously one presented here noted by the similarity between the band structure and projected DOS. However in the first case the computational cust is smaller.

The TiO_2:Ag semiconductor–metal heterostructure is a good example of space-charge layers, band bending, and formation of a Schottky barrier, as shown in Fig. 10. Electrically neutral and isolated from each other, the metal and the semiconductor have different Fermi level positions. As seen with the heterostructure obtained in the present study, the metal has a higher Fermi level position than the semiconductor. When the two materials are electrically connected, electron migration from the semiconductor to the metal occurs until the two Fermi levels are aligned, as shown in Fig. 10. The electrical contact thus forms a space-charge layer. The surface of the metal acquires excess negative charge, while the semiconductor exhibits excess positive charge, because of the migration of an electron from the barrier region; the electronic bands of the semiconductor bend upward, toward its surface, and the space-charge layer is said to be depleted. The barrier formed at the metal:semiconductor interface is termed the Schottky barrier. The diagram in Fig. 10 illustrates an ideal metal:semiconductor contact, i.e., no surface states exist on the semiconductor. The Schottky barrier produced at the metal:semiconductor interface can serve as an efficient electron trap, preventing electron–hole recombination [54].

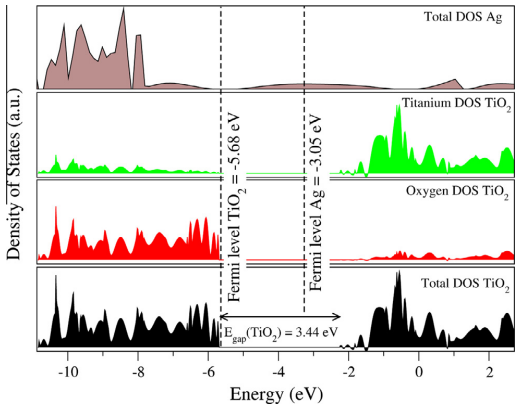


Fig. 8. Projected total density of states of TiO_2 and metallic Ag, and projected atomic states with regard to oxygen and titanium in TiO_2.

In nanoparticles, oxygen vacancies can function as a point defect and are present in three different charge states: neutral oxygen vacancy (V_O^x), singly occupied oxygen vacancy (V_O^x), and doubly occupied ($V_O^{\bullet\bullet}$) states. It can be inferred that increased disorder in the lattice is associated with the presence of $[TiO_5 \cdot V_O^x]$, $[TiO_5 \cdot V_O^{\bullet}]$, and $[TiO_5 \cdot V_O^{\bullet\bullet}]$ complex clusters, and that these complex defects are shallow and/or deeply inserted in the band gap [24].

Clusters of Ag nanoparticles exhibit collective oscillation of their electrons in the CB, which is known as localized surface plasmon resonance. The complex defects of TiO_2 allow interactions with the $[Ag_4]^x$ clusters of Ag nanoparticles, i.e., an association between the semiconductor and the metal plasmon [52]. The association between the semiconductor and metal changes the effectiveness and mechanism of antimicrobial activity of each.

In the model proposed here, the most important events occur at the interface of the plasmon and semiconductor. This involves an electron-transfer process at the metal:semiconductor interface, with the formation of superoxide, hydrogen ions (H^+), and/or OOH^* radicals by electron–hole reactions, which causes protein inactivation and eventual apoptosis [16]. Moreover, an effective charge separation exists between the TiO_2 bulk and surface, and the metal at the semiconductor surface is able to conduct these charges to the solution.

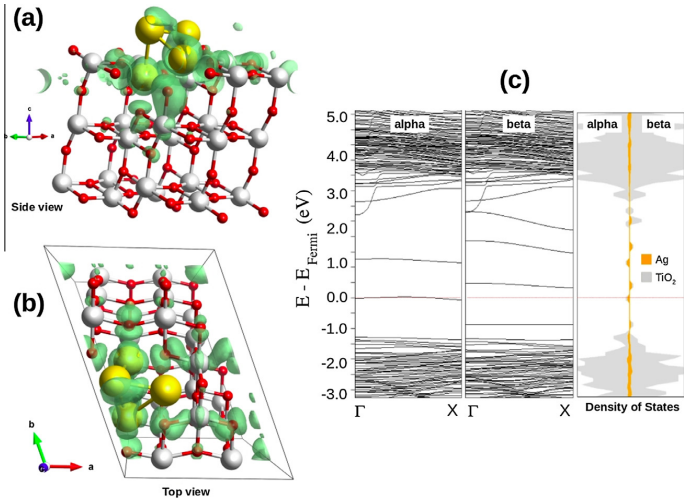


Fig. 9. (a) Side view, (b) top view of $[Ag_4]$ cluster adsorbed on reduced TiO_{2-x} (101) surface with the electronic spin density isosurface (green surface; isovalue 0.001 e/Å^3) at the topmost layers of the heterostructure around $[Ag_4]$ cluster, and (c) band structure and DOS shown the appearance of intermediary levels at the TiO_2 gap by the adsorbed silver atoms. The silver, titanium and oxygen atoms are shown in yellow, white and red, respectively. (For interpretation of the references to colour in this figure legend, the reader is referred to the web version of this article.)

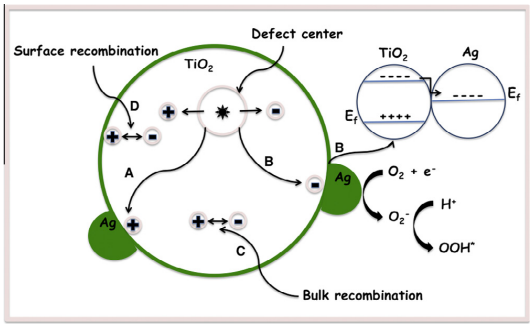


Fig. 10. Possible mechanisms in the heterostructure formed by TiO_2 and Ag nanoparticles. (a) Hole trap at the surface; (b) electron conduction by the Ag nanoparticle; (c) bulk recombination; (d) surface recombination.

Consequently, the effect of surface properties on the electron–hole reaction performance should be considered in terms of the following:

$$[TiO_6]^x + [TiO_5 \cdot V_O^x] \longrightarrow [TiO_6]' + [TiO_5 \cdot V_O^\bullet]$$

$$[TiO_6]' + [Ag]^x \longrightarrow [TiO_5 \cdot V_O^x] + [Ag]'$$

The reactivity of molecular oxygen with a complex $[Ag]'$ on the Ag surface results in a chemisorbed species and subsequent oxygen incorporation into the lattice:

$$[Ag_4]' + O_2 \longrightarrow [Ag_4]' \ldots O_{2(ads)}$$

$$[Ag_4]' \ldots O_{2(ads)} \longrightarrow [Ag_4]^x \ldots O'_{2_{(ads)}}$$

$$[Ag_4]^\bullet + O_2 \longrightarrow [Ag_4]^\bullet \ldots O_{2(ads)}$$

$$[Ag_4]^\bullet \ldots O_{2(ads)} + [TiO_6]' \longrightarrow [Ag_4]^\bullet \ldots O'_{2(ads)} + [TiO_6]^x$$

The clusters formed by the Ag complex also interact with H^+ and split into peroxide oxygen according to the following reaction:

$$[Ag_4]^x \ldots O'_{2(ads)} + H^+ \longrightarrow [OOH]^*$$

The HO_2^* radical may react with microbial cells, ultimately resulting in the oxidation of cellular components. Therefore, even with an agglomerate morphology, nanoparticles exhibit antimicrobial activity due to their physicochemical property of oxidation.

5. Conclusions

An Ag nanoparticle-coated TiO_2 heterostructure was synthesized using the safe, ecofriendly, and reproducible HTMW method. These nanoparticles exhibited physicochemical properties that conferred antimicrobial activity against planktonic and biofilm-forming cells of MRSA and *Candida* spp. Biofilm-forming strains showed increased tolerance compared to planktonic strains. To the best of our knowledge, this is the first report on the effect of TiO_2:Ag nanoparticles, produced via HTMW, on *Candida* spp. and MRSA biofilms. Moreover, the mechanism underlying the antimicrobial activity of TiO_2:Ag nanoparticles is suggested on the basis of theoretical calculations.

Conflict of interest

No conflict of interest.

Acknowledgments

The authors are grateful for the financial support provided by the Brazilian research-funding institutions CAPES, CNPq, and FAPESP under the Grants 2011/06786-0, 2011/06900-8, 2011/24004-0, and 2013/07296-2 (CEPID Program).

References

[1] A.Y. Zhang, M.H. Zhou, L. Han, Q.X. Zhou, J. Hazard. Mater. 186 (2011) 1374.
[2] C. Botta, J. Labille, M. Auffan, D. Borschneck, H. Miche, M. Cabie, A. Masion, J. Rose, J.Y. Bottero, Environ. Pollut. 159 (2011) 1543.

[3] H.J. Yun, H. Lee, J.B. Joo, N.D. Kim, J. Yi, J. Nanosci. Nanotechnol. 11 (2011) 1688.
[4] W.Q. Peng, M. Yanagida, L.Y. Han, S. Ahmed, Nanotechnology 22 (2011).
[5] W.S. Tung, W.A. Daoud, J. Mater. Chem. 21 (2011) 7858.
[6] A. Fujishima, K. Honda, Nature 238 (1972) 37.
[7] F. Haghighi, S.R. Mohammadi, P. Mohammadi, M. Eskandari, S. Hosseinkhani, Med. J. 113 (2012) 707.
[8] R.G. Nair, J.K. Roy, S.K. Samdarshi, A.K. Mukherjee, Colloid Surf. B Biointerfaces 86 (2011) 7.
[9] M. Potara, E. Jakab, A. Damert, O. Popescu, V. Canpean, S. Astilean, Nanotechnology 22 (2011).
[10] A. Bokare, A. Sanap, M. Pai, S. Sabharwal, A.A. Athawale, Colloid Surf. B Biointerfaces 102 (2013) 273.
[11] P.V. Sanita, A.C. Pavarina, E.T. Giampaolo, M.M. Silva, E.G. de Oliveira Mima, D.G. Ribeiro, C.E. Vergani, Oral Surg. Oral Med. Oral Pathol. Oral Radiol. Endodontol. 111 (2011) 726.
[12] V. Krcmery, A.J. Barnes, J. Hosp. Infect. 50 (2002) 243.
[13] I.M. Gould, M.Z. David, S. Esposito, J. Garau, G. Lina, T. Mazzei, G. Peters, Int. J. Antimicrob. Agents 39 (2012) 96.
[14] I. Perelshtein, G. Applerot, N. Perkas, J. Grinblat, A. Gedanken, Chem. Eur. J. 18 (2012) 4575.
[15] N. Hoiby, T. Bjarnsholt, M. Givskov, S. Molin, O. Ciofu, Int. J. Antimicrob. Agents 35 (2010) 322.
[16] C.A. Zamperini, R.S. Andre, V.M. Longo, E.G. Mima, C.E. Vergani, A.L. Machado, J.A. Varela, E. Longo, J. Nanomater. (2013).
[17] A.s.M.-A. National Committee for Clinical Laboratory Standards: Methods for Dilution Antimicrobial Susceptibility Tests for Bacteria That Grow Aerobically, NCCLS, seventh ed. (Ed.), Wayne, PA, USA, 2006.
[18] A.S. Clinical and Laboratory Standards Institute: Reference Method for Broth Dilution Antifungal Susceptibility Testing of Yeasts, CLSI Document M27-A3, third ed. (Ed.), Wayne, PA, 2008.
[19] A.R. Albuquerque, J. Maul, E. Longo, I.M.G. dos Santos, J.R. Sambrano, J. Phys. Chem. C 117 (2013) 7050.
[20] A.R. Albuquerque, I.M.G. Santos, J.R. Sambrano, Quim. Nova 37 (2014) 1318.
[21] A.D.R. Albuquerque, M.L. Garzim, I.M.G.D. Santos, V. Longo, E. Longo, J.R. Sambrano, J. Phys. Chem. A 116 (2012) 11731–11735.
[22] A.R. Albuquerque, A. Bruix, I.M.G. dos Santos, J.R. Sambrano, F. Illas, J. Phys. Chem. C 118 (2014) 9677.
[23] C.W. Raubach, Y.V.B. de Santana, M.M. Ferrer, V.M. Longo, J.A. Varela, W. Avansi, P.G.C. Buzolin, J.R. Sambrano, E. Longo, Chem. Phys. Lett. 536 (2012) 96.
[24] V.M. Longo, F.C. Picon, C. Zamperini, A.R. Albuquerque, J.R. Sambrano, C.E. Vergani, A.L. Machado, J. Andres, A.C. Hernandes, J.A. Varela, E. Longo, Chem. Phys. Lett. 577 (2013) 114.
[25] V.M. Longo, C.C. De Foggi, M.M. Ferrer, A.F. Gouveia, R.S. Andre, W. Avansi, C.E. Vergani, A.L. Machado, J. Andres, L.S. Cavalcante, A.C. Hernandes, E. Longo, J. Phys. Chem. A 118 (2014) 5769.
[26] R. Dovesi, V.R. Saunders, C. Roetti, R. Orlando, C.M. Zicovich-Wilson, F. Pascale, B. Civalleri, K. Doll, N.M. Harrison, I.J. Bush, P. D'Arco, M. Llunell, M. Causà, Y. Noël, CRYSTAL14 User's Manual, University of Torino, Torino, 2014.
[27] H.P. Hratchian, A.V. Krukau, P.V. Parandekar, M.J. Frisch, K. Raghavachari, J. Chem. Phys. 136 (2012).
[28] M.L. Moreira, E.C. Paris, Acta Mater. 57 (2009) 5174.
[29] M.L. Moreira, J. Andres, J.A. Varela, E. Longo, Cryst. Growth Des. 9 (2009) 833.
[30] V.M. Longo, L.S. Cavalcante, E.C. Paris, J.C. Sczancoski, P.S. Pizani, M.S. Li, J. Andres, E. Longo, J.A. Varela, J. Phys. Chem. C 115 (2011) 5207.
[31] M.L. Moreira, P.G.C. Buzolin, V.M. Longo, N.H. Nicoleti, J.R. Sambrano, M.S. Li, J.A. Varela, E. Longo, J. Phys. Chem. A 115 (2011) 4482.
[32] D.L. Wood, J. Tauc, Phys. Rev. B 5 (1972) 3144.
[33] V.M. Longo, L.S. Cavalcante, R. Erlo, V.R. Mastelaro, A.T. de Figueiredo, J.R. Sambrano, S. de Lazaro, A.Z. Freitas, L. Gomes, N.D. Vieira, J.A. Varela, E. Longo, Acta Mater. 56 (2008) 2191.
[34] M. Rycenga, C.M. Cobley, J. Zeng, W. Li, C.H. Moran, Q. Zhang, D. Qin, Y. Xia, Chem. Rev. 111 (2011) 3669.
[35] M.L. Brongersma, V.M. Shalaev, Science 328 (2010) 440.
[36] D.P. Volanti, D. Keyson, L.S. Cavalcante, A.Z. Simoes, M.R. Joya, E. Longo, J.A. Varela, P.S. Pizani, A.G. Souza, J. Alloys Compd. 459 (2008) 537.
[37] I. Bilecka, M. Niederberger, Nanoscale 2 (2010) 1358.
[38] M. Jose-Yacaman, C. Gutierrez-Wing, M. Miki, D.Q. Yang, K.N. Piyakis, E. Sacher, J. Phys. Chem. B 109 (2005) 9703.
[39] H.C. Zeng, Int. J. Nanotechnol. 4 (2007) 329.
[40] G.J. Wilson, A.S. Matijasevich, D.R.G. Mitchell, J.C. Schulz, G.D. Will, Langmuir 22 (2006) 2016.
[41] <http://rsbweb.nih.gov/ij/>.
[42] K.M. Rahulan, N. Padmanathan, L.D. Stephen, C.C. Kanakam, J. Alloys Compd. 554 (2013) 432.
[43] M.N. Iliev, V.G. Hadjiev, A.P. Litvinchuk, Vib. Spectrosc. 64 (2013) 148.
[44] G.A. Tompsett, G.A. Bowmaker, R.P. Cooney, J.B. Metson, K.A. Rodgers, J.M. Seakins, J. Raman Spectrosc. 26 (1995) 57.
[45] J.F. Meng, G.T. Zou, Q.L. Ciu, Y.N. Zhao, Z.Q. Zhu, J. Phys. Condens. Matter 6 (1994) 6543.
[46] L. Saviot, D. Machon, L. Debbichi, A. Girard, J. Margueritat, P. Krueger, M.C.M. de Lucas, A. Mermet, J. Phys. Chem. C 118 (2014) 10495.
[47] A. Jebali, F.H.E. Hajjar, F. Pourdanesh, S. Hekmatimoghaddam, B. Kazemi, A. Masoudi, K. Daliri, N. Sedighi, Med. Mycol. 52 (2014) 65.
[48] K.-J. Kim, W.S. Sung, S.-K. Moon, J.-S. Choi, J.G. Kim, D.G. Lee, J. Microbiol. Biotechnol. 18 (2008) 1482.
[49] D.R. Monteiro, S. Silva, M. Negri, L.F. Gorup, E.R. de Camargo, R. Oliveira, D.B. Barbosa, M. Henriques, Mycoses 56 (2013) 672.
[50] A. Panacek, L. Kvitek, R. Prucek, M. Kolar, R. Vecerova, N. Pizurova, V.K. Sharma, T. Nevecna, R. Zboril, J. Phys. Chem. B 110 (2006) 16248.
[51] K. Kowal, K. Wysocka-Krol, M. Kopaczynska, E. Dworniczek, R. Franiczek, M. Wawrzynska, M. Vargova, M. Zahoran, E. Rakovsky, P. Kus, G. Plesch, A. Plecenik, F. Laffir, S.A.M. Tofail, H. Podbielska, J. Colloid Interface Sci. 362 (2011) 50.
[52] J.R. Morones, J.L. Elechiguerra, A. Camacho, K. Holt, J.B. Kouri, J.T. Ramirez, M.J. Yacaman, Nanotechnology 16 (2005) 2346.
[53] N.G. Durmus, T.J. Webster, Adv. Healthcare Mater. 2 (2013) 165.
[54] A.L. Linsebigler, G.Q. Lu, J.T. Yates, Chem. Rev. 95 (1995) 735.

3.2 Publicação 2·

PLOS ONE

RESEARCH ARTICLE

Encapsulation of curcumin in polymeric nanoparticles for antimicrobial Photodynamic Therapy

Jeffersson Krishan Trigo Gutierrez, Gabriela Cristina Zanatta, Ana Laura Mira Ortega, Maria Isabella Cuba Balastegui, Paula Volpato Sanitá, Ana Cláudia Pavarina, Paula Aboud Barbugli, Ewerton Garcia de Oliveira Mima*

Department of Dental Materials and Prosthodontics, School of Dentistry, Araraquara, São Paulo State University (UNESP), Araraquara, São Paulo, Brazil

* ewertonmima@foar.unesp.br

Check for updates

OPEN ACCESS

Citation: Trigo Gutierrez JK, Zanatta GC, Ortega ALM, Balastegui MIC, Sanitá PV, Pavarina AC, et al. (2017) Encapsulation of curcumin in polymeric nanoparticles for antimicrobial Photodynamic Therapy. PLoS ONE 12(11): e0187418. https://doi.org/10.1371/journal.pone.0187418

Editor: Michael Hamblin, Massachusetts General Hospital, UNITED STATES

Received: July 17, 2017

Accepted: October 19, 2017

Published: November 6, 2017

Copyright: © 2017 Trigo Gutierrez et al. This is an open access article distributed under the terms of the Creative Commons Attribution License, which permits unrestricted use, distribution, and reproduction in any medium, provided the original author and source are credited.

Data Availability Statement: All relevant data are within the paper.

Funding: This study was supported by São Paulo Research Foundation (FAPESP): grant numbers 2013/23165-5 (EGOM), 2014/18345-7 (ALMO), 2014/20119-5 (EGOM), www.fapesp.br; São Paulo Research Foundation (FAPESP, RIDC, CEPOF): grant number 2013/07276-1 (ACP), http://cepid.fapesp.br/en/centro/17/; National Counsel of Technological and Scientific Development: grant number 446401/2014-5 (EGOM), www.cnpq.br;

Abstract

Curcumin (CUR) has been used as photosensitizer in antimicrobial Photodynamic Therapy (aPDT). However its poor water solubility, instability, and scarce bioavalibility hinder its in vivo application. The aim of this study was to synthesize curcumin in polymeric nanoparticles (NP) and to evaluate their antimicrobial photodynamic effect and cytoxicity. CUR in anionic and cationic NP was synthesized using polylactic acid and dextran sulfate by the nanoprecipitation method. For cationic NP, cetyltrimethylammonium bromide was added. CUR-NP were characterized by physicochemical properties, photodegradation, encapsulation efficiency and release of curcumin from nanoparticles. CUR-NP was compared with free CUR in 10% dimethyl sulfoxide (DMSO) as a photosensitizer for aPDT against planktonic and biofilms (mono-, dual- and triple-species) cultures of *Streptococcus mutans*, *Candida albicans* and Methicillin-Resistant *Staphylococcus aureus*. The cytotoxicity effect of formulations was evaluated on keratinocytes. Data were analysed by parametric (ANOVA) and non-parametric (Kruskal-Wallis) tests ($\alpha = 0.05$). CUR-NP showed alteration in the physicochemical properties along time, photodegradation similar to free curcumin, encapsulation efficiency up to 67%, and 96% of release after 48h. After aPDT planktonic cultures showed reductions from 0.78 $\log_{10}$ to complete eradication, while biofilms showed no antimicrobial effect or reductions up to 4.44 $\log_{10}$. Anionic CUR-NP showed reduced photoinactivation of biofilms. Cationic CUR-NP showed microbicidal effect even in absence of light. Anionic formulations showed no cytotoxic effect compared with free CUR and cationic CUR-NP and NP. The synthesized formulations improved the water solubility of CUR, showed higher antimicrobial photodynamic effect for planktonic cultures than for biofilms, and the encapsulation of CUR in anionic NP reduced the cytotoxicity of 10% DMSO used for free CUR.

· Artigo nas normas do periódico *PLos One*.

Coordination for the Improvement of Higher Education Personnel (CAPES) (JKTG), www.capes.gov.br; Program of Scientific Initiation: 30641, 34828 (MICB), 30288, and 34848 (GCZ), http://prope.unesp.br/pibic/; PROINTER PROPe/PROPG 03/2017, grant 1732 (EGOM), www.unesp.br/prope.

Competing interests: The authors declare a competing financial interest, a patent deposited on National Institute for Industrial Property-INPI in Brazil on July 4, 2016, process number BR 10 2016 015631 9, entitled "Processo de Obtenção de Nanopartículas Poliméricas Aniônicas e Catiônicas de Curcumina, Nanopartículas Obtidas e Seus Usos". This does not alter our adherence to PLOS ONE policies on sharing data and materials. There is no other competing interest.

Introduction

Oral microbiota involves a wide range of species, including bacteria and fungi coexisting with each other in polymicrobial biofilms. Often, these microorganisms are inoffensive inhabitants of the oral cavity, but they can be infective pathogens and promote infections when an imbalance of the local or systemic homeostasis occurs. Among these species, *Streptococcus mutans* is the main etiological factor of dental caries due to its capacity to produce organic acids from dietary sugars (acidogenicity), especially sucrose, and to survive in low pH environment (aciduricity). Additionally, *S. mutans* may also be associated with severe systemic infections, such as acute endocarditis [1].

Other important microorganisms that should be highlighted are the fungi of the *Candida* genus, particularly *Candida albicans*, the most prevalent and virulent species [2]. This opportunistic pathogen is able to alter its morphology from yeast (blastopore) to filamentous forms (hyphal and pseudohyphal invasive forms), a process called polymorphism. The infection caused by *C. albicans*, called candidiasis, is one of the most common oral infections, especially in immunocompromised patients, affecting 90% of HIV-positive patients [3]. In more severe cases, the infection may spread to the blood stream and cause systemic infection, known as candidemia, whose mortality rate is high, varying between 40 and 60%, especially in patients in intensive care units [4].

Another pathogen that has been receiving great attention is Methicillin-Resistant *Staphylococcus aureus* (MRSA), responsible for high mortality rates in critically ill patients. MRSA is frequently found in long-stay hospital patients and an increasing trend in a community setting has also been reported [5]. Although MRSA is not considered part of the oral microbiota, it is able to co-exist with *C. albicans* in biofilms without antagonism and with bacteria cells preferentially associated to *C. albicans* hyphal invasive forms [6]. Similarly, *C. albicans* and *S. mutans* are also able to form mixed biofilms, beneficially affecting the growth of both microorganisms [7]. Thus, in addition to the fact that the three above-mentioned microorganisms are able to cause a relevant number of infections independently, they can also be commonly associated as co-infector microorganisms.

The widespread use of conventional antimicrobials (antibiotics and antifungals) has emerged the problem of microbial resistance [2,5], which results in persistence of infection, treatment failure, and side-effects of drugs especially when multiple antimicrobials are used. Due to these shortcomings of the currently available drug treatments, antimicrobial alternatives have been sought. A promising therapeutic modality for microbial inactivation is antimicrobial Photodynamic Therapy (aPDT), which uses the association of a photosensitizing agent (PS) [e.g., curcumin (CUR)] with a light at a suitable wavelength. The interaction between PS and light in the presence of oxygen results in the production of a reactive species, mainly the singlet oxygen and free radicals that promote cell damage and death [8,9].

Curcumin (diferuloymethane) is a polyphenol having a low molecular weight compound isolated from *Curcuma longa* L. It has been demonstrated that CUR presents antimicrobial effects [10] and recent studies have proved that the antifungal effect is potentiated when CUR is associated with blue light [11–13]. However, CUR is not water soluble, it has a limited bioavailability and instability, reasons that hinder its clinical applicability. An alternative in order to improve the properties of CUR is to encapsulate it in drug delivery systems, such as nanoparticles, nanoemulsions, and ciclodextrins [14]. Polylactic acid (PLA) is a natural, stable, biodegradable, and biocompatible polyester polymer used to encapsulate hydrophobic drugs [15].

Previous studies have encapsulated CUR in nanoformulations for antimicrobial purposes [16–20]. Hegge et al. [16] solubilized CUR in polyethylene glycol 400, Pluronic F127, and hydroxypropyl-γ-cyclodextrin and found the survival of *Staphylococcus epidermidis* biofilms to

be between 13% and 29% after aPDT without significant differences between the solubilizing agents. CUR encapsulated in chitosan and polyethylene glycol had several effects in the absence of light: they inhibited the planktonic growth of MRSA and *Pseudomonas aeruginosa*, they caused a significant reduction in the number of both bacterial colonies, they reduced the amount of MRSA present in skin burns of mice, and they accelerated the healing process [17]. Using this same CUR encapsulation system at a concentration of 10 μg/mL, a complete elimination of the planktonic culture of the dermatophyte fungi *Trichophyton rubrum* was observed after the application of blue light at 10 J/cm^2 [18]. The combination of silver nanoparticles (NP) with CUR in polymeric micelles inhibited the biofilm formation and reduced the biomass of *P. aeruginosa* and *S. aureus* [19]. Inhibition of biofilm formation was also observed when *S. mutans* was grown with CUR in chitosan, alginate, and starch [20]. Although these studies have evaluated the antimicrobial effect of CUR in nanoformulations, most investigations evaluated their antimicrobial effect in absence of light [17,19,20]. Moreover, few studies that evaluated the antimicrobial photodynamic effect of CUR are restricted to non-oral species [16,18].

Therefore, the purpose of the current study was to synthesize and characterize CUR-loaded into polymeric NP and to evaluate its cytotoxicity and photodynamic effects compared with free CUR as PSs against planktonic cultures and biofilms of oral species (*S. mutans* and *C. albicans*) and MRSA. The scientific hypothesis of this research was: water solubility and cytotoxity of CUR are improved with encapsulation in NP, whose antimicrobial effect is similar or higher than free CUR. Thus, the statistic hypothesis were: null hypothesis (H0)—CUR-NP does not improve water solubility, cytotoxicity and the antimicrobial photodynamic effect of CUR; alternative hypothesis (H1)—CUR-NP improves water solubity, cytotoxicity and the antimicrobial photodynamic effect of CUR. The synthesized formulations demonstrated solubility in water, and higher antimicrobial photodynamic effect for planktonic cultures compared with biofilms, and anionic CUR-NP showed no cytotoxicity compared with free CUR and cationic CUR-NP.

Materials and methods

CUR (purity $\geq$ 65%), dextran sulfate (DEX), cetyltrimethylammonium bromide (CTAB) and bacitracin were purchased from Sigma Aldrich (St Louis, MO, USA). Dimethyl sulfoxide (DMSO), acetone PA/ACS, NaCl, sucrose were purchased from Labsynth *Produtos para Laboratório*, Ltda (Diadema, SP, Brazil). Brain Heart Infusion (BHI) was purchased from HiMedia Laboratories (Mumbai, India). Yeast Nitrogen Broth (YNB), Mitis Salivarius Agar (MSB), Mannitol Salt Agar (MSA) were purchased from Difco (Detroit, MI, USA). Tryptic Soy Broth (TSB), Sabouraud Dextrose Agar with 5 mg/mL of chloramphenicol (SDA) were purchased from Acumedia Manufactures Inc (Lansing, Michigan, USA).

Photosensitizer and light source

Free CUR was used as a PS in ratio 9:1 of sterile distilled water: DMSO [11].

A Light Emitting Diodes (LED, LXHL- PR09, Luxeon® III Emitter, Lumileds Lighting, San Jose, CA, USA) device having a wavelength from 440 nm to 460 nm (peak at 455 nm) and a light intensity of 33.58 mW/cm^2 was designed by Physics Institute of São Carlos (University of São Paulo) and used as a light source for photodegradation and aPDT experiments.

Encapsulation of CUR in polymeric nanoparticle (CUR-NP)

CUR-NP were synthesized using a nanoprecipitation method [21]. CUR stock solution at 4 mg/mL was prepared in acetone. For CUR encapsulation in NP, the aqueous phase containing

DEX 1% in sterile ultrapure water was dropped into polymer/organic phase (PLA 0.5% in acetone) under moderate magnetic stirring. After 10 minutes of magnetic stirring, the solution was left resting at room temperature for 24 hours to completely evaporate the solvent (acetone). The resultant formulation had a negative (anionic) charge and maximum CUR concentration of 260 μM. PLA was kindly provided by Professor Valtencir Zucolotto from University of São Paulo.

To synthesize cationic (positive charge) CUR-NP, CTAB [22] 2% in sterile ultrapure water with NaCl 1.76% was added as surfactant after completely evaporating the solvent. Anionic and cationic NP without CUR were also synthesized as described above but without the CUR solution in the organic phase. This process was subjected to a patent deposited on National Institute for Industrial Property-INPI (process number BR 10 2016 015631 9).

Characterization of CUR-NP

Physicochemical characterization. After encapsulation of CUR-NP, the samples were diluited in sterile ultrapure water (10 μL/mL) and characterized by Dynamic Light Scattering (DLS). The properties of average particle size, polydispersity index (PDI), and zeta potential were determined at 25˚C in a Zetasizer Nano ZS (Malvern Instruments Ltd, Malvern, UK) in the absence of light. These properties of the formulations were evaluated for up to 40 days after the synthesis to determine the formulation stability.

Nanoparticles analysis by Field Emission Gun Scanning Electron Microscopy (FEG-SEM). The CUR-NP diluted in sterile ultrapure water (1:50) were dropped on silicon conductive paper, which was placed in stub conductors. Samples were dried in a Sputter Coater apparatus (BAL-TEC SCD 050, Bridgend, UK) and observed in a FEG-SEM (JEOL model 7500F, Peabody, MA, USA) from the Institute of Chemistry, Araraquara, São Paulo State University (UNESP), Araraquara, SP, Brazil.

Absorption spectrum and photostability. Absorption spectrum of free CUR and both anionic and cationic CUR-NP at the concentration of 130 μM was determined in a UV-visible spectrophotometer (SQ 4802 UV-Visible Double Beam Spectrophotometer UNICO, United Products & Instruments Inc, Dayton, NJ, USA) at wavelengths range of 200–700 nm.

For the photodegradation test, free CUR and both anionic and cationic CUR-NP at 130 μM were illuminated by the LED device (see "Photosensitizer and light source" above) for four different times (5, 10, 15 and 20 minutes, corresponding to 10.8, 21.6, 32.4 and 43.2 J/cm^2, respectively), and then the absorbances of the samples were read from the spectrophotometer as described above. The photostability of both CUR-NPs was compared with the free CUR.

Encapsulation efficiency (EE). For the EE, samples of both CUR-NP at 52 μM were centrifuged at 6,000 x*g* for 10 minutes. The pellet (nanoparticles) was resuspended in ultrapure water and the absorbance of the samples was determined before (B) and after (A) centrifugation. Absorbance was determined in a UV-visible spectrophotometer at wavelengths that showed maximum absorbance for each sample [23]. The EE was calculated using the formula: EE% = A x 100/B.

Curcumin release from nanoparticles. The release test was carried out according to the technique proposed by Krausz et al. [17] with some modifications. Samples of both anionic and cationic CUR-NP were diluted in phosphate buffer saline (PBS- NaCl = 0.136 M; KH_2PO_4 = 1 mM; KCl = 2 mM; Na_2HPO_4 = 10 mM; pH 7.4) at a concentration of 52 μM and incubated at 37˚C at 100 rpm. At interval of 2 hours, samples were centrifuged at 6,000 x*g* for 10 minutes to separate the nanoparticles from the solution, and then the nanoparticles (pellet) were diluted in acetone to solubilize the unreleased CUR, whose absorbance was determined by a

UV-visible spectrophotometer. The total released CUR was calculated by dividing the absorbance read at each time interval by the absorbance of the encapsulated CUR estimated as maximum.

Antimicrobial assays

aPDT against planktonic cultures of *S. mutans*, *C. albicans* and MRSA. Standard strains from the American Type Culture Collection (ATCC; Rockville, MD, USA) of *S. mutans* (UA159 ATCC 700610), *C. albicans* (ATCC 90028) and MRSA (ATCC 33591) were kept in -80˚C in BHI with 1% of sucrose, YNB, and TSB, respectively, with 50% glycerol. Each strain was thawed and one loopful of each microorganism was spread on its respective agar plate (MSB supplemented with 15% sucrose and 0.2 IU/mL of bacitracin for *S. mutans*, SDA for *C. albicans*, and MSA for MRSA). The agar plates were then incubated at 37˚C for 48 hours. All experiments with *S. mutans* were performed in a 5% CO_2 incubator (L212 Laboven, Qingdao, China). After incubation, 5–10 colonies were resuspended in BHI for *S. mutans*, YNB for *C. albicans*, and TSB for MRSA, and the plates were incubated at 37˚C for 16 hours. Aliquots of each suspension were diluted in each specific broth and incubated until optical density (OD) reached the mid-log phase of growth. The suspensions of each microorganism were standardized at OD of 0.613 arbitrary units (a.u.), 0.473 a.u. and 0.510 a.u. for *S. mutans*, *C. albicans* and MRSA, respectively, determinated in a spectrophotometer (Bioespectro SP 220 Equipar Ltda, Curitiba, PR, Brazil), equivalent to 10^7–10^8 CFU/mL for bacteria and 10^6–10^7 CFU/mL for yeast, respectively.

Since the aim of this study was to evaluate the photoinactivation of biofilms, the aPDT parameters used for planktonic cultures was the same as those used for the biofilms in order to verify whether the aPDT efficacy was due to biofilm organization or to cell susceptibility to the synthesized formulations. These parameters were previously established in a pilot study (non-published data), in which CUR concentrations, the pre-irradiation times, and the illumination times were progressively increased from previous investigations [11–13] until photoinactivation of the multispecies biofilm was achieved. For aPDT, aliquots of 100 μL of each microbial suspension were individually transferred to 96-well flat-bottom microtiter plates (TPP Techno Plastic Products, Trasadingen, Switzerland). In each well, additional aliquots of 100 μL of the PS (free CUR or anionic or cationic CUR-NP at 260 μM) were added to each microbial suspension resulting in a final concentration of 130 μM. The plate was then kept in the dark for 40 minutes (pre-irradiation time) and, after this period, it was illuminated from above by LED light for 20 minutes, corresponding to a fluence of 43.2 J/cm^2 (C+L+ groups). In order to evaluate the toxicity of the PS alone, samples of each microbial suspension were incubated with each PS (free CUR or anionic or cationic CUR-NP) and maintained in the dark for 60 minutes, corresponding to the pre-irradiation and illumination times (C+L- groups). The toxicity of the NPs were evaluated by incubating each microbial suspension with anionic or cationic NPs without CUR in the dark for 60 minutes (N groups). The effect of light alone was verified by adding 100 μL of PBS to each microbial suspension, incubating it for 40 minutes and illuminating it for 20 minutes (43.2 J/cm^2, C-L+ group). The untreated control group did not receive any PS nor light (C-L-). Afterwards, each sample was submitted to tenfold serial dilutions that were spread on specific agar media for each microorganism as described previously. All agar plates were incubated at 37˚C for 48 hours for colony quantification (CFU/mL). The diagram of all the experimental conditions is illustrated in Fig 1.

aPDT against mono-, dual- and triple-species biofilms. After the cultivation and standardization of each microorganism as described previously for the planktonic cultures, tests

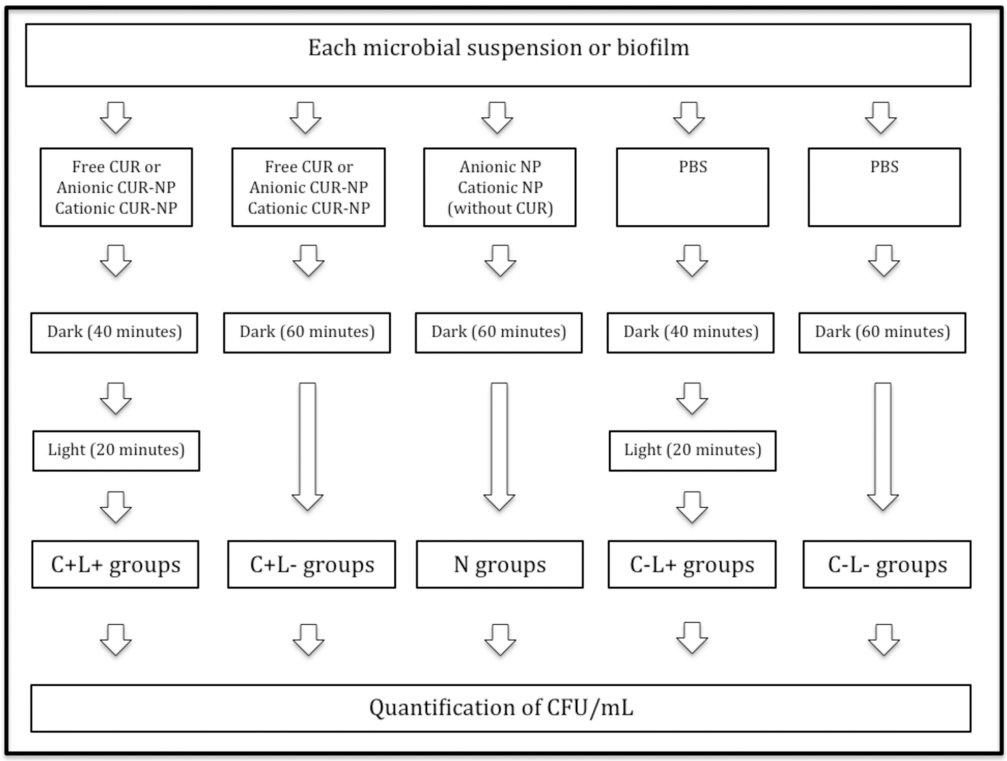


Fig 1. Diagram of the experimental conditions for planktonic cultures and biofilms.

https://doi.org/10.1371/journal.pone.0187418.g001

were made against mono-, dual-, and triple-species biofilms formed by *C. albicans*, *S. mutans*, and MRSA.

Biofilms were formed on a 96-well flat-bottom microtiter plate with a final microbial volume of 150 μL (150 μL of each microbial suspension for mono-species biofilms, 75 μL of each microbial suspension for dual-species biofilms, and 50 μL of each microbial suspension for triple-species biofilms). The plates were incubated at 37˚C for 90 minutes (adhesion phase). Then, the culture broth was removed and wells were washed twice using PBS in order to remove the non-adherent cells. Afterwards, 150 μL of BHI were added to each well and the plate was incubated at 37˚C for 48 hours to form the biofilms. After 24 hours, 75 μL of broth were removed from each well and the same volume of fresh BHI was added. All experiments with *S. mutans* were performed in a 5% CO_2 incubator.

After the biofilm was formed, the medium broth was removed and the biofilm was washed twice with PBS. The same groups described for planktonic cultures were evaluated for the single and multispecies biofilm viability (C+L+, C+L-, N, C-L+, and C-L- / Fig 1). However, the concentration of free CUR was 1200 μM, since lower concentrations were not effective against these multispecies biofilms (non-published data), and the maximum concentration of the synthesized CUR-NP (260 μM for anionic and cationic formulations) was used. The same pre-

irradiation time (40 minutes) and light fluence used for the planktonic cultures were employed for the biofilms. Additional samples (n = 3 or 6) of the triple-species biofilm had the PS (free CUR, anionic CUR-NP or cationic CUR-NP) washed thrice with PBS after pre-irradiation time and before illumination. After the treatments, the biofilms were mechanically disrupted using the pipette tip and tenfold serial dilutions were plated on specific agar medium for each microorganism as described previously. The agar plates were incubated at 37˚C for 48 hours for colonies quantification (CFU/mL).

Confocal Scanning Laser Microscopy (CSLM) analysis. In order to evaluate the uptake of the synthesized formulations and the free CUR by the triple-species biofilm, samples were grown onto cover glass-bottom dishes (SPL Life Sciences, Pocheon, Korea) as described above in duplicate or triplicate. Biofilms were incubated for 40 minutes with free CUR, and anionic and cationic CUR-NP, and control biofilms were incubated for 40 minutes with SYTO-9 (Molecular Probes, Invitrogen Corp., Carlsbad, USA) prepared according to the manufacturer's instructions. For each group, samples were washed thrice with PBS or not before being observed under a confocal laser microscope (Carl Zeiss LSM 800 with Airyscan, Germany) with laser at 488 nm, and images were acquired using 40x oil-immersion objective and z-stack sections of 1 μm.

Cell viability assay. Spontaneously immortalized Normal Oral Keratinocytes (NOK-si) were kindly provided by Prof. Carlos Rossa Junior (Department of Periodontology, School of Dentistry, Araraquara, UNESP, Brazil) [24]. Cells were cultured in Dulbecco's Modified Eagles Medium (DMEM-GIBCO BRL, Grand Island, NJ, USA) suplemeted with fetal bovine serum (10%), glutamine 2 mM (GIBCO BRL, Grand Island, NJ, USA) and penicillin 100 IU/mL-streptomycin 100 mg/mL (Sigma Chemical Co., St. Louis, MO, USA) [25]. Cells were grown at 37˚C under 5% CO_2 and 80% humidity (Series II water jacket CO_2 incubator, Thermo Fisher Scientific, Marietta OH, USA) until 90% confluence.

A total of 20,000 cells quantified in a cell counter (Countess II FL, Lifetechnologies, Carlsbad, CA, USA) were transferred to wells of a black 96-well culture plate (NUNC; Thermo Scientific, Roskilde, Denmark). Cells were incubated for 40 minutes with the formulations (anionic CUR-NP, anionic NP, cationic CUR-NP and cationic NP), free CUR, 10% DMSO (free CUR vehicle), and Triton X-100 (positive control). For the negative control group, cells were grown with culture medium only. For all groups, DMEM was used as vehicle (anionic and cationic NP and CUR-NP were centrifuged at 6,000 *xg* for 10 minutes, and pellets were resuspended in DMEM). Then the cells were washed twice with PBS, and a solution of Alamar blue (Invitrogen,TREK Diagnostic Systems, OH, USA) and DMEM (1:9) was immediately added onto samples, which were incubated for 4 and 24 hours. After each period, the fluorescence intensity of the Alamar blue with its samples was mensured in a Fluoroskan Ascent FL fluorometer (Labsystems, Helsinki, Finland) having a 540 nm excitation wavelength and a 590 nm emission wavelength [26].

Statistical analyzes. The experiments were performed in triplicate on three different occasions for all experimental conditions unless otherwise stated. The CFU/mL values were transformed to logarithms. For the cytotoxic assay, the percentage of cell viability (survival) was calculated considering the negative control as 100%. Normal and homoscedastic data were analyzed by ANOVA and Tukey post-hoc tests. Normal and heteroscedastic data were analyzed by ANOVA/Welch and Games-Howell post-hoc tests. Non-normal data were evaluated by non-parametric Kruskall-Walis test. The significance level was 5%. Mean reductions in $\log_{10}$ were calculated only for normal data, since mean and standard deviation (SD) do not represent non-normal data. Therefore, normal data was plotted in bar charts as mean and SD, while non-normal data was plotted as box-plots.

Table 1. DLS mean values of size, PDI and zeta potential (± standard deviation) of anionic CUR-NP, anionic NP, cationic CUR-NP and cationic NP.

Formulation	Days	Size (nm)	PDI (a.u.)	Zeta Potential (mV)
Anionic CUR-NP	0	237.9 (± 34.2)	0.08 (± 0.08)	-35.2 (± 6.52)
	7	259.1 (± 27.9)	0.22 (± 0.02)	-25.4 (± 2.95)
	15	270.2 (± 64.2)	0.16 (± 0.1)	-16.3 (± 2.64)
	35	273.3 (± 48.7)	0.27 (± 0.04)	-13.9 (± 5.17)
	40	326.1 (± 61.4)	0.28 (± 0.07)	-04.3 (± 3.32)
Anionic NP	0	203.6 (± 19.1)	0.10 (± 0.01)	-32.7 (± 0.96)
	7	266.9 (± 23.7)	0.21 (± 0.09)	-25.8 (± 1.76)
	15	284.3 (± 08.2)	0.25 (± 0.02)	-17.8 (± 2.24)
	35	289.4 (± 43.9)	0.29 (± 0.04)	-12.8 (± 5.44)
	40	399.5 (± 17.7)	0.31 (± 0.02)	-04.9 (± 0.96)
Cationic CUR-NP	0	239.0 (± 47.6)	0.20 (± 0.07)	+32.0 (± 1.45)
	7	305.6 (± 22.8)	0.27 (± 0.04)	+28.8 (± 5.75)
	15	256.6 (± 34.1)	0.29 (± 0.08)	+24.7 (± 1.89)
	35	266.9 (± 13.5)	0.25 (± 0.04)	+13.8 (± 0.53)
	40	279.9 (± 42.7)	0.25 (± 0.08)	+06.9 (± 3.23)
Cationic NP	0	205.3 (± 27.1)	0.20 (± 0.03)	+30.0 (± 1.36)
	7	248.8 (± 27.8)	0.24 (± 0.03)	+29.3 (± 2.51)
	15	297.6 (± 09.2)	0.32 (± 0.01)	+23.3 (± 3.90)
	35	263.3 (± 13.3)	0.25 (± 0.04)	+14.3 (± 1.48)
	40	290.3 (± 25.9)	0.30 (± 0.08)	+05.5 (± 1.62)

DLS: Dynamic Light Scattering; PDI: polydispersity index; a.u.: arbitrary units.

https://doi.org/10.1371/journal.pone.0187418.t001

Results

CUR-NP synthesis and characterization

Physicochemical characterization. With the nanoprecipitation method used, the maximum concentration of CUR encapsulated in the NPs was 260 μM. Higher concentrations resulted in CUR aggregation. Physicochemical properties of the nanoformulations are presented in Table 1. According to the DLS characterization, the mean values of the size, the PDI, and the zeta potential of the 4 formulations were similar at the baseline (day 0). As can be seen, these values have changed over time and, in general, the highest variations occurred after 15 days.

The FEG-SEM showed the CUR-NP having a spherical shape and sizes of 193 and 214 nm for the anionic and the cationic solutions, respectively, after their synthesis (Fig 2).

Absorption spectrum and photostability. Fig 3 shows the absorption spectrum of the free CUR, and the anionic and cationic CUR-NPs. All PSs demonstrated maximum absorbance values from 1.645 a.u. to 2.272 a.u. at wavelengths of 425–429 nm (blue region).

PS photostability is shown in Fig 4. The highest reduction of absorbance, verified after 43.2 J/cm^2 of light (20 minutes), corresponded to 75.06%, 88.95%, and 71.67% of free CUR, anionic CUR-NPs and cationic CUR-NPs, respectively.

EE and CUR release. The mean EE of the anionic and cationic CUR-NP were 67% and 64.67%, respectively. Fig 5 shows CUR release from anionic and cationic NP. There was a gradual and incomplete CUR release over time and, after 48 hours, 96% of the CUR was released from both anionic and cationic NP.

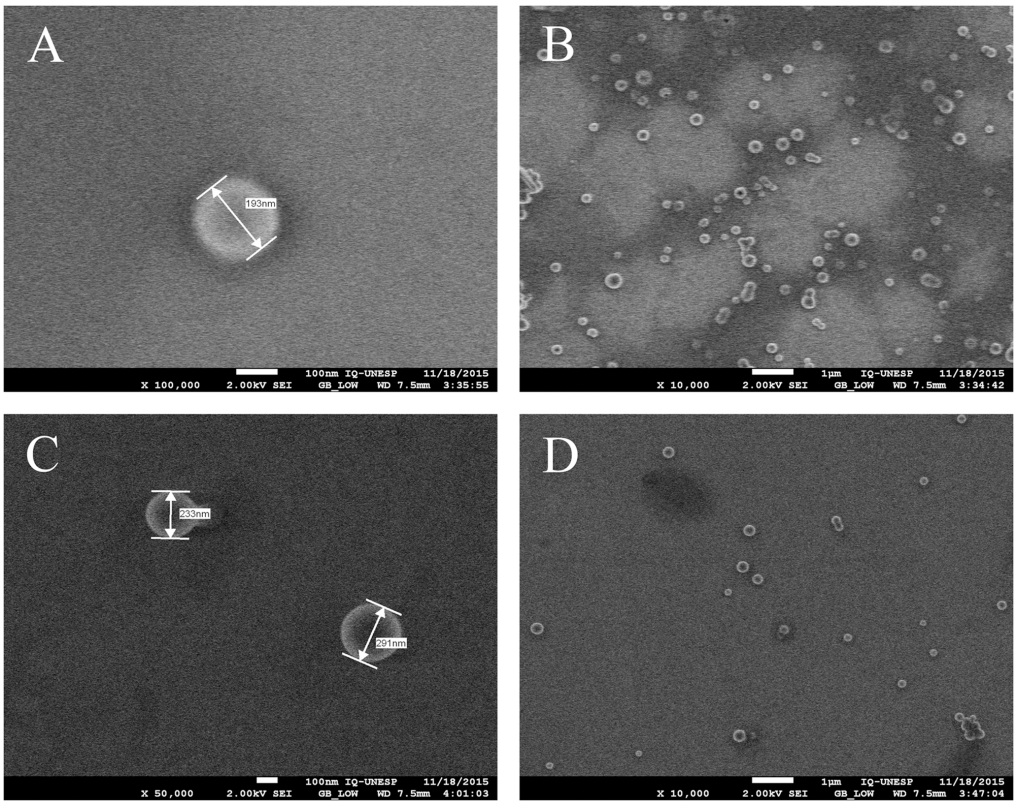


Fig 2. FEG-SEM of CUR–NP solutions. (A and B) Anionic CUR-NP solution; (C and D) cationic CUR-NP solution.

https://doi.org/10.1371/journal.pone.0187418.g002

Antimicrobial assays

aPDT against planktonic cultures of *S. mutans*, *C. albicans* and MRSA. Fig 6 shows the results of planktonic cultures of *S. mutans* (Fig 6A), *C. albicans* (Fig 6B), and MRSA (Fig 6C).

The results obtained from planktonic cultures of *S. mutans* and *C. albicans* showed that treatments with aPDT mediated by free CUR (C+L+ free groups) resulted in the eradication of the microbial growth. In addition, the samples treated with free CUR only (C+L- groups with free CUR) showed a significant reduction of $\log_{10}$(CFU/mL) values (ANOVA/Welch; $p<0.010$ for bacteria and $p<0.001$ for yeast) when compared to the control group (C-L-; reduction of 0.75 $\log_{10}$ for *S. mutans* and 2.43 $\log_{10}$ for *C. albicans*). aPDT mediated by anionic CUR-NP (C+L+ anionic groups) also resulted in significant reductions (ANOVA/Welch; $p<0.001$) of the microbial growth compared with the other groups (C-L-, C-L+, N anionic, and C+L- anionic). Compared with the control, aPDT mediated by anionic CUR-NP showed reductions of 6.54 $\log_{10}$ and 0.78 $\log_{10}$ for *S. mutans* and *C. albicans*, respectively. It was also observed that cationic nanoparticles, with or without CUR (C+L- and N groups, respectively), eradicated the growth (no colony on agar plates) of *S. mutans* and *C. albicans*, indicating a microbicidal effect

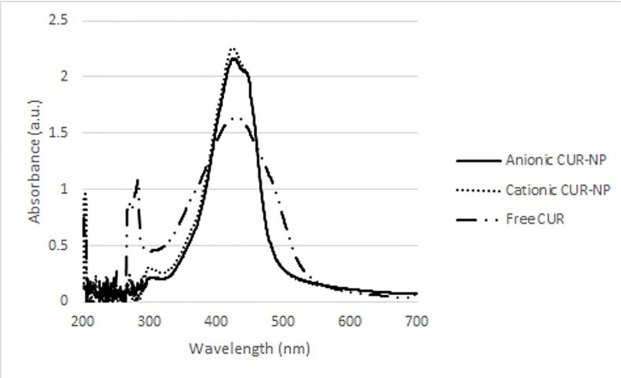


Fig 3. Absorption spectrum of free CUR, anionic CUR-NP, and cationic CUR-NP.

https://doi.org/10.1371/journal.pone.0187418.g003

of cationic nanoparticles. Consequently, the samples treated with the cationic CUR-NP and light (C+L+ group) also showed no microbial growth.

For planktonic cultures of MRSA (Fig 6C), bacteria eradication was also observed for C+L + free CUR, cationic N, cationic C+L-, and cationic C+L+ groups, similar to the outcomes observed for *S. mutans* and *C. albicans*. In addition, the samples treated with aPDT mediated by anionic CUR-NP (C+L+ group) resulted in significant reduction ($p<0.001$) of $\log_{10}$(CFU/mL) values compared with the other groups with bacterial growth (C-L-, C-L+, C+L- free, anionic N, and anionic C+L- groups). This reduction was equivalent to 6.47 $\log_{10}$ compared to the control group. In opposition to the results verified for *S. mutans* and *C. albicans*, MRSA samples treated with free CUR (C+L- group) showed no significant difference ($p\geq0.261$) compared to the C-L-, C-L+, N, and C+L- (anionic formulation) groups. Additionally, MRSA samples treated with anionic NP without CUR (N group) showed a significant difference ($p = 0.048$) compared to the control. Despite the fact that this difference may be statistically significant, it was not relevant from the microbiological point of view, since the mean values of the control and the anionic N groups were 7.64 and 7.36 $\log_{10}$(CFU/mL), a difference lower than 1 $\log_{10}$ (0.28 $\log_{10}$).

aPDT against mono-species biofilms. When the free CUR was evaluated, a significant reduction of $\log_{10}$(CFU/mL) of biofilms of *C. albicans* ($p\leq0.043$), *S. mutans* ($p<0.001$) and MRSA ($p\leq0.05$) (Fig 7A, 7B and 7C) was observed after the aPDT compared with the control (C-L-), which did not show a significant difference ($p>0.05$) compared with the other groups (C+L- and C-L+). The mean reductions observed for each species were: 1.24, 2.26, and 2.47 $\log_{10}$ for MRSA, *C. albicans* and *S. mutans*, respectively.

For the anionic CUR-NPs, aPDT promoted no significant difference ($p\geq0.532$) in the viability of *C. albicans* biofilm compared with the control (C-L-) and C+L- groups. However a significant difference ($p\leq0.038$) was observed between the N group and the C-L-, C-L+ and C+L + groups, and also between the C-L+ group and the C+L- and C+L+ groups ($p\leq0.034$) (Fig 8A). For *S. mutans* (Fig 8B), the aPDT mediated by the anionic CUR-NP promoted a significant reduction ($p<0.001$) in its viability compared with the other groups, which showed no significant difference ($p\geq0.067$) among them. Compared with the control (C-L-) group, a reduction of 1.70 $\log_{10}$ was verified. Conversely, ANOVA demonstrated no significant difference ($p = 0.222$) for MRSA (Fig 8C).

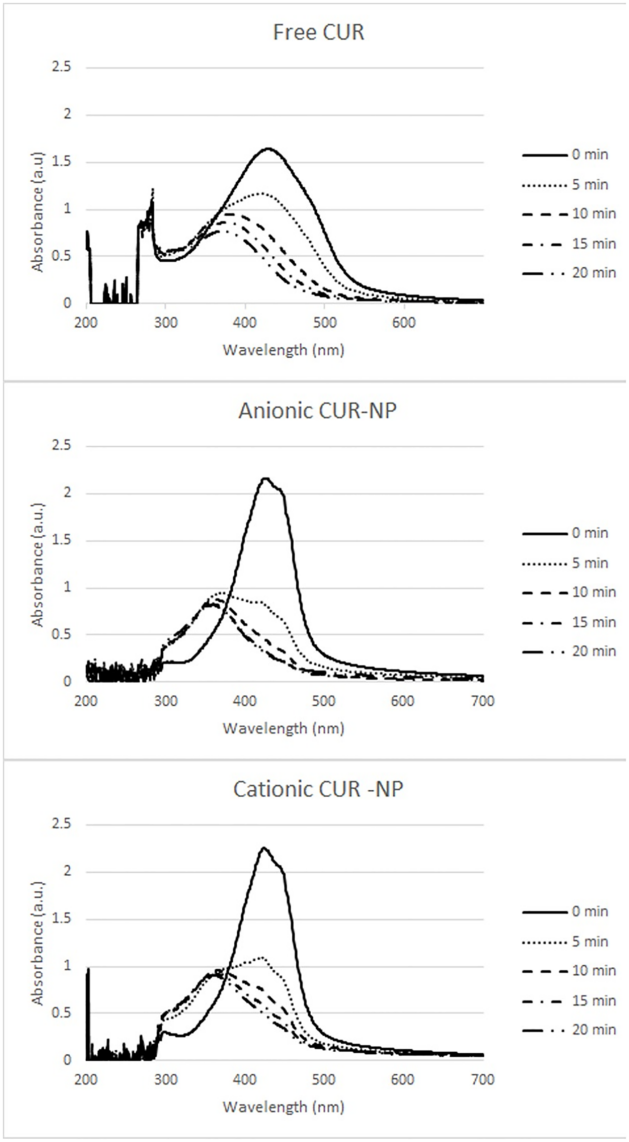


Fig 4. Photostability (values of absorbance) after different irradiation times observed for free CUR, anionic and cationic CUR-NP.

https://doi.org/10.1371/journal.pone.0187418.g004

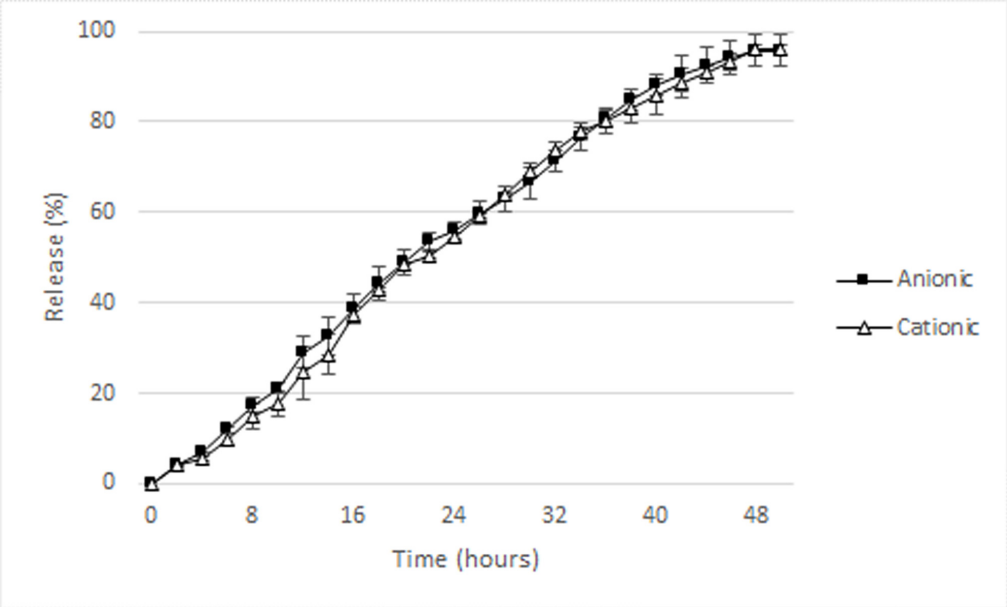


Fig 5. CUR release (% values) from anionic and cationic NP.

https://doi.org/10.1371/journal.pone.0187418.g005

The evaluation of the cationic CUR-NPs against *C. albicans* demonstrated that the values of all experimental groups (C+L-, C-L+, N and C+L+) were significantly lower ($p \leq 0.008$) than the control group (C-L-). The fungal monospecies biofilm submitted to light only showed $\log_{10}$(CFU/mL) values significantly ($p \leq 0.041$) lower than the control and higher than the other groups. The groups treated with cationic CUR-NPs with and without light, and with NPs without CUR (C+L-, C+L+ and N) showed no significant difference among themselves. When *S. mutans* was evaluated, the non-parametric Kruskal-Wallis test demonstrated that biofilm treated with cationic NPs (N, C+L- and C+L+ groups) were significantly lower ($p \leq 0.010$) than the control and light-only groups (C-L- and C-L+). For biofilms of MRSA, ANOVA demonstrated no significant difference ($p = 0.108$) (Fig 9A, 9B and 9C).

aPDT against dual-species biofilms. For the free CUR, the biofilm of *S. mutans* and *C. albicans* (Fig 10A) showed a significant reduction ($p \leq 0.002$) of 1.50 $\log_{10}$ after the aPDT only for *C. albicans* compared with the control (C-L-) and C-L+ groups, which did not differ significantly ($p > 0.05$) from the C+L- group. On the other hand, *S. mutans* showed no significant difference ($p > 0.05$) among all the groups evaluated. On the other hand, the biofilms of MRSA and *C. albicans* (Fig 10B) showed a significant reduction in the viability of both species after aPDT equivalent to 1.39 $\log_{10}$ ($p < 0.001$) and 2.06 $\log_{10}$ ($p = 0.002$), respectively. For *C. albicans*, a significant difference ($p = 0.004$) was also observed between the C+L+ and C+L- groups and no significant difference ($p \geq 0.130$) among C-L-, C-L+ and C+L- groups and similarly none between C+L+ and C-L+ groups. For the biofilms of *S. mutans* and MRSA (Fig 10C), the ANOVA/Welch demonstrated a significant effect ($p = 0.003$) in the viability of *S. mutans*, since a significant ($p = 0.005$) reduction of 2.86 $\log_{10}$ after aPDT was observed compared with the control group. aPDT also promoted a significant reduction ($p \leq 0.007$) compared with the

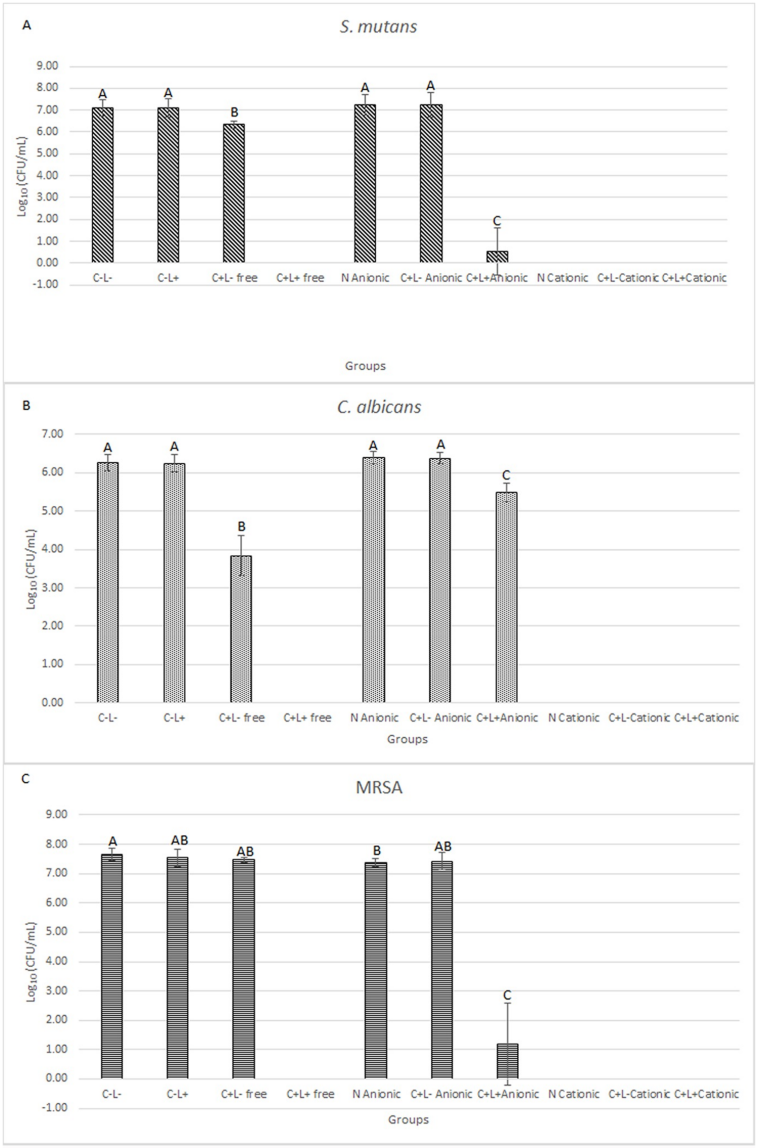


Fig 6. Mean values of log_{10}(CFU/mL) of planktonic cultures. (A) *S. mutans*, (B) *C. albicans* and (C) MRSA. Error bars: standard deviation. The same letters show no statistical difference. C-L-: control group without PS nor light. C-L+: Planktonic culture treated with light only (43.2 J/cm^2). C+L- free: Planktonic culture treated with free Cur only at 130 μM. C+L+ free: Planktonic culture submitted to aPDT with free Cur at 130 μM and 43.2 J/cm^2. N Anionic: Planktonic culture treated with anionic NP without CUR. C+L- Anionic: Planktonic cultures treated only with anionic CUR-NP at 130 μM. C+L+ Anionic: Planktonic culture submitted to aPDT with anionic CUR-NP at 130 μM and 43.2 J/cm^2. N Cationic: Planktonic culture treated with cationic NP without CUR. C+L- Cationic: Planktonic culture treated only with cationic CUR-NP at 130 μM. C+L+ Cationic: Planktonic culture submitted to aPDT with cationic CUR-NP at 130 μM and 43.2 J/cm^2.

https://doi.org/10.1371/journal.pone.0187418.g006

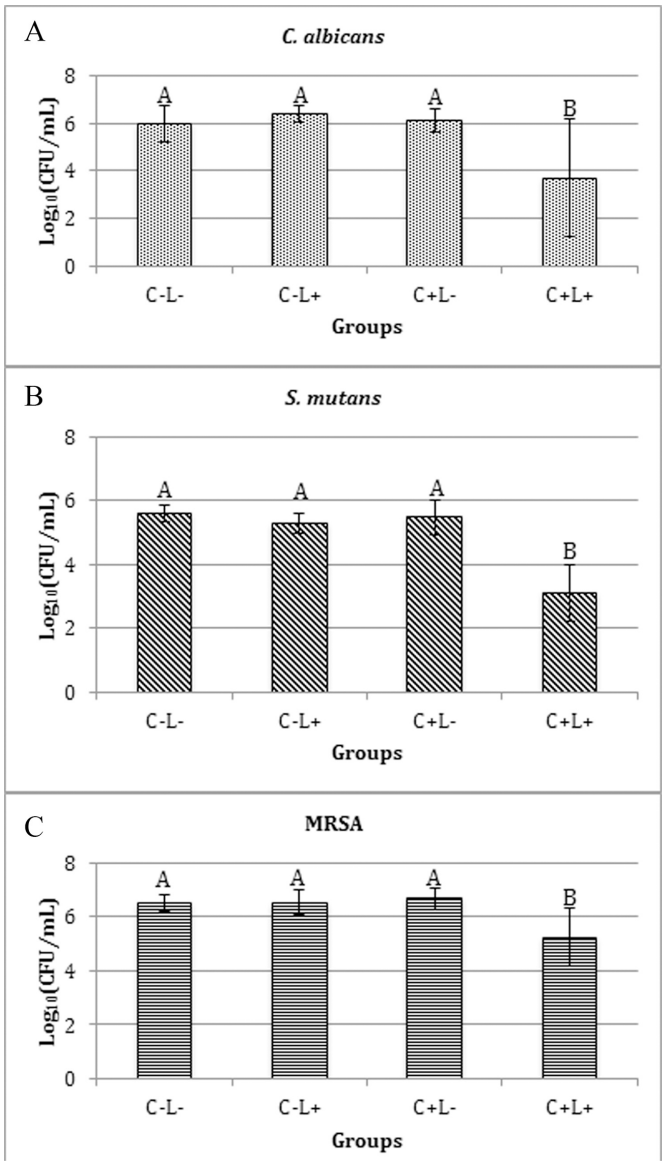


Fig 7. Values of log_{10}(CFU/mL) of mono-species biofilm treated with free CUR. (A) *C. albicans*, (B) *S. mutans* and (C) MRSA. Bars charts show mean and standard deviation (error bars). The same letters show no statistical difference. C-L-: Control group without PS nor light. C-L+: Biofilm treated only with light (43.2 J/cm^2). C+L-: Biofilm treated only with Cur at 1200 μM. C+L+: Biofilm submitted to aPDT with Cur at 1200 μM and 43.2 J/cm^2.

https://doi.org/10.1371/journal.pone.0187418.g007

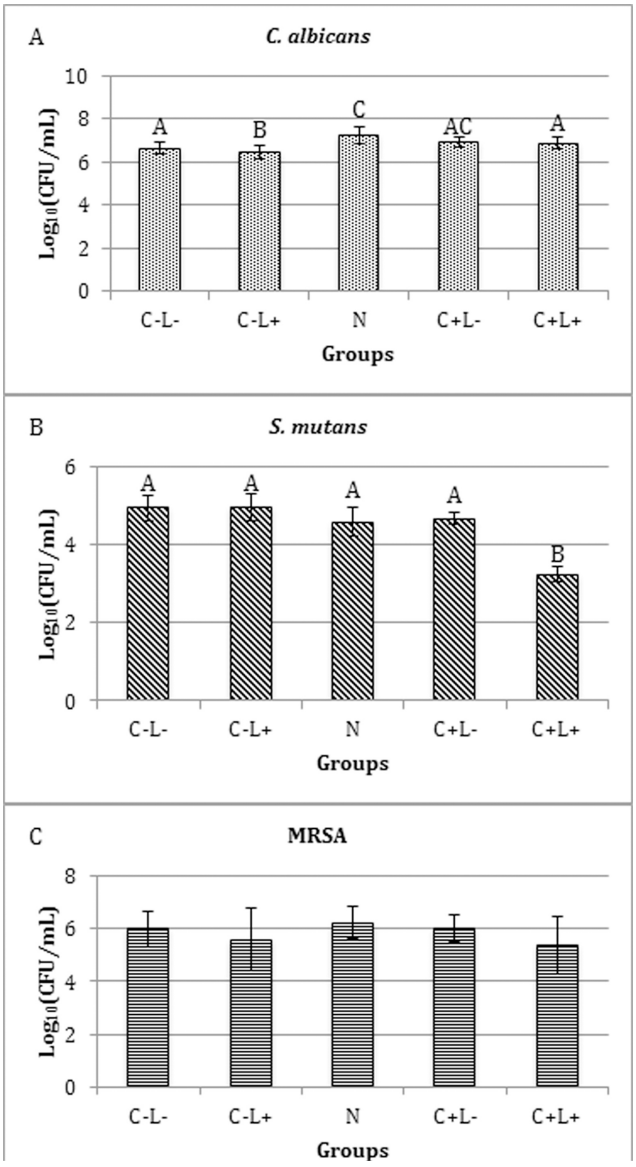


Fig 8. Values of log_{10}(CFU/mL) of mono-species biofilm treated with anionic CUR-NP. (A) *C. albicans*, (B) *S. mutans* and (C) MRSA. Bars charts show mean and standard deviation (error bars). The same letters show no statistical difference. C-L-: Control group without PS nor light. N: Biofilm treated with anionic NP without CUR. C-L+: Biofilm treated only with light (43.2 J/cm^2). C+L-: Biofilm treated only with anionic CUR-NP at 260 μM. C+L+: Biofilm submitted to aPDT with anionic CUR-NP at 260 μM and 43.2 J/cm^2.

https://doi.org/10.1371/journal.pone.0187418.g008

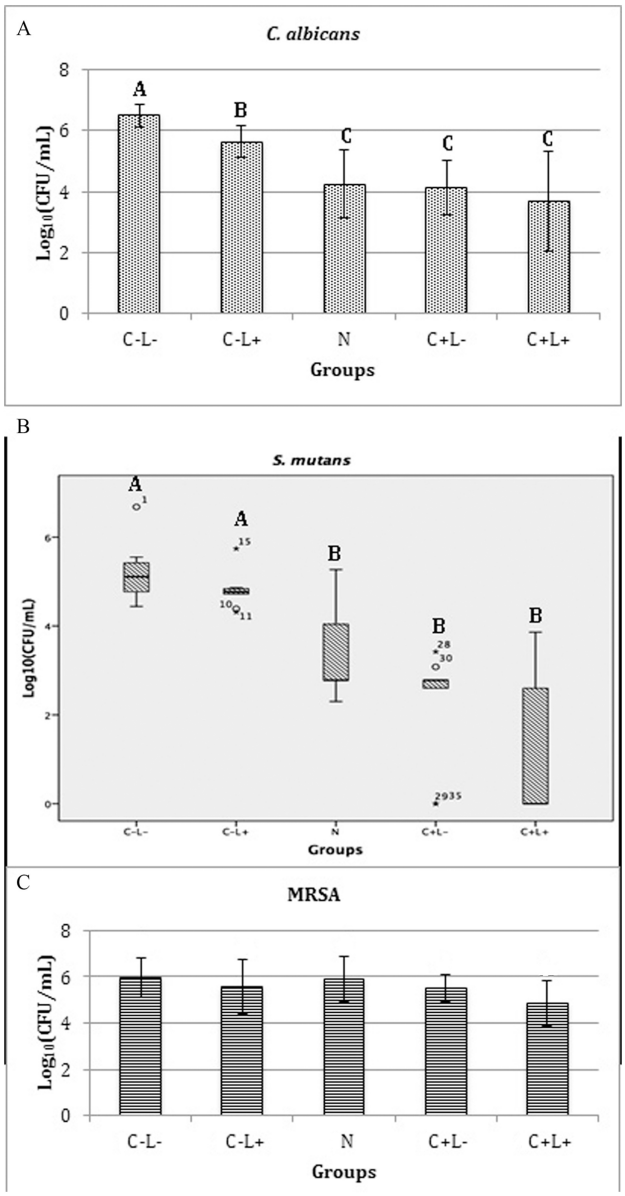


Fig 9. Values of log_{10}(CFU/mL) of mono-species biofilms treated with cationic CUR-NP. (A) *C. albicans*, (C) MRSA. Bars charts show mean and standard deviation (error bars). (B) Box-plot of *S. mutans* shows median (dash) first and third quartiles (boxes), highest and lowest values (error bars). Bar charts were used for normal data submitted to parametric analysis, while box-plot was used for non-normal data submitted to non-parametric analysis. The same letters show no statistical difference. C-L-: Control group without PS

nor light. N: Biofilm treated with cationic NP without CUR. C-L+: Biofilm treated only with light (43.2 J/cm^2). C+L-: Biofilm treated only with cationic CUR-NP at 260 μM. C+L+: Biofilm submitted to aPDT with cationic CUR-NP at 260 μM and 43.2 J/cm^2.

https://doi.org/10.1371/journal.pone.0187418.g009

C-L+ and C+L- groups, which did not differ significantly ($p \geq 0.813$) from the control. On the other hand, ANOVA/Welch did not demonstrate a significant ($p = 0.156$) difference in the viability of MRSA among the groups.

The evaluation of the anionic CUR-NPs against the biofilm of *S. mutans* and *C. albicans* demonstrated, for *S. mutans* according to the Kruskal-Wallis test, a significant difference ($p = 0.010$) between the C+L+ group (aPDT) and the N and C-L- (control) groups. The other groups showed no significant difference ($p \geq 0.184$) among themselves. For *C. albicans* viability, the aPDT resulted in a significant reduction ($p = 0.004$) of 0.78 $\log_{10}$ compared with the control (C-L-) group. The other groups showed no significant difference ($p \geq 0.106$) among themselves (Fig 11A).

In the biofilm of MRSA and *C. albicans*, the aPDT mediated by the anionic CUR-NP resulted in a significant difference ($p \leq 0.033$) in the fungal viability compared with the other groups, which showed no significant difference ($p \geq 0.536$) among themselves. Compared with the control group (C-L-), the aPDT reduced the viability of *C. albicans* by 1.37 $\log_{10}$. On the other hand, for MRSA, no significant reduction ($p \geq 0.950$) was verified between the C+L+ group (aPDT) and the control (C-L-) and the C-L+ groups. Significant differences ($p \leq 0.033$) were observed only between the C+L+ group (aPDT) and the N and C+L- groups (Fig 11B).

For the biofilm of *S. mutans* and MRSA, the aPDT using the anionic CUR-NP promoted no significant difference ($p \geq 0.063$) in the viability of *S. mutans* compared with the other groups, except for the C-L+ group, which showed a significant difference ($p < 0.001$) compared with the other groups. A significant difference ($p = 0.003$) was also observed between the C+L- groups and the control (C-L-) groups. For MRSA, ANOVA demonstrated no significant difference ($p = 0.094$) among the groups (Fig 11C).

When the cationic CUR-NPs were evaluated against the biofilm of *S. mutans* and *C. albicans*, the Kruskal-Wallis test demonstrated a significant difference in the viability of both species ($p \leq 0.004$ and $p \leq 0.005$, respectively) between the control group (C-L-) and the other groups (C+L+, C+L- and C-L+), except for the N group ($p = 0.708$ and $p = 0.089$, respectively). The other groups did not show a significant difference ($p \geq 0.134$ and $p = 1.000$) (Fig 12A).

In the biofilm of MRSA and *C. albicans*, ANOVA demonstrated no significant ($p = 0.206$) difference for MRSA. Conversely for *C. albicans*, the Kruskal-Wallis test showed a significant ($p \leq 0.010$) difference between the control group (C-L-) and the N, C+L- and C+L+ groups, which showed no significant difference among themselves ($p = 1.000$). The C-L+ group did not show any significant difference ($p = 1.000$) either when compared with the other groups (Fig 12B).

Finally, in the biofilm of *S. mutans* and MRSA, the aPDT using the cationic CUR-NPs promoted a significant ($p < 0.001$) reduction in the viability of *S. mutans* compared with the other groups, with a reduction of 4.11 $\log_{10}$ compared with the control (C-L-). A significant difference ($p = 0.009$) was also observed between the N group and the control (C-L-), while the other groups showed no significant difference ($p \geq 0.208$) among themselves. For MRSA, the aPDT promoted a significant ($p \leq 0.029$) reduction in its viability compared with the other groups, except for the C+L- group ($p = 0.058$). The reduction in the aPDT group (C+L+) was equivalent to 1.58 $\log_{10}$ compared with the control group (C-L-). The other groups demonstrated no significant difference ($p \geq 0.765$) among themselves (Fig 12C).

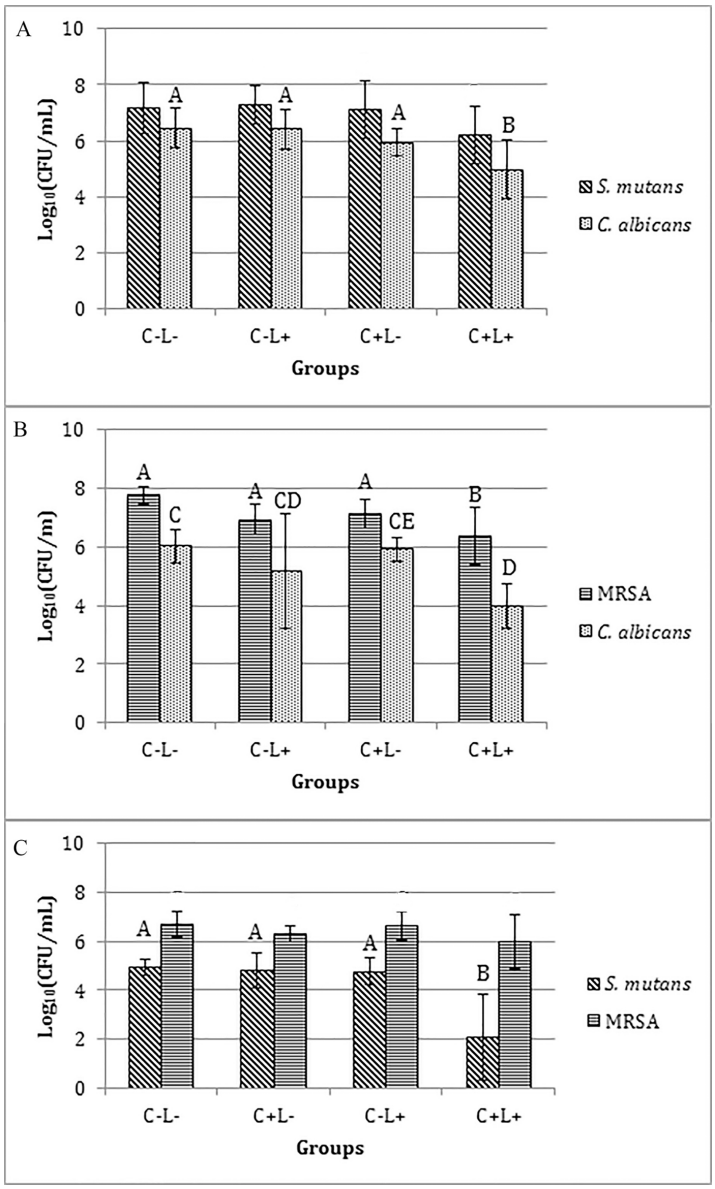


Fig 10. Values of log_{10}(CFU/mL) of dual-species biofilm treated with free CUR. (A) *S. mutans* and *C. albicans*, (B) MRSA and *C. albicans*, (C) *S. mutans* and MRSA. Bars charts show mean and standard deviation (error bars). The same letters show no statistical difference. C-L-: Control group without PS nor light. C-L+: Biofilm treated only with light (43.2 J/cm^2). C+L-: Biofilm treated only with free Cur at 1200 μM. C+L+: Biofilm submitted to aPDT with free Cur at 1200 μM and 43.2 J/cm^2.

https://doi.org/10.1371/journal.pone.0187418.g010

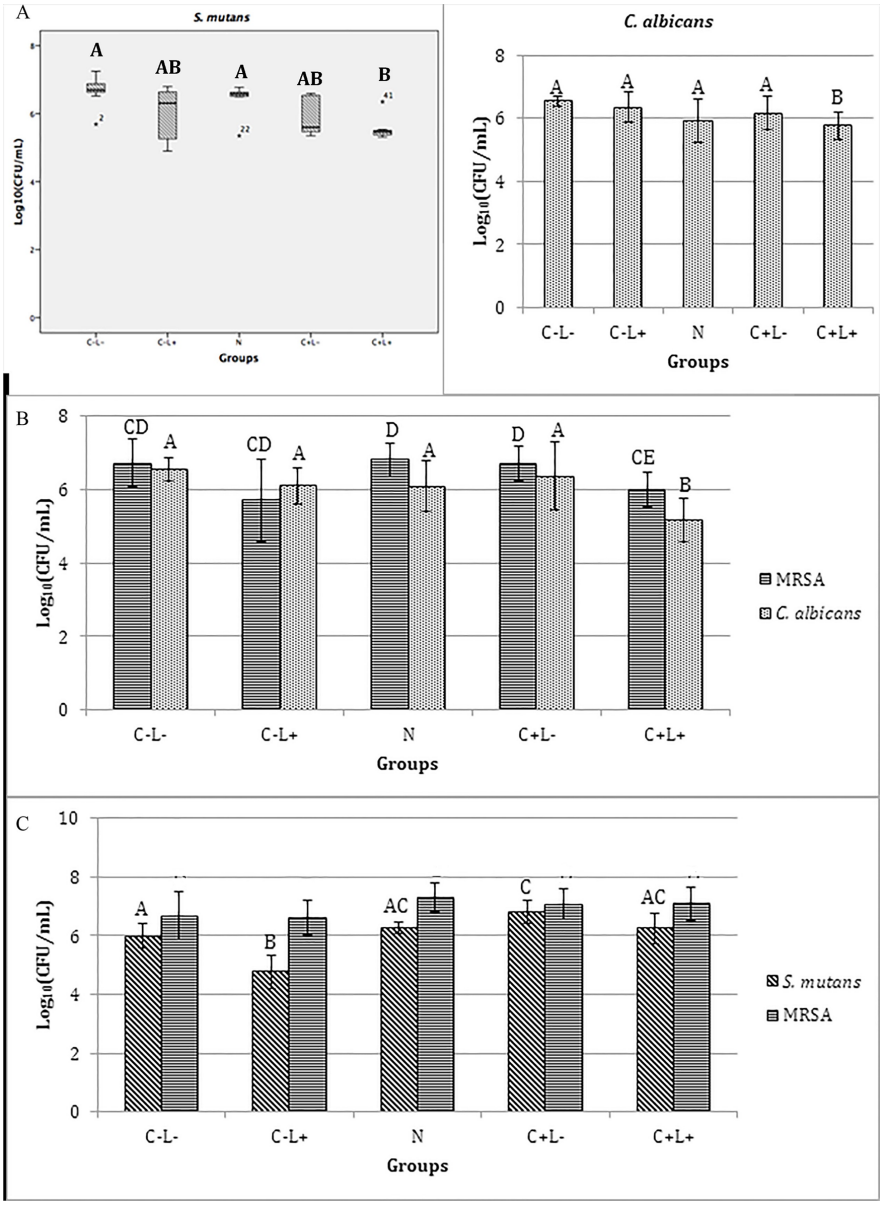


Fig 11. Values of log_{10}(CFU/mL) of dual-species biofilms treated with anionic formulation. (A) *S. mutans* and *C. albicans*, (B) MRSA and *C. albicans*, and (C) *S. mutans* and MRSA. Bars charts show mean and standard deviation (error bars) values of log_{10}(CFU/mL). Box-plot shows median (dash), first and third quartiles (boxes), highest and lowest values (error bars). The same letters showed no statistical difference. Bar charts were used for normal data submitted to parametric analysis, while box-plot was used for non-normal data submitted to non-parametric analysis. C-L-: Control

group without PS nor light. N: Biofilm treated with anionic NP without CUR. C-L+: Biofilm treated only with light (43.2 J/cm^2). C+L-: Biofilm treated only with anionic CUR-NP at 260 μM. C+L+: Biofilm submitted to aPDT with anionic CUR-NP at 260 μM and 43.2 J/cm^2.

https://doi.org/10.1371/journal.pone.0187418.g011

aPDT against triple-species biofilm. Table 2 shows the results of the treatments with free CUR, anionic and cationic formulations against the triple-species biofilm. Washed biofilms demonstrated reductions of 1 to 2 $\log_{10}$ compared with non-washed biofilms for each species.

The results obtained for free CUR showed significant differences among the treatment groups for all microorganisms ($p<0.001$). The aPDT promoted a significant reduction in the viability of the three species evaluated in comparison to the control and the other treatments (p values were <0.001 for *S. mutans*, ≤ 0.007 for *C. albicans*, and ≤ 0.002 for MRSA). There was no significant difference among the other groups for *S. mutans* ($p\geq 0.840$), *C. albicans* ($p\geq 0.668$), and MRSA ($p\geq 0.314$). Compared with control (C-L-), the aPDT mediated by the free CUR promoted reductions of 1.05, 2.41, and 0.90 $\log_{10}$ for *S. mutans*, *C. albicans*, and MRSA, respectively. For washed samples submitted to aPDT, only bacteria showed reduction of viability compared with control (1.81 and 1.07 $\log_{10}$ for *S. mutans* and MRSA, respectively).

The evaluation of the triple-species biofilm after treatments with the anionic formulations demonstrated a significant difference only for *C. albicans* when the anionic groups N and C+L+ were compared ($p = 0.036$), while no significant difference among the other groups ($p\geq 0.129$) was observed. There was also no significant difference among the groups for *S. mutans* ($p\geq 0.548$) and MRSA ($p\geq 0.579$), since bacterial growth was observed after all treatments. After aPDT, washed samples showed reduction in viability only for bacteria (0.99 and 0.37 $\log_{10}$ for *S. mutans* and MRSA, respectively) compared with control.

When cationic formulations were compared, significant differences were observed for the three microorganisms, which showed similar growth behavior after the treatments. The cationic formulations, with or without CUR, in the presence or absence of light (NP, C+L-, and C+L+ groups), resulted in a significant reduction of $\log_{10}$(CFU/mL) values ($p\leq 0.036$) in comparison with the control group, with no significant difference between the C+L- and C+L+ groups ($p\geq 0.088$). There was no significant difference ($p\geq 0.849$) between the control group (C-L-) and the C-L+ groups in the $\log_{10}$(CFU/mL) values for the three microbial species. Compared with the control (C-L-), the highest reductions observed for *S. mutans*, *C. albicans*, and MRSA were 5.05 $\log_{10}$ (C+L- group), 2.32 $\log_{10}$ (C+L- group) and 4.21 $\log_{10}$ (C+L+ group), respectively. For washed samples, all species showed reduction in viability after aPDT (2.42, 1.75, and 1.2 $\log_{10}$ for *S. mutans*, *C. albicans*, and MRSA, respectively) and after being treated only with the cationic CUR-NP (1.63, 1.18, and 0.94 $\log_{10}$ for *S. mutans*, *C. albicans*, and MRSA, respectively) compared with control.

CSLM analysis. The images showed brighter fluorescence for non-washed samples (Fig 13A, 13C, 13E and 13F) than those washed thrice with PBS (Fig 13B, 13D, 13F and 13G), which suggests that the washing step reduced the PS uptake. Control biofilms stained with SYTO-9 (Fig 13A and 13B) demonstrated the fluorescence of coccus, yeast, and hyphae, and a mean thickness of 14.62 μm and 12.9 μm for non-washed and washed samples, respectively. Biofilms incubated with free CUR (Fig 13C and 13D) showed a mean thickness of 6.24 μm (non-washed) and 7.02 μm (washed) and brighter fluorescence for coccus than for yeast, suggesting a better uptake of free CUR by the bacteria than by the yeast. For anionic CUR-NP no yeast was observed, only a high amount of coccus suggesting an uptake only by the bacteria, and a mean thickness of 7.46 μm and 7.31 μm for non-washed and washed samples, respectively. Finally, biofilms treated with cationic CUR-NP demonstrated fluorescence of coccus, yeast, and hyphae, suggesting that all microoganisms had taken up the cationic formulation,

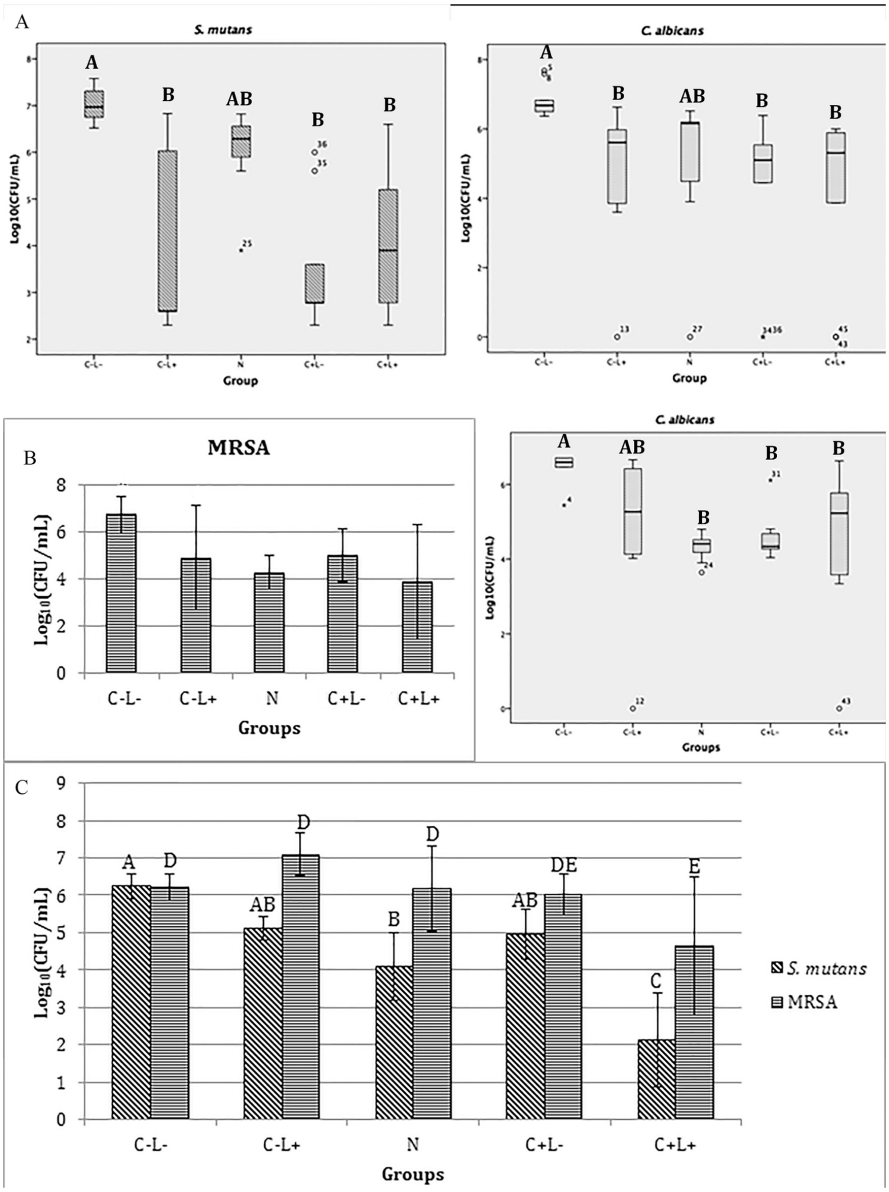


Fig 12. Values of log_{10}(CFU/mL) of dual-species biofilms treated with cationic formulation. (A) *S. mutans* and *C. albicans*, (B) MRSA and *C. albicans*, and (C) *S. mutans* and MRSA treated with cationic CUR-NP. Bars charts show mean and standard deviation (error bars) values of log_{10}(CFU/mL). Box-plot shows median (dash), first and third quartiles (boxes), highest and lowest values (error bars). The same letters showed no statistical difference. Bar charts were used for normal data submitted to parametric analysis, while box-plot was used for non-normal data submitted to non-parametric analysis. C-L-: Control group without PS nor light. N: Biofilm treated with cationic NP without CUR. C-L+: Biofilm treated only with light (43.2 J/cm^2). C+L-: Biofilm treated only with cationic CUR-NP at 260 μM. C+L+: Biofilm submitted to aPDT with cationic CUR-NP at 260 μM and 43.2 J/cm^2.

https://doi.org/10.1371/journal.pone.0187418.g012

Table 2. Mean values of log_{10}(CFU/mL) and standard deviation of the triple-species biofilm for each group evaluated.

	Groups								
	C-L-		C-L+		N	C+L-		C+L+	
	not washed	washed	not washed	washed		not washed	washed	not washed	washed
Free CUR									
S. mutans	6.59 (0.27)^{A}	5.18 (0.28)	6.60 (0.15)^{A}	5.51 (0.10)	-	6.53 (0.21)^{A}	5.26 (0.02)	5.54 (0.57)^{B}	3.37 (0.62)
C. albicans	6.03 (0.51)^{A}	5.09 (0.04)	5.84 (0.39)^{A}	5.29 (0.10)	-	5.67 (0.96)^{A}	5.17 (0.02)	3.62 (2.00)^{B}	5.15 (0.07)
MRSA	7.53 (0.39)^{A}	6.32 (0.13)	7.23 (0.44)^{A}	6.56 (0.06)	-	7.30 (0.32)^{A}	6.53 (0.03)	6.63 (0.45)^{B}	5.25 (0.08)
Anionic CUR-NP									
S. mutans	7.57 (0.23)^{A}	5.58 (0.23)	7.43 (0.42)^{A}	5.47 (0.28)	7.39 (0.11)^{A}	7.58 (0.25)^{A}	5.56 (0.26)	7.48 (0.22)^{A}	4.59 (0.25)
C. albicans	6.54 (0.19)^{ABC}	5.42 (0.15)	6.64 (0.24)^{ABC}	5.50 (0.23)	6.74 (0.12)^{B}	6.55 (0.13)^{ABC}	5.53 (0.11)	6.49 (0.17)^{C}	5.40 (0.15)
MRSA	7.77 (0.18)^{A}	6.63 (0.28)	7.67 (0.19)^{A}	6.57 (0.14)	7.73 (0.16)^{A}	7.64 (0.25)^{A}	6.52 (0.26)	7.65 (0.14)^{A}	6.26 (0.41)
Cationic CUR-NP									
S. mutans	7.72 (0.13)^{A}	5.82 (0.25)	7.74 (0.16)^{A}	5.73 (0.38)	3.23 (1.49)^{B}	2.67 (1.81)^{B}	4.19 (0.09)	3.28 (1.01)^{B}	3.40 (0.23)
C. albicans	6.61 (0.31)^{A}	5.34 (0.19)	6.47 (0.26)^{A}	5.54 (0.16)	5.35 (0.53)^{B}	4.29 (0.53)^{C}	4.16 (0.40)	4.35 (0.53)^{C}	3.59 (0.15)
MRSA	7.75 (0.27)^{A}	6.44 (0.17)	7.81 (0.06)^{A}	6.62 (0.21)	6.47 (0.26)^{B}	5.23 (1.01)^{C}	5.50 (0.28)	3.54 (1.51)^{C}	5.24 (0.26)

-: not evaluated; different letters denote significant difference ($p<0.05$) for non-washed samples; washed samples: n = 6 for anionic and cationic CUR-NP, and n = 3 for free CUR in each group (no statistical inference was performed).

https://doi.org/10.1371/journal.pone.0187418.t002

and a mean thickness of 9.75 μm (non-wahsed) and 13.47 μm (washed). Furthermore, washing the PSs did not reduce the biofilm thickness.

Cell viability assay. After 4 hours of incubation with Alamar blue (Fig 14A), cells treated with anionic formulations (NP and CUR-NP) showed no significant difference of viability (percentage of survival) compared between themselves and with the negative control group ($p \geq 0.998$). However, these groups showed significant difference compared to the others groups ($p < 0.001$). On the other hand, cells incubated with cationic formulations (NP and CUR-NP), free CUR, and 10% DMSO did not show statistical differcence among themselves ($p \geq 0.657$). Additionaly, cells treated with cationic solutions (NP and CUR-NP) and 10% DMSO did not demonstrate any significant difference compared with the positive control group (Triton X-100).

Similar to the test performed at 4 hours, after 24 hours of incubation the negative control group and groups treated with anionic formulation (NP and CUR-NP) did not show significant difference among themselves ($p \geq 0.999$), and these groups showed significant difference ($p \leq 0.001$) compared with the other groups (positive control group, cationic NP, cationic CUR-NP, 10% DMSO, and free CUR). Additionaly, the positive control group also showed significant difference compared with those of cationic NP and free CUR ($p \leq 0.049$). However, the positive control group (Triton X-100) did not show any significant difference compared with groups treated with cationic CUR-NP and 10% DMSO ($p \geq 0.061$). Finally, for samples treated with cationic formulations (NP and CUR-NP), the organic solvent (10% DMSO) and free CUR, no significant difference was observed among them ($p \geq 0.186$) (Fig 14B).

Discussion

Although previous studies have evaluated antimicrobial effects of CUR in nanocarriers, these studies were focused on the prevention of biofilm formation [19] or tested against planktonic cultures [18]. Only a few studies have used CUR in nanoformulations against planktonic oral species [20] or as PS in aPDT against non-oral biofilm [16]. Moreover, the susceptibility of different kinds of biofilms (mono-, dual-, and triple-species biofilms) to aPDT is not extensively

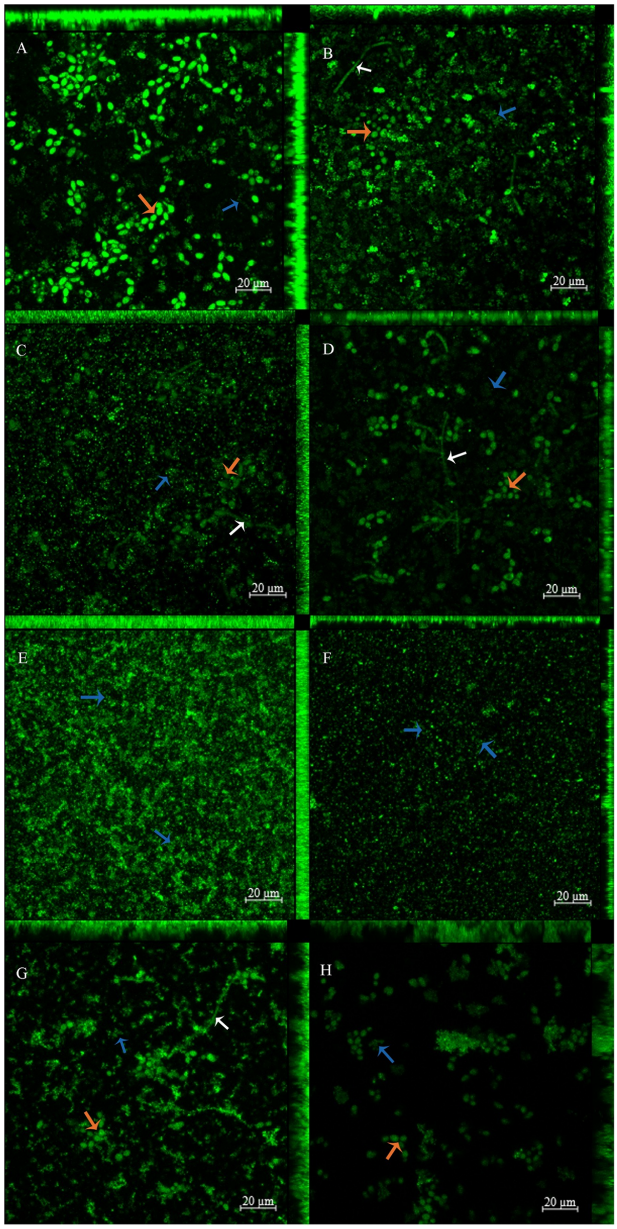


Fig 13. CLSM images showing uptake of free CUR (C and D), anionic CUR-NP (E and F), and cationic CUR-NP (G and H) by the triple-species biofilm. Controls (A and B) were stained with SYTO-9. Samples were washed thrice with PBS (B, D, F, and H) or not washed at all (A, C, E, and G). Magnification: 20 µm. Blue arrows: coccus; red arrows: yeasts; white arrows: hyphaes.

https://doi.org/10.1371/journal.pone.0187418.g013

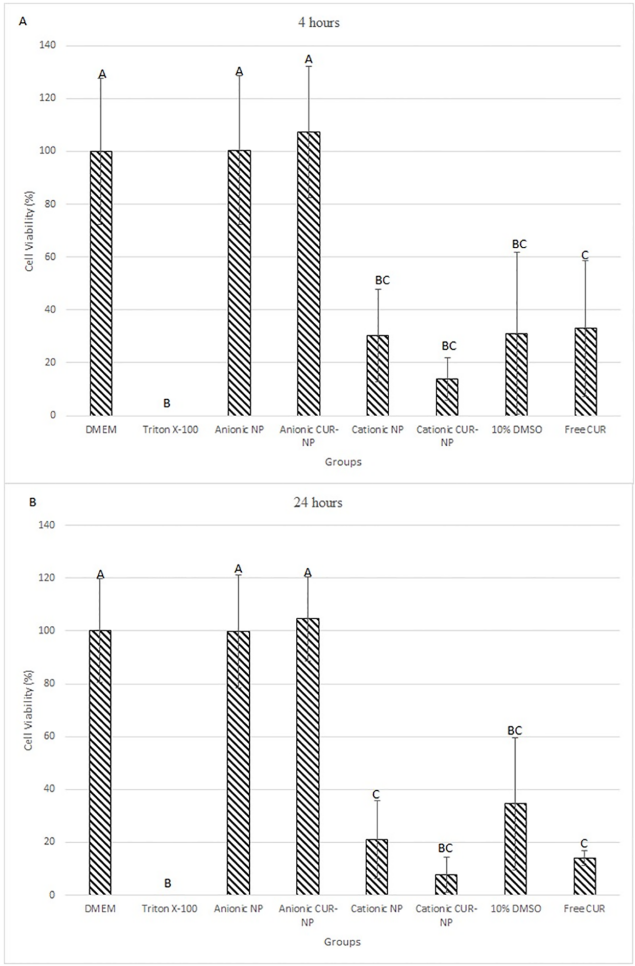


Fig 14. Cell viability (mean percentage of survival) after 4 hours (A) and 24 hours (B) of incubation with Alamar blue in all groups evaluated. Error bars: standard deviation. Different letters denote significant differences.

https://doi.org/10.1371/journal.pone.0187418.g014

explored. Thus, the present investigation evaluated the photodynamic effect of CUR-NP on planktonic cultures and mixed biofilms of microbial species found in the oral cavity. Due to good physico-chemical properties and capacity to encapsulate drugs, polymeric NP represents one of most successful nanocarrier [27]. In this research, we used PLA as polymer, since this compound is biodegradable, biocompatible, and its sub-products of degradation are non-toxic in superficial tissues. Moreover, PLA was approved for direct contact with biological fluids [28]. Furthermore, PLA could be degradated by microorganisms (fungi and bacteria) via esterease enzymatic action [29]. These features make PLA an attractive compound to use as a nanocarrier for antimicrobial purpose. In addition, the nanoprecipitation method used to

synthesize CUR-NP in the present research is simple, reproductible, fast, economic, and easy to apply in industrial scale [30].

The results demonstrated that the encapsulation of CUR in NPs was performed successfully. When the formulations were characterized, their values of mean size, PDI, and zeta potential changed along time after synthesis, since at each time variations begin to appear. Although this was not the goal of this investigation, it could be suggested that these formulations may be stable for short periods after synthesis. The stability of these nanoformulations could be related to the fact that NPs with high zeta potential (in modulus) produces repulsion among the NPs avoiding NP aggregation [31]. Since the PDI values may range from 0 to 1, the PDI value obtained in this study may be considered homogeneous, although only values lower than 0.1 are associated to high homogeneity [32]. Moreover, the size of NP were smaller when they were evaluated by SEM compared with DLS, but this may a consequence of the shinkrage of the NP after the drying procedure for SEM [32].

The physicochemical properties of nanoparticles are related to the polymer and the method used to produce them. Polylactic co-glycolic acid (PLGA) was used in previous studies to synthesize nanoparticles containing CUR by different methods, such as oil/water emulsion-solvent evaporation [33], nanoprecipitation [23], and emulsion-difussion-evaporation [34]. The physicochemical properties obtained by these methods were, in general, similar to those obtained in the present study. The mean sizes, PDI, and zeta potential of the formulations synthesized by emulsion-solvent evaporation [33]/nanoprecipitation [23] methods were 176/76.2–560.4 nm, PDI 0.105/0.19–0.41 and -23.2/+0.06 and -0.06 mV, respectively [33,23]. Another study that used the emulsion-evaporation method obtained nanospheres with size of 264 nm [34]. Gosh et al. [35] prepared CUR-NPs with PLGA and observed by Atomic Force Microscopy nanoparticles with a diameter of 15 nm. PLGA was also used to synthesize NPs loaded with CUR by the single emulsion solvent evaporation technique, where particles with a size of 161.93 nm and a PDI of 0.042 were obtained [36]. PLA and PLGA are polymers approved by the FDA due to their biodegradability and biocompatibility. The difference between PLA and PLGA are the products produced after their metabolism in the body: while PLA breaks into monomers of lactic acid, PLGA produces monomers of lactic acid and glycolic acid [21].

The maximum absorbance of anionic and cationic CUR-NPs were 2.272 a.u. (425 nm) and 2.256 a.u. (426 nm), respectively, while the free CUR absorbance was 1.645 a.u. at 429 nm wavelength. These data are in agreement with the data found in other studies, which showed that CUR absorbs blue light at wavelength between 408–434 nm [11,18]. The anionic and cationic CUR-NPs showed a reduction in the absorbance band of 60.48% and 42.19%, respectively, after 5 min of irradiation, corresponding to 10.85 J/cm^2, while the free CUR showed a decrease of 20.26% after the same light dose. The results observed with the CUR-NPs were similar to a previous investigation [16] that demonstrated a CUR degradation of 50% with a light dose of 9.4 J/cm^2. However, Dovigo et al. [11], observed a degradation of 70% after a lower light dose of 0.4 J/cm^2. These differences could be explained by the different concentrations of free CUR and CUR-NPs used in this study and in the another investigation [11].

In the present investigation, the EE percentage was 67% for the anionic CUR-NPs and 64.67% for the cationic CUR-NPs. Previous studies showed higher EE, varying from 78.95% to 97% [31,33,37,38]. The difference in the EE percentage could be explained by the centrifugation speed and time. In the present investigation, a centrifugation of 6,000 *xg* for 10 minutes was applied, while others studies have used higher velocities and longer times to determine the EE (15,000 rpm for 1 hour [31], 15,000 xg for 15 minutes [38]). This difference in the EE percentage could also be explained by the different methods employed in others studies, such as High Performance Liquid Chromatography (HPLC), which achieved EE values of 46.9, 77.07,

89, and 90% [33,36,39,40]. The chromatographic condition could be adjusted to the physico-chemical characteristics of the nanocarrier without interfering in the structure of the polymeric nanoformulation, which is an advantage of the HPLC method over the UV-VIS method [41].

The present study also evaluated the CUR release from the NPs and the results showed a gradual release of 96% after 48 hours. Krausz et al. [17] obtained similar results, since a CUR release of 42.3% occured in the first 6 hours, achieving 81.5% after 24 hours. However, these high release values are different from those found in other studies, which demonstrated CUR releases of 40.5% and 75.7% after the first 24 hours and eight days [33], 21% and 56.9% after 24 hours and 9 days [36], and 20% and 80% after 24 hours and 360 hours [19]. When CUR was encapsulated in chitosan, alginate, and starch, release values of 92.8% after 96 hours, 51.4% after 24 hours, and 73.4% after 96 hours, respectively, were found [20]. These differences may be attributed to the polymers used for the encapsulation process and the methodology employed to evaluate the drug release (HPLC [36], dialysis membrane [31]).

Eradication of planktonic cultures of *S. mutans*, *C. albicans*, and MRSA was observed when free CUR was associated with blue light after 40 minutes of pre-irradiation and a light dose of 43.2 J/cm^2. The light dose used in this research is similar to that used by Paschoal et al. [42], who used 42 J/cm^2 for CUR at 0.75 μM, and they observed a reduction of 5.37 $\log_{10}$ in the planktonic culture of *S. mutans*. Another study showed that 15 mg/mL of CUR used as PS and a light dose of 5.7 J/cm^2 yielded inactivation of *S. mutans* culture [43]. Regarding the photoinactivation of planktonic cultures of *C. albicans*, previous studies exhibited yeast eradication using CUR at 20 μM and a light dose of 5.28 J/cm^2 [11,13]. In another study, aPDT mediated by CUR and blue light against MRSA planktonic cultures [44] was tested, and it showed a reduction of 9.8 $\log_{10}$, associated with free CUR at 20 μM and a light dose of 37.5 J/cm^2.

In this study, 130 μM of CUR-NPs and free CUR were used for the antimicrobial evaluation of the planktonic cultures. A lower Minimum Inhibitory Concentration (MIC) was found in previous studies [10], corresponding to 23.5 μM against *C. albicans*. This could explain the reduction of 2.43 $\log_{10}$ of *C. albicans* and 0.75 $\log_{10}$ for *S. mutans* when treated only with free CUR (C+L- group), but this result was not observed for MRSA. MIC values of 0.128 mg/mL [45] and 125 μmol/L [46] have been reported against *S. mutans*, and values of 125–250 mg/mL [47] and 217 mg/mL [48] have been found for MRSA. MIC values of 6 mg/mL was also found for *S. aureus* and *S. mutans* and 1.5 mg/mL for *C. albicans*, but no microbicidal effect (absence of colonies growth) was observed for these species [31].

As expected, in the present investigation the planktonic cultures showed higher susceptibility to aPDT compared with the biofilms. Few studies showed photoinactivation of multispecies biofilm. Results obtained in this research using free CUR agree with previous studies which showed inhibition of dual-species biofilm composed of *S. mutans* and *Lactobacillus acidophilus* by aPDT mediated by CUR at 0.75, 1.5, and 3.0 g/L, resulting in reductions of 97.5, 95 and 99.9%, respectively, of microbial inactivation [43]. A higher concentration of PS was used in this research to inhibit the multispecies biofilm, similar to the study performed by Quishida et al. [49] who observed a significant reduction of a 48h-multispecies biofilm formed by *C. albicans*, *C. glabrata*, and *S. mutans* after aPDT mediated by CUR at 120 μM. In another study using a multispecies biofilm of *C. albicans*, *S. aureus*, and *S. mutans*, inhibitions of 1.00, 1.4,7 and 1.25 $\log_{10}$, respectively, were observed using 0.1 mg/mL of methylene blue as PS [50]. On the other hand, some studies applied aPDT against monospecies biofilm, and observed a reduction of 85% in the metabolism of *C. albicans* biofilm using CUR at a concentration of 40 μM and 20 minutes of pre-irradiation time with a light fluence of 18 J/cm^2 [12].

The anionic CUR-NPs demonstrated an antimicrobial photodynamic effect against planktonic cultures, since a microbicidal effect was observed only when CUR-NPs were exposed to

light, and no antimicrobial effect was verified for samples submitted to CUR-NPs without light, nor with NPs by themselves. However this photoinactivation was low, since there was no complete photoinactivation of the three microorganisms evaluated (*S. mutans*, *C. albicans*, and MRSA), as was observed with the free CUR. However, it's important to emphasize that free CUR at the same concentrarion of CUR-NP (260 μM) did not reduce the triple-species biofilm evaluated in this investigation (data not shown); so higher concentrations were evaluated and only 1,200 μM resulted in photoinactivation. When the anionic formulation was applied to the biofilms, only *S. mutans* was susceptible to aPDT in mono-species biofilm. Conversely, for the triple-species biofilm, no photodynamic inactivation was verified, since the three species were able to grow after aPDT similar to the control (C-L- group). This result could be explained by the surface charge (anionic) of the CUR-NPs, because some studies have shown that cationic PSs demonstrated an improved antimicrobial effect when compared with anionic ones [51,52]. Exopolysaccharides of the biofilm matrix have an anionic charge [53], which generates repulsion against anionic external agents. Therefore, the effect of anionic PSs is limited. Moreover, the slow release of CUR from the NPs demonstrated in this investigation may also explain the reduced antimicrobial photodynamic effect of anionic CUR-NP. In addition, washing the triple-species biofilm after incubation with free CUR and anionic CUR-NP abolished the photodynamic effect against *C. albicans*. This result corroborates with a previous investigation that demonstrated that washing CUR from planktonic suspension of *C. albicans* reduced the fungal photoinactivation [11].

Due to the limited effect of the anionic CUR-NP against biofilm, CTAB was incorporated in the formulation in order to produce cationic CUR-NP [22]. The results of the microbiological evaluation demonstrated that cationic nanoparticles, CUR-NPs, and NPs, had a microbicidal effect since they were able to eradicate the growth of the three microorganisms evaluated in the planktonic cultures. When these species were grown as biofilms, an antimicrobial effect against the three microorganisms was observed for cationic NPs with or without CUR, even in the absence of light, since reductions of colonies were observed. Even washing biofilms after incubation with cationic CUR-NP resulted in decreased viability for all species. Therefore, the reduction in the microbial viability observed for samples submitted to cationic formulations may be attributed to the their toxic effect to microbial cells, as also observed in the viability assay with mammalian cells (keratinocytes). The microbicidal effect could be explained by the CTAB incorporation in the formulation, since it was demonstrated that this compound causes lysis in the cell wall of *S. aureus*, *Enterococcus faecalis*, and *Escherichia coli* [54].

Several studies have demonstrated antimicrobial activity of CUR-NP, but only against planktonic cultures. The minimum inhibitory concentration (MIC) of 100 μg/mL of the CUR-NPs synthesized by the wet milling technique in planktonic cultures of *S. aureus* compared to CUR in DMSO (150 mg/mL) was observed in a previous study [55]. Another investigation demonstrated a MIC of 30 mg/mL against planktonic MRSA cultures using up-conversion nanoparticles conjugated with CUR after infrared light irradiation for 30 minutes [56]. Nanoparticles containing CUR produced a reduction of 97% in the viability of the planktonic MRSA cultures after incubation of 4 hours [17]. Hazzah et al. [31] synthesized solid lipid CUR-NPs and they observed lower MIC values against *S. aureus*, *S. mutans*, and *C. albicans* compared with raw CUR. CUR nanospheres at 1 mg/mL inhibited *E. coli*, *S. aureus*, and *C. albicans* after incubation of 24 hours [57]. CUR loaded in chitosan, alginate and starch showed MIC values of 0.114, 0.204, and 0.204 mg/mL, lower than free CUR (0.438 mg/mL), to inhibit *S. mutans* growth [20]. Inhibition zones of 17 mm for MRSA and *S. aureus*, 18 mm for *E. coli* and *Klebsiella pneumonia*, both resistant and not resistant to extended-spectrum β-lactamase, was observed on agar culture using electro-spun CUR loaded into poly-(2-hydroxyethyl methacrylate) nanofiber incubated overnight on suspensions of these microorganisms [58].

Few studies have evaluated aPDT mediated by CUR in nanocarriers. Baltazar et al. [18] found complete inactivation of the planktonic culture of *T. rubrum* treated with a nanoparticle containing CUR at 10 μg/mL for 10 minutes of pre-irradiation time and blue light at 10 J/cm^2. Fungal growth was inhibited by 7 days after treatment. An aquous solution of CUR in polyvinylpyrrolidone (PVP-C) at 5 μM incubated for 5 minutes with planktonic cultures of *S. aureus* followed by a light fluence of 33.8 J/cm^2 resulted in bacterial photoinactivation of more than 6 $\log_{10}$. Increasing the PVP-C concentration to 50 μM and the incubation period to 25 minutes prior illumination resulted in the complete eradication of the Gram(+) bacterium [59]. When aPDT was used for food decontamination, PVP-C at 50 μM and at 100 μM immediately associated to the same light fluence reduced *S. aureus* in 2.6 $\log_{10}$ and 2.5 $\log_{10}$ from cucumber and pepper [60]. In an ex vivo porcine model, the same parameters of aPDT mediated by PVP-C resulted in a higher reduction (1.7 $\log_{10}$ and 1.3 $\log_{10}$) of *S. aureus* than those observed for *E. coli* (0.0 $\log_{10}$ and 0.3 $\log_{10}$). When a cationic derivative of CUR at 50 μM and 100 μM was associated to light at 33.8 J/cm^2, photoinactivation of the Gram(-) species was improved, since reductions of 2.2 $\log_{10}$ and 1.8 $\log_{10}$ for *S. aureus* and 3.2 $\log_{10}$ and 3.3 $\log_{10}$ for *E. coli* were observed [61].

The results of the present investigation against biofilms agree with other studies, in which erradication of biofilm was not observed. Hegge et al. [16], observed less than 1 $\log_{10}$ reduction of *S. epidermidis* biofilm after aPDT mediated by CUR solubilized in polyethylene glycol 400, pluronic F127, and hydroxypropyl-γ-cyclodextrin. CUR in micellar NP combined with silver NP at 30 μg/mL CUR and 3.75 μg/mL Ag supressed the biofilm formation of *S. aureus* and *P. aeruginosa*. However, a higher concentration (400 μg/mL of CUR-NP and 50 μg/mL of AgNP) was necessary to reduce by 70% the biomass of pre-formed biofilms [19]. Inhibition of biofilm formation from 89.48% to 99.38% was observed when *S. mutans* was incubated with CUR loaded in polysaccharide NP [20]. In the present investigation, the susceptibility of each species to aPDT varied, and the reduction rates (near to 1–3 $\log_{10}$) were similar in mono-, dual-, and triple-species biofilms. Conversely, Pereira et al. verified that singlespecies biofilm of *S. mutans*, *S. aureus* and *C. albicans* showed a higher susceptibility to aPDT mediated by methylene blue and laser compared with dual- and triple-species biofilms [50]. The difference between the outcomes of these studies may be atributted to the different PS, light source, and aPDT parameters employed for biofilm inactivation.

In the present investigation, anionic CUR-NP showed the lowest antimicrobial photodynamic effect, while cationic CUR-NP was cytotoxic. However, free CUR needed a concentration 4.62 times higher than CUR-NPs to promote a significant reduction in mixed-species biofilms. Since the maximum CUR concentration able to be encapsulated in NP was 260 μM, we couldn't conclude that CUR-NP was more effective than free CUR. Regarding the biological relevance, several investigations reported that, according to the American Society for Microbiology and CLSI standards, reduction of 3 $\log_{10}$ are considered to be biologically relevant [62,63,64,65]. Thus, although the results of this investigation showed significant reductions of $\log_{10}$(CFU/ml) values, reductions lower than 3 $\log_{10}$, such as those observed for some biofilms, may not be considered biologically relevant. Future studies should be conducted in order to improve the formulation of CUR and the efficacy of aPDT.

CUR is auto-fluorescent and emits a green fluorescence [37]. In this research, confocal microscopy showed that washing the PS from the biofilm reduced the fluorescence, although its intensity was not measured. This result agrees with that of the viability assay [$\log_{10}$(CFU/mL)] with washed biofilms, which demonstrated lower values compared with non-washed biofilms. Therefore, washing the PS reduced the photoinactivation of the biofilm, as demonstrated in previous studies that report that CUR in the bulk solution increases the photoinactivation of

bacteria [66] and mono-species biofilm of *C. albicans* [11]. While cationic CUR-NP showed uptake by all cell morphologies found in the triple-species biofilm evaluated, free CUR demonstrated better uptake by bacteria, but anionic CUR-NP was not taken up by yeast, which justify the low photoinactivation of planktonic *C. albicans* with anionic CUR-NP (only 0.78 $\log_{10}$). This result was similar to that obtained in another study performed with free CUR, in which CUR was taken up by *S. aureus* [58]. The mechanism of incorporating the CUR-NPs into the bacteria is the fixation of the PS onto the bacterial wall, followed by breaking the peptidoglycan layer and finally the penetration of the PS to within the microorganism [55,67,68]. Andrade et al. [13] observed CUR uptake in *C. albicans* after a five- and a twenty-minute incubation using confocal laser scanning microscopy. In the present investigation, the biofilm labeled with SYTO-9 (control group) was thicker than those treated with free CUR and anionic CUR-NP, suggesting that these PSs were not able to penetrate deeply into the biofilm. This result agrees with Andrade et al. [13], who reported that CUR does not photosensitise the deepest cells inside the biofilm, but only the cells located in the outermost layers, which may explain the incomplete inactivation of the biofilm in this study. On the other hand, cationic CUR-NP showed thickness values more similar to the control group, which suggests that the atractive force between the positive charge of the formulation and the negative charge of the biofilm increases the PS penetration into the biofilm. However, it is important to emphasize that the thickness measured in the z-stack produced by the confocal microscope is related to the fluorescence of the labeled biofilm. This being the case, the deepest layers of cells may not have been labeled even by the SYTO-9, since it was used on pre-formed biofilms. Ideally, the biofilm should grow in the presence of the fluorophore to label the whole biofilm and for its thickness to be measured accurately.

In the present research, the anionic formulations (NP and CUR-NP) showed a similar cell viability percentage compared to the negative control group cultured with DMEM, which demonstrates that the anionic CUR-NP developed in this investigation is not cytotoxic. It confirms that PLA is a biocompatible polymer having low toxicity and is an attractive compound to encapsulate drugs. Similar to keratinocytes treated with Triton X-100, cationic CUR-NP and 10% DMSO (free CUR vehicle) showed cellular toxicity. Although samples treated with cationic NP after 24 hours and with free CUR in both periods showed significant difference compared with the positive control group (Triton X-100), they demonstrated cell viabilities under 40%, which is considered cytotoxic [69]. As observed in the microbiological assays, the cytotoxicity observed for cationic formulations (NP and CUR-NP) may be atributed to CTAB. Moreover, the cytotoxic effect of free CUR may be explained by the high concentration of DMSO (10%) used in the present investigation, since the same concentration used in antimicrobial assays was evaluated in the cytotoxic assay. However, the concentration of DMSO recommended to test cell viability is lower than 1% [70]. Therefore, the encapsulation of CUR with NP overcomes the cytotoxic effect of organic solvents.

In conclusion, encapsulation of CUR in polymeric nanoparticles was performed successfully using PLA as polymer, and the properties of the CUR-NPs were similar to those of the free CUR. The anionic CUR-NPs showed reduced photoinactivation of biofilms and no cytotoxicity, while the cationic CUR-NPs and NPs showed antimicrobial activity even without light but they were cytotoxic. However, only mature biofilms were evaluated in this study. It was demonstrated that micro-organisms growing in the presence of CUR-NP resulted in inhibition of biofilm formation [19,20]. Nonetheless, the ability of CUR to inhibit multispecies biofilm formation was not assessed in this investigation. In addition, further studies developing cationic systems of faster release of drugs should be investigated for aPDT.

Acknowledgments

The authors wish to thank the Institute of Chemistry (UNESP) for the FEG-SEM, Jessica Bernegossi and Professor Marlus Chorilli for supporting the use of ZetaSizer Nano, and Geisiane Helena Gomes Bueno for the technical support in the microbiological experiments.

Author Contributions

Conceptualization: Paula Aboud Barbugli, Ewerton Garcia de Oliveira Mima.

Data curation: Jeffersson Krishan Trigo Gutierrez, Ewerton Garcia de Oliveira Mima.

Formal analysis: Jeffersson Krishan Trigo Gutierrez, Ewerton Garcia de Oliveira Mima.

Funding acquisition: Ana Cláudia Pavarina, Paula Aboud Barbugli, Ewerton Garcia de Oliveira Mima.

Investigation: Jeffersson Krishan Trigo Gutierrez, Ewerton Garcia de Oliveira Mima.

Methodology: Jeffersson Krishan Trigo Gutierrez, Gabriela Cristina Zanatta, Ana Laura Mira Ortega, Maria Isabella Cuba Balastegui, Paula Aboud Barbugli, Ewerton Garcia de Oliveira Mima.

Project administration: Ewerton Garcia de Oliveira Mima.

Resources: Ewerton Garcia de Oliveira Mima.

Supervision: Ewerton Garcia de Oliveira Mima.

Writing – original draft: Jeffersson Krishan Trigo Gutierrez, Ewerton Garcia de Oliveira Mima.

Writing – review & editing: Jeffersson Krishan Trigo Gutierrez, Paula Volpato Sanitá, Ana Cláudia Pavarina, Paula Aboud Barbugli, Ewerton Garcia de Oliveira Mima.

References

1. Lemos JA, Quivey RG Jr, Koo H, Abranches J. *Streptococcus mutans*: a new Gram-positive paradigm?. Microbiology. 2013; 159: 436–445. https://doi.org/10.1099/mic.0.066134-0 PMID: 23393147
2. Sardi JC, Scorzoni L, Bernardi T, Fusco-Almeida AM, Mendes Giannini MJ. *Candida* species: current epidemiology, pathogenicity, biofilm formation, natural antifungal products and new therapeutic options. J Med Microbiol. 2013; 62: 10–24. https://doi.org/10.1099/jmm.0.045054-0 PMID: 23180477
3. Cassone A, Cauda R. *Candida* and candidiasis in HIV-infected patients: where commensalism, opportunistic behavior and frank pathogenicity lose their borders. AIDS. 2012; 26: 1457–1472. https://doi.org/10.1097/QAD.0b013e3283536ba8 PMID: 22472853
4. Oud L. Secular trends in utilization of critical care services among candidemia-associated hospitalizations: a population-based cohort study. J Clin Med Res. 2016; 8: 40–43. https://doi.org/10.14740/jocmr2387w PMID: 26668681
5. Russotto V, Cortegiani A, Graziano G, Saporito L, Raineri SM, Mammina C, et al. Bloodstream infections in intensive care unit patients: distribution and antibiotic resistance of bacteria. Infect Drug Resist. 2015; 10: 287–296.
6. Zago CE, Silva S, Sanitá PV, Barbugli PA, Dias CM, Lordello VB, et al. Dynamics of biofilm formation and the interaction between *Candida albicans* and methicillin-susceptible (MSSA) and -resistant *Staphylococcus aureus* (MRSA). PloS One. 2015; 10: e0123206. https://doi.org/10.1371/journal.pone.0123206 PMID: 25875834
7. Falsetta ML, Klein MI, Colonne PM, Scott-Anne K, Gregoire S, Pai CH, et al. Symbiotic relationship between *Streptococcus mutans* and *Candida albicans* synergizes virulence of plaque biofilms in vivo. Infect Immun. 2014; 82: 1968–1981. https://doi.org/10.1128/IAI.00087-14 PMID: 24566629
8. Soukos NS, Goodson JM. Photodynamic therapy in the control of oral biofilms. Periodontol 2000. 2011; 55: 143–166. https://doi.org/10.1111/j.1600-0757.2010.00346.x PMID: 21134233

9. Hamblim MR Antimicrobial photodynamic inactivation: a bright new technique to kill resistant microbes. Curr Opin Microbiol. 2016; 33: 67–73. https://doi.org/10.1016/j.mib.2016.06.008 PMID: 27421070

10. Martins CV, da Silva DL, Neres AT, Magalhães TF, Watanabe GA, Modolo LV, et al. Curcumin as a promising antifungal of clinical interest. J Antimicrob Chemother. 2009; 63: 337–339. https://doi.org/10.1093/jac/dkn488 PMID: 19038979

11. Dovigo LN, Pavarina AC, Ribeiro AP, Brunetti IL, Costa CA, Jacomassi DP, et al. Investigation of the photodynamic effects of curcumin against *Candida albicans*. Photochem Photobiol. 2011; 87: 895–903. https://doi.org/10.1111/j.1751-1097.2011.00937.x PMID: 21517888

12. Dovigo LN, Pavarina AC, Carmello JC, Machado AL, Brunetti IL, Bagnato VS. Susceptibility of clinical isolates of *Candida* to photodynamic effects of curcumin. Lasers Surg Med. 2011; 43: 927–934. https://doi.org/10.1002/lsm.21110 PMID: 22006736

13. Andrade MC, Ribeiro AP, Dovigo LN, Brunetti IL, Giampaolo ET, Bagnato VS, et al. Effect of different pre-irradiation times on curcumin-mediated photodynamic therapy against planktonic cultures and biofilms of *Candida* spp. Arch Oral Biol. 2013; 58: 200–210. https://doi.org/10.1016/j.archoralbio.2012.10.011 PMID: 23153629

14. Vrignaud S, Benoit JP, Saulnier P. Strategies for the nanoencapsulation of hydrophilic molecules in polymer-based nanoparticles. Biomaterials. 2011; 32: 8593–8604. https://doi.org/10.1016/j.biomaterials.2011.07.057 PMID: 21831421

15. Mohamed F, van der Walle CF. Engineering biodegradable polyester particles with specific drug targeting and drug release properties. J Pharm Sci. 2008; 97: 71–87. https://doi.org/10.1002/jps.21082 PMID: 17722085

16. Hegge AB, Bruzell E, Kristensen S, Tønnesen HH. Photoinactivation of *Staphylococcus epidermidis* biofilms and suspensions by the hydrophobic photosensitizer curcumin—effect of selected nanocarrier: studies on curcumin and curcuminoides XLVII. Eur J Pharm Sci. 2012; 47: 65–74. https://doi.org/10.1016/j.ejps.2012.05.002 PMID: 22609527

17. Krausz AE, Adler BL, Cabral V, Navati M, Doerner J, Charafeddine RA, et al. Curcumin-encapsulated nanoparticles as innovative antimicrobial and wound healing agent. Nanomedicine. 2015; 11: 195–206. https://doi.org/10.1016/j.nano.2014.09.004 PMID: 25240595

18. Baltazar LM, Krausz AE, Souza AC, Adler BL, Landriscina A, Musaev T, et al. *Trichophyton rubrum* is inhibited by free and nanoparticle encapsulated curcumin by induction of nitrosative stress after photodynamic activation. PLoS ONE. 2015; 10: e0120179. https://doi.org/10.1371/journal.pone.0120179 PMID: 25803281

19. Loo CY, Rohanizadeh R, Young PM, Traini D, Cavaliere R, Whitchurch CB, et al. Combination of silver nanoparticles and curcumin nanoparticles for enhanced anti-biofilm activities. J Agric Food Chem. 2016; 64: 2513–2522. https://doi.org/10.1021/acs.jafc.5b04559 PMID: 26595817

20. Maghsoudi A, Yazdian F, Shahmoradi S, Ghaderi L, Hemati M, Amoabediny G. Curcumin-loaded polysaccharide nanoparticles: optimization and anticariogenic activity against *Streptococcus mutans*. Mater Sci Eng C Mater Biol Appl. 2017; 75: 1259–1267. https://doi.org/10.1016/j.msec.2017.03.032 PMID: 28415415

21. Kumari A, Yadav SK, Yadav SC. Biodegradable polymeric nanoparticles based drug delivery systems. Colloids Surf B Biointerfaces. 2010; 75: 1–18. https://doi.org/10.1016/j.colsurfb.2009.09.001 PMID: 19782542

22. Zou W, Liu C, Chen Z, Zhang N. Preparation and characterization of cationic PLA-PEG nanoparticles for delivery of plasmid DNA. Nanoscale Res Lett. 2009; 4: 982–992. https://doi.org/10.1007/s11671-009-9345-3 PMID: 20596550

23. Yallapu MM, Gupta BK, Jaggi M, Chauhan SC. Fabrication of curcumin encapsulated PLGA nanoparticles for improved therapeutic effects in metastatic cancer cells. J Colloid Interface Sci. 2010; 351: 19–29. https://doi.org/10.1016/j.jcis.2010.05.022 PMID: 20627257

24. Castilho RM, Squarize CH, Leelahavanichk L K, Zheng Y, Bugge T, Gutkind JS. Rac1 is required for epithelial stem cell function during dermal and oral mucosal wound healing but not for tissue homeostasis in mice. PLoS One. 2010; 5: e10503. https://doi.org/10.1371/journal.pone.0010503 PMID: 20463891

25. de Carvalho Dias K, Barbugli PA, de Patto F, Lordello VB, de Aquino Penteado L, Medeiros AI, Vergani CE. Soluble factors from biofilm of *Candida albicans* and *Staphylococcus aureus* promote cell death and inflammatory response. BMC Microbiol. 2017; 17: 146. https://doi.org/10.1186/s12866-017-1031-5 PMID: 28666415

26. O'Brien J, Wilson I, Orton T, Pognan F. Investigation of the Alamar Blue (resazurin) fluorescent dye for the assessment of mammalian cell cytotoxicity. Eur J Biochem. 2000; 267: 5421–5426. PMID: 10951200

27. Couvreur P, Barratt G, Fattal E, Legrand P, Vauthier C. Nanocapsule technology: a review. Crit Rev Ther Drug Carrier Syst. 2002; 19: 99–134. PMID: 12197610

28. Farah S, Anderson DG, Langer R. Physical and mechanical properties of PLA, and their functions in widespread applications—A comprehensive review. Adv Drug Deliv Rev. 2016; 107: 367–392. https://doi.org/10.1016/j.addr.2016.06.012 PMID: 27356150

29. Shah AA, Kato S, Shintani N, Kamini NR, Nakajima-Kambe T. Microbial degradation of aliphatic and aliphatic-aromatic co-polyesters. Appl Microbiol Biotechnol. 2014; 98: 3437–3447. https://doi.org/10.1007/s00253-014-5558-1 PMID: 24522729

30. Vauthier C, Bouchemal K. Methods for the preparation and manufacture of polymeric nanoparticles. Pharm Res. 2009; 26: 1025–1058. https://doi.org/10.1007/s11095-008-9800-3 PMID: 19107579

31. Hazzah HA, Farid RM, Nasra MM, Hazzah WA, El-Massik MA, Abdallah OY. Gelucire-based nanoparticles for curcumin targeting to oral mucosa: preparation, characterization, and antimicrobial activity assessment. J Pharm Sci. 2015; 104: 3913–3924. https://doi.org/10.1002/jps.24590 PMID: 26202796

32. Gaumet M, Vargas A, Gurny R, Delie F. Nanoparticles for drug delivery: the need for precision in reporting particle size parameters. Eur J Pharm Biopharm. 2008; 69: 1–9. https://doi.org/10.1016/j.ejpb.2007.08.001 PMID: 17826969

33. Chereddy KK, Coco R, Memvanga PB, Ucakar B, des Rieux A, Vandermeulen G, et al. Combined effect of PLGA and curcumin on wound healing activity. J Control Release. 2013; 171: 208–215. https://doi.org/10.1016/j.jconrel.2013.07.015 PMID: 23891622

34. Shaikh J, Ankola D, Beniwal V, Singh D, Kumar MN. Nanoparticle encapsulation improves oral bioavailability of curcumin by at least 9-fold when compared to curcumin administered with piperine as absorption enhancer. Eur J Pharm Sci. 2009; 37: 223–230. https://doi.org/10.1016/j.ejps.2009.02.019 PMID: 19491009

35. Ghosh D, Choudhury ST, Ghosh S, Mandal AK, Sarkar S, Ghosh A, et al. Nanocapsulated curcumin: oral chemopreventive formulation against diethylnitrosamine induced hepatocellular carcinoma in rat. Chem Biol Interact. 2012; 195: 206–214. https://doi.org/10.1016/j.cbi.2011.12.004 PMID: 22197969

36. Khalil NM, do Nascimento TC, Casa DM, Dalmolin LF, de Mattos AC, Hoss I, et al. Pharmacokinetics of curcumin-loaded PLGA and PLGA-PEG blend nanoparticles after oral administration in rats. Colloids Surf B Biointerfaces. 2013; 101: 353–360. https://doi.org/10.1016/j.colsurfb.2012.06.024 PMID: 23010041

37. Udompornmongkol P, Chiang BH. Curcumin-loaded polymeric nanoparticles for enhanced anti-colorectal cancer applications. J Biomater Appl. 2015; 30: 537–546. https://doi.org/10.1177/0885328215594479 PMID: 26170212

38. Mukerjee A, Vishwanatha JK. Formulation, characterization and evaluation of curcumin-loaded PLGA nanospheres for cancer therapy. Anticancer Res. 2009; 29: 3867–3875. PMID: 19846921

39. Tsai YM, Chien CF, Lin LC, Tsai TH. Curcumin and its nano-formulation: the kinetics of tissue distribution and blood–brain barrier penetration. Int J Pharm. 2011; 416: 331–338. https://doi.org/10.1016/j.ijpharm.2011.06.030 PMID: 21729743

40. Mohanty C, Sahoo SK. The in vitro stability and in vivo pharmacokinetics of curcumin prepared as an aqueous nanoparticulate formulation. Biomaterials. 2010; 31: 6597–6611. https://doi.org/10.1016/j.biomaterials.2010.04.062 PMID: 20553984

41. Sartori T, Seigi Murakami F, Pinheiro Cruz A, Machado de Campos A. Development and validation of a fast RP-HPLC method for determination of methotrexate entrapment efficiency in polymeric nanocapsules. J Chromatogr Sci. 2008; 46: 505–509. PMID: 18647471

42. Paschoal MA, Tonon CC, Spolidório DMP, Bagnato VS, Giusti JSM, Santos-Pinto L. Photodynamic potential of curcumin and blue LED against *Streptococcus mutans* in a planktonic culture. Photodiagnosis Photodyn Ther. 2013; 10: 313–319. https://doi.org/10.1016/j.pdpdt.2013.02.002 PMID: 23993858

43. Araújo NC, Fontana CR, Bagnato VS, Gerbi ME. Photodynamic effects of curcumin against cariogenic pathogens. Photomed Laser Surg. 2012; 30: 393–399. https://doi.org/10.1089/pho.2011.3195 PMID: 22693952

44. Ribeiro AP, Pavarina AC, Dovigo LN, Brunetti IL, Bagnato VS, Vergani CE, et al. Phototoxic effect of curcumin on methicillin-resistant *Staphylococcus aureus* and L929 fibroblasts. Lasers Med Sci. 2013; 28: 391–398. https://doi.org/10.1007/s10103-012-1064-9 PMID: 22358772

45. Song J, Choi B, Jin EJ, Yoon Y, Choi KH. Curcumin suppresses *Streptococcus mutans* adherence to human tooth surfaces and extracellular matrix proteins. Eur J Clin Microbiol Infect Dis. 2012; 31: 1347–1352. https://doi.org/10.1007/s10096-011-1448-y PMID: 22009290

46. Hu P, Huang P, Chen MW. Curcumin reduces *Streptococcus mutans* biofilm formation by inhibiting sortase A activity. Arch Oral Biol. 2013; 58: 1343–1348. https://doi.org/10.1016/j.archoralbio.2013.05.004 PMID: 23778072

47. Moghadamtousi SZ, Kadir HA. Hassandarvish P, Tajik H, Abubakar S, Zandi K. A review on antibacterial, antiviral, and antifungal activity of curcumin. BioMed Res Int. 2014; 2014: 186864. https://doi.org/10.1155/2014/186864 PMID: 24877064

48. Gunes H, Gulen D, Mutlu R, Gumus A, Tas T, Topkaya AE. Antibacterial effects of curcumin: an in vitro minimum inhibitory concentration study. Toxicol Ind Health. 2016; 32: 246–250. https://doi.org/10.1177/0748233713498458 PMID: 24097361

49. Quishida CC, De Oliveira Mima EG, Jorge JH, Vergani CE, Bagnato VS, Pavarina AC. Photodynamic inactivation of a multispecies biofilm using curcumin and LED light. Lasers Med Sci. 2016; 31: 997–1009. https://doi.org/10.1007/s10103-016-1942-7 PMID: 27126412

50. Pereira CA, Romeiro RL, Costa AC, Machado AK, Junqueira JC, Jorge AO. Susceptibility of *Candida albicans*, *Staphylococcus aureus*, and *Streptococcus mutans* biofilms to photodynamic inactivation: an in vitro study. Lasers Med Sci. 2011; 26: 341–348. https://doi.org/10.1007/s10103-010-0852-3 PMID: 21069408

51. Junqueira JC, Jorge AO, Barbosa JO, Rossoni RD, Vilela SF, Costa AC, et al. Photodynamic inactivation of biofilms formed by *Candida* spp., *Trichosporon mucoides*, and *Kodamaea ohmeri* by cationic nanoemulsion of zinc 2,9,16,23-tetrakis(phenylthio)-29H, 31H-phthalocyanine (ZnPc). Lasers Med Sci. 2012; 27: 1205–1212. https://doi.org/10.1007/s10103-012-1050-2 PMID: 22278349

52. Ribeiro AP, Andrade MC, Bagnato VS, Vergani CE, Primo FL, Tedesco AC, et al. Antimicrobial photodynamic therapy against pathogenic bacterial suspensions and biofilms using chloro-aluminum phthalocyanine encapsulated in nanoemulsions. Lasers Med Sci. 2015; 30: 549–559. https://doi.org/10.1007/s10103-013-1354-x PMID: 23748800

53. Al-Fattani MA, Douglas LJ. Biofilm matrix of *Candida albicans* and *Candida tropicalis*: chemical composition and role in drug resistance. J Med Microbiol. 2006; 55: 999–1008. https://doi.org/10.1099/jmm.0.46569-0 PMID: 16849719

54. Salton MR. The adsorption of cetyltrimethylammonium bromide by bacteria, its action in releasing cellular constituents and its bactericidal effects. J Gen Microbiol. 1951; 5: 391–404. https://doi.org/10.1099/00221287-5-2-391 PMID: 14832428

55. Mun SH, Kim SB, Kong R, Choi JG, Kim YC, Shin DW, et al. Curcumin reverse methicillin resistance in *Staphylococcus aureus*. Molecules. 2014; 19: 18283–18295. https://doi.org/10.3390/molecules191118283 PMID: 25389660

56. Ye Y, Li Y, Fang F. Upconversion nanoparticles conjugated with curcumin as a photosensitizer to inhibit methicillin-resistant *Staphylococcus aureus* in lung under near infrared light. Int J Nanomedicine. 2014; 9: 5157–5165. https://doi.org/10.2147/IJN.S71365 PMID: 25395852

57. Arunraj TR, Sanoj Rejinold N, Mangalathilham S, Saroj S, Biswas R, Jayakumar R. Synthesis, characterization and biological activities of curcumin nanospheres. J Biomed Nanotech. 2014; 10: 238–250.

58. Ramalingam N, Natarajan TS, Rajiv S. Preparation and characterization of electrospun curcumin loaded poly(2-hydroxyethyl methacrylate) nanofiber-a biomaterial for multidrug resistant organisms. J Biomed Mater Res A. 2015; 103: 16–24. https://doi.org/10.1002/jbm.a.35138 PMID: 24578218

59. Winter S, Tortik N, Kubin A, Krammer B, Plaetzer K. Back to the roots: photodynamic inactivation of bacteria based on water-soluble curcumin bound to polyvinylpyrrolidone as a photosensitizer. Photochem Photobiol Sci. 2013; 12: 1795–1802. https://doi.org/10.1039/c3pp50095k PMID: 23828307

60. Tortik N, Spaeth A, Plaetzer K. Photodynamic decontamination of foodstuff from *Staphylococcus aureus* based on novel formulations o curcumin. Photochem Photobiol Sci. 2014; 13: 1402–1409. https://doi.org/10.1039/c4pp00123k PMID: 24957403

61. Tortik N, Steinbacher P, Maisch T, Spaeth A, Plaetzer K. A comparative study on the antibacterial photodynamic efficiency of a curcumin derivative and a formulation on a porcine skin model. Photochem Photobiol Sci. 2016; 15: 187–195. https://doi.org/10.1039/c5pp00393h PMID: 26751838

62. Nakonieczna J. Comment on "Effectiveness of antimicrobial photodynamic therapy (AmPDT) on *Staphylococcus aureus* using phenothiazine compound with red laser". Lasers Med Sci. 2017; 32: 1667–1668.

63. Cieplik F, Tabenski L, Buchalla W, Maisch T. Antimicrobial photodynamic therapy for inactivation of biofilms formed by oral key pathogens. Front Microbiol. 2014; 5: 405. https://doi.org/10.3389/fmicb.2014.00405 PMID: 25161649

64. Taraszkiewicz A, Grinholc M, Bielawski KP, Kawiak A, Nakonieczna J. Imidazoacridinone derivatives as efficient sensitizers in photoantimicrobial chemotherapy. Appl Environ Microbiol. 2013; 79: 3692–3702. https://doi.org/10.1128/AEM.00748-13 PMID: 23563951

65. Kiesslich T, Gollmer A, Maisch T, Berneburg M, Plaetzer K. A comprehensive tutorial on in vitro characterization of new photosensitizers for photodynamic antitumor therapy and photodynamic inactivation of microorganisms. Biomed Res Int. 2013; 2013: 840417. https://doi.org/10.1155/2013/840417 PMID: 23762860

66. Dahl TA, McGowan WM, Shand MA, Srinivasan VS. Photokilling of bacteria by the natural dye curcumin. Arch Microbiol. 1989; 151: 183–185. PMID: 2655550

67. Tyagi P, Singh M, Kumari H, Kumari A, Mukhopadhyay K. Bactericidal activity of curcumin I is associated with damaging of bacterial membrane. PLoS ONE. 2015; 10: e0121313. https://doi.org/10.1371/journal.pone.0121313 PMID: 25811596

68. Basniwal RK, Buttar HS, Jain VK, Jain N. Curcumin nanoparticles: preparation, characterization, and antimicrobial study. J Agric Food Chem. 2011; 59: 2056–2061. https://doi.org/10.1021/jf104402t PMID: 21322563

69. Hamid R, Rotshteyn Y, Rabadi L, Parikh R, Bullock P. Comparison of alamar blue and MTT assays for high through-put screening. Toxicol in Vitro. 2004; 18: 703–710. https://doi.org/10.1016/j.tiv.2004.03.012 PMID: 15251189

70. Trivedi AB, Kitabatake N, Doi E. Toxicity of dimethyl sulfoxide as a solvent in bioassay system with HeLa cells evaluated colorimetrically with 3-(4,5-dimethyl thiazol-2-yl)-2,5-diphenyl-tetrazolium bromide. Agric Biol Chem. 1990; 54: 2961–2966. PMID: 1368650

3.3 Publicação 3·

molecules

MDPI

Article

Antimicrobial Photodynamic Therapy Mediated by Curcumin-Loaded Polymeric Nanoparticles in a Murine Model of Oral Candidiasis

Vinicius Tatsuyuji Sakima [1], Paula Aboud Barbugli [1], Paulo Sérgio Cerri [1], Marlus Chorilli [2], Juliana Cabrini Carmello [1], Ana Cláudia Pavarina [1] and Ewerton Garcia de Oliveira Mima [1,*]

[1] School of Dentistry, São Paulo State University (UNESP), Araraquara 14801-903, São Paulo, Brazil; sakima888@gmail.com (V.T.S.); pabfarma@yahoo.com.br (P.A.B.); pcerri@foar.unesp.br (P.S.C.); cabrini.juliana@gmail.com (J.C.C.); pavarina@foar.unesp.br (A.C.P.)

[2] School of Pharmaceutical Sciences, São Paulo State University (UNESP), Araraquara 14800-903, São Paulo, Brazil; chorilli@fcfar.unesp.br

* Correspondence: ewertonmima@foar.unesp.br; Tel.: +55-16-33016557; Fax: +55-16-33016406

Received: 14 July 2018; Accepted: 14 August 2018; Published: 19 August 2018



Abstract: Antimicrobial photodynamic therapy (aPDT) has been proposed as an alternative method for oral candidiasis (OC), while nanocarriers have been used to improve the water solubility of curcumin (CUR). The aim of this study is to encapsulate CUR in polymeric nanoparticles (NPs) and to evaluate its photodynamic effects on a murine model of OC. Anionic and cationic CUR-NP is synthesized using poly-lactic acid and dextran sulfate and then characterized. Female mice are immunosuppressed and inoculated with *Candida albicans* (Ca) to induce OC. aPDT is performed by applying CUR-NP or free CUR on the dorsum of the tongue, followed by blue light irradiation for five consecutive days. Nystatin is used as positive control. Afterward, Ca are recovered and cultivated. Animals are euthanized for histological, immunohistochemical, and DNA damage evaluation. Encapsulation in NP improves the water solubility of CUR. Nystatin shows the highest reduction of Ca, followed by aPDT mediated by free CUR, which results in immunolabelling of cytokeratins closer to those observed for healthy animals. Anionic CUR-NP does not show antifungal effect, and cationic CUR-NP reduces Ca even in the absence of light. DNA damage is associated with Ca infection. Consecutive aPDT application is a safe treatment for OC.

Keywords: photochemotherapy; nanoparticles; keratins; mice; *Candida albicans*; oral candidiasis; curcumin

1. Introduction

Candida albicans is an opportunist pathogen found in human mucosa that, under local or systemic conditions, might invade tissues and promote infection. *C. albicans* is the most prevalent species found in oral candidiasis (OC) [1]. OC is a common condition found in immunocompromised patients, especially those infected by human immunodeficiency virus (HIV), but also subjects under treatment with immunosuppressant agents, such as transplanted patients and those under chemotherapy [2]. Regarding those patients, the infection might spread from its original site and reach the bloodstream, causing a systemic infection known as candidaemia. Candidaemia is the fourth nosocomial infection with a high mortality rate—up to 50% [3].

OC is characterized by invasion of the hosts mucosal epithelium by the filamentous form (hyphae) of *C. albicans* [4]. Invasion occurs via two different ways: endocytosis, a process mediated by epithelial cells; or active penetration, in which a viable hypha penetrates through or between the epithelial cells. Regardless of the mechanism, invasion results in damage of the epithelium via necrosis and/or apoptosis [5]. To resist the external mechanical stress, the cytoplasm of epithelial cells has filaments of

· Artigo nas normas do periódico *Molecules*.

keratins called cytokeratins (CKs). CKs are protein constituents of the epithelial cytoskeleton found in the whole oral cavity and their specific level of expression is used to diagnose oral pathologies such as carcinomas [6]. While the CK13 is distributed in suprabasal layers of the stratified epithelium, the CK14 is expressed in non-differentiated basal cells of the stratified squamous epithelium. Both cytokeratins are expressed during morphogenesis of filiform and circumvallate papillae of rats [7,8]. However, to the best of the authors' knowledge, the expression of CKs in *C. albicans* infection is still unknown.

The conventional antifungal agents used for local and systemic candidiasis have shown some drawbacks, with the development of resistant strains being a serious health concern [9]. Therefore, new therapies have been investigated, such as antimicrobial photodynamic therapy (aPDT), which combines a photosensitizer agent (PS) and a light source. The interaction between PS and light in the presence of oxygen produces reactive species, such as singlet oxygen and free radicals that promote cell damage and death [10,11]. aPDT has been extensively used against cancer [12] and some studies have demonstrated its potential in the treatment of infections [13], including those of the oral cavity [11].

Curcumin (diferuloymethane, CUR) is a natural compound found in turmeric with several therapeutic properties such as anti-inflammatory, antioxidant, anticancer, and antimicrobial activity [14]. Previous studies demonstrated that, for an antifungal effect, CUR requires lower concentrations (7.4 mg/L, equivalent to 20 μM) when used as PS in aPDT [15,16] than when used alone without light (minimum inhibitory concentration of 64 mg/L or 173.73 μM) [17]. Associated with a blue light source (440–485 nm), CUR promotes complete photoinactivation of planktonic cultures and 87.22% reduction in the metabolic activity of biofilm cultures of *C. albicans* [15]. When clinical isolates of *Candida* spp. are evaluated, CUR-mediated aPDT results in complete photoinactivation of planktonic cultures of *C. albicans* and *Candida tropicalis* and significant reduction of *Candida glabrata*, while biofilms show more than a 73% reduction in the metabolic activity and more than 52% in the total biomass [16]. Confocal laser scanning microscopy shows photosensitization of *C. albicans* biofilm only in the outmost layers of the biofilm [18]. When a murine model of oral candidiasis is evaluated, a single application of aPDT with CUR results in reduction of over 4.00 $\log_{10}$ of yeast from the tongue of mice, without histological features of fungal infection [19]. To extend the period of oral candidiasis and to evaluate a therapeutic protocol of consecutive aPDT applications in mice, Carmello et al., 2016 [20] performed four immunosuppression and five aPDT applications with photodithazine (PDZ) and light-emitting diode (LED) light on the tongues of mice. They observed a significant reduction of 3.00 $\log_{10}$ in the viability of *C. albicans* after aPDT compared with the control (untreated animals), as well as a significant increase in the expression of the tumor necrosis factor α (TNF-α) [20].

CUR also improves the wound healing process acting in several pathways. It inhibits the production of pro-inflammatory cytokines; stimulates healing growth factors; increases antioxidant enzymes, fibroblast numbers, granulation tissue formation, and collagen deposition; and accelerates neovascularization, re-epithelialisation, and wound closure [21–24]. However, the wound healing process has usually been evaluated by topical application of CUR in cutaneous [25] and burn wounds [26], and few studies have evaluated infected tissues [27,28].

Despite these therapeutic effects, clinical use of CUR is limited because of insolubility in water (hydrophobicity), poor stability (hydrolytic, proteolytic, and photodegradation), and low bioavailability. Therefore, drug delivery systems have been investigated to overcome these drawbacks [24,29,30]. Research has been carried out to find more efficient drug delivery systems, associating CUR with different polymers forming a stable nano-structured polymeric system in this context. Nanoformulations of CUR have been used in infected tissues of rodents to evaluate its antimicrobial and healing efficacy. An ethosomal formulation of CUR inhibited the growth of *Pseudomonas aeruginosa* and improved the healing of burn wounds of rats [27]. CUR in nanoparticles (NP) of chitosan and polyethylene glycol reduced the viability of planktonic cultures of methicillin-resistant *Staphylococcus aureus* (MRSA) and *P. aeruginosa* in vitro, as well as that of MRSA in burn wounds of mice, which showed a faster wound closure, better maturation of granulation tissue, and improved neovascularization and collagen maturation after topical application [28].

A recent study synthesized CUR in nanoparticles (CUR-NPs) of poly-lactic acid (PLA) and dextran (DEX) and evaluated its antimicrobial efficacy in vitro. CUR-NP showed light absorbance and photodegradation similar to free CUR, and its photodynamic antimicrobial activity against planktonic cultures of *C. albicans*, *Streptococcus mutans*, and MRSA was higher compared with the results of biofilms of these species [31]. The synthesized CUR-NP is used in a murine model of oral candidiasis to evaluate its photodynamic effect in the present investigation. Moreover, the detection of epithelial CKs and the DNA damage in the host's tissue also are evaluated.

2. Results

2.1. Synthesis and Characterization of CUR-NPs

2.1.1. Physicochemical Properties and Morphology Analysis

The highest CUR concentration encapsulated in NPs was 260 µM, as higher concentrations resulted in aggregation of CUR. Anionic and cationic CUR-NPs were synthesized, and anionic and cationic NPs without CUR were synthesized as controls. The physicochemical properties were evaluated within a period interval of 0–29 days after the synthesis (Table 1). Images of field emission gun scanning electron microscopy (FEG-SEM) (Figure 1A–D) were captured nine days after the synthesis, showing spherical nanoparticles.

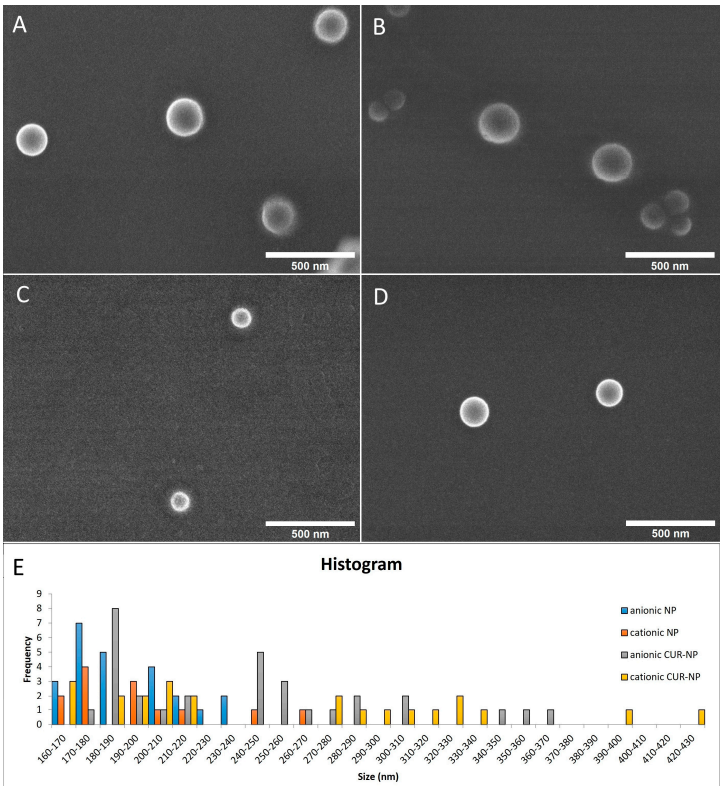


Figure 1. FEG-SEM of NP formulations with and without CUR: (**A**) anionic CUR-NP (magnification: ×60,000); (**B**) cationic CUR-NP (magnification: ×60,000); (**C**) anionic NP without CUR (magnification: ×60,000); (**D**) cationic NP without CUR (magnification: ×60,000); and (**E**) histogram showing size of all formulations.

Table 1. Mean values of size, poly-dispersion index (PDI), and zeta potential (± standard deviation) of NPs formulations with and without CUR determined in dynamic light scattering (DLS) in a period interval of 0–29 days after the synthesis (n = 12).

	Size (nm)	PDI	Zeta Potential (mV)
Anionic CUR-NP	225 (±60.38)	0.15 (± 0.06)	−30 (±12.58)
Cationic CUR-NP	248 (±86.39)	0.21 (± 0.09)	+35 (±7.23)
Anionic NP	193 (±17.95)	0.15 (± 0.05)	−32 (±11.86)
Cationic NP	186 (±14.97)	0.14 (± 0.04)	+33 (±2.69)

2.1.2. Absorption Spectrum and Photostability

During the light absorption study, the absorbance signals of free CUR, and anionic and cationic CUR-NP were similar in the blue range of the UV-visible spectrum. The free CUR presented maximum absorbance at 430 nm and both anionic and cationic CUR-NP at 426 nm and 424 nm, respectively (Figure 2). Although the wavelength values were close, the absorbance of the free CUR formulation was lower than those of the CUR-NPs, with values of 0.53, 0.712, and 0.602 a.u. observed for free CUR, and anionic and cationic CUR-NP, respectively.

During the photostability study, the authors observed a reduction of the maximum absorption signal of the formulations proportional to the illumination time for all the formulations. The free CUR showed a degradation of 44.7% after illumination of 43.2 J/cm^2, corresponding to 20 min. Concerning anionic and cationic CUR-NP, we observed degradation of 84.0% and 94.0%, respectively, after 20 min of illumination (Figure 3).

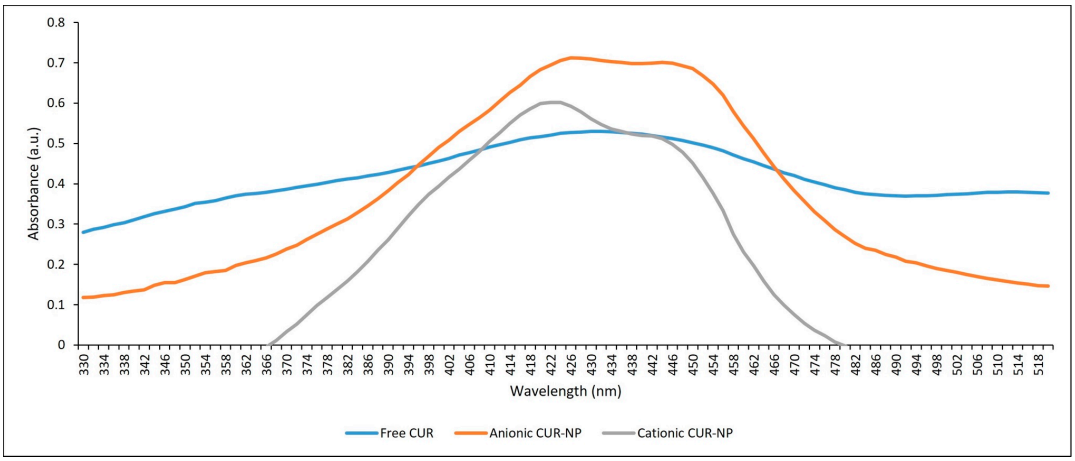


Figure 2. Absorption spectrum of free CUR, anionic and cationic CUR-NP.

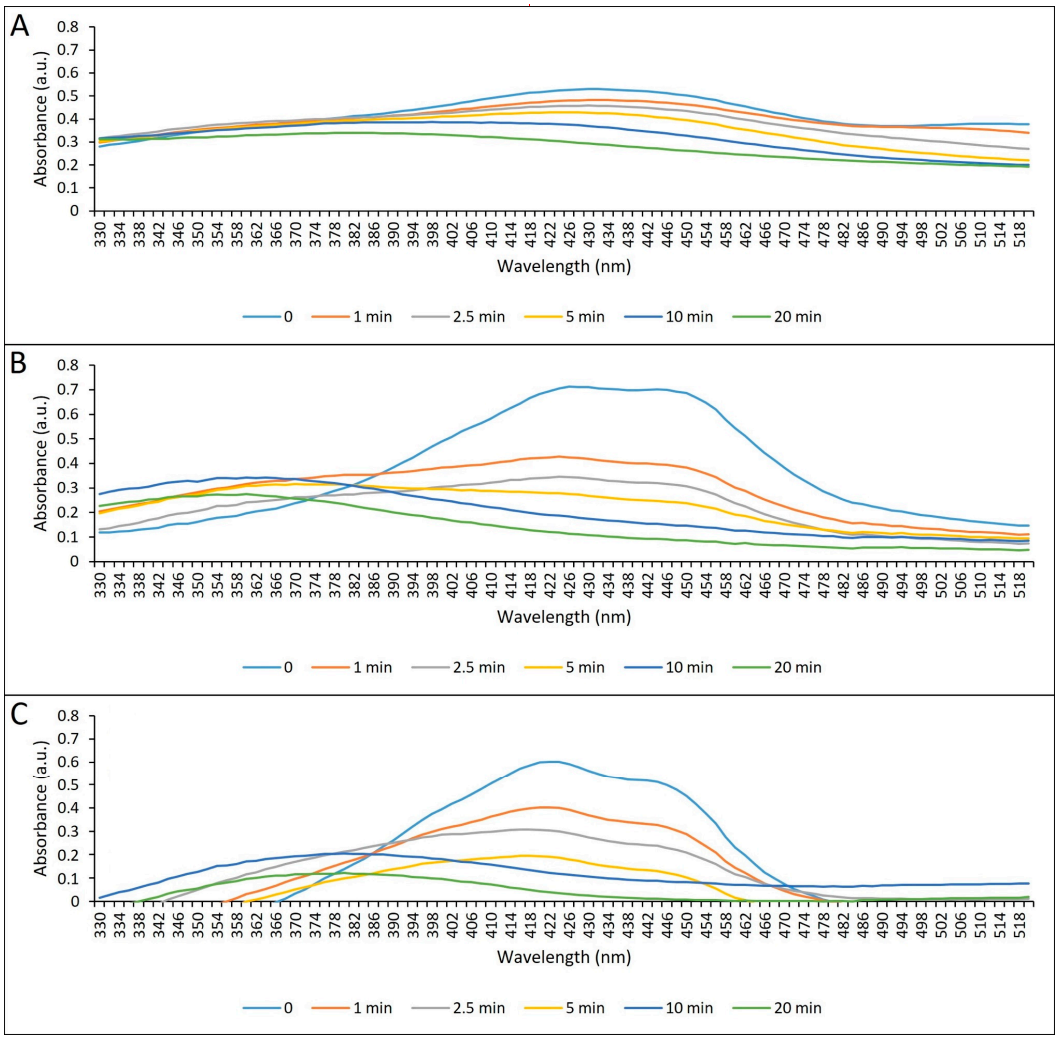


Figure 3. Photodegradation of free CUR, and anionic and cationic CUR-NPs after different periods of illumination with blue LED. (**A**) Free CUR; (**B**) anionic CUR-NP; (**C**) cationic CUR-NP.

2.1.3. Encapsulation Efficiency (EE) and Release of CUR from NPs

Regarding EE, values of 60.84% and 73.81% were observed for the anionic and cationic CUR-NPs, respectively.

Concerning CUR release, a slow and progressive CUR release from NPs was observed. After 12 h, release values of 52.6% and 51.6% of CUR from the anionic and cationic NP, respectively, were observed. (Figure 4).

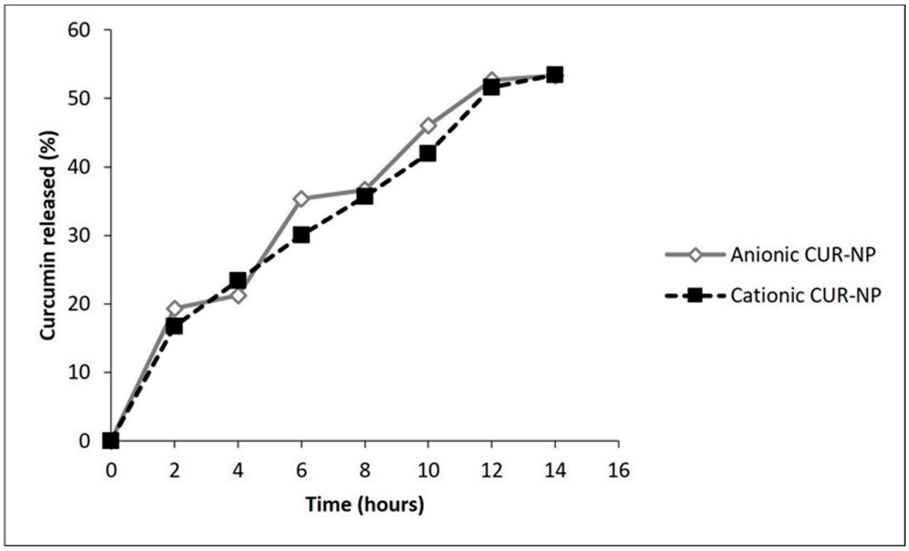


Figure 4. Release of CUR from anionic and cationic NPs (in percentage).

2.2. In Vivo Study

2.2.1. Antifungal Treatments of Oral Candidiasis in Mice

Tongues of mice inoculated with yeast showed the mean value of 4.95 $\log_{10}$ of colony-forming units per mL (CFU/mL) of *C. albicans* (control group). However, white patches on the dorsum of the tongue were observed only for some animals, consequently, a macroscopic analysis of lesions was not performed. When free CUR at 80 μM was evaluated, no antifungal photodynamic effect was observed (data not shown). Therefore, free CUR at 260 μM was evaluated because this was the highest CUR concentration encapsulated in NPs. A total of 13 animals died before the end of the experiments (six died during *C. albicans* inoculation, and seven after being allocated in the groups of treatments). Each treatment was performed daily during five consecutive days.

The quantification of *C. albicans* recovered from tongues of mice after five days of treatment in all groups is depicted in Figure 5. aPDT mediated by free CUR (C + L+ group) resulted in a significant ($p < 0.001$) reduction of 1.11 $\log_{10}$ in the viability of *C. albicans* recovered from tongues of mice compared with the control group (C − L−). Mice treated only with free CUR (C + L− group) showed no significant difference compared with the control ($p = 1.000$). Regarding anionic CUR-NP, no significant difference in the $\log_{10}$ (CFU/mL) was observed ($p \geq 0.421$) for animals submitted to photosensitizer (PS) only (AC + L−) or aPDT (AC + L+) compared with the control. Conversely, cationic CUR-NP promoted a significant reduction ($p < 0.009$) of 0.74 and 0.44 $\log_{10}$ in the presence of (CC + L+) and absence of light (CC + L−), respectively, compared with the control group. Although mice treated only with cationic CUR-NP (CC + L−) showed no significant difference ($p = 0.928$) to those treated with cationic CUR-NP-mediated aPDT (CC + L+), the former demonstrated a significant difference ($p = 0.048$) compared with aPDT mediated by free CUR (C + L+), which was similar ($p = 0.360$) to aPDT mediated by cationic CUR-NP (CC + L+).

Higher reductions were observed for mice treated with nystatin (NYS), as significant reductions ($p < 0.001$) of 1.58 and 2.57 $\log_{10}$ were obtained for NYS four times/day (NYS4) and NYS once a day under anesthesia (NYS1), respectively, compared with the control group. When all effective antifungal groups were compared, NYS4 and NYS1 demonstrated no significant difference between themselves ($p = 0.109$), but lower values ($p \leq 0.011$) than those found in groups treated with cationic CUR-NP (CC + L− and CC + L+). Moreover, NYS1 showed the highest reduction of $\log_{10}$ (CFU/mL) with a

significant difference (p = 0.001) compared with aPDT mediated by free CUR (C + L+), which was similar to NYS4 (p = 0.516).

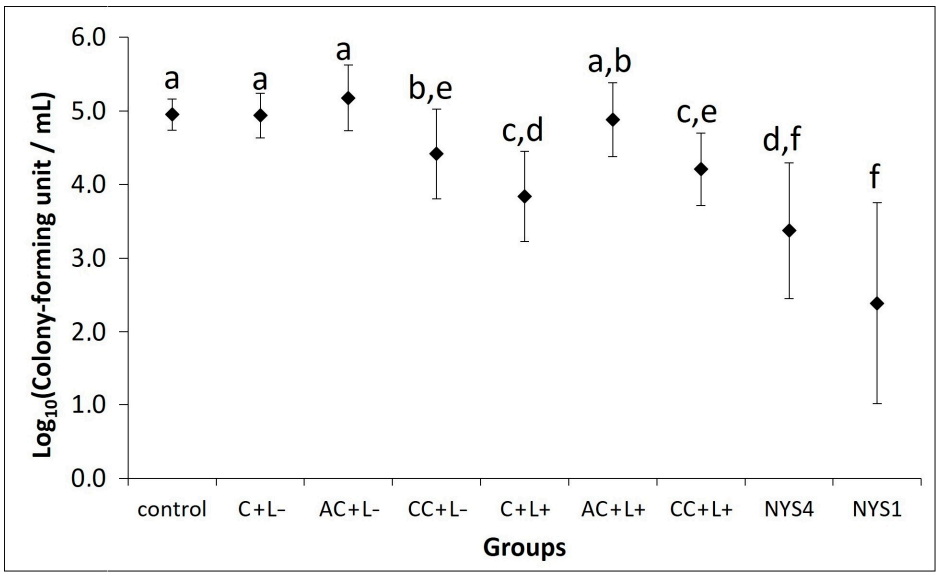


Figure 5. Mean values of $\log_{10}$ (CFU/mL) of *C. albicans* recovered from the tongue dorsum on the last day of treatment (n = 24). The control group corresponded to infected animals that did not receive any treatment (C − L −); C + L+, AC + L+, and CC + L+ groups: animals treated with free CUR, and anionic and cationic CUR-NP, respectively, associated with blue LED light; C + L−, AC + L–, and CC + L− groups: evaluation of each PS alone (free CUR, anionic and cationic CUR-NP, respectively); NYS1 and NYS4 groups: animals treated with Nystatin 100,000 international units (IU) once (under anesthesia) and four times daily, respectively. Different letters represent statistical differences between the groups ($p < 0.05$). Error bars: standard deviation.

2.2.2. Histological Analysis—Periodic Acid-Schiff (PAS)

Histological images from tongues of mice from all groups are shown in Figure 6. The epithelium showed alteration of the filiform papillae in the keratin region, presence of the filamentous form of *C. albicans* in the epithelium stratum corneum with invasion in the stratum spinosum, and few inflammatory cells in the lamina propria of the lingual mucosa in all infected animals compared with the healthy animals (negative control, NC group). Mice treated with aPDT (C + L+) with free CUR and NYS4 also showed these histological alterations, but with fewer fungal cells compared with animals from the control (C − L−), PS only (free CUR, anionic and cationic CUR-NP), and aPDT groups with anionic and cationic CUR-NP, which showed similar histological features for both periods of observation (24 h and seven days after treatment). The group of animals NYS1 (euthanized 24 h and seven days after the treatment) exhibited the lowest number of fungal filaments in the epithelium tissue.

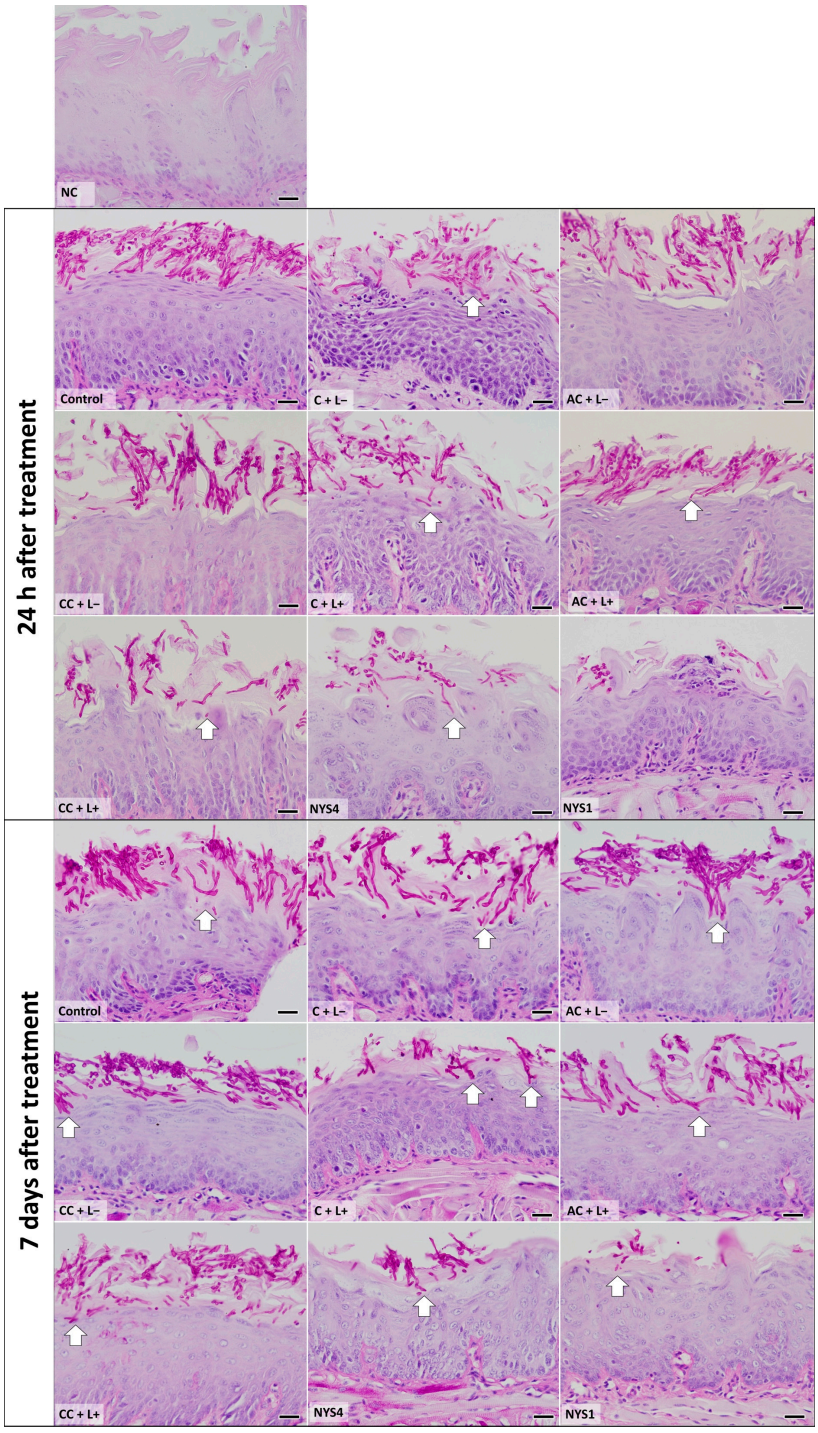


Figure 6. Light micrographs showing sections of tongue mucosa submitted to the periodic acid-Schiff (PAS) histochemical method. The light micrographs show the epithelium tongue of healthy, infected, and treated animals, euthanized 24 h and seven days after treatment. NC group: healthy and untreated animals; Control group: infected animals that did not receive any treatment (C − L−); C + L+, AC +

L+, and CC + L+ groups corresponded to the animals treated with aPDT mediated by free CUR, anionic and cationic CUR-NP, respectively, and blue LED light; C + L−, AC + L−, and CC + L− groups corresponded to evaluation of each PS alone (free CUR, and anionic and cationic CUR-NP, respectively); NYS1 and NYS4 groups: animals treated with Nystatin 100,000 IU once (under anesthesia) and four times daily, respectively. Arrows: invasion of *C. albicans* in the subjacent epithelium. Magnification: ×40. Scale bar: 20 μm.

2.2.3. Cytokeratins (CKs) 13 and 14 Immunolabelling

The evaluation of CK13 and CK14 by immunohistochemistry (IHC) (Figures 7 and 8) demonstrated different patterns in the immunolabelling according to the groups of treatments and periods. However, inferential statistics were not performed because only two animals from each group were evaluated (three sections for each animal). In healthy animals (NC), the lowest CK13 and CK14 immunolabelling was observed (only 5% and 11% of the epithelial area, respectively, was immunolabelled). Conversely, the non-treated infected mice (control group, C − L−) showed a more intense immuno-expression of both CKs at 24 h and seven days after treatment (46–47% for CK13, and 37–39% for CK14). Compared with the control group, a less intense immuno-expression for CK13 was observed in the animals treated with free CUR (C + L−) assessed after 24 h (37%) and NYS1 for both periods (40–44%), and the lowest immuno-expression among the infected animals was observed in the aPDT group with free CUR (C + L+) for both periods evaluated (22–24%, Figure 9). The highest CK13 immunolabelling was observed in groups treated with both CUR-NP (without and with light: AC + L−, CC + L−, AC + L+, CC + L+) and NYS4 (48–60%). A similar finding was observed for CK14 (Figure 10), as infected animals submitted to aPDT with free CUR showed the lowest immuno-expression (12–18%), followed by NYS1 (27–30%). The highest immunolabelling was verified in mice treated with cationic CUR-NP (without and with light, CC + L− and CC + L+, respectively) at both periods, and NYS4 after seven days (55–57%), while animals treated with anionic CUR-NP without and with light (AC + L− and AC + L+, respectively) for both periods and NYS4 evaluated after 24 h showed values (37–44%) similar to the control group.

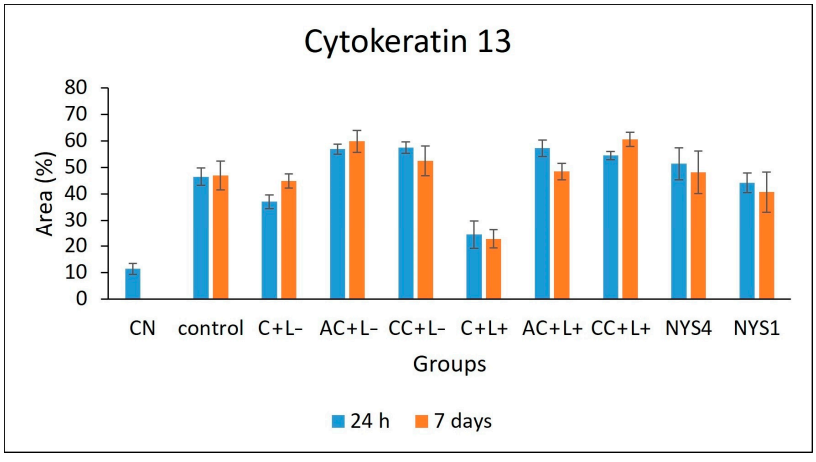


Figure 7. Mean values of CK13 immunolabelling area measured by ImageJ software (n = 2). NC group: healthy and untreated animals; control group: infected animals that did not receive any treatment (C − L−); C + L+, AC + L+, and CC + L+ groups: animals treated with aPDT mediated by free CUR, anionic and cationic CUR-NP, respectively, and blue LED light; C + L−, AC + L−, and CC + L− groups: evaluation of each PS alone (free CUR, and anionic and cationic CUR-NP, respectively); NYS1 and NYS4 groups: animals treated with Nystatin 100,000 IU once (under anesthesia) and four times daily, respectively. Error bars: standard deviation.

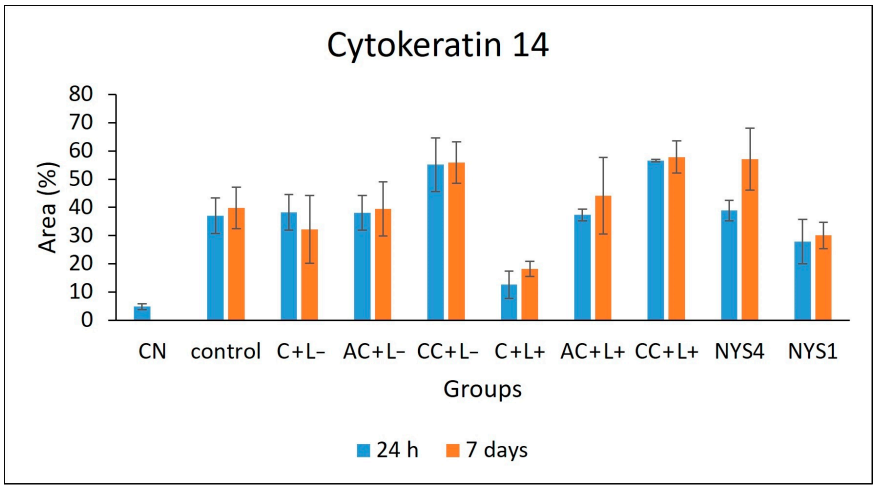


Figure 8. Mean values of CK14 immunolabelling area measured by ImageJ software (n = 2). NC group: healthy and untreated animals; control group: infected animals that did not receive any treatment (C − L−); C + L+, AC + L+, and CC + L+ groups: animals treated with aPDT mediated by free CUR, anionic and cationic CUR-NP, respectively, and blue LED light; C + L−, AC + L−, and CC + L− groups: evaluation of each PS alone (free CUR, and anionic and cationic CUR-NP, respectively); NYS1 and NYS4 groups: animals treated with Nystatin 100,000 IU once (under anesthesia) and four times daily, respectively. Error bars: standard deviation.

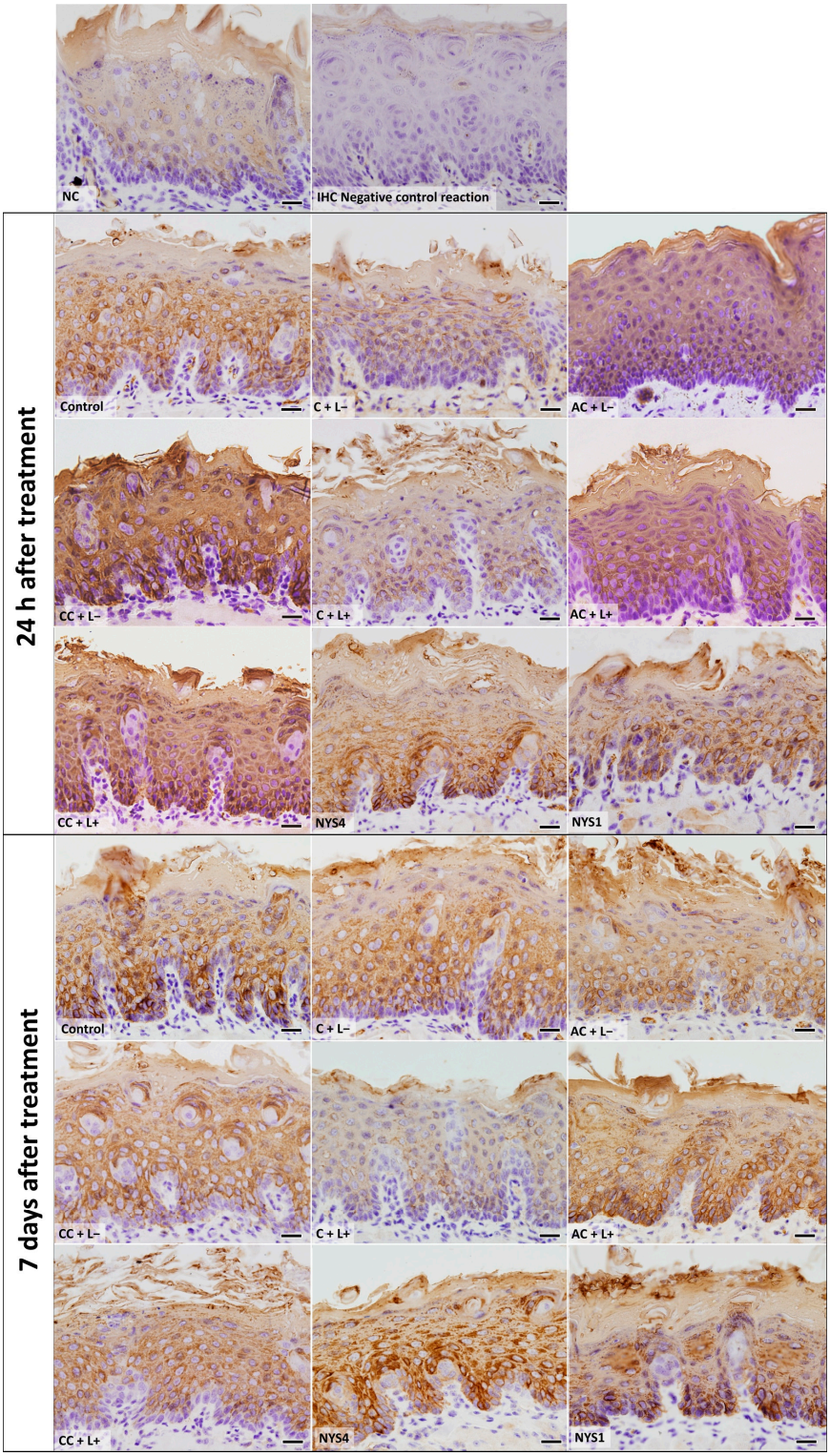


Figure 9. Light micrographs showing portions of sections of the tongue dorsal mucosa submitted to IHC for CK13 detection and counterstained with haematoxylin. NC group: healthy and untreated animals; Control group: infected animals that did not receive any treatment (C − L−); C + L+, AC +

L+, and CC + L+ groups: animals treated with aPDT mediated by free CUR, anionic and cationic CUR-NP, respectively, and blue LED light; C + L−, AC + L−, and CC + L− groups: evaluation of each PS alone (free CUR, and anionic and cationic CUR-NP, respectively); NYS1 and NYS4 groups: animals treated with Nystatin 100,000 IU once (under anesthesia) and four times daily, respectively. Magnification: ×40. Scale bar: 20 µm.

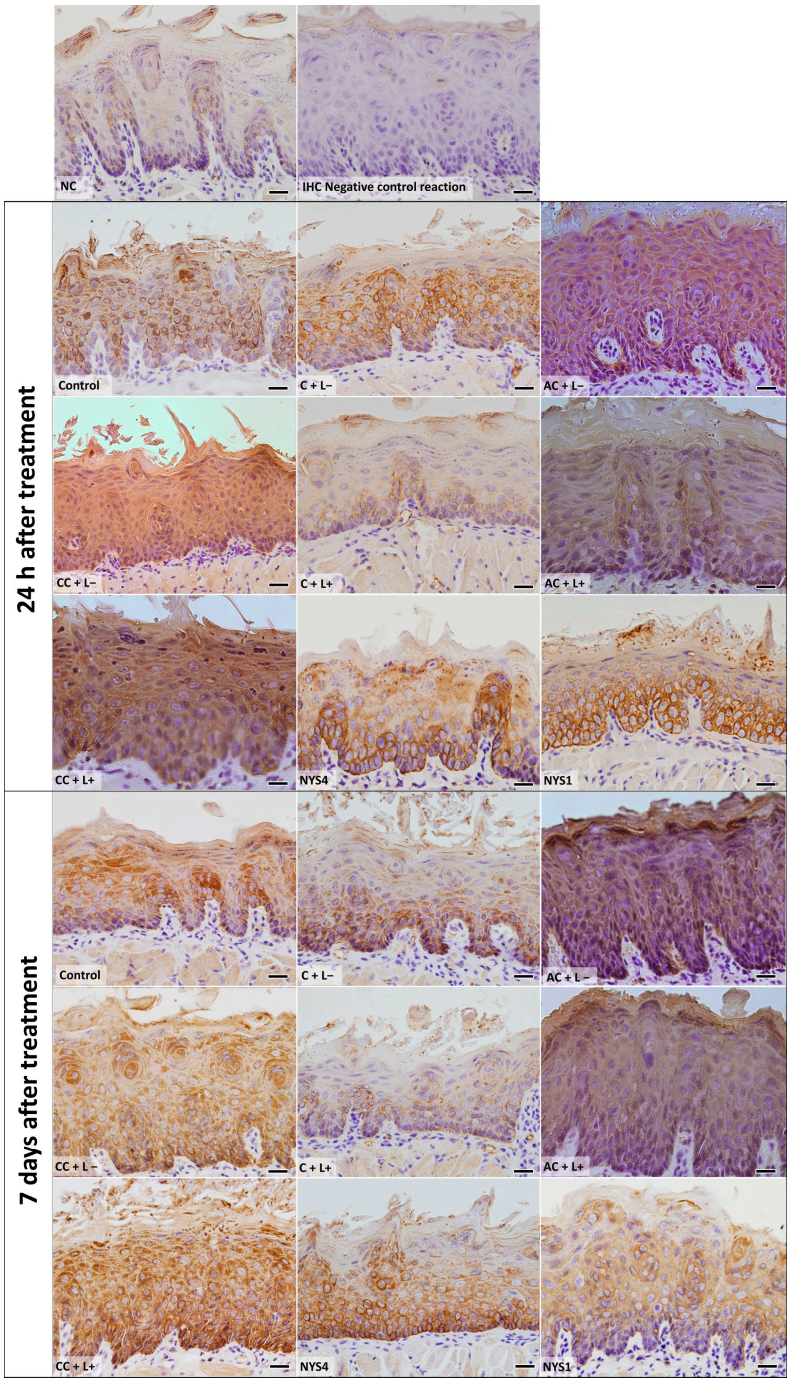


Figure 10. Light micrographs showing portions of sections of the tongue dorsal mucosa submitted to

IHC for CK14 detection and counterstained with haematoxylin. NC group: healthy and untreated animals; Control group: infected animals that did not receive any treatment (C − L−); C + L+, AC + L+, and CC + L+ groups: animals treated with aPDT mediated by free CUR, anionic and cationic CUR-NP, respectively, and blue LED light; C + L−, AC + L−, and CC + L− groups: evaluation of each PS alone (free CUR, and anionic and cationic CUR-NP, respectively); NYS1 and NYS4 groups: animals treated with Nystatin 100,000 IU once (under anesthesia) and four times daily, respectively. Magnification: ×40. Scale bar: 20 μm.

2.2.4. Terminal Deoxynucleotidyl Transferase (TdT)-Mediated Deoxyuridine Triphosphate (dUTP)-Biotin Nick End Labeling (TUNEL) Assay

Following 24 h of treatments, mice from the experimental groups showed no/few epithelial cells with DNA damage (red fluorescence) on the tongue mucosa (Figure 11B), as well as animals from NC, C + L+, NYS1, NYS4, CC + L−, and CC + L+ killed seven days after the treatments, similar to healthy mice (negative control, NC group). Increased number of DNA-damaged cells were observed on the tongue tissue of mice from C − L−, C + L−, AC + L−, and AC + L+ seven days after treatments (Figure 11C). The slide used as a positive control of the reaction showed many DNA-damaged cells in the tongue tissue, especially in the epithelial layers (Figure 11A).

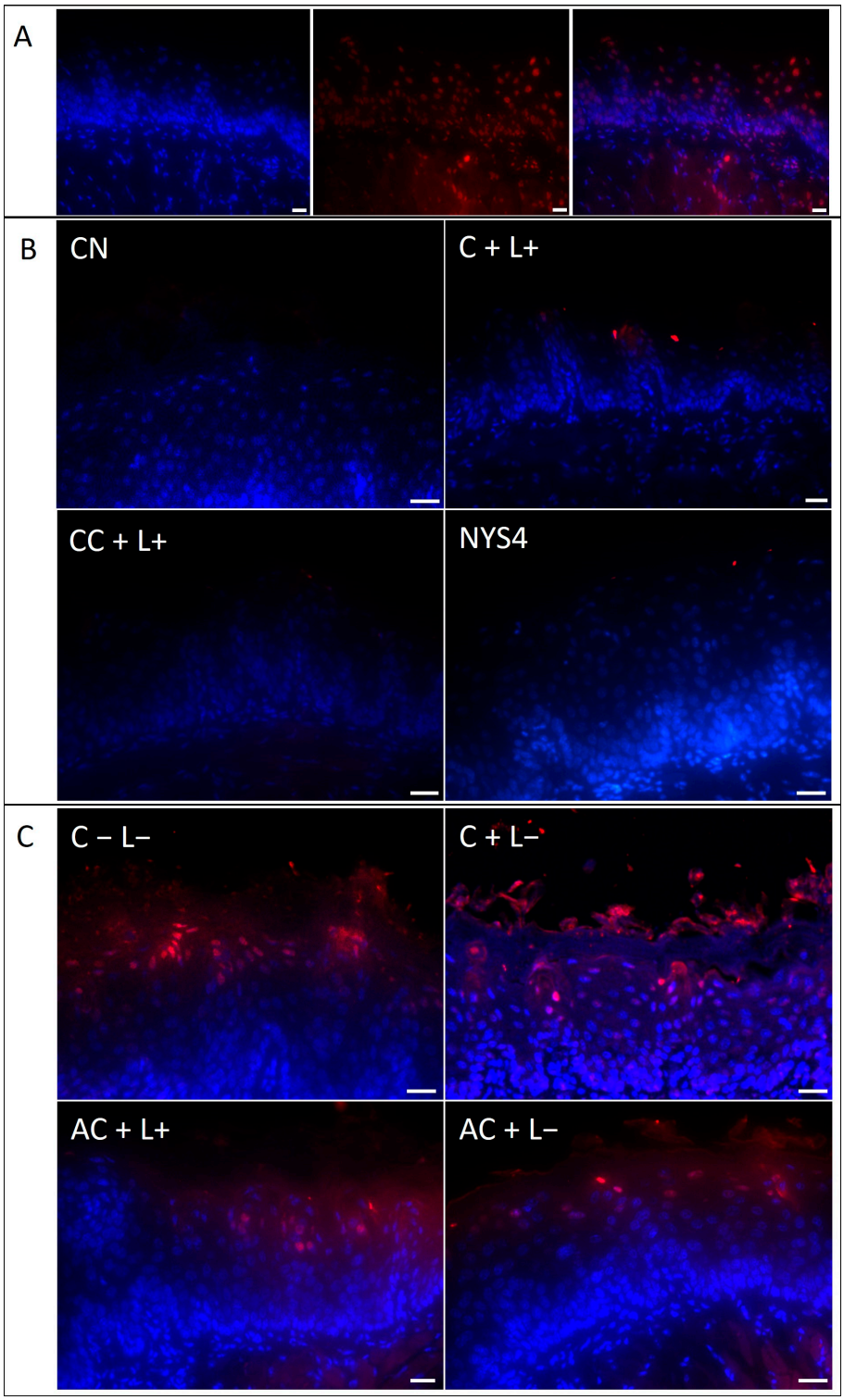


Figure 11. TUNEL assay of sections from the tongue of mice. (**A**) Positive control of the reaction (DNAse-treated sample) showing blue channel, red channel and overlay from left to right. (**B**) These

four images show no/few cells with DNA damage (red fluorescence) on the tongue mucosa and represent animals killed at 24 h after treatments and mice from the groups NC, C + L+, CC + L−, CC + L+, NYS4, and NYS1 seven days after treatments. (**C**) High number of DNA-damaged cells (red fluorescence) of the animals from C − L−, C + L−, AC + L+, and AC + L− groups seven days after treatment. Scale bar: 20 μm.

3. Discussion

CUR-NPs synthesized by the nanoprecipitation [32] method using PLA and DEX showed similar properties to those previously described [31], demonstrating that the synthesis process used to obtain CUR-NP was reproducible. Although the synthesized formulations were stable in solution, their physicochemical features (size, PDI and Zeta potential) might change over time. Therefore, all experiments were performed immediately after the synthesis. Even 29 days after the synthesis, the values found in DLS were comparable to other studies [33–37], which employed different polymers and methods to synthesize CUR-NP. During the present investigation, the size of CUR-NPs was also evaluated by FEG-SEM, which demonstrated a smaller size than that found in DLS, due to the shrinkage of the NPs as a consequence of the drying procedure required for FEG-SEM [38].

The encapsulation process did not change the absorption spectra of CUR in this study, as the maximum absorbance values obtained from free CUR, and anionic and cationic CUR-NP were observed at blue wavelengths, similar to those reported in previous studies in which CUR showed absorbance between 400–470 nm [15,39]. Moreover, the photostability assay showed that all the PSs demonstrated photodegradation higher than 44.7% after 43.2 J/cm^2 of blue light. This result agrees with a previous investigation [31], in which free CUR showed lower photodegradation compared with CUR-NP. Other studies found degradation values of 46–86% after 9.4 J/cm^2 of light [39], and 70% after 0.4 J/cm^2 of light [15].

In the present study, the percentage of EE was observed to be 60.84% for anionic CUR-NP and 73.81% for cationic CUR-NP. These values agree with other investigations that verified EE from 46.9% to 97% [33,37,40–43]. The release of CUR from NP was slow and progressive. After 12 h, approximately 52% of CUR was released from the NP. The authors' previous study verified that 48 h was needed to release 96% of CUR from NP [31], and other investigations also observed a progressive release of CUR from 20% to 92.8% during periods from 6 h to 15 days [28,33,37,44,45].

During the present study, a treatment protocol of aPDT with free CUR topically applied on the dorsum of the tongue of mice with OC resulted in a reduction of 1.11 $\log_{10}$ in the viability of *C. albicans*, while aPDT mediated by anionic CUR-NP demonstrated no antifungal effect, and cationic CUR-NP reduced the fungal load (0.44–0.74 $\log_{10}$) even in the absence of light. These results agree with the authors' previous in vitro study, in which the same PSs were used against biofilm of *C. albicans* and resulted in photoinactivation of 2.26 $\log_{10}$ for free CUR, no antifungal effect for anionic CUR-NP and reductions higher than 2.00 $\log_{10}$ for cationic CUR-NP even in the absence of light [31]. The inefficacy of anionic CUR-NP in inactivating the biofilm of *C. albicans* could be explained by the negative charge of the formulation that promotes repulsion against the negative charge of biofilm matrix [46] and the *C. albicans* cell wall [47]. Some studies have demonstrated that cationic PSs are more effective in aPDT compared with anionic PSs [48,49]. Hence, a cationic CUR-NP was also synthesized and evaluated in this study, and the antifungal effect observed even in the absence of light could be ascribed to the cetyltrimethylammonium bromide (CTAB) in the formulation, which, per se, has an antimicrobial effect [50]. This finding reinforces the authors' previous in vitro study, which demonstrated that cationic CUR-NP was toxic to microbial and mammal cells, while anionic CUR-NP was non-toxic [31].

Another possible reason for the absence of an antifungal effect of anionic CUR-NP is the slow CUR release from NP; the aPDT protocol established for the pre-irradiation time of PS in the tongue of animals corresponded to 20 min. During the release test of CUR, less than 10% of CUR in the CUR-NP formulations was released in 20 min, which could have reduced the antimicrobial efficacy of aPDT. CUR in NP of chitosan and polyethylene glycol promoted a significant reduction in bacterial counts

when applied topically for seven days on the burn wounds of mice infected with MRSA (more than 1.00 $\log_{10}$) [28]. During the present study, application of CUR-NP for five consecutive days would result in total release of CUR from NP. However, the topical application on the tongue does not keep the CUR-NPs in the mucosa because animals eliminate the formulation.

The results of the present investigation demonstrate that aPDT resulted in reduced photoinactivation of *C. albicans*. According to the American Society of Microbiology (ASM), an antimicrobial approach should promote reduction of at least 3.00 $\log_{10}$ [51]. A previous study demonstrated that the CUR-mediated aPDT promoted reduction of 4.00 $\log_{10}$ of *C. albicans* recovery from the tongues of mice with induced OC when a single topical application of aPDT was used [19]. The low reduction in the fungal viability after aPDT in the present research might be associated with the purity of CUR used (>65%). In another investigation, five aPDT applications with PDZ reduced the fungal viability in 3.00 $\log_{10}$ [20], and no death was observed. This higher reduction might be associated with the different PS used. Another reason for the higher reduction in the fungal viability in these studies might be the method of inoculum cultivation; while the present investigation used a suspension of *C. albicans* in the mid-log phase of growth, the other studies used an overnight culture. Conversely, in the present investigation, 13 mice died during the experiments, which was an unexpected result. The death of these mice might be attributed to the extended period of infection and the consecutive aPDT application, which required daily anesthesia of animals. A long period of OC might predispose animals to a systemic infection due to the immunosuppressive condition of mice and the ability of *C. albicans* to invade tissues, which was observed in the histological analysis. Moreover, after anesthesia, a recovery period for animals of longer than 24 h would be necessary before another aPDT application. Although the previous study [20] reported no death, no weight loss, and no behavior alteration, the possibility of systemic infection and death should be taken into consideration when OC is reproduced. The deaths observed in the present investigation suggest that impaired systemic health of mice would also reduce the efficacy of the treatments performed. Therefore, the impaired health of mice might also explain the reduced antifungal efficacy of aPDT in this study, because a competent immune system is also required to improve the host defense against *C. albicans*.

Treatment with nystatin four times a day was performed in order to simulate a clinical antifungal therapy, and it showed similar antifungal efficacy to aPDT. A clinical trial also demonstrated that topical application of nystatin showed similar results to aPDT for denture-associated OC [52]. Surprisingly, nystatin once a day in anesthetized animals was the most effective treatment in this study, resulting in 2.57 $\log_{10}$ of reduction. The highest reduction of fungal viability achieved by nystatin once a day might be justified by the anesthesia, which enables a longer period of action by the antifungal agent. Nystatin applied in non-anesthetized mice is removed from the mouth when mice feed, intake water, lick, and more. However, even the best result achieved with nystatin in the present investigation is below that recommended by ASM. Carmello et al., 2016 [20] also observed a high reduction of *C. albicans* (3.20 $\log_{10}$) after nystatin once a day in anesthetized mice. Although aPDT was performed in anesthetized animals, its antimicrobial action occurs only when the PS is activated by light, because the produced reactive oxygen species have a very short lifetime (microseconds) [11]. Therefore, as the reduction in the viability of *C. albicans* observed with aPDT once a day was similar to nystatin four times a day, the antifungal effect of aPDT might be considered relevant.

The histological analysis demonstrated that the amount of *C. albicans* on the keratin layer of the tongue corroborates with the CFU/mL results. Therefore, few filamentous cells were observed in the groups treated with nystatin and aPDT with free CUR. Few/scarce inflammatory cells were observed in all mice infected with *C. albicans*, suggesting that the treatments did not exacerbate the inflammatory response of tissues. These histological findings were similar for both periods of observation (24 h and seven days after the treatments), corroborating with a previous study [20]. However, Carmello et al, 2016 [20] did not observe fungal invasion in the epithelium of animals treated with nystatin, while in the present investigation, fungal invasion was also verified in animals treated with nystatin. Other

in vivo studies evaluated the histopathological features of epidermal wound healing treated with CUR-NP. When the healing of burn wounds of mice was evaluated, CUR-NP reduced the inflammatory infiltrate, and improved the collagen deposition and the neovascularization of wounds [28]. CUR in NP of poly (lactic-co-glycolic acid) also improved the healing of excisional wounds of mice, which showed better re-epithelialization, and an increase in the collagen formation in the connective tissue [33]. A composite of hydrogel with CUR encapsulated in micelles also improved the wound healing of rats, which showed increased re-epithelialization, granulation tissue, fibroblast proliferation, and deposition of collagen [53]. CUR in pluronic gel also accelerates the wound healing of diabetic rats [25]. However, in these studies of wound healing, slow release of CUR from the delivery systems is a positive factor because CUR is maintained in the tissue during the wound-healing period. Conversely, for topical aPDT, the maximum of CUR should ideally be released from the nanocarrier during light activation to produce reactive oxygen species and, consequently, the antimicrobial effect.

As this study evaluated a superficial infection of an oral mucosa rather than an epidermal wound healing model, the effect of aPDT mediated by CUR-NP on the tongue mucosa was assessed. During the present study, the fungal infection increased the immuno-expression of both CKs evaluated, which might be attributed to the epithelial disarrangement and response to the fungal invasion. To the best of the authors' knowledge, this was the first study that observed an increased expression of CKs as a result of OC. Other investigations reported alteration of CK expression as a result of oral lesions, such as lichen planus [54,55], and actinic cheilitis [56], but they did not associate CK expression with microbial biofilm. Kaminagakura et al, 2006 [57] evaluated the pattern of CK expression by IHC in biopsies of oral mucosa from patients with paracoccidioidomycosis showing pseudoepitheliomatous hyperplasia. In the oral mucosa of these patients, they found that CK1 and CK10 were not expressed in the hard palate, gingiva, and lips, and CK14 expression increased in the buccal mucosa and lips of oral infected mucosa [57]. Therefore, in accordance with this study, this investigation demonstrated that CK expression is altered in cases of oral infection.

Moreover, the present study showed that treatment with PS alone and nystatin also increased the immunolabelling for CK13 and CK14, similar to the untreated control group. As the treatment with PS alone did not reduce the fungal load, a high expression of both CKs observed in these groups was expected. However, although nystatin had reduced the fungal viability from tongues of mice, the expression of CK13 and CK14 was similar to the untreated control group, suggesting that nystatin was not able to improve the reorganization of the cytoskeleton of the epithelium even after seven days from the end of the treatment. Surprisingly, aPDT with free CUR resulted in reduced expression of both CKs. This was an unexpected outcome, as aPDT did not completely eliminate the fungal load from the tongue; therefore, CK expression was expected to be more intense, as observed in mice treated with nystatin. This result suggests that, concurrent with the reduction in the fungal viability, aPDT also contributed to the normal expression of CK13 and CK14 of the epithelial cells. However, the mechanism of such effects should be further investigated. Alternately, treatment with anionic and cationic CUR-NP (with and without light) resulted in expression of CK13 and CK14 similar to the infected mice. Concerning anionic CUR-NP, this result might be explained by the absence of antimicrobial activity. Although cationic CUR-NP had reduced the fungal viability, the increased expression of both CK might be justified by the CTAB in its composition, which showed in vitro cytotoxicity [31].

C. albicans is able to invade the epithelial layers and promote tissue damage by necrosis or apoptosis [5]. aPDT mediated by silicon phthalocyanine Pc4 promoted nuclear alterations in *C. albicans* similar to apoptosis, such as externalization of phosphatidylserine, chromatin condensation, and DNA fragmentation [58]. The reactive oxygen species produced by anticancer photodynamic therapy kill neoplastic cells by necrosis, apoptosis, or autophagy [59]. Therefore, in the present investigation, the TUNEL assay was performed in order to evaluate the safety of the consecutive applications of the aPDT on the hosts' tissues. The findings showed that DNA damage was not observed after the treatments, especially after 24 h. An in vitro study, which also evaluated the safety of aPDT, observed

no induction of apoptosis on human gingival fibroblasts and osteoblasts submitted to methylene blue at 50 μg/mL for 10 min followed by irradiation with a red diode laser at 12 J/cm^2 [60]. During an ex vivo study, the TUNEL assay demonstrated that porcine skin samples inoculated with MRSA and submitted to aPDT (10 μM of porphyrin-based PS and 13.7 J/cm^2) showed a slight increase in dead cells within the epidermis (16.55–35.8% ± 5%) compared with non-treated samples (15.3% ± 5%) [61]. Some studies have reported that blue light alone has an antimicrobial effect without harming the host tissue [62,63]. Mice burns infected with *P. aeruginosa* and irradiated with blue light (415 ± 20 nm, 55.8 J/cm^2) not only showed a reduction of bacterial burden, but also rescued mice from death, and no DNA damage in the host tissue was observed [62]. Irradiation with blue light (415 ± 20 nm) of burned skin of mice infected with multidrug-resistant *Acinetobacter baumannii* reduced the bacterial load (55.8 J/cm^2) and resulted in no significant DNA damage (195 J/cm^2) in the cells of the epidermis evaluated by the TUNEL assay [63].

The present investigation demonstrated that the number of cells showing DNA damage after seven days increased in groups with a high amount of fungi, but not in groups with a reduction of fungal viability (cationic CUR-NP with and without light, aPDT with free CUR, and nystatin), which might indicate that DNA damage is due to the persistence of *C. albicans* in the tissue. Although, in the authors' previous in vitro study, the cationic CUR-NP was toxic to mammal cells [31], in the present investigation, this formulation was not able to harm the tissue, probably because of the low CTAB concentration (2%).

To respond to *Candida* infection, the host cells synthesize pro-inflammatory cytokines and chemokines that mediate immune protection against *Candida* [64]. An in vitro study demonstrated that human oral and vaginal epithelial cells co-cultured with *C. albicans* produced tumor necrosis factor α (TNF-α) and interleukin 1α (IL-1α), but not interleukin 6 (IL-6) [65]. A protective response against *C. albicans* has also been associated with T helper (Th) in 17 cells induced by interleukin 1β (IL-1β), IL-6, and transforming growth factor β (TGF-β) [66], more so than with the classical Th1 response [67]. Unfortunately, the authors could not demonstrate the genetic expression of the inflammatory cytokines after treatments of OC because of the loss of samples during RNA extraction and purification (see Supplementary Material). The authors tried to improve the method previously reported [20], after careful considerations with an expert in molecular biology, by including the evaluation of RNA integrity. However, the authors observed a low yield and degradation of RNA. Only in the last attempts, with the remaining samples pooled, could they obtain a minimum amount of RNA for cDNA synthesis. Considering these samples (from AC + L−, CC + L−, AC + L+, and CC + L+ groups), the authors did not observe any increase in the inflammatory cytokines evaluated (TNF-α, IL-1β, and IL-6), although the control groups (C − L− and healthy mice) were not included (Figure S1). Other in vivo studies observed reduction of cytokine expression after aPDT associated or not with scaling/root planning for treating periodontitis [68,69].

4. Materials and Methods

4.1. Synthesis and Characterization of CUR-NPs

4.1.1. PS and Light Source

Free CUR and CUR-NPs were used as PSs in this study. A stock solution of free CUR (260 μM) was prepared in dimethyl sulfoxide (DMSO) 10% diluted in sterile milli-Q water [15,16,18,19]. A blue (≈ 455 nm) LED (LXHL-PR09, Luxeon III Emitter, Lumileds Lighting, San Jose, CA, USA) device was elaborated as a handpiece by the Physical Institute of São Carlos—University of São Paulo (USP). The light emission end of the device had a diameter of 5 mm and a power output of 75 mW.

4.1.2. Encapsulation of CUR in NPs

CUR-NPs were synthesized by the nanoprecipitation method [32], characterized as previously reported [31], and submitted to a patent deposited on the National Institute for Industrial Property (INPI) (process number BR 10 2016 015631 9). To perform this, a stock solution of CUR 0.4% was prepared in acetone. During the encapsulation process, an organic phase containing PLA (kindly provided by Professor Valtencir Zucolotto from University of São Paulo) at 0.5% in acetone was mixed with the stock solution of CUR. Then, an aqueous phase containing DEX 1% (Sigma-Aldrich Brasil Ltda, São Paulo, SP, Brazil) in milli-Q water was added by dropping to the organic phase. This procedure was performed at room temperature (25 °C) under slow magnetic rotation (90–100 rpm). Afterward, the solution was maintained under magnetic stirring for 10 min. The NP solution was kept at room temperature for 24 h to evaporate the solvent. This procedure resulted in anionic NP. To synthesize cationic CUR-NP, after the 24 h of acetone evaporation, CTAB (Sigma-Aldrich Brasil Ltda) 2% in sterile water and NaCl 1.76% was added [70]. The maximum concentration of CUR encapsulated in NP was 260 µM. Anionic and cationic NPs without CUR were also synthesized by the same method as the controls.

4.1.3. Physicochemical Properties

Nanometric properties of CUR-NPs were characterized by size, PDI, and Zeta potential (determination of the superficial charge) using a Zeta Sizer NANO ZS (Malvern Instruments Ltd., Malvern, UK) at 25 °C.

4.1.4. Morphology Analysis

CUR-NPs solutions were diluted in sterile ultra-pure water (1:200) and dried in a vacuum desiccator for 48 h, protected from light. The samples were placed in conductive stubs for carbon coating in the Sputter Coater (SCD 050 BAL-TEC). Particle morphology was analyzed by a FEG-SEM (Jeol, JSM 7500 F). Size was measured by ImageJ software (1.51j, National Institutes of Health, Bethesda, MD, USA).

4.1.5. Encapsulation Efficiency (EE)

Regarding EE, 5 mL of the CUR-NPs at 52 µM were centrifuged at 6000× g for 10 min. The absorbance of the supernatant (free portion) was determined in a UV-visible spectrophotometer (SQ 4802 UV-Visible Double Beam Spectrophotometer UNICO, United Products and Instruments Inc., Dayton, NJ, USA). The EE was calculated using the following formula: EE% = (PStotal − PSfree) × 100/PStotal [31,35].

4.1.6. Absorption Spectrum and Photostability

The absorbance of each PS (free CUR, and cationic and anionic CUR-NPs) at a concentration of 80 µM was determined in a plate reader in the UV-visible spectrum of 300–800 nm (Fluostar Omega, BMG LabTech, Offenburg, Germany). The photostability of CUR-NPs was compared with free CUR. Photodegradation was monitored by absorption spectrum between the wavelengths of 300–800 nm of the samples after illumination. CUR and CUR-NPs were exposed to different illumination intervals of a LED light source (≈455 nm) of 36 mW/cm^2. Sample absorption was determined before (0 min) and after each irradiation time (1, 2.5, 5, 10, and 20 min, corresponding to 2.16, 5.4, 10.8, 21.6, and 43.2 J/cm^2, respectively). Blank samples corresponded to NP solutions, whose absorbance was read to verify the hypothesis of absorption of the excipient solution (PLA and DEX) [31].

4.1.7. Release of CUR from NPs

Samples of cationic and anionic CUR-NPs at 130 µM were incubated at 37 °C under agitation (100 rpm). Every 2 h, 2 mL of the samples was centrifuged at 6000× *g* for 10 min to separate the NPs

from the solution and then the pellets were diluted in acetone to solubilize the unreleased CUR, whose absorbance was determined in a UV-visible spectrophotometer. The total CUR released was calculated by dividing the absorbance of each interval time by the maximum absorbance of the encapsulated CUR determined in the EE study [28,31].

4.2. In Vivo Study

4.2.1. Animals

The authors used 235 female Swiss mice of 4–6 weeks of age, weighing approximately 20 g. The research protocol was approved by the Ethical Committee for Animal Research ("Comissão de Ética no Uso De Animais" CEUA; process 19/2015 approved on 8 December 2015) of the School of Dentistry, Araraquara, São Paulo State University (UNESP). The animals were kept in polypropylene cages with five animals in each cage, with controlled temperature (23 ± 2 °C) and humidity (55 ± 10%). The mice were maintained under a 12:12 light/dark cycle with light onset at 07:00 a.m. Standard chow (Guabi Rat Chow, Paulinia, SP, Brazil) and water were provided ad libitum.

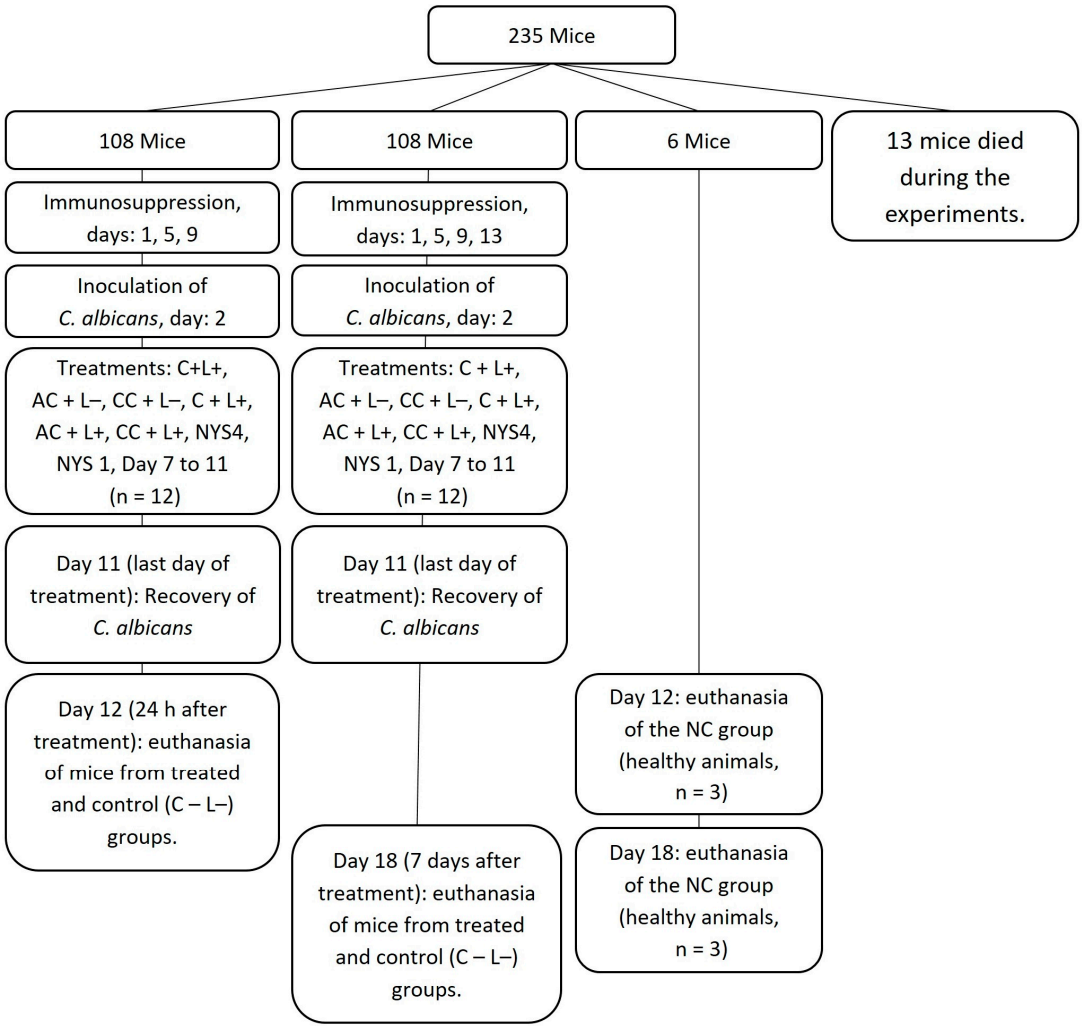
4.2.2. Oral Infection and Treatments

A reference strain of *C. albicans* ATCC 90028 (Rockville, MD, USA) was kept in yeast nytrogen broth with 100 mM of glucose (YNBg) and glycerol 50% at −80 °C. During each experiment, the strain was thawed and grown in sabouraud dextrose agar with 5 mg/mL of chloramphenicol (SDAc), which was incubated at 37 °C for 48 h. Colonies were resuspended in YNBg and incubated at 37 °C for 16 h. This suspension was then diluted 1:20 in a fresh YNBg and incubated at 37 °C until the mid-log phase of growth (OD_{540}: 0.548 ± 0.048), whose concentration was standardized at 5.8×10^6 ± 4.2×10^6 (mean ± standard deviation) CFU/mL. To induce the OC in animals, the methodology of Takakura et al., 2003 [71] was used with the modifications of Carmello et al., 2016 [20] to prolong the period of infection and to perform successive aPDT applications (Scheme 1). The animals were immunosuppressed with subcutaneous injections of prednisolone at the dose of 100 mg/kg on days 1, 5, 9, and 13. Tetracycline hydrochloride at 0.83 mg/mL was provided to the animals in the drinking water during the entire period. Oral inoculation of *C. albicans* was performed on day 2 by scrubbing a cotton swab immerged in the yeast suspension in the entire oral cavity. To do this, animals were anesthetized by an intramuscular injection of 50 µL of chlorpromazine hydrochloride at 2 mg/mL in each femur.

Treatments were performed daily from days 7 to 11. The groups PS only and aPDT involved free CUR (C + L− and C + L+, respectively), anionic CUR-NPs (AC + L− and AC + L+, respectively), and cationic CUR-NP (CC + L− and CC + L+, respectively). Each experiment was performed with 16–20 mice divided into four different groups (control, PS only, aPDT, and nystatin). Animals were allocated to the following groups: for aPDT, animals were anesthetized with an intraperitoneal injection of ketamine hydrochloride (100 mg/kg of body weight) associated with xylazine hydrochloride (10 mg/kg of body weight). Then, 50 µL of the PS at 260 µM was pipetted on the dorsum of the tongue. Following 20 min in the dark (pre-irradiation time), the tongue of the animals was illuminated for 7 min at 37.5 J/cm^2 (C + L+, AC + L+, and CC + L+ groups). To verify a possible toxic effect of the applied PS, additional animals were treated only with the PS during the pre-irradiation and illumination times (C + L−, AC + L+, and CC + L+ groups). The control group (C − L−) received only sterile phosphate-buffered saline (PBS) during the same pre-irradiation and illumination times. The effect of light alone was not evaluated, as previous studies demonstrated no fungicidal effect of blue light at 37.5 J/cm^2 [19,72]. To compare, two additional groups received topical application of nystatin 100,000 IU. Regarding the NYS1 group, nystatin was applied once a day for five consecutive days under anesthesia. To simulate the clinical use of nystatin, another group received nystatin for four times a day (intervals of four hours) during five consecutive days without anesthesia (NYS4). Moreover, in the NC group, animals were not inoculated with the fungi and did not receive any

treatment. Twelve animals from each group were evaluated in each period of euthanasia [20], which was performed 24 h and 7 days after the last day of treatment for each group, with the exception of the NC group (n = 3).

Subsequent to the last fifth day of each treatment, *C. albicans* was recovered from the tongue of each animal by swabbing a mini cotton swab for 1 min on the dorsum of the tongue. The mini-swabs were kept in 1 mL of sterile saline solution, which was vortexed and serially diluted. Aliquots of 25 µL were spread in duplicate in SDA plates, which were incubated at 37 °C for 48 h for colony quantification (CFU/mL). No fungal recovery was performed seven days after the treatment because a previous study reported no significant difference between the $\log_{10}$ (CFU/mL) of *C. albicans* recovered 24 h and seven days after aPDT/no treatment [20].



Scheme 1. Study design. C + L+, AC + L+, and CC + L+ groups: animals treated with aPDT mediated by free CUR, and anionic or cationic CUR-NPs, respectively, and blue LED light; C + L−, AC + L−, and CC + L− groups: evaluation of each PS alone (free CUR, and anionic or cationic CUR-NP, respectively); NYS1 or NYS4 groups: animals treated with Nystatin 100,000 IU once (under anesthesia) or four times daily, respectively; C − L− (control) group: infected animals that did not receive any treatment; and negative control (NC) group: healthy and untreated. During the entire experimental period (18 days), tetracycline hydrochloride was given in drinking water.

4.2.3. Euthanasia

The animals were euthanized 24 h (on day 12) or seven days (on day 18) after the fifth application of each treatment by a lethal dose of ketamine hydrochloride by intramuscular injection into the femur region. Then, the tongue of each animal was surgically removed. The anterior third and posterior third were removed and the dorsal region was divided in the longitudinal plane. One half of the tissue was fixed in 4% formaldehyde for histological, immunohistochemical (IHC), and terminal deoxynucleotidyl transferase (TdT)-mediated deoxyuridine triphosphate (dUTP)-biotin nick end labeling (TUNEL, DNA fragmentation) analyses. The other half was stored in RNA LATER at −80 °C for quantitative reverse transcription-polymerase chain reaction (RT-qPCR) analyses (Supplementary material).

4.2.4. Histological Analyses

Following fixation in 4% formaldehyde buffered at Hidrogenionic potential (pH) of 7.2 with 0.1 M sodium phosphate, the samples were processed for paraffin embedding. The sections (5-µm thick) were adhered to glass slides and submitted to the periodic acid-Schiff (PAS) histochemical method and counterstained with hematoxylin to be observed in light microscopy (BX-51, Olympus Corporation, Shinjuku, Tokyo, Japan). The morphological alterations were evaluated according to the presence of yeast and filamentous cells, the organization of the epithelial layer, and the presence of inflammatory cells in the connective tissue.

4.2.5. Immunohistochemistry (IHC) for Cytokeratins (CKs)

The sections of the tongue adhered to silanized glass slides were deparaffinized for avidin-biotin complex detection of CK13 and CK14. Antigenic retrieval was performed by heating the sections in 10 mM sodium citrate buffer, pH = 6 (for CK14), or 10 mM of tris(hydroxymethyl) aminomethane-ethylenediaminetetraacetic acid (TRIS-EDTA, TE) buffer, pH = 9 (for CK13), in a microwave oven (98 °C for 10 min). The samples were washed and immersed in 4% H_2O_2 for 10 min to inactivate the endogenous peroxidase. Following washing, the samples were incubated in a solution containing 2% bovine serum albumin (BSA, Sigma-Aldrich)/1% sodium azide (Sigma-Aldrich)/1% Triton X-100 (Sigma-Aldrich) for 20 min at room temperature. Subsequently, the sections were incubated in a humidified chamber at 4 °C overnight with mouse monoclonal anti-CK13 antibody (ab16112, ABCAM®), or mouse monoclonal anti-CK14 antibody (ab7800, ABCAM®), both diluted 1:500. The next day, the samples were washed in PBS and incubated with the second antibodies [goat anti-mouse horseradish peroxidase (HRP)/dihydrochloride (DAB) (ab64259, ABCAM®)] for 20 min. Subsequently, the samples were washed and incubated in streptavidin for 20 min (ab64259, ABCAM®). Next, the samples were marked by 4,6-diamino-2-phenylidole dihydrochloride (DAB; Invitrogen) and counterstained with Carazzi's hematoxylin for analysis under light microscope (BX-51, Olympus Corporation, Shinjuku, Japan), and photographed at magnification 200× and 400×.

4.2.6. Tissue Damage: Detection of Cell Death by the TUNEL Method

To evaluate the treatment safety, the TUNEL assay was performed using Click-iT® TUNEL Alexa Fluor® 594 Imaging Assay kit (Molecular Probes®), according to the manufacturer's instructions. Briefly, sections were deparaffinized for a prolonged time, to remove paraffin as much as possible. Then, the samples were incubated with proteinase-K, a permeabilizing agent used to expose the DNA fragments, and fixed with 4% formaldehyde. A positive control of the reaction was made by incubating a slide from negative control (NC) group in 1 unit/µL of TURBO DNAse (Ambion, AM2238). Afterward, all samples were incubated with terminal deoxynucleotidyl transferase (TdT) reaction mixture, washed with 3% BSA and 0.1% Triton X-100 in PBS, followed by Click-iT Plus TUNEL reaction cocktails to mark cells with DNA fragmentation. Slides were washed with 3% BSA in PBS for 5 min. The DNA intercalator 4,6-diamidino-2-phenylindole (DAPI, Molecular Probes, NucBlue® Fixed cell stain ready Probes, R37606) was used to counterstain the nuclei. Finally, the slides were assembled

with fluoromount (CAT # 17984-25, Electron Microscopy Sciences, Fort Washington, WA, USA) and visualized in a fluorescence microscopy (Leica DMI3000 B).

4.3. Statistical Analyses

The values of $\log_{10}$ (CFU/mL) recovery from tongues of mice were submitted for statistical analyses. Normality and homoscedasticity were evaluated by Shapiro-Wilk and Levene tests, respectively. As the assumption of normality was met, but the homogeneity of variance was not met, data were analyzed by analysis of variance (ANOVA)/Welch and post-hoc of Games–Howell. The significance level adopted was 5% ($\alpha = 0.05$). All analyses were performed using SPSS software version 20.0 (SPSS Inc., Chicago, IL, USA).

To quantify the IHC immunolabelling, the software ImageJ (1.51j, National Institutes of Health, Bethesda, MD, USA) was used as previously described [73,74]. The colorful images (.tiff) at magnification 200× were converted to gray scale, and the blue channel of the red-green-blue (RGB) stack was selected to remove the background. Then, the threshold was manually adjusted to separate the positive-IHC immunolabelling from the negative-IHC ones, by comparing with the original colorful image. Afterward, the epithelium region was selected (basal and spinous cell layers), and the immunolabelled area was measured as a percentage. Sections of two animals from each group were analyzed. Therefore an inferential statistical analyze was not performed [only descriptive statistics (mean and standard deviation) were shown].

The histopathological and TUNEL analyses were performed qualitatively.

5. Conclusions

This study encapsulated CUR in NPs, which improved the water solubility of CUR. However, free CUR showed a better photodynamic effect than CUR-NP, and nystatin once a day in anesthetized animals showed the best antifungal effect. DNA damage of the host tissue was related to the fungal infection, and not to the treatments performed. Furthermore, aPDT with free CUR resulted in expression of CK13 and CK14 of the epithelium of the tongue close to that observed in healthy mice, an outcome not observed for nystatin. Further studies should be developed to improve the release of CUR from NP and its antimicrobial effect, and to better understand the expression of CKs of the infected tissue after aPDT.

6. Patents

Authors report a patent deposited in the National Institute for Industrial Property (INPI) in Brazil on 4 July 2016, process BR 10 2016 015631 9, entitled "Processo de Obtenção de Nanopartículas Poliméricas Aniônicas e Catiônicas de Curcumina, Nanopartículas Obtidas e Seus Usos".

Supplementary Materials: The following are available.

Author Contributions: Conceptualization, E.G.O.M. and P.A.B.; Methodology, V.T.S., E.G.O.M., P.A.B. (synthesis and characterization of CUR-NP), J.C.C. (animals and RT-qPCR), and P.S.C. (IHC and TUNEL assay); Formal Analysis, V.T.S., E.G.O.M., M.C., and P.S.C.; Investigation, all authors; Resources, E.G.O.M. and A.C.P.; Data Curation, V.T.S. and E.G.O.M.; Writing—Original Draft Preparation, V.T.S. and E.G.O.M.; Writing—Review & Editing, all authors; Supervision, E.G.O.M.; Project Administration, E.G.O.M.; Funding Acquisition, E.G.O.M. and A.C.P.

Funding: This study was supported by São Paulo Research Foundation (FAPESP grants 2013/23165-5, 2014/20119-5, and RIDC/CEPOF 2013/07276-1) and National Counsel of Technological and Scientific Development (CNPq grant 446401/2014-5).

Acknowledgments: Authors thank Marlise Inêz Klein for the helpful considerations in the RT-qPCR methodology, Geisiane Helena Gomes Bueno for the technical support in the microbiological assays, Jéssica Bernegossi for scheduling and instructing the DLS use, and the Institute of Chemistry for the FEG-SEM.

Conflicts of Interest: The authors declare a patent deposited on INPI. There is no other conflict of interest.

References

1. Rautemaa, R.; Ramage, G. Oral candidosis-clinical challenges of a biofilm disease. *Crit. Rev. Microbiol.* **2011**, *37*, 328–336. [CrossRef] [PubMed]
2. Telles, D.R.; Karki, N.; Marshall, M.W. Oral fungal infections: Diagnosis and management. *Dent. Clin. N. Am.* **2017**, *61*, 319–349. [CrossRef] [PubMed]
3. Kim, J.; Sudbery, P. *Candida albicans*, a major human fungal pathogen. *J. Microbiol.* **2011**, *49*, 171–177. [CrossRef] [PubMed]
4. Gow, N.A.; van de Veerdonk, F.L.; Brown, A.J.; Netea, M.G. *Candida albicans* morphogenesis and host defence: Discriminating invasion from colonization. *Nat. Rev. Microbiol.* **2011**, *10*, 112–122. Available online: Https://www.ncbi.nlm.nih.gov/pubmed/22158429 (accessed on 12 July 2018). [CrossRef] [PubMed]
5. Moyes, D.L.; Richardson, J.P.; Naglik, J.R. *Candida albicans*-epithelial interactions and pathogenicity mechanisms: Scratching the surface. *Virulence* **2015**, *6*, 338–346. Available online: Https://www.ncbi.nlm.nih.gov/pubmed/25714110 (accessed on 12 July 2018). [CrossRef] [PubMed]
6. Rao, R.S.; Patil, S.; Ganavi, B.S. Oral cytokeratins in health and disease. *J. Contemp. Dent. Pract.* **2014**, *15*, 127–136. [CrossRef] [PubMed]
7. Iwasaki, S.; Aoyagi, H.; Yoshizawa, H. Localization of keratins 13 and 14 in the lingual mucosa of rats during the morphogenesis of circumvallate papillae. *Acta Histochem.* **2011**, *113*, 395–401. [CrossRef] [PubMed]
8. Iwasaki, S.; Yoshizawa, H.; Aoyagi, H. Immunohistochemical expression of keratins 13 and 14 in the lingual epithelium of rats during the morphogenesis of filiform papillae. *Arch. Oral Biol.* **2006**, *51*, 416–426. [CrossRef] [PubMed]
9. Roca, I.; Akova, M.; Baquero, F.; Carlet, J.; Cavaleri, M.; Coenen, S.; Cohen, J.; Findlay, D.; Gyssens, I.; Heuer, O.E.; et al. The global threat of antimicrobial resistance: Science for intervention. *New Microbes New Infect.* **2015**, *6*, 22–29. [CrossRef] [PubMed]
10. Santezi, C.; Reina, B.D.; Dovigo, L.N. Curcumin-mediated Photodynamic Therapy for the treatment of oral infections-A review. *Photodiagnosis Photodyn. Ther.* **2018**, *21*, 409–415. [CrossRef] [PubMed]
11. Soukos, N.S.; Goodson, J.M. Photodynamic therapy in the control of oral biofilms. *Periodontol. 2000.* **2011**, *55*, 143–166. [CrossRef] [PubMed]
12. Van Straten, D.; Mashayekhi, V.; de Bruijn, H.S.; Oliveira, S.; Robinson, D.J. Oncologic Photodynamic Therapy: Basic principles, current clinical status and future directions. *Cancers (Basel)* **2017**, *9*, 19. [CrossRef] [PubMed]
13. Hamblin, M.R. Antimicrobial photodynamic inactivation: A bright new technique to kill resistant microbes. *Curr. Opin. Microbiol.* **2016**, *33*, 67–73. [CrossRef] [PubMed]
14. Amalraj, A.; Pius, A.; Gopi, S.; Gopi, S. Biological activities of curcuminoids, other biomolecules from turmeric and their derivatives-A review. *J. Tradit. Complement. Med.* **2016**, *7*, 205–233. [CrossRef] [PubMed]
15. Dovigo, L.N.; Pavarina, A.C.; Ribeiro, A.P.; Brunetti, I.L.; Costa, C.A.; Jacomassi, D.P.; Bagnato, V.S.; Kurachi, C. Investigation of the photodynamic effects of curcumin against *Candida albicans*. *Photochem. Photobiol.* **2011**, *87*, 895–903. [CrossRef] [PubMed]
16. Dovigo, L.N.; Pavarina, A.C.; Carmello, J.C.; Machado, A.L.; Brunetti, I.L.; Bagnato, V.S. Susceptibility of clinical isolates of *Candida* to photodynamic effects of curcumin. *Lasers Surg. Med.* **2011**, *43*, 927–934. [CrossRef] [PubMed]
17. Martins, C.V.; da Silva, D.L.; Neres, A.T.; Magalhães, T.F.; Watanabe, G.A.; Modolo, L.V.; Sabino, A.A.; de Fátima, A.; de Resende, M.A. Curcumin as a promising antifungal of clinical interest. *J. Antimicrob. Chemother.* **2009**, *63*, 337–339. [CrossRef] [PubMed]
18. Andrade, M.C.; Ribeiro, A.P.; Dovigo, L.N.; Brunetti, I.L.; Giampaolo, E.T.; Bagnato, V.S.; Pavarina, A.C. Effect of different pre-irradiation times on curcumin-mediated photodynamic therapy against planktonic cultures and biofilms of *Candida* spp. *Arch. Oral Biol.* **2013**, *58*, 200–210. [CrossRef] [PubMed]
19. Dovigo, L.N.; Carmello, J.C.; de Souza Costa, C.A.; Vergani, C.E.; Brunetti, I.L.; Bagnato, V.S.; Pavarina, A.C. Curcumin-mediated photodynamic inactivation of *Candida albicans* in a murine model of oral candidiasis. *Med. Mycol.* **2013**, *51*, 243–251. [CrossRef] [PubMed]
20. Carmello, J.C.; Alves, F.; Basso, F.G.; de Souza Costa, C.A.; Bagnato, V.S.; Mima, E.G.; Pavarina, A.C. Treatment of oral candidiasis using photodithazine®-mediated Photodynamic Therapy in vivo. *PLoS ONE* **2016**, *11*, e0156947. [CrossRef] [PubMed]

21. Akbik, D.; Ghadiri, M.; Chrzanowski, W.; Rohanizadeh, R. Curcumin as a wound healing agent. *Life Sci.* **2014**, *116*, 1–7. [CrossRef] [PubMed]
22. Fonseca-Santos, B.; Dos Santos, A.M.; Rodero, C.F.; Gremião, M.P.; Chorilli, M. Design, characterization, and biological evaluation of curcumin-loaded surfactant-based systems for topical drug delivery. *Int. J. Nanomed.* **2016**, *11*, 4553–4562. [CrossRef] [PubMed]
23. Tejada, S.; Manayi, A.; Daglia, M.; Nabavi, S.F.; Sureda, A.; Hajheydari, Z.; Gortzi, O.; Pazoki-Toroudi, H.; Nabavi, S.M. Wound healing effects of curcumin: A short review. *Curr. Pharm. Biotechnol.* **2016**, *17*, 1002–1007. [CrossRef] [PubMed]
24. Hussain, Z.; Thu, H.E.; Ng, S.F.; Khan, S.; Katas, H. Nanoencapsulation, an efficient and promising approach to maximize wound healing efficacy of curcumin: A review of new trends and state-of-the-art. *Colloids Surf. B Biointerface* **2017**, *150*, 223–241. [CrossRef] [PubMed]
25. Kant, V.; Gopal, A.; Pathak, N.N.; Kumar, P.; Tandan, S.K.; Kumar, D. Antioxidant and anti-inflammatory potential of curcumin accelerated the cutaneous wound healing in streptozotocin-induced diabetic rats. *Int. Immunopharmacol.* **2014**, *20*, 322–330. [CrossRef] [PubMed]
26. Mehrabani, D.; Farjam, M.; Geramizadeh, B.; Tanideh, N.; Amini, M.; Panjehshahin, M.R. The healing effect of curcumin on burn wounds in rat. *World J. Plast. Surg.* **2015**, *4*, 29–35. [PubMed]
27. Partoazar, A.; Kianvash, N.; Darvishi, M.H.; Nasoohi, S.; Rezayat, S.M.; Bahador, A. Ethosomal curcumin promoted wound healing and reduced bacterial flora in second degree burn in rat. *Drug Res. (Stuttg)* **2016**, *66*, 660–665. [CrossRef] [PubMed]
28. Krausz, A.E.; Adler, B.L.; Cabral, V.; Navati, M.; Doerner, J.; Charafeddine, R.A.; Chandra, D.; Liang, H.; Gunther, L.; Clendaniel, A.; et al. Curcumin-encapsulated nanoparticles as innovative antimicrobial and wound healing agent. *Nanomedicine* **2015**, *11*, 195–206. [CrossRef] [PubMed]
29. Salmazi, R.; Calixto, G.; Bernegossi, J.; Ramos, M.A.; Bauab, T.M.; Chorilli, M. A curcumin-loaded liquid crystal precursor mucoadhesive system for the treatment of vaginal candidiasis. *Int. J. Nanomed.* **2015**, *10*, 4815–4824. [CrossRef]
30. Gonçalez, M.L.; Rigon, R.B.; Pereira-da-Silva, M.A.; Chorilli, M. Curcumin-loaded cationic solid lipid nanoparticles as a potential platform for the treatment of skin disorders. *Pharmazie* **2017**, *72*, 721–727. [CrossRef] [PubMed]
31. Trigo Gutierrez, J.K.; Zanatta, G.C.; Ortega, A.L.M.; Balastegui, M.I.C.; Sanitá, P.V.; Pavarina, A.C.; Barbugli, P.A.; Mima, E.G.O. Encapsulation of curcumin in polymeric nanoparticles for antimicrobial Photodynamic Therapy. *PLoS ONE* **2017**, *12*, e0187418. [CrossRef] [PubMed]
32. Kumari, A.; Yadav, S.K.; Yadav, S.C. Biodegradable polymeric nanoparticles based drug delivery systems. *Colloids Surf. B Biointerfaces* **2010**, *75*, 1–18. [CrossRef] [PubMed]
33. Chereddy, K.K.; Coco, R.; Memvanga, P.B.; Ucakar, B.; des Rieux, A.; Vandermeulen, G.; Préat, V. Combined effect of PLGA and curcumin on wound healing activity. *J. Control. Release* **2013**, *171*, 208–215. [CrossRef] [PubMed]
34. Shaikh, J.; Ankola, D.D.; Beniwal, V.; Singh, D.; Kumar, M.N. Nanoparticle encapsulation improves oral bioavailability of curcumin by at least 9-fold when compared to curcumin administered with piperine as absorption enhancer. *Eur. J. Pharm. Sci.* **2009**, *37*, 223–230. [CrossRef] [PubMed]
35. Yallapu, M.M.; Gupta, B.K.; Jaggi, M.; Chauhan, S.C. Fabrication of curcumin encapsulated PLGA nanoparticles for improved therapeutic effects in metastatic cancer cells. *J. Colloid Interface Sci.* **2010**, *351*, 19–29. [CrossRef] [PubMed]
36. Ghosh, D.; Choudhury, S.T.; Ghosh, S.; Mandal, A.K.; Sarkar, S.; Ghosh, A.; Saha, K.D.; Das, N. Nanocapsulated curcumin: Oral chemopreventive formulation against diethylnitrosamine induced hepatocellular carcinoma in rat. *Chem. Biol. Interact.* **2012**, *195*, 206–214. [CrossRef] [PubMed]
37. Khalil, N.M.; do Nascimento, T.C.; Casa, D.M.; Dalmolin, L.F.; de Mattos, A.C.; Hoss, I.; Romano, M.A.; Mainardes, R.M. Pharmacokinetics of curcumin-loaded PLGA and PLGA-PEG blend nanoparticles after oral administration in rats. *Colloids Surf. B Biointerfaces* **2013**, *101*, 353–360. [CrossRef] [PubMed]
38. Gaumet, M.; Vargas, A.; Gurny, R.; Delie, F. Nanoparticles for drug delivery: The need for precision in reporting particle size parameters. *Eur. J. Pharm. Biopharm.* **2008**, *69*, 1–9. [CrossRef] [PubMed]
39. Hegge, A.B.; Nielsen, T.T.; Larsen, K.L.; Bruzell, E.; Tønnesen, H.H. Impact of curcumin supersaturation in antibacterial photodynamic therapy—effect of cyclodextrin type and amount: Studies on curcumin and curcuminoides XLV. *J. Pharm. Sci.* **2012**, *101*, 1524–1537. [CrossRef] [PubMed]

40. Hazzah, H.A.; Farid, R.M.; Nasra, M.M.; Hazzah, W.A.; El-Massik, M.A.; Abdallah, O.Y. Gelucire-based nanoparticles for curcumin targeting to oral mucosa: Preparation, characterization, and antimicrobial activity assessment. *J. Pharm. Sci.* **2015**, *104*, 3913–3924. [CrossRef] [PubMed]
41. Udompornmongkol, P.; Chiang, B.H. Curcumin-loaded polymeric nanoparticles for enhanced anti-colorectal cancer applications. *J. Biomater. Appl.* **2015**, *30*, 537–546. [CrossRef] [PubMed]
42. Mukerjee, A.; Vishwanatha, J.K. Formulation, characterization and evaluation of curcumin-loaded PLGA nanospheres for cancer therapy. *Anticancer Res.* **2009**, *29*, 3867–3875. [PubMed]
43. Mohanty, C.; Sahoo, S.K. The in vitro stability and in vivo pharmacokinetics of curcumin prepared as an aqueous nanoparticulate formulation. *Biomaterials* **2010**, *31*, 6597–6611. [CrossRef] [PubMed]
44. Loo, C.Y.; Rohanizadeh, R.; Young, P.M.; Traini, D.; Cavaliere, R.; Whitchurch, C.B.; Lee, W.H. Combination of silver nanoparticles and curcumin nanoparticles for enhanced anti-biofilm activities. *J. Agric. Food Chem.* **2016**, *64*, 2513–2522. [CrossRef] [PubMed]
45. Maghsoudi, A.; Yazdian, F.; Shahmoradi, S.; Ghaderi, L.; Hemati, M.; Amoabediny, G. Curcumin-loaded polysaccharide nanoparticles: Optimization and anticariogenic activity against *Streptococcus mutans*. *Mater. Sci. Eng. C Mater. Biol. Appl.* **2017**, *75*, 1259–1267. [CrossRef] [PubMed]
46. Al-Fattani, M.A.; Douglas, L.J. Biofilm matrix of *Candida albicans* and *Candida tropicalis*: Chemical composition and role in drug resistance. *J. Med. Microbiol.* **2006**, *55*, 999–1008. [CrossRef] [PubMed]
47. Ruiz-Herrera, J.; Elorza, M.V.; Valentín, E.; Sentandreu, R. Molecular organization of the cell wall of *Candida albicans* and its relation to pathogenicity. *FEMS Yeast Res.* **2006**, *6*, 14–29. [CrossRef] [PubMed]
48. Lambrechts, S.A.; Aalders, M.C.; Van Marle, J. Mechanistic study of the photodynamic inactivation of *Candida albicans* by a cationic porphyrin. *Antimicrob. Agents Chemother.* **2005**, *49*, 2026–2034. [CrossRef] [PubMed]
49. Ribeiro, A.P.; Andrade, M.C.; da Silva Jde, F.; Jorge, J.H.; Primo, F.L.; Tedesco, A.C.; Pavarina, A.C. Photodynamic inactivation of planktonic cultures and biofilms of *Candida albicans* mediated by aluminum-chloride-phthalocyanine entrapped in nanoemulsions. *Photochem. Photobiol.* **2013**, *89*, 111–119. [CrossRef] [PubMed]
50. Salton, M.R. The adsorption of cetyltrimethylammonium bromide by bacteria, its action in releasing cellular constituents and its bactericidal effects. *J. Gen. Microbiol.* **1951**, *5*, 391–404. [CrossRef] [PubMed]
51. Cieplik, F.; Tabenski, L.; Buchalla, W.; Maisch, T. Antimicrobial photodynamic therapy for inactivation of biofilms formed by oral key pathogens. *Front. Microbiol.* **2014**, *5*, 405. [CrossRef] [PubMed]
52. Mima, E.G.; Vergani, C.E.; Machado, A.L.; Massucato, E.M.; Colombo, A.L.; Bagnato, V.S.; Pavarina, A.C. Comparison of Photodynamic Therapy versus conventional antifungal therapy for the treatment of denture stomatitis: A randomized clinical trial. *Clin. Microbiol. Infect.* **2012**, *18*, E380–E388. [CrossRef] [PubMed]
53. Gong, C.; Wu, Q.; Wang, Y.; Zhang, D.; Luo, F.; Zhao, X.; Wei, Y.; Qian, Z. A biodegradable hydrogel system containing curcumin encapsulated in micelles for cutaneous wound healing. *Biomaterials* **2013**, *34*, 6377–6387. [CrossRef] [PubMed]
54. Rivarola de Gutierrez, E.; Innocenti, A.C.; Cippitelli, M.J.; Salomón, S.; Vargas-Roig, L.M. Determination of cytokeratins 1, 13 and 14 in oral lichen planus. *Med. Oral Patol. Oral Cir. Bucal* **2014**, *19*, e359–e365. [CrossRef] [PubMed]
55. Jacques, C.M.; Pereira, A.L.; Maia, V.; Cuzzi, T.; Ramos-e-Silva, M. Expression of cytokeratins 10, 13, 14 and 19 in oral lichen planus. *J. Oral Sci.* **2009**, *51*, 355–365. [CrossRef] [PubMed]
56. Dos Santos, J.N.; de Sousa, S.O.; Nunes, F.D.; Sotto, M.N.; de Araújo, V.C. Altered cytokeratin expression in actinic cheilitis. *J. Cutan. Pathol.* **2003**, *30*, 237–241. [CrossRef] [PubMed]
57. Kaminagakura, E.; Bonan, P.R.; Lopes, M.A.; Almeida, O.P.; Scully, C. Cytokeratin expression in pseudoepitheliomatous hyperplasia of oral paracoccidioidomycosis. *Med. Mycol.* **2006**, *44*, 399–404. [CrossRef] [PubMed]
58. Lam, M.; Jou, P.C.; Lattif, A.A.; Lee, Y.; Malbasa, C.L.; Mukherjee, P.K.; Oleinick, N.L.; Ghannoum, M.A.; Cooper, K.D.; Baron, E.D. Photodynamic therapy with Pc 4 induces apoptosis of *Candida albicans*. *Photochem. Photobiol.* **2011**, *87*, 904–909. [CrossRef] [PubMed]
59. Buytaert, E.; Dewaele, M.; Agostinis, P. Molecular effectors of multiple cell death pathways initiated by photodynamic therapy. *Biochim. Biophys. Acta* **2007**, *1776*, 86–107.

60. Xu, Y.; Young, M.J.; Battaglino, R.A.; Morse, L.R.; Fontana, C.R.; Pagonis, T.C.; Kent, R.; Soukos, N.S. Endodontic antimicrobial photodynamic therapy: Safety assessment in mammalian cell cultures. *J. Endod.* **2009**, *35*, 1567–1572. [CrossRef] [PubMed]
61. Maisch, T.; Bosl, C.; Szeimies, R.M.; Love, B.; Abels, C. Determination of the antibacterial efficacy of a new porphyrin-based photosensitizer against MRSA ex vivo. *Photochem. Photobiol. Sci.* **2007**, *6*, 545–551. [CrossRef] [PubMed]
62. Dai, T.; Gupta, A.; Huang, Y.Y.; Yin, R.; Murray, C.K.; Vrahas, M.S.; Sherwood, M.E.; Tegos, G.P.; Hamblin, M.R. Blue light rescues mice from potentially fatal *Pseudomonas aeruginosa* burn infection: Efficacy, safety, and mechanism of action. *Antimicrob. Agents Chemother.* **2013**, *57*, 1238–1245. [CrossRef] [PubMed]
63. Zhang, Y.; Zhu, Y.; Gupta, A.; Huang, Y.; Murray, C.K.; Vrahas, M.S.; Sherwood, M.E.; Baer, D.G.; Hamblin, M.R.; Dai, T. Antimicrobial blue light therapy for multidrug-resistant *Acinetobacter baumannii* infection in a mouse burn model: Implications for prophylaxis and treatment of combat-related wound infections. *J. Infect. Dis.* **2014**, *209*, 1963–1971. [CrossRef] [PubMed]
64. Dongari-Bagtzoglou, A.; Fidel, P.L., Jr. The host cytokine responses and protective immunity in oropharyngeal candidiasis. *J. Dent. Res.* **2005**, *84*, 966–977. [CrossRef] [PubMed]
65. Steele, C.; Fidel, P.L., Jr. Cytokine and chemokine production by human oral and vaginal epithelial cells in response to *Candida albicans*. *Infect. Immun.* **2002**, *70*, 577–583. [CrossRef] [PubMed]
66. Conti, H.R.; Gaffen, S.L. Host responses to *Candida albicans*: Th17 cells and mucosal candidiasis. *Microbes Infect.* **2010**, *12*, 518–527. [CrossRef] [PubMed]
67. Richardson, J.P.; Moyes, D.L. Adaptive immune responses to *Candida albicans* infection. *Virulence* **2015**, *6*, 327–337. [CrossRef] [PubMed]
68. De Oliveira, R.R.; Schwartz-Filho, H.O.; Novaes, A.B.; Garlet, G.P.; de Souza, R.F.; Taba, M.; Scombatti de Souza, S.L.; Ribeiro, F.J. Antimicrobial photodynamic therapy in the non-surgical treatment of aggressive periodontitis: Cytokine profile in gingival crevicular fluid, preliminary results. *J. Periodontol.* **2009**, *80*, 98–105. [CrossRef] [PubMed]
69. De Oliveira, R.R.; Novaes, A.B., Jr.; Garlet, G.P.; de Souza, R.F.; Taba, M., Jr.; Sato, S.; de Souza, S.L.; Palioto, D.B.; Grisi, M.F.; Feres, M. The effect of a single episode of antimicrobial photodynamic therapy in the treatment of experimental periodontitis. Microbiological profile and cytokine pattern in the dog mandible. *Lasers Med. Sci.* **2011**, *26*, 359–367. [CrossRef] [PubMed]
70. Zou, W.; Liu, C.; Chen, Z.; Zhang, N. Preparation and characterization of cationic PLA-PEG nanoparticles for delivery of plasmid DNA. *Nanoscale Res. Lett.* **2009**, *4*, 982–992. [CrossRef] [PubMed]
71. Takakura, N.; Sato, Y.; Ishibashi, H.; Oshima, H.; Uchida, K.; Yamaguchi, H.; Abe, S. A novel murine model of oral candidiasis with local symptoms characteristic of oral thrush. *Microbiol. Immunol.* **2003**, *47*, 321–326. [CrossRef] [PubMed]
72. Mima, E.G.; Pavarina, A.C.; Dovigo, L.N.; Vergani, C.E.; Costa, C.A.; Kurachi, C.; Bagnato, V.S. Susceptibility of *Candida albicans* to photodynamic therapy in a murine model of oral candidosis. *Oral Surg. Oral Med. Oral Pathol. Oral Radiol. Endod.* **2010**, *109*, 392–401. [CrossRef] [PubMed]
73. Zhang, G.; Chen, Y.; BilalWaqar, A.; Han, L.; Jia, M.; Xu, C.; Yu, Q. Quantitative analysis of rabbit coronary atherosclerosis. Practical techniques utilizing open-source software. *Anal. Quant. Cytopathol. Histpathol.* **2015**, *37*, 115–122. [PubMed]
74. Jensen, E.C. Quantitative analysis of histological staining and fluorescence using ImageJ. *Anat. Rec. (Hoboken)* **2013**, *296*, 378–381. [CrossRef] [PubMed]

Sample Availability: Samples of the compounds are not available from the authors.



© 2018 by the authors. Licensee MDPI, Basel, Switzerland. This article is an open access article distributed under the terms and conditions of the Creative Commons Attribution (CC BY) license (http://creativecommons.org/licenses/by/4.0/).

Supplementary Material

Genetic Expression of the Inflammatory Cytokines by Quantitative Reverse Transcription-Polymerase Chain Reaction (RT-qPCR)

The expression of inflammatory cytokines was evaluated as previously described [20]. After the storage of the samples in RNA LATER (Ambion), samples were transferred to vials containing 1 mL of TRIZOL (Ambion), which were manually ground or mechanically homogenized in a mini-BEADBATER-16 processor (Model 607; 3450 rpm; Biospec product) with 500 mg of glass spheres (0,1 mm diameter glass, Biospec product) by vibration during 8 cycles of 40 seconds with intervals of 20 seconds at 4 °C. An aliquot of 500 μL was transferred to another microtube containing 0.1 mL of chloroform, which was homogenized and incubated for 3 minutes at room temperature. Following, the samples were centrifuged at 12,000 rcf (Microcentrifuge Eppendorf model 5415R, Hamburg, Germany) for 15 minutes at 4 °C. Then, the aqueous phase containing RNA was transferred to a new tube followed by the addition of 100 μL of isopropanol and 10% of sodium acetate (Ambion) to promote the precipitation of the RNA. The samples were incubated at –80 °C overnight. After the incubation time, samples were centrifuged at 12,000 RCF for 30 minutes at 4 °C. The supernatant was removed, and 0.5 mL of ethanol 75% was added to the pellet. Samples were centrifuged at 7,500 rcf for 5 minutes at 4 °C, and the supernatant was removed again. This process of washing samples was repeated thrice, and in the last washing ethanol 99% was used. Then, the pellet of RNA was dried at room temperature for 45 minutes. The RNA was resuspended in 10 mL of ultra-pure water (Invitrogen). The total RNA extracted was purified and DNAse-treated using a column-based purification kit (Qiagen micro-elute KIT), following the manufacturer's instructions. A second DNAse treatment was performed with Turbo DNAse, and RNA was purified using the Qiagen RNeasy MinElute kit (Qiagen). To quantify the RNA of the samples, their absorbance was read at 260 nm, and the ratio of 260 nm/280 nm was also determined in order to evaluate the purity of the samples. The absorbance was read after extraction and purification steps (3 stages), using a NANODROP DS-11+ Spectophotometer (DeNovix). The RNA integrity was evaluated running RNA samples in 1% agarose gel electrophoresis.

For each sample of total RNA, the cDNA was synthetized using the High Capacity DNA reverse Transcriptase KIT (Applied Byosystem), according to recommendations of the manufacturer. The cDNA was stored at –20 °C for posterior quantitative reverse transcription-polymerase chain reaction (RT-qPCR). After cDNA synthesis, the expression of the pro-inflammatory cytokines [interleukin 1β (IL-1β), interleukin 6 (IL-6), and tumor necrosis factor α (TNF-α)] involved in the inflammatory processes were assessed by each specific primer (TaqmanAssay - Applied Biosystems): βActin (control gene) = Mm00607939_S1; TNFα = Mm00443260_G1; IL-1β = Mm00434228_M1; IL-6 = Mm00446190_M1.

For the RT-qPCR reaction, 1 μL of the cDNA sample was added in 14 μL of the Taqman mix reaction. This mix consisted of 6.25 μL of the Taqman Assay kit (Applied Biosystems), 0.75 μL of the primer specific to each gene, and 7 μL of ultra-pure water. The samples were pipetted into PCR plates and sealed with adhesive. All procedures were performed on PCR Workstation and the surfaces were treated with RNAse (Applied Biosystens). Amplification analyzes were performed on thermocycler (CFX96 touch™ real time PCR detection system, BioRad) and the amplification cycles were analyzed in the software BioRad CFX manager (BioRad). The thermal cycling consisted of 40 cycles of 2 min at 50 °C, 2 min at 95 °C for reverse transcription, 15 sec at 95 °C, 30 sec at 57 °C and 30 sec at 60 °C. In all experiments, negative controls (samples without primers) were performed to exclude possibilities of RNA or genomic DNA contamination

Individual samples manually ground showed low yield of genetic material (84.73% of genetic material was lost after purification procedures), hindering the cDNA synthesis. Therefore, samples were pooled according to their groups and mechanically homogenized, which increased the genetic material yielded after purification (56.11% of genetic material was lost). However, electrophoresis demonstrated degradation of RNA. Another attempt was performed with the remaining samples, which were pooled according to their groups (AC + L−, CC + L−, AC + L+, and CC + L+) and manually ground. Although a low yield was observed after purification (84.88% of genetic material was lost), electrophoresis demonstrated no degradation of RNA, and it was possible to standardize the samples in 1 μg/μL for cDNA synthesis. After qPCR, expression of

inflammatory cytokines was normalized by the expression of βActin gene. Each cytokine evaluated (TNF-α, IL-1β, and IL-6) showed similar expression among the groups (Figure 1S). Unfortunately, the samples of the other groups (C − L−, C + L−, C + L+, NYS1, and NYS4) were lost during the attempts to extract the RNA as described.

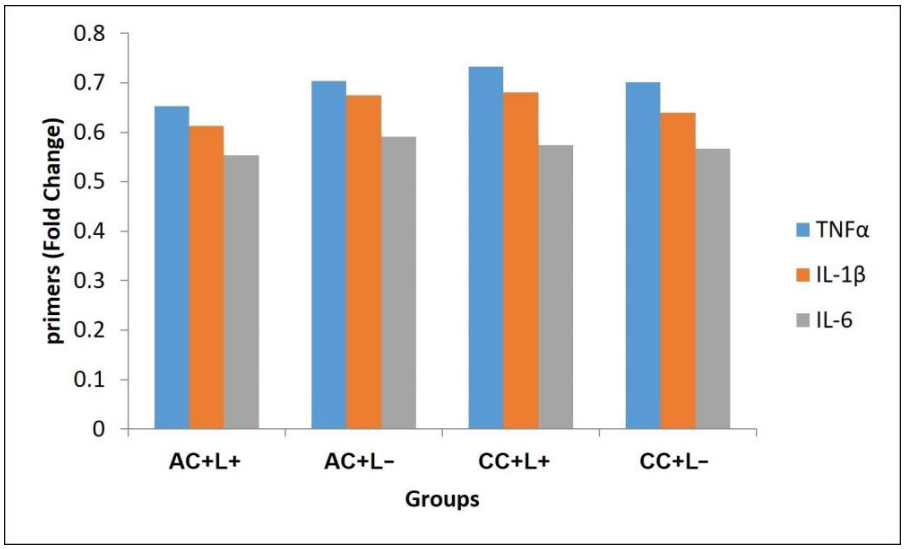


Figure S1. Mean values of gene expression for pooled samples normalized by the β-actin gene.

3.4 Publicação 4·

Photodiagnosis and Photodynamic Therapy 24 (2018) 212–219

Contents lists available at ScienceDirect

Photodiagnosis and Photodynamic Therapy

journal homepage: www.elsevier.com/locate/pdpdt

Effect of Chloroaluminium phthalocyanine in cationic nanoemulsion on photoinactivation of multispecies biofilm

Jeffersson Krishan Trigo-Gutierrez[a], Paula Volpato Sanitá[a], Antonio Claudio Tedesco[b], Ana Cláudia Pavarina[a], Ewerton Garcia de Oliveira Mima[a,*]

[a] Department of Dental Materials and Prosthodontics, São Paulo State University (UNESP), School of Dentistry, Araraquara, São Paulo, Brazil
[b] Center of Nanotechnology and Tissue Engineers, Photobiology and Photomedicine Research Group, FFCLRP—São Paulo University, Ribeirão Preto, São Paulo, Brazil

ARTICLE INFO

Keywords:
Biofilm
Fungi
Bacteria
Photochemotherapy
Nanocarriers
Antimicrobial photodynamic therapy

ABSTRACT

Background: Photosensitizers in nanocarriers have been investigated for antimicrobial Photodynamic Therapy (aPDT). However, most studies are focused against microorganisms in planktonic or monospecies biofilm. Thus, this in vitro study evaluated the effect of aPDT using Chloroaluminium phthalocyanine (ClAlPc) in cationic nanoemulsion (NE) against *Candida albicans*, *Candida glabrata* and *Streptococcus mutans* grown as multispecies biofilm.

Methods: Standard suspensions of each microorganism were added into wells of a microtiter plate for biofilm growth for 48 h in a candle jar. The biofilms were incubated with ClAlPc in cationic NE at 31.8 μM for 30 min and illuminated with red light fluence of 39.3 J/cm^2 (P + L + group). Additional samples were treated only with photosensitizer (P + L-) or red light (P-L +) or neither (P-L-, control group). aPDT efficacy was assessed by colony quantification, biofilm's metabolic activity, total biomass, and confocal microscopy. Data were analyzed by ANOVA/Welch and post-hoc Tukey/Games-Howell tests ($\alpha = 0.05$).

Results: aPDT (P + L +) reduced the colony count in 1.30 to 2.24 lg_{10} and the metabolic activity in 53.7% compared with the control group (P-L-). The total biomass showed no statistical difference among the groups. The confocal microscopy analyzes showed uptake of the PS in the biofilm, and dead cells were observed in the biofilm treated with aPDT.

Conclusion: aPDT mediated by ClAlPc in cationic NE promoted photoinactivation of the multispecies biofilm, which was confirmed by colony quantification, metabolic activity, and confocal microscopy. However, the total biomass of the biofilm was not affected by the treatment.

1. Introduction

Oral candidiasis is a common fungal infection that affects humans. The main factor associated with this multi-etiological disease is *Candida*-gender fungi, and *Candida albicans* is the most prevalent species [1]. Although *Candida* spp. live commensally in the oral cavity, under local and systemic conditions, such as patients wearing a dental prosthesis, xerostomia, and the use of antibiotics and immunosuppressive drugs, yeasts can become pathogenic. Besides *C. albicans*, other fungal species, such as *Candida glabrata, Candida tropicalis, Candida parapsilosis, Candida pseudotropicalis, Candida krusei*, and *Candida guilliermondi* were isolated from the palatal mucosa and from the denture's acrylic surface of patients with denture stomatitis [2], a prevalent type of oral candidiasis found in denture users. *C. glabrata* is the second most prevalent yeast isolated [3], and its innate resistance to many azole antifungal agents, especially fluconazole, is concerning [4]. Furthermore, *C. glabrata* is responsible for fungemia cases along with *C. albicans* [5].

Although *Candida* spp. are considered the main pathogens in oral candidiasis development, bacteria from oral microbiota also contribute to the colonization and proliferation of fungal species [6]. The high prevalence of *Streptococcus mutans* has been reported on dental prosthesis surfaces [7], and its virulence is influenced by the ability to (i) produce high amounts of organic acids from carbohydrate metabolism, (ii) survive in low-pH environments, and (iii) synthesize extracellular glucan from sucrose, which is important in early stages of microorganism adhesion and colonization in order to form biofilm [8]. Both microorganisms, bacteria and fungi, coexist in harmony as a multispecies biofilm in the oral cavity [9]. Several microbial infections are strongly associated with biofilms, which confer mutual beneficial

* Corresponding author at: R. Humaitá nº 1680, Araraquara, São Paulo, CEP 14801-903, Brazil.
E-mail address: ewerton.mima@unesp.br (E.G.d.O. Mima).

https://doi.org/10.1016/j.pdpdt.2018.10.005
Received 23 March 2018; Received in revised form 30 September 2018; Accepted 5 October 2018
Available online 09 October 2018
1572-1000/ © 2018 Elsevier B.V. All rights reserved.

· Artigo nas normas do periódico *Photodiagnosis and Photodynamic Therapy*.

interactions between microorganisms and improve protection against host defenses. The clinical relevance of these interactions between microorganisms is that multispecies biofilms have different phenotypic properties and an increased resistance to antimicrobial agents compared to free planktonic microorganisms [10].

Beyond the increased resistance of microorganisms in biofilm, another concern is the development of resistant strains due to the indiscriminate use of antimicrobials [11]. Due to deficiencies of available treatments, antimicrobial alternatives have been widely investigated and, in this context, an alternative method to inactivate pathogenic microorganisms is the antimicrobial Photodynamic Therapy (aPDT). aPDT associates a photosensitizing agent (PS) with a light source of a suitable wavelength. The interaction between the PS and light in the presence of oxygen results in the production of reactive species, mainly the singlet oxygen and free radicals that promote cell damage and death [12,13]. Due to a great diversity of microorganisms in infections, and the limitation of the majority of available treatments, the option of aPDT is feasible. Research of PSs with high efficacy is also a challenge for biofilm inactivation. Among the PSs, phthalocyanines (Pc) are second generation PSs which require metals in its structure to have a photodynamic effect and are activated by red light [14]. Since Chloroaluminium phthalocyanine (ClAlPc) is a hydrophobic PS, drug delivery systems are needed to carry it in an aqueous solution without aggregation (Fig. 1), enabling its in vivo use [15].

Previous studies demonstrated that aPDT mediated by ClAlPc encapsulated in cationic nanoemulsions (NE) and red light emitting diodes (LED) promoted a significant reduction of 70% in the metabolism of *C. albicans* biofilm [16] and decrease 2.26 lg_{10} of *C. albicans* counts recovered from oral candidiasis lesions on tongues of mice [17]. Despite the promising results with ClAlPc in NE against monospecies biofilm, the effect of aPDT mediated by this PS against multispecies biofilm remains unknown. Since this is an alternative treatment modality for microbial infections, the knowledge of this outcome could be important before its clinical application. Thus, the aim of this study was to evaluate the effect of aPDT mediated by ClAlPc encapsulated in cationic NE associated with red LED (660 nm) against multispecies biofilm of *C. albicans*, *C. glabrata*, and *S. mutans*.

2. Materials and methods

2.1. Photosensitizer synthesis

The ClAlPc encapsulated in cationic NE was prepared by Photobiology and Photomedicine of Nanotechnology and Tissue Engineering Research Group of the São Paulo University (USP) in Ribeirão Preto - SP as described previously [16–19]. The ClAlPc was entrapped in NE at the concentration of 68.8 μM, then it was dissolved in Brain Heart Infusion (BHI) broth (Difco, Detroit, Michigan, USA) at the final concentration of 31.8 μM. At this concentration, the ClAlPc in NE showed similar photophysical, photochemical, and photobiological properties to those previously described [19,20] in which no aggregation of the PS was observed. The concentration of this formulation was previously tested against planktonic cultures and monospecies biofilms of *C. albicans* [16], methicillin-resistant (MRSA) and susceptible (MSSA) *Staphylococcus aureus* [18].

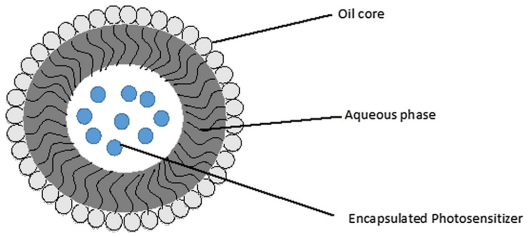


Fig. 1. Representative scheme of nanoemulsion (NE) used to encapsulate ClAlPc.

2.2. Light source

The device used for aPDT was composed by two sets of LED (LXHL-PR09, Luxeon III Emitter; Lumileds Lighting, San Jose, CA) sources, localized on the top and the bottom of a glass plate, where the culture plate was placed for irradiation. This light source had coolers at the top of the upper LED and at the bottom of the lower LEDs to avoid heating of the samples. This apparatus was called "Biotable" and Fig. 2 depicts its layout. The distances from the top and bottom of LED to the glass plate were 3.3 cm and 2.5 cm, respectively.

The light source was calibrated at the Physics Institute of São Carlos, São Paulo University, using a spectrophotometer (USB 2000, Ocean Optics, Metric Drive, Winter Park, FL, USA) coupled to a Sony ILX511B charged-couple device detector (Sony Ocean Optics, Metric Drive, Winter Park, FL, USA) with wavelength from 200 nm to 1,100 nm, with an area of 0.120011046 cm^2. For calibration procedures, the 96 well-microtiter plate used in the microbiological experiments was positioned in the Biotable in the same way as in the aPDT experiments, and the intensity and power of each well were measured during irradiation (see Supplementary data). In all experiments of our study, the wells with the lowest difference in light intensity were chosen to grow the biofilm and to perform the aPDT.

The LED device had maximum emission at 660 nm (red), with 20 nm bandwidth, and mean light intensity of 21.84 mW/cm^2. The light dose used was calculated using the following formula:

fluence (J/cm^2) = *intensity* (W/cm^2) / *time* (seconds).

2.3. Microorganisms and multispecies biofilm growth

Standard strains (American Type Culture Collection, ATCC, Rockville, MD, USA) of *C. albicans* (ATCC 90028), *C. glabrata* (ATCC 2001), and *S. mutans* (ATCC 25175) were used for biofilm formation. Previously to the experiments, the strains of *C. albicans* and *C. glabrata* were individually streaked onto Sabouraud Dextrose Agar (SDA, Acumedia Inc., Baltimore, MD, USA) medium with chloramphenicol at 5 μg/mL, and *S. mutans* onto Brain Heart Infusion (BHI Agar, Difco, Detroit, Michigan, USA) medium supplemented with amphotericin B (Sigma Aldrich, St. Louis, MO, USA) at 25 μg/mL. Then, the plates were incubated at 37 °C for 48 h. Two loops of each microorganism newly grown were transferred to RPMI 1640 (Sigma Aldrich, St. Louis, MO, USA) for *C. albicans* and *C. glabrata,* and BHI broth with 1% of glucose for *S. mutans* and incubated at 37 °C for 16 h under agitation at 75 rpm. All experiments with *S. mutans* were performed in candle jars, since biofilm formation by *S. mutans* is dramatically impaired in presence of oxygen, which results in alteration in the microbial cell surface composition, affecting the expression and maturation of Autolysin A, which is critical for biofilm formation [21,22]. After incubation, the cells were centrifuged at 2683.2 x*g* for 5 min and washed twice with sterile phosphate buffer saline (PBS; 100 mM NaCl, NaH_2PO_4 100 mM, pH 7.2). The cells of *C. albicans, C. glabrata*, and *S. mutans* were then resuspended in RPMI and BHI broth, and the optical density of the suspension was standardized in a spectrophotometer at a concentration of 1×10^7 CFU/mL for *C. albicans* and *C. glabrata* and 1×10^8 CFU/mL for *S. mutans* [23].

For the development of the biofilm, aliquots of 50 μL of each standardized suspension were transferred to the wells of a 96-well flat-bottom microtiter plate, which was incubated for 90 min (adhesion phase) at 37 °C in an orbital shaker (75 rpm). After this period, the wells were carefully washed twice with 200 μL of sterile PBS for removal of non-adherent cells. Then, 150 μL of BHI broth with glucose was added

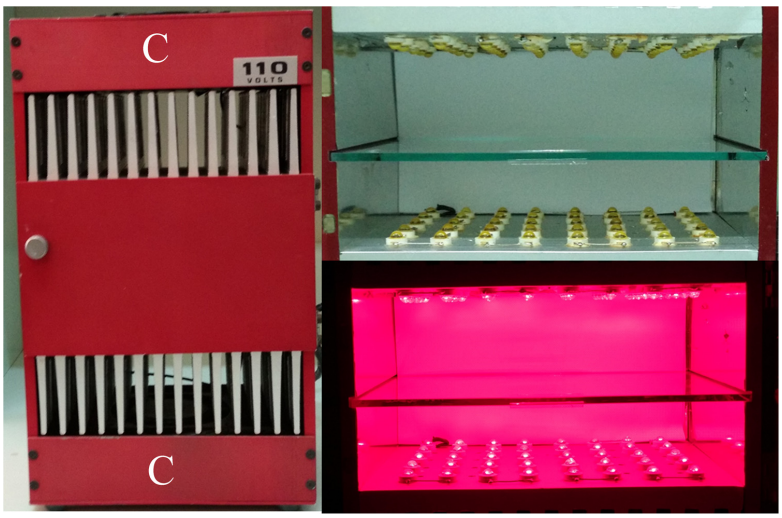


Fig. 2. The LED light source used for aPDT (left: "Biotable"; upper right: top and bottom LEDs turned off; lower right: top and bottom LEDs turned on). C: coolers.

to the wells and the microtiter plate was incubated for 48 h in an orbital shaker (37 °C; 75 rpm) for the development of biofilms [16,18,23]. After 24 h of incubation, 75 µL of the culture medium was removed of each well and renewed through the addition of 75 µL of fresh BHI.

2.4. Antimicrobial photodynamic therapy (aPDT)

After the 48-hour period of biofilm formation, the culture medium was carefully aspirated from each well using a micropipette, and biofilms were washed twice with sterile PBS for the removal of remaining non-adherent cells and culture medium. Aliquots of 150 µL of ClAlPc in NE at 31.8 µM were added in each well containing the biofilms, and the plate was incubated for 30 min (pre-irradiation time) [16]. Afterwards, the PS was removed and 150 µL of sterile saline was added in each well. Biofilms were then illuminated with a dose of 39.3 J/cm^2 during 30 min (P + L + group).

In order to find a dose-response relationship, aPDT experiments using ClAlPc in NE at the concentrations of 16 and 68.8 µM, pre-irradiation time of 30 min, and light fluences of 39.3 and 78.63 J/cm^2 (corresponding to 30 and 60 min of illumination, respectively) were performed as follow: 16 µM of PS was associated with 39.3 J/cm^2 of light, 31.8 and 68.8 µM of PS were associated with 78.63 J/cm^2 of light.

To verify a possible toxic effect of the PS, the same experiments were conducted in additional samples of biofilms exposed only to ClAlPc in NE in the dark (P + L- group). Another group was exposed only to irradiation with saline instead of the PS (P-L +). The control group consisted of biofilms not exposed to PS nor light (P-L-, biofilms received sterile saline instead of PS).

Then, biofilms from each group were evaluated by the following assays:

2.5. Quantification of colonies - CFU/mL assay

After treatments, samples from all test groups were washed twice with PBS, the biofilm was mechanically disrupted from the bottom of the wells using the pipette tip, and serial tenfold dilutions were performed. Aliquots of 25 µL of each dilution were transferred to specific culture agar: CHROMAgar *Candida* (Difco Laboratories, Detroit, Mich.) for yeasts and BHI agar with amphotericin B for *S. mutans*. Then, the agar plates were incubated at 37 °C by 48 h for quantification of colonies (green colonies on CHROMAgar *Candida* were counted as *C. albicans* and pink colonies were counted as *C. glabrata*). Plates containing *S. mutans* were incubated in an atmosphere of 5% CO_2.

2.6. Metabolic activity - XTT assay

XTT ({2,3-bis(2-methoxy-4-nitro-5-sulfophenyl)-5-[(phenylamino) carbonyl]-2H-tetrazolium hyadroxide}, Sigma Chemical Co., St. Louis, MO, USA), a yellow salt, is reduced by enzymes of metabolically active cells in a water-soluble product (formazan), which is measured spectrophotometrically. XTT solution was prepared using ultrapure water at a concentration of 1 mg/mL and kept at -70 °C until the time of the experiments. A solution of menadione (Sigma Aldrich, St. Louis, MO, USA) was prepared in acetone at 0.4 mM immediately before each experiment. The XTT solution prepared in all experiments was constituted of PBS with 200 mM of glucose previously prepared, XTT solution, and menadione in the following proportion: 158 µL, 40 µL, and 2 µL, respectively [25]. After washing twice the biofilms with PBS solution, the XTT solution was added in the wells with the biofilms, which were incubated at 37 °C for 3 h [25]. After this period, 200 µL aliquots of the degradation product of the XTT solution (supernatant) were transferred to wells of another 96-well flat-bottom microtiter plate. The results of the chemical reaction of the XTT test were measured (absorbance) using a spectrophotometer at 492 nm (Thermo Plate - TP Reader).

The use of menadione and glucose is important in the XTT assay, because menadione, when reduced by electrons transported by NADH, is responsible for reducing the XTT [26], and glucose stimulates the mitochondrial activity of *C. albicans* biofilm due to the low metabolic activity in cells located at the basal layers of the biofilm [25].

2.7. Total biomass - crystal violet (CV) assay

The CV staining was used to determine the total biomass of biofilms, including the cells and the extracellular matrix [27]. After the treatments, samples from each group were washed with 200 µL of PBS solution, and 200 µL of 80% methanol (Synth, Diadema, SP, Brasil) was added in each well and maintained for 15 min for biofilm fixation. Then, the methanol was removed and the CV dye (Synth, Diadema, SP, Brasil) at 1% v/v was added and maintained for 5 min. Subsequently, the samples were washed with PBS, and acetic acid (Synth, Diadema,

SP, Brasil) at 33% v/v was added to remove the dye from the biofilms. An aliquot of 200 µL of the resulting product was transferred to the wells of a microtiter plate and the absorbance of the solution was measured using a spectrophotometer at 570 nm (Thermo Plate - TP Reader) [23,27].

2.8. Confocal scanning laser microscopy (CSLM) analysis

The multispecies biofilm was grown onto cover glass-bottom dishes (SPL Life Sciences, Pocheon, Korea) for 48 h. After this period, biofilms were distributed in the same groups described above (P + L +, P + L-, P-L +, and P-L-) in duplicate. After 60 min (simulating 30 min of pre-irradiation time and 30 min of illumination or dark period), biofilms were washed twice with PBS and immediately incubated by 10 min with Live/Dead viability kit containing SYTO-9 and Propidium Iodide (PI) (Molecular Probes, Invitrogen Corp., Carlsbad, USA) prepared according to the manufacturer's instructions. Samples were observed under a confocal laser microscope (Carl Zeiss LSM 800 with Airyscan, Germany) with a laser set at 640 nm (intensity of 6.19%), 488 nm (0.20%), and 561 nm (0.69%) for ClAlPc in NE, SYTO-9, and PI, respectively, and detection range of 618–700 nm, 410–544 nm, and 544–618 nm, respectively, to avoid overlap among the spectra (especially between ClAlPc in NE and PI). In order to differentiate the red fluorescence of ClAlPc from the PI fluorescence, the purple color was chosen for ClAlPc in NE as an alternative to red color. The biofilm thickness was measured with the z-stack set at 1 µm [i.e. images (xy) were taken at each 1 µm of biofilm thickness in order to build the z-stack; 10 to 16 images were obtained for each biofilm].

2.9. Statistical analyzes

For the experiments performed with the PS at the concentration of 31.8 µM associated with 30 min of light irradiation (39.3 J/cm^2), the assays of CFU/mL, metabolic activity, and total biomass were performed in triplicate on three different occasions (n = 9 for each group in each assay). For the statistical analyzes, normal and homoscedastic data from XTT assay and CV staining were analyzed by ANOVA and Tukey post-hoc test. Normal and heteroscedastic data from CFU/mL assay were evaluated by ANOVA/Welch and Games–Howell post-hoc test. The significance level was 5%. Samples treated with 16 µM of PS associated with 39.3 J/cm^2 of light, 31.8 and 68.8 µM of PS associated with 78.63 J/cm^2 of light were evaluated only by quantification of colonies (CFU/mL). Due to the reduced number of samples in each group (n = 3), only descriptive statistical analyze was performed.

3. Results

Fig. 3 shows the results of the CFU/mL assay for *C. albicans*, *C. glabrata*, and *S. mutans* using the PS at the concentration of 31.8 µM associated with the light fluence of 39.3 J/cm^2. For the three microorganisms, statistical analyzes showed significant differences from P + L + groups compared with the groups P-L-, P + L-, and P-L + ($p \leq 0.010$, $p \leq 0.006$, and $p \leq 0.013$ for *C. albicans*, *C. glabrata*, and *S. mutans*, respectively). No significant differences were observed among P-L-, P + L-, and P-L + groups for the three microorganisms ($p \geq 0.077$ for *C. albicans*, $p \geq 0.447$ for *C. glabrata*, and $p \geq 0.620$ for *S. mutans*), indicating no toxic effect of PS and light only. aPDT promoted reductions of 1.30, 1.39, and 2.24 lg_{10} for *C. albicans*, *C. glabrata*, and *S. mutans* counts, respectively, when compared with the control group (P-L-).

The analysis of the XTT absorbance values by ANOVA showed a significant effect of the treatments on the metabolic activity of the biofilms ($p < 0.001$). Tukey post-hoc test demonstrated that the metabolic activity of biofilms submitted to aPDT (P + L + group) was significantly lower ($p \leq 0.001$) than those of the samples from the other groups (P-L-, P + L-, and P-L +). A reduction of 53.7% was observed for aPDT group when compared with the control group. Additionally,

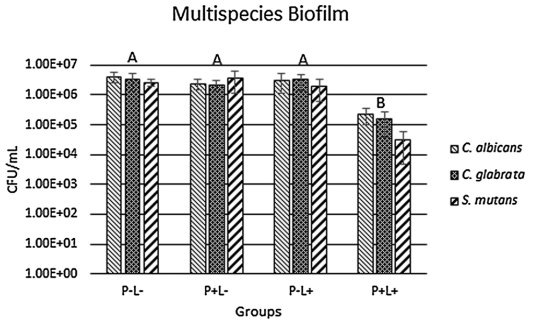


Fig. 3. Mean values of CFU/mL for each microorganism of multispecies biofilm. (A) *C. albicans*, (B) *C. glabrata*, and (C) *S. mutans*; errors bars: standard deviation. Different letters show a significant difference among groups ($p \leq 0.013$).

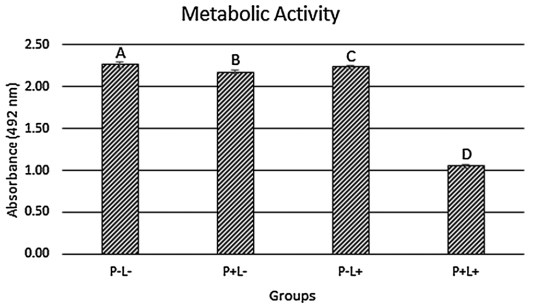


Fig. 4. Mean values of metabolic activity of multispecies biofilm for each group evaluated. Error bars: standard deviation. Different letters show significant differences among groups ($p \leq 0.042$).

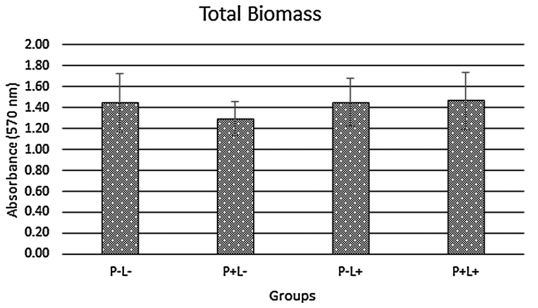


Fig. 5. Mean values of the total biomass of multispecies biofilm. Error bars: standard deviation ($p \geq 0.444$).

significant differences ($p \leq 0.042$) were also observed among the others groups (P-L +, P + L-, and P-L-) (Fig. 4).

Fig. 5 shows the results of the total biomass of the multispecies biofilm. The statistical analyzes of the data demonstrated no significant differences ($p \geq 0.444$) in the total biomass among the groups evaluated.

CSLM showed, in green fluorescence, the presence of viable microorganisms in biofilms from P-L- and P-L + groups (Fig. 6A and 6B), whose mean thickness was 6.6 µm and 6 µm, respectively. Biofilm incubated only with PS (P + L- group) was observed in purple, suggesting PS uptake by the microorganisms grown as multispecies biofilm (Fig. 6C), which showed 14 µm of mean thickness. Fig. 6D shows

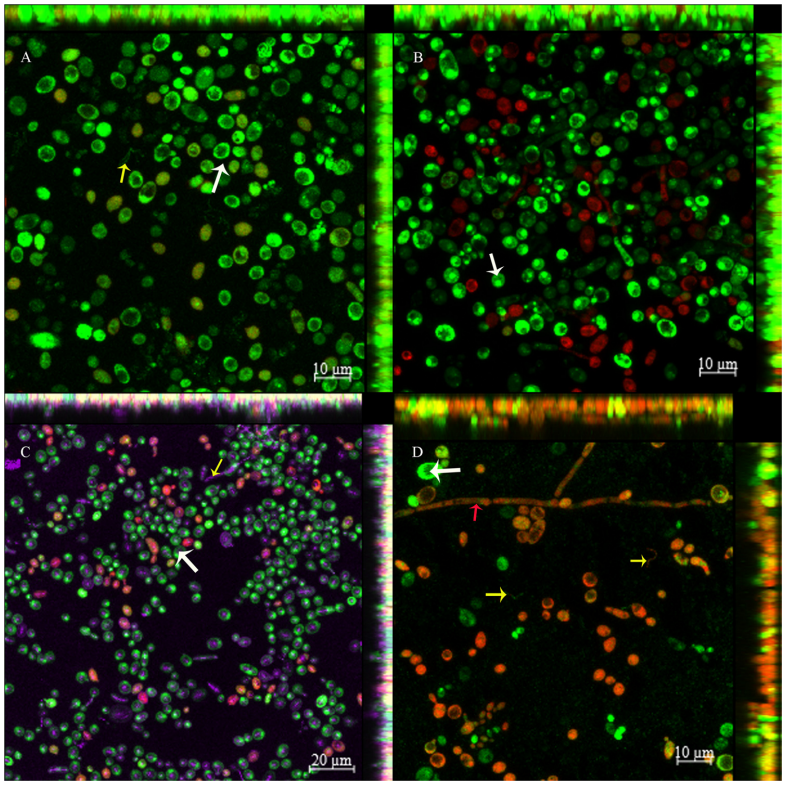


Fig. 6. CSLM images of multispecies biofilm. (A) P-L- and (B) P−L+ groups show viable cells (in green fluorescence); (C) P+L- group shows PS uptake (in purple); (D) P+L+ group shows increased dead cells (in red fluorescence). Magnification: 10 µm for A, B, and D; 20 µm for C. White arrows: yeasts (*C. albicans* and *C. glabrata*); red arrow: filamentous form (*C. albicans*); yellow arrow: coccus (*S. mutans*) (For interpretation of the references to colour in this figure legend, the reader is referred to the web version of this article).

multispecies biofilm submitted to aPDT (P+L+ group), in which the red fluorescence (non-viable cells) was visually increased compared to the others images (6A, 6B, and 6C); additionally, the mean thickness of this sample was 12.5 µm.

When the concentrations of 16 and 68.8 µM of the ClAlPc in NE were used, similar values of CFU/mL among the groups were observed (Table 1). Moreover, increasing the irradiation time to 1 h (78.63 J/cm^2) did not increase the photoinactivation rate of the biofilm using 31.8 µM of the PS (reductions of 0.804, 0.850, and 1.182 lg_{10} were observed for *S. mutans*, *C. albicans*, and *C. glabrata*, respectively). Therefore, a dose-dependent result was not observed. With the light dose of 78.63 J/cm^2, CFU/mL values were similar for all groups evaluated (with and without light) for the three microorganism (Table 1), suggesting that the heating effect due to light irradiation had no effect on the multispecies biofilm. Similar findings were observed with the light dose of 39.3 J/cm^2, which showed no toxic effect to the multispecies biofilm (no significant difference compared with the control group, P-L-) (Fig. 3).

Table 1
Mean values and standard deviation of CFU/mL values of the multispecies biofilm for each group evaluated.

Groups				
PS/species	P-L-	P+L-	P-L+	P+L+
16 µM				
S. mutans	1.34E + 06 (6.00E + 04)	1.53E + 06 (1.63E + 05)	1.51E + 07 (2.02E + 07)	1.80E + 07 (7.25E + 06)
C. albicans	1.29E + 06 (7.57E + 04)	1.42E + 06 (1.71E + 05)	2.30E + 06 (6.41E + 05)	2.45E + 06 (6.07E + 05)
C. glabrata	1.39E + 06 (1.03E + 05)	1.31E + 06 (1.15E + 04)	1.46E + 06 (1.40E + 05)	1.69E + 06 (2.93E + 05)
68.8 µM				
S. mutans	1.87E + 06 (2.93E + 06)	2.82E + 07 (3.46E + 07)	3.63E + 06 (3.48E + 06)	7.26E + 06 (8.17E + 06)
C. albicans	2.93E + 06 (1.48E + 06)	4.61E + 06 (1.44E + 06)	2.52E + 06 (9.85E + 05)	3.46E + 06 (1.68E + 06)
C. glabrata	1.95E + 06 (1.03E + 05)	1.31E + 06 (6.22E + 05)	1.53E + 06 (1.30E + 05)	1.95E + 06 (9.24E + 05)

The PS concentration of 16 µM was associated with 39.3 J/cm^2 while 68.8 µM was associated with 78.63 J/cm^2 (in both associations, 30 min of pre-irradiation time was employed).
n = 3 for each group (no statistical inference was performed).

4. Discussion

ClAlPc has been used as PS in previous studies [16–18], which focused on planktonic cultures or monospecies biofilm. To the best of our knowledge, few studies used Pc as PS against multispecies biofilm [28]. The oral environment is colonized by fungal and bacterial species, which have the ability to grow as multispecies biofilms [29]. These multispecies biofilms are surrounded by an extracellular matrix (ECM), which protects microorganisms against some medications, host

immunity defenses, and external agents [30,31], hindering their eradication. In addition, a previous study suggested that, due to interactions between the different microorganisms, multispecies biofilms might have a more viscous ECM, resulting in increased resistance compared with single biofilms [32]. This ECM may also impede diffusion of substances, such as the contact of PS with microorganisms, hindering the photosensitization process [33,34]. The results of the present investigation showed that ClAlPc at a concentration of 31.8 μM associated to 39.3 J/cm^2 of light fluence reduced the CFU/mL values and metabolic activities of *C. albicans*, *C. glabrata*, and *S. mutans* growing as a multispecies biofilm. This outcome highlights aPDT mediated by ClAlPc as an alternative method against multispecies biofilm.

In the present investigation, reductions of 1.30, 1.39, and 2.24 lg_{10} in CFU values of *C. albicans*, *C. glabrata*, and *S. mutans*, respectively, were observed after aPDT mediated by ClAlPc in NE at 31.8 μM and 39.3 J/cm^2 of light. Increasing the PS concentration and/or the light dose did not increase the microbial photoinactivation. Therefore, a dose-dependent inactivation was not observed. Previous studies demonstrated a reduction of up to 3.1 lg_{10} of *C. albicans* [16] and 5 lg_{10} of MSSA and MRSA [18] after aPDT using the same ClAlPc in cationic NE. However, in these studies, a light fluence of 50 [16] or 100 J/cm^2 [18] were employed, against the 39.3 J/cm^2 used here. These previous studies [16–18] used a light fluence of 100 J/cm^2, since the intensity of the light source employed (38.1 and 44.6 mW/cm^2) was higher than that used in the present investigation (21.84 mW/cm^2). Therefore, with the light source used in the present investigation, a light fluence of 100 J/cm^2 would require an irradiation time higher than 76 min (more than 1 h of illumination), which is clinically unfeasible. Moreover, these studies evaluated planktonic cultures of those species, while the present investigation evaluated the effect of aPDT on a 48-hour multispecies biofilm. In fact, it is important to emphasize that the age or degree of maturation, the nutritional condition of the biofilm, and the cell density may have influenced the effect of the aPDT. A study evaluated the effect of the aPDT mediated by curcumin at 80, 100, and 120 μM on multispecies biofilms of *C. albicans*, *C. glabrata*, and *S. mutans* and verified that the 24-hour biofilm showed a higher susceptibility to aPDT than the 48-hour biofilm [35].

An in vivo study also used ClAlPc in cationic NE as PS and showed a decrease of 2.26 lg_{10} of *C. albicans* in oral candidiasis lesion on tongues of mice [17]. In the present study, the lower lg_{10} reduction of *C. albicans* in the multispecies biofilm could be explained by the fact that the cell density in the tongue of the animals was on the scale of 10^5 CFU/mL [17], while in this in vitro study the multispecies biofilm showed mean values higher than 10^6 CFU/mL. It has been shown that the higher the cell density, the lower the aPDT effect [36], explaining the reduced susceptibility of the biofilm to aPDT verified in the present study. Moreover, some differences that exist between the dynamics of the in vitro and in vivo biofilms, such as the maturation of the biofilm, constant presence of nutritive culture medium during the formation process, the substrate where the biofilm grows, etc., may help to explain the different susceptibility.

The CFU/mL values found in the present research partially agree with those observed in the study performed by Vilsinki et al. [37]. They synthesize ClAlPc in micelles (0.36 and 0.64 μmol/L), which was associated with laser light (42.5 and 63.6 J/cm^2) against planktonic microorganisms [37]. A dose-dependent reduction in the viability of *S. aureus* and *C. albicans* was observed, achieving 3 lg-fold for bacterium and less than 1 lg-fold for yeast [37]. Other kinds of Pc, such as Lutetium (III) acetate Pc (Lu-Pc) [38] or cationic Zn-Pc onto Cellulose Nanocrystals [39], have been evaluated in aPDT. Lu-Pc at 30 μM and 20 μM with 50 J/cm^2 of LED light (665 nm) showed complete photoinactivation of planktonic cultures of *C. albicans* and *Pseudomonas aeruginosa*, while biofilms of these species showed reduced photoinactivation (< 3 lg) [38].

Other investigations also observed reduced susceptibility of multispecies biofilm to aPDT. A polymicrobial biofilm composed of *Actinomyces naeslundii, Veillonella dispar*, *Fusobacterium nucleatum, Streptococcus sobrinus, Streptococcus oralis*, and *C. albicans* grown on bovine enamel discs and exposed to aPDT mediated by methylene blue and soft laser showed reduction lower than 1 lg_{10} [34]. A root canal biofilm formed in vitro by *Actinomyces israelii*, *Fusobacterium nucleatum* subspecies *nucleatum*, *Porphyromonas gingivalis,* and *Prevotella intermedia* was also reduced by less than 1 lg_{10} after aPDT mediated by methylene blue and laser light [40]. The same multispecies biofilm used in the present investigation demonstrated similar reduction rates (1.21, 1.19, and 2.39 lg_{10} for *C. albicans*, *C. glabrata,* and *S. mutans*, respectively) after aPDT with Photodithazine® (PDZ) and LED light [22]. However, when this biofilm was grown on acrylic resin and submitted to three applications of aPDT, only *S. mutans* showed significant reduction compared with control [41]. Therefore, the results of CFU found in the present investigation using aPDT with ClAlPc in NE may be considered similar or superior to those found by other studies. Nevertheless, more studies are needed in order to obtain 3 lg_{10} of reduction, which is considered biologically relevant [42].

Although the determination of CFUs may be the “gold standard” for quantifying microbial growth, it has some drawbacks. The method is time-consuming and labor-intensive. Therefore, other methods for biofilm quantification were used (metabolic activity and biofilm biomass). In contrast to the 48 h required for colony growth and counting, the XTT assay allows measuring the biofilm viability immediately after the treatments. The results showed that aPDT reduced the metabolic activity of multispecies biofilm by 53.7% compared with the control group. This result is in agreement with previous studies that used the same multispecies biofilm and observed significant reductions in the metabolic activity after aPDT mediated by PDZ [23,41] and curcumin [35]. When the ClAlPc in cationic NE was used as PS associated with different light doses against single-species biofilms, reductions in metabolic activity of up to 80% for MSSA biofilm, 76.5% for MRSA biofilm [18], and 70% for *C. albicans* biofilm [16] were observed. Aqueous Pc formulations, such silicon-Pc PEGylated dendrimers, also showed significant reduction in fungal viability of *C. albicans* suspensions [43].

The results of the XTT assay also showed significant differences ($p \leq 0.042$) among the groups P-L-, P+L-, and P-L+. Despite these significant differences, the reductions in the metabolic activity for P+L- and P-L+ groups (3.9% and 1.3%, respectively) in comparison with the control group were considerably lower than that observed for P+L+ group (53.7%). These results are different from those of CFU assay, in which no differences were seen among P-L-, P+L-, and P-L+ groups ($p \geq 0.077$). The XTT assay evaluates metabolic activity immediately after treatments when the viability of the biofilm could be affected temporarily by the treatment. Conversely, in order to evaluate quantification of colonies, 48 h of colony growth is necessary, and during this period, microorganisms can recover from a sub-lethal transitory effect caused by treatments, and subsequently develop colonies on agar plates. Another difference between these assays is the need to disrupt the biofilm for quantification of colonies, while the metabolic activity is measured on intact biofilm. Since the XTT solution is added over the intact biofilm, only the metabolic activity of cells located in the outmost layers of the biofilm could be measured [26], while the cells located in the deeper layers of the biofilm, which probably have not suffered the effects of the treatments, could not be evaluated. In fact, it is well known that the cells located in the top layers of the biofilms have a higher metabolic activity than those in the bottom layers, which are in a state of latency [44]. Therefore, these explanations may justify the significant differences in the metabolic activity between the non-treated biofilms (control) and those submitted to PS or light only, differences not observed in the CFU assay, which may exclude a possible toxic effect of PS and light only. Consequently, XTT assay should not replace the quantification of colonies as a viability test in antimicrobial assays.

The evaluation of total biomass using crystal violet staining quantifies all biofilm components, including living and dead cells and ECM.

Thus, although CV is not adequate to measure the inactivation of biofilm, it may show detachment of the biofilm after any treatment [45]. So, in this investigation, the CV assay was employed to evaluate this possible effect of aPDT on the multispecies biofilm biomass. The results showed that aPDT had no effect in disrupting multispecies biofilm. Other investigations that tested PDZ as PS also verified no disruption of the biofilm biomass formed by *C. albicans*, *C. glabrata*, and *S. mutans* after aPDT [23,41]. On the other hand, previous studies demonstrated, by CV staining, that aPDT may detach biofilms of *Candida* spp. [24,35,46]. The differences in these studies may be attributed to the PS used, since the investigations that found a detachment of biofilm used curcumin as PS [24,35,46]. So, the PS may have a crucial role in the antibiofilm effect of the aPDT. Another important factor that could explain the results of CV staining in the present investigation is the features of the ECM. It is well acknowledged that biofilms are attached communities of cells surrounded by a self-produced ECM, which is responsible for the three-dimensional architecture and cohesiveness of the biofilm [30]. In some multispecies biofilms, there is a synergic relationship among the microorganisms. Zago et al. verified that the growth of *C. albicans* with MRSA resulted in a higher biofilm biomass than the respective monospecies biofilms [47]. In addition, a dual species biofilm of *C. albicans* and *S. mutans* had more biomass than their monospecies biofilms, and this was caused by both the higher growth of *S. mutans* and an increased production of ECM [48]. It was also verified in vivo that this dual species biofilm was more virulent, promoting aggressive dental caries in rats [48]. Therefore, the increased ECM of multispecies biofilm may explain the results obtained here.

CSLM images showed PS uptake by the microorganisms grown as a 48-hour biofilm and few hyphaes. Hyphaes are usually observed in biofilms grown in RPMI 1640 media, which is scarce in nutrients. Due to the presence of *S. mutans* in the biofilm evaluated in the present study, we selected a more nutrient-rich culture media (BHI supplemented with glucose). Previous studies also demonstrated uptake of the PS by *C. albicans* monospecies biofilm using the same PS employed in the present study and free ClAlPc [16] and a Lu-Pc [38]. Uptake of a cationic liposome ClAlPc by cariogenic bacteria suspension was also observed [49], as well as silicon-Pc PEGylated dendrimers and cationic Zn-Pc by planktonic cultures of *C. albicans* [43] and *S. aureus* [50], respectively. Another study reported that oral biofilm formed in situ also showed uptake of pyridinium Zn-Pc, and after aPDT, a more intense fluorescence of PI (suggesting cell killing), less dense biofilm formed by columns of bacterial aggregates were observed [28]. However, it is not possible to visualize the images in the online available manuscript. The PS uptake by the microorganisms is fundamental to the photoinactivation process in order to photosensitize the microbial cells. In fact, the illumination of the photosensitized cells resulted in microbial death, which was observed by the visual increase of red fluorescence of PI after aPDT in Fig. 6D.

Biofilm treated only with light (P-L+) showed red fluorescence (Fig. 6B), indicative of dead cells. This result agrees with that observed in the XTT assay, since the CSLM samples were evaluated immediately after the treatments. However, this result does not agree with Fig. 3 (CFU assay), since cells may recover from a sub-lethal dose during the period of 48 h required for colony growth. Moreover, the cells observed in the CSLM do not necessarily grow individually as colonies, since agglomerated cells and hyphae/pseudohyphae with several branches grow as a single colony. On the other hand, CSLM images from the P-L- group showed live microorganism (green fluorescence of SYTO-9) within the biofilm, corroborating the CFU outcomes. These results are in agreement to previous studies, in which microbial death was observed after aPDT mediated by PDZ [23] or curcumin [35] against the same multispecies biofilm used in the present study. The CSLM images also gave additional information about the biofilm thickness. In the present investigation, the thickness of the 48-hour multispecies biofilm ranged from 6 μm to 14 μm, which partially agree to a previous study in which the 48-hour *C. albicans* biofilm showed thickness between 14 μm and 21 μm [38]. However, in this investigation, the biofilm submitted to aPDT was thicker than the controls. Conversely, aPDT mediated by pyridinium Zn-Pc reduced the thickness of an in situ biofilm [28]. It is important to emphasize that thickness measured by CSLM corresponded to the penetration of the fluorophores into the biofilm. So, the real thickness of the biofilm may not be determined. Another study also observed limited to full penetration of the PS into the biofilm [38].

In conclusion, aPDT mediated by ClAlPc at 31.8 μM associated to 39.9 J/cm^2 of light fluence promoted reduction in CFU/mL values and metabolic activity, but not in the total biomass of the multispecies biofilm formed by *C. albicans*, *C. glabrata*, and *S. mutans*. Therefore, aPDT mediated by ClAlPc in NE and LED light may be an alternative or an adjuvant method for polimicrobial inactivation. However, in the present investigation, only standard strains of *C. albicans*, *C. glabrata*, and *S. mutans* were tested, which is a limitation of this study. The inhibition observed may be strain specific, so it would be important to evaluate clinical isolates in the analysis. Thus, further studies are needed in order to assess the efficacy of the aPDT parameters tested here against clinical isolates and in conditions closer to a clinical scenario, such as in situ and in vivo assays.

Acknowledgments

This work was supported by Pró-Reitoria de Pesquisa (PROPe) UNESP, grant 0199/004/13. Authors thank the Centro de Pesquisa em Óptica e Fotônica (CEPOF) - RIDC/FAPESP (São Paulo Research Foundation, grant 2013/07276-1) for developing and calibrating the LED device used in this study. We also thank Geisiane Helena Gomes Bueno and Dr. Paula Aboud Barbugli for the technical support in the microbiological assays and CSLM, respectively.

Appendix A. Supplementary data

Supplementary material related to this article can be found, in the online version, at doi:https://doi.org/10.1016/j.pdpdt.2018.10.005.

References

[1] A. Singh, R. Verma, A. Murari, A. Agrawal, Oral candidiasis: an overview, J. Oral. Maxillofac. Pathol. 18 (2014) S81–S85, https://doi.org/10.4103/0973-029X.141325.

[2] P.V. Sanitá, A.C. Pavarina, E.T. Giampaolo, M.M. Silva, E.G.O. Mima, D.G. Ribeiro, C.E. Vergani, *Candida* spp. prevalence in well controlled type 2 diabetic patients with denture stomatitis, Oral Surg. Oral Med. Oral Pathol. Oral Radiol. Endod. 6 (2011) 726–733, https://doi.org/10.1016/j.tripleo.2011.02.033.

[3] M. Cavalheiro, M.C. Teixeira, *Candida* biofilms: threats, challenges, and promising strategies, Front. Med. (Lausanne) 28 (2018), https://doi.org/10.3389/fmed.2018.00028.

[4] P.L.J. Fidel, J.A. Vazquez, J.D. Sobel, *Candida glabrata*: review of epidemiology, pathogenesis, and clinical disease with comparison to *C. albicans*, Clin. Microbiol. 12 (1999) 80–96.

[5] G.P. Bodey, M. Mardani, H.A. Hanna, M. Boktour, J. Abbas, E. Girgawy, R.Y. Hachem, D.P. Kontoyiannis, I.I. Raad, The epidemiology of *Candida glabrata* and *Candida albicans* fungemia in immunocompromised patients with cancer, Am. J. Med. 5 (2002) 380–385.

[6] L.Y. Hsu, G.E. Minah, D.E. Peterson, J.R. Wingard, W.G. Merz, V. Altomonte, C.A. Tylenda, Coaggregation of oral *Candida* isolates with bacteria from bone marrow transplant recipients, J. Clin. Microbiol. 28 (1990) 2621–2626.

[7] D.G. Ribeiro, A.C. Pavarina, L.N. Dovigo, A.L. Machado, E.T. Giampaolo, C.E. Vergani, Prevalence of *Candida* spp. associated with bacteria species on complete dentures, Gerodontology 29 (2012) 203–208, https://doi.org/10.1111/j.1741-2358.2011.00578.

[8] W.H. Bowen, H. Koo, Biology of *Streptococcus mutans*-derived glucosyltransferases: role in extracellular matrix formation of cariogenic biofilms, Caries Res. 45 (2011) 69–86, https://doi.org/10.1159/000324598.

[9] Z.M. Thein, J.C. Seneviratne, Y.H. Samaranayake, L.P. Samaranayake, Community lifestyle of *Candida* in mixed biofilms: a mini review, Mycoses 6 (2009) 467–475, https://doi.org/10.1111/j.1439-0507.2009.01719.

[10] H.C. Flemming, J. Wingender, U. Szewzyk, P. Steinberg, S.A. Rice, S. Kjelleberg, Biofilms: an emergent form of bacterial life, Nat. Rev. Microbiol. 14 (2016) 563–575, https://doi.org/10.1038/nrmicro.2016.94.

[11] R.D. Cannon, E. Lamping, A.R. Holmes, K. Niimi, K. Tanabe, M. Niimi, B.C. Monk, *Candida albicans* drug resistance another way to cope with stress, Microbiol. 153 (2007) 3211–3217, https://doi.org/10.1099/mic.0.2007/010405-0.

[12] R.F. Donnelly, P.A. Mccarron, M.M. Tunney, Antifungal photodynamic therapy, Microbiol. Res. 1 (2008) 1–12, https://doi.org/10.1016/j.micres.2007.08.001.
[13] N.S. Soukos, J.M. Goodson, Photodynamic therapy in the control of oral biofilms, Periodontol. 55 (2011) (2000) 143–166, https://doi.org/10.1111/j.1600-0757.2010.00346.x.
[14] R. Abrahamse, M.R. Hamblin, New photosensitizers for photodynamic therapy, Biochem. J. 473 (2016) 347–364, https://doi.org/10.1042/BJ20150942.
[15] P.L. Goto, M.P. Siqueira-Moura, A.C. Tedesco, Application of aluminum chloride phthalocyanine-loaded solid lipid nanoparticles for photodynamic inactivation of melanoma cells, Int. J. Pharm. 518 (2017) 228–241, https://doi.org/10.1016/j.ijpharm.2017.01.004.
[16] A.P.D. Ribeiro, M.C. Andrade, J.F. da Silva, J.H. Jorge, F.L. Primo, A.C. Tedesco, A.C. Pavarina, Photodynamic inactivation of planktonic cultures and biofilms of *Candida albicans* mediated by aluminum-chloride-phthalocyanine entrapped in nanoemulsions, Photochem. Photobiol. 89 (2013) 111–119, https://doi.org/10.1111/j.1751-1097.2012.01198.
[17] J.C. Carmello, F. Alves, A.P.D. Ribeiro, F.G. Basso, C.A. de Souza Costa, A.C. Tedesco, F.L. Primo, E.G. Mima, A.C. Pavarina, In vivo photodynamic inactivation of Candida albicans using chloro-aluminum phthalocyanine, Oral Dis. 22 (5) (2016) 415–422, https://doi.org/10.1111/odi.12466.
[18] A.P.D. Ribeiro, M.C. Andrade, V.S. Bagnato, C.E. Vergani, F.L. Primo, A.C. Tedesco, A.C. Pavarina, Antimicrobial photodynamic therapy against pathogenic bacterial suspensions and biofilms using chloro-aluminum phthalocyanine encapsulated in nanoemulsions, Lasers Med. Sci. 30 (2015) 549–559, https://doi.org/10.1007/s10103-013-1354.
[19] F.L. Primo, M.V. Bentley, A.C. Tedesco, Photophysical studies and in vitro skin permeation/retention of Foscan®/nanoemulsion (NE) applicable to photodynamic therapy skin cancer treatment, J. Nanosci. Nanotechnol. 8 (2008) 340–347, https://doi.org/10.1166/jnn.2008.004.
[20] S. Séguier, S.L. Souza, A.C. Sverzut, A.R. Simioni, F.L. Primo, A. Bodineau, V.M. Corrêa, B. Coulomb, A.C. Tedesco, Impact of photodynamic therapy on inflammatory cells during human chronic periodontitis, J. Photochem. Photobiol. B 101 (2010) 348–354, https://doi.org/10.1016/j.jphotobiol.2010.08.007.
[21] A. Sang-Joon, R.A. Burne, Effects of oxygen on biofilm formation and the AtlA autolysin of Streptococcus mutans, J. Bacteriol. 189 (2007) 6293–6302.
[22] A. Sang-Joon, T.W. Zezhang, R.A. Burne, Effects of oxygen on virulence traits of Streptococcus mutans, J. Bacteriol. 189 (2007) 8519–8527.
[23] C.C.C. Quishida, J.C. Carmello, E.G.O. Mima, V.S. Bagnato, A.L. Machado, A.C. Pavarina, Susceptibility of multispecies biofilm to photodynamic therapy using photodithazine®, Lasers Med. Sci. 30 (2015) 685–694, https://doi.org/10.1007/s10103-013-1397.
[24] L.N. Dovigo, A.C. Pavarina, A.P.D. Ribeiro, I.L. Brunetti, C.A.S. Costa, D.P. Jacomassi, V.S. Bagnato, C. Kurachi, Investigation of the photodynamic effects of curcumin against Candida albicans, Photochem. Photobiol. 4 (2011) 895–903, https://doi.org/10.1111/j.1751-1097.2011.00937.
[25] W.J. Silva, J. Seneviratne, N. Parahitiyawa, E.A.R. Rosa, L.P. Samaranayake, A.A. Del Bel Cury, Improvement of XTT assay performance of studies involving *Candida albicans* biofilms, Braz. Dent. J. 4 (2008) 364–369, https://doi.org/10.1590/S0103-64402008000400014.
[26] B.J. Moss, Y. Kim, M.P. Nandakumar, M.R. Marten, Quantifying metabolic activity of filamentous fungi using a colorimetric XTT assay, Biotechnol. Prog. 24 (2008) 780–783.
[27] S. Stepanovic, D. Vukovic, I. Dakic, B. Savic, M. Svabic-Vlahovic, A modified microtiter-plate test for quantification of staphylococcal biofilm formation, J. Microbiol. Methods 40 (2000) 175–179.
[28] S. Wood, B. Nattress, J. Kirkham, R. Shore, S. Brookes, J. Griffiths, C. Robinson, An in vitro study of the use of photodynamic therapy for the treatment of natural oral plaque biofilms formed in vivo, J. photochem. Photobiol. B 1 (1999) 1–7, https://doi.org/10.1016/S1011-1344(99)00056-1.
[29] L.E. O'Donnell, E. Millhouse, L. Sherry, R. Kean, J. Malcolm, C.J. Nile, G. Ramage, Polymicrobial *Candida* biofilms: friends and foe in the oral cavity, FEMS Yeast Res. 15 (2015), https://doi.org/10.1093/femsyr/fov077 fov077.
[30] H. Koo, K.M. Yamada, Dynamic cell-matrix interactions modulate microbial biofilm and tissue 3D microenvironments, Curr. Opin. Cell. Biol. 42 (2016) 102–112, https://doi.org/10.1016/j.ceb.2016.05.005.
[31] M.M. Harriott, M.C. Noverr, *Candida albicans* and *Staphylococcus aureus* form polymicrobial biofilms: effects on antimicrobial resistance, Antimicrob. Agents. Chemother. 54 (2009) 3746–3755, https://doi.org/10.1128/AAC.00657-09.
[32] C.A. Pereira, R.L. Romeiro, A.C. Costa, A.K. Machado, J.C. Junqueira, A.O. Jorge, Susceptibility of *Candida albicans*, *Staphylococcus aureus*, and *Streptococcus mutans* biofilms to photodynamic inactivation: an in vitro study, Lasers Med. Sci. 26 (2011) 341–348, https://doi.org/10.1007/s10103-010-0852-3.
[33] A.C. Costa, V.M. de Campos Rasteiro, C.A. Pereira, E.S. da Silva Hashimoto, M.J. Beltrame Jr., J.C. Junqueira, A.O. Jorge, Susceptibility of *Candida albicans* and *Candida dubliniensis* to erythrosine- and LED-mediated photodynamic therapy, Arch. Oral. Biol. 11 (2011) 1299–1305, https://doi.org/10.1016/j.archoralbio.2011.05.013.
[34] P. Müller, B. Guggenhem, P.R. Schmidlin, Efficacy of gasiform ozone and photodynamic therapy on a multispecies oral biofilm in vitro, Eur. J. Oral. Sci. 1 (2007) 77–80, https://doi.org/10.1111/j.1600-0722.2007.00418.x.
[35] C.C.C. Quishida, E.G.O. Mima, J.H. Jorge, C.E. Vergani, V.S. Bagnato, A.C. Pavarina, Photodynamic inactivation of a multispecies biofilm using curcumin and LED light, Lasers Med. Sci. 31 (2016) 997–1009, https://doi.org/10.1007/s10103-016-1942-7.
[36] T.N. Demidova, M.R. Hamblin, Effect of cell-photosensitizer binding and cell density on microbial photoinactivation, Antimicrob. Agents. Chemother. 49 (2005) 2329–2335, https://doi.org/10.1128/AAC.49.6.2329-2335.2005.
[37] B.H. Vilsinki, A.P. Gerola, J.A. Enumo, K.D.S.S. Campanholi, P.C.D.S. Pereira, G. Braga, N. Hioka, E. Kimura, A.L. Tessaro, W. Caetano, Formulation of aluminum chloride phthalocyanine in pluronic P-123 and F-127 block copolymer micelles: photophysical properties and photodynamic inactivation of microorganisms, Photochem. Photobiol. 3 (2015) 518–525, https://doi.org/10.1111/php.12421.
[38] V. Mantareva, V. Kussovski, M. Durmuş, E. Borisova, I. Angelov, Photodynamic inactivation of pathogenic species *Pseudomonas aeruginosa* and *Candida albicans* with lutetium (III) acetate phthalocyanines and specific light irradiation, Lasers Med. Sci. 31 (2016) 1591–1598, https://doi.org/10.1007/s10103-016-2022-8.
[39] E. Anaya-Plaza, E. van de Winckel, J. Mikkilä, J.M. Malho, O. Ikkala, O. Gulías, R. Bresolí-Obach, M. Agut, S. Nonell, T. Torres, M.A. Kostiainen, A. de la Escosura, Photoantimicrobial biohybrids by supramolecular immobilization of cationic phthalocyanines onto cellulose nanocrystals, Chemistry 23 (2017) 4320–4326, https://doi.org/10.1002/chem.201605285.
[40] J.L. Fimple, C.R. Fontana, F. Foschi, K.B.S. Ruggiero, X. Song, T.C. Pagonis, A.C.R. Tanner, R. Kent, A.G. Doukas, P.P. Stashenko, N.S. Soukos, Photodynamic treatment of endodontic polymicrobial infection in vitro, J. Endod. 34 (2008) 728–734, https://doi.org/10.1016/j.joen.2008.03.011.
[41] C.C.C. Quishida, E.G.O. Mima, L.N. Dovigo, J.H. Jorge, V.S. Bagnato, A.C. Pavarina, Photodynamic inactivation of a multispecies biofilm using Photodithazine® and LED light after one and three successive applications, Lasers Med. Sci. 9 (2015) 2303–2312, https://doi.org/10.1007/s10103-015-1811-9.
[42] F. Cieplik, L. Tabenski, W. Buchalla, T. Maisch, Antimicrobial photodynamic therapy for inactivation of biofilms formed by oral key pathogens, Front. Microbiol. 5 (92014) (2018) 405, https://doi.org/10.3389/fmicb.2014.00405.
[43] M.A. Hutnick, S. Ahsanuddin, L. Guan, M. Lam, E.D. Baron, J.K. Pokorski, PEGylated dendrimers as drug delivery vehicles for the photosensitizer silicon phthalocyanine Pc 4 for Candidal infections, Biomacromolecules 18 (2017) 379–385, https://doi.org/10.1021/acs.biomac.6b01436.
[44] C.J. Seneviratne, W.J. Silva, L.J. Jin, Y.H. Samaranayake, L.P. Samaranayake, Architectural analysis, viability assessment and growth kinetics of *Candida albicans* and *Candida glabrata* biofilms, Arch. Oral Biol. 54 (2009) 1052–1060, https://doi.org/10.1016/j.archoralbio.2009.08.002.
[45] B. Pitts, M.A. Hamilton, N. Zelver, P.S. Stewart, A microtiter-plate screening method for biofilm disinfection and removal, J. Microbiol. Methods 54 (2003) 269–276, https://doi.org/10.1016/S0167-7012(03)00034-4.
[46] L.N. Dovigo, A.C. Pavarina, J.C. Carmello, A.L. Machado, I.L. Brunetti, V.S. Bagnato, Susceptibility of clinical isolates of *Candida* to photodynamic effects of curcumin, Lasers Surg. Med. 9 (2011) 927–934, https://doi.org/10.1002/lsm.21110.
[47] C.E. Zago, S. Silva, P.V. Sanitá, P.A. Barbugli, C.M.I. Dias, V.B. Lordello, C.E. Vergani, Dynamics of biofilm formation and the interaction between *Candida albicans* and methicillin-susceptible (MSSA) and -resistant *Staphylococcus aureus* (MRSA), PloS One 10 (4) (2015), https://doi.org/10.1371/journal.pone.0123206 e0123206.
[48] M.L. Falsetta, M.I. Klein, P.M. Colonne, K. Scott-Anne, S. Gregoire, C.H. Pai, M. Gonzalez-Begnea, G. Watson, D.J. Krysan, W.H. Bowen, H. Koo, Symbiotic relationship between *Streptococcus mutans* and *Candida albicans* synergizes virulence of plaque biofilms in vivo, Infect. Immun. 5 (2014) 1968–1981, https://doi.org/10.1128/IAI.00087-14.
[49] J.P.F. Longo, S.C. Leal, A.R. Simioni, M.F.M. Almeida-Santos, A.C. Tedesco, R.B. Azevedo, Photodynamic therapy disinfection of carious tissue mediated by aluminum-chloride-phthalocyanine entrapped in cationic liposomes: an in vitro and clinical study, Lasers Med. Sci. 27 (2012) 575–584, https://doi.org/10.1007/s10103-011-0962-6.
[50] Y. Gao, B. Mai, A. Wang, M. Li, X. Wang, K. Zhang, Q. Liu, S. Wei, P. Wang, Antimicrobial properties of a new type of photosensitizer derived from phthalocyanine against planktonic and biofilm forms of *Staphylococcus aureus*, Photodiagn. Photodyn. Ther. 21 (2018) 316–326, https://doi.org/10.1016/j.pdpdt.2018.01.003.

Supplementary Material:

Chart 1. Intensity of light power in mW/cm^2 on each well in 96-microtiter plate.

	1	2	3	4	5	6	7	8	9	10	11	12
A	13.91	17.33	17.32	18.17	17.83	18.32	17.48	17.72	17.10	16.81	14.66	11.13
B	17.22	20.83	21.04	22.04	21.57	22.30	21.36	21.94	20.92	21.00	18.33	13.60
C	16.74	20.54	20.40	21.44	20.80	21.93	20.85	21.60	20.55	20.91	17.68	13.33
D	16.12	19.27	19.78	20.78	20.52	21.66	20.61	21.36	20.31	20.44	17.41	13.14
E	16.16	19.95	19.91	20.93	20.54	21.73	20.83	21.57	20.57	20.51	17.63	13.34
F	17.12	21.20	21.00	22.29	21.93	22.81	22.10	22.70	21.34	21.71	18.70	14.10
G	17.75	21.78	21.41	22.51	21.67	22.53	21.94	21.95	21.54	21.54	19.26	14.72
H	14.63	17.51	17.50	18.40	18.15	18.85	18.51	18.46	18.01	17.81	16.17	12.04

3.5 Publicação 5·

BIOFOULING, 2018
https://doi.org/10.1080/08927014.2018.1439935

Taylor & Francis
Taylor & Francis Group

Check for updates

Antimicrobial sonodynamic and photodynamic therapies against *Candida albicans*

Fernanda Alves[a], Ana Cláudia Pavarina[a], Ewerton Garcia de Oliveira Mima[a], Anthony P. McHale[b] and John Francis Callan[b]

[a]Department of Dental Materials and Prosthodontics, School of Dentistry, São Paulo State University (UNESP), Araraquara, Brazil; [b]School of Pharmacy and Pharmaceutical Sciences, Faculty of Life & Health Sciences, Ulster University, Coleraine, UK

ABSTRACT

Candida albicans biofilms exhibit unique characteristics and are highly resistant to antifungal agents. Antimicrobial photodynamic therapy (aPDT) is an alternative treatment limited to treating superficial infections due to the poor light penetration. In this manuscript, the antifungal properties of sonodynamic therapy (SDT) were assessed. SDT uses ultrasound instead of light, enabling the treatment of deeper infections. Planktonic cells and biofilms of *C. albicans* were treated with aPDT or SDT, in addition to combined aPDT/SDT, with cell survival determined using colony forming units. The total biomass and structural integrity of the biofilms were also investigated. The results demonstrated that while individual aPDT or SDT eradicated suspensions, they had little impact on biofilms. However, combined aPDT/SDT significantly reduced the viability and total biomass of biofilms. Microscopic images revealed that biofilms treated with aPDT/SDT were thinner and comprised mainly of dead cells. These results highlight the potential of combined aPDT/SDT for the inactivation of *C. albicans* biofilms.

ARTICLE HISTORY
Received 23 June 2017
Accepted 6 February 2018

KEYWORDS
Candida albicans; photodynamic therapy; sonodynamic therapy; biofilms; antimicrobial; antifungal

Introduction

Oropharyngeal candidosis (OPC) is one of the most common manifestations of mucocutaneous candidiasis in patients receiving corticosteroid therapy, prolonged use of antibiotics, cancer chemotherapy and in those suffering from immunosuppression after transplantation or human immunodeficiency virus (HIV) infections (Peres-Bota et al. 2004). Depending on the stage of immunosuppression, up to 90% of HIV-positive patients present with OPC, which consequently is considered an indicator of the development of HIV infection (Pfaller and Diekema 2007). *Candida albicans* is the main etiological agent of OPC and the switching from commensal to the pathogenic condition has been widely known to be associated with its ability to grow in filamentous form that facilitates invasion of epithelial tissue (Sudbery 2011). Furthermore, *Candida* species have the ability to form a biofilm that is a highly structured community of microorganisms attached to a surface and are embedded in a self-produced protective extracellular matrix (Costerton et al. 1999; Ramage et al. 2009). The extracellular matrix contributes to the preservation of the biofilm architecture and to the maintenance of stable cell-cell, cell-surface and cell-environment interactions (Flemming and Wingender 2010). The benefits of organisms being organized as biofilms include protection from environmental changes, protection against host defense, enabling metabolic cooperation and regulation of gene expression (Ramage et al. 2009). For these reasons, cells in biofilms exhibit unique phenotypic characteristics compared to their planktonic counterparts and from a therapeutic perspective, tend to be more resistant to antimicrobial agents (Ramage et al. 2009). *Candida* spp. can also be associated with disseminated forms of disease, such as candidemia, which exhibit a high morbidity and mortality rate (Pfaller and Diekema 2007).

Considering the high frequency of *Candida* infections in immunocompromised patients, it is clear that an effective antifungal therapy is necessary. Topical antifungal agents are often prescribed to manage OPC (Lombardi and Budtz-Jorgensen 1993; Banting et al. 1995). However, these agents achieve only a transient response and relapses are frequent (Samaranayake and MacFarlane 1981; Kulak et al. 1994). As the recurrence rate is high, systemic azole antifungals (eg fluconazole and itraconazole) have mainly been used to treat fungal infections (Samaranayake and

CONTACT John Francis Callan j.callan@ulster.ac.uk

© 2018 Informa UK Limited, trading as Taylor & Francis Group

· Artigo nas normas do periódico *Biofouling*.

MacFarlane 1981; Barchiesi et al. 1998; Ellepola and Samaranayake 2000). Nevertheless, the increased use of azoles, combined with several cases of treatment failures, has drawn attention to the problem of antifungal resistance (Hunter et al. 1998; White et al. 1998; Goldman et al. 2004). Clinical resistance to antifungal drugs is a broad concept describing failure of an antifungal therapy, which results in persistence or progression of an infection (White et al. 1998). It has been reported that exposure to fluconazole led to the development of *C. albicans* resistance in HIV-positive patients (Hunter et al. 1998), and also led to the replacement of fluconazole-susceptible *C. albicans* strains with other species that are intrinsically less sensitive to fluconazole, such as *Candida glabrata* and *Candida krusei* (Hunter et al. 1998; White et al. 1998).

To overcome the problems associated with antifungal resistance, studies have been performed to search for new alternative therapies for resistant infections. One potential alternative approach is antimicrobial photodynamic therapy (aPDT). aPDT requires the association of oxygen, a visible light source and photosensitizer (PS) to exert antimicrobial activity (Bonnett and Martínez 2001). In general, the PS is applied externally to the cell, thus the cell membrane is considered the initial target of the photodynamic process (Strakhovskaia et al. 2002; Donnelly et al. 2008). Different PSs have been evaluated for the inactivation of *Candida* species through aPDT, including porphyrins (Bliss et al. 2004; Dovingo, Pavarina, Carmello et al. 2011; Mima et al. 2012), phenothiazine dyes (Paardekopper et al. 1992; Pereira et al. 2011), chlorins (Park et al. 2010; Dovigo et al. 2013), curcumin (Dovigo, Pavarina, Carmello et al. 2011) and rose bengal (RB) (Costa et al. 2012). However, studies have shown that *Candida* biofilms are less susceptible to aPDT when compared with their planktonic counterparts (Dovigo, Pavarina, Mima et al. 2011; Dovigo et al. 2013; Costa et al. 2012).

It has been demonstrated that certain PS can also be activated by ultrasound (US), and as a result, the PS may also be referred to as a sonosensitizer (SS). This approach is known as sonodynamic therapy (SDT) (Ma et al. 2009; Serpe and Giuntini 2015). The advantage of SDT when compared to aPDT is that US propagates deeper into the tissue than light; therefore, SDT may be used to treat deeper lesions overcoming the limitations of light propagation and delivery presented by aPDT (Ma et al. 2009; Costley et al. 2015; Serpe and Giuntini 2015). It has been suggested that in SDT, singlet oxygen generation may result by the indirect photo-activation of the sensitizer drug *via* sonoluminescence (Umemura et al. 1999). Once excited the sensitizer generates singlet oxygen in the same way as in the aPDT (Umemura et al. 1999; Hiraoka et al. 2006). An alternative hypothesis suggests that the elevated temperatures resulting from cavitation can result in the generation of radicals directly from the PS, and ROS are subsequently produced in much the same way as a Type I photodynamic reaction.

The use of SDT as an antimicrobial treatment to overcome antimicrobial resistance is a relatively new approach and publications in the field are rare. A number of studies in this area have reported US-mediated inactivation of bacteria using different sensitizers, including rose-bengal (RB) (Nakonechny et al. 2013; Costley et al. 2017), curcumin (Wang et al. 2014) and porphyrin (Zhuang et al. 2014).

In this manuscript, the ability of aPDT, SDT and a combination of these treatments was evaluated, using the sensitizers RB and Photodithazine®, to inactivate *C. albicans*. Cell viability was assessed by colony forming units (CFU), the total biomass of the biofilm was measured by crystal violet staining and biofilm architecture was analyzed by light and fluorescence microscopy.

Materials and methods

Sensitizers, light sources and ultrasound device

The chlorin e6 derivative Photodithazine® (PDZ, produced by Veta-Grand Co., Moskva, Russia) and RB (Sigma-Aldrich, St Louis, MO, USA) were used as sensitizers. The PDZ has I band absorption maxima at longer wavelengths (650–670 nm). Prior to the beginning of each experiment, the work solution of PDZ was obtained by diluting the commercial solution of PDZ (5,000 mg l^{-1}) in physiological saline (0.85% NaCl). RB has an absorption maximum of 560 nm and was also diluted in physiological solution. A range of concentrations of each sensitizer was evaluated.

The PDZ sensitizer was irradiated by a light emitting diode (LED) in the red region of the spectrum (peak at 660 nm). This device is composed of red LEDs (LXHL-PR09, Luxeon® III Emitter, Lumileds Lighting, San Jose, CA, USA) uniformly distributed, with a constant power output of 30 mW cm^{-2}. The RB sensitizer was illuminated by a white LED device (Fenix™, LD01, Shanghai, China) with a constant power output of 370 mW cm^{-2}.

A Sonidel SP100 sonoporator was used for sonication, at a frequency of 1 MHz and pulse repetition frequency of 100 Hz (Sonidel Ltd, Dublin, Ireland).

Strain and growth conditions

C. albicans ATCC 90028 obtained from American Type Culture Collection was used in this study. *C. albicans* was maintained in yeast peptone glucose medium (YEPD: 1% yeast extract, 2% Bacto peptone and 2% D-glucose, 2% agar) with glycerol and frozen at –80°C until use. The yeast was subcultured onto Sabouraud dextrose agar plates (SDA) supplemented with chloramphenicol (0.05 g l^{-1}) and incubated at 37°C for 48 h to grow the colonies used for each experiment.

Treatment against planktonic cultures

To prepare the yeast inoculum, five colonies of the agar stock culture were individually transferred to 10 ml of yeast nitrogen base broth (YNB) supplemented with 100 mM glucose, and incubated at 37°C overnight. After incubation, 500 µl of the culture were transferred to 9.5 ml of fresh YNB and the tube was incubated for 8 h, until *C. albicans* cells reached the mid-log phase of growth. *C. albicans* suspension was spectrophotometrically standardized (540 nm) at an OD of 0.7, which corresponds to a final concentration of 10^7 CFU ml^{-1}. Next, a 100 µl aliquot of the inoculum was added to each well of a 96-well polystyrene plate and then submitted to the aPDT or SDT.

Initially, the effect of US application on the viability of planktonic cultures was evaluated. To apply US to the samples, an US gel Rothband (Haslingden, UK) was used to ensure contact between the bottom of the 96-well plate and the US transducer. A wide range of parameters were investigated including duty cycle (50, 55, 60, 65, 70 and 75%), exposure time (2.5, 5, 7.5 and 10 min) and power density (intensity) (1, 1.5, 2, 2.5 and 3 W cm^{-2}). To determine yeast survival, aliquots of the contents of each well were serially diluted 10-fold in sterile saline. Duplicate 25 µl aliquots were spread over the surfaces of SDA plates. All plates were aerobically incubated at 37°C for 48 h. Then, the colony forming units (CFU ml^{-1}) were calculated and the effectiveness of aPDT and SDT mediated by PDZ or RB against the planktonic cultures was evaluated.

For SDT mediated by PDZ, suspensions of *C. albicans* were incubated with 100 µl of the sensitizer solution to yield final PDZ concentrations of 25, 50 or 100 mg l^{-1}, and the plates were incubated in the dark for 20 min. Afterwards, the US gel was used between the plate and the transducer of the US device for the US application. US conditions used were a frequency of 1 MHz, a power density of 2.5 W cm^{-2}, 50% of duty cycle and pulse frequency of 100 Hz for 5 min (SDT/PDZ groups). For the RB-mediated SDT, suspensions of *C. albicans* were incubated with 100 µl of the sensitizer solution to give final RB concentrations of 1, 5 and 10 µM, and the plate was incubated in the dark for 30 min (Costley et al. 2015). Afterwards, the same US parameters as previously described for PDZ were used (SDT/RB groups).

For aPDT mediated by PDZ (aPDT/PDZ groups), *C. albicans* suspensions were incubated for 20 min (Dovigo et al. 2013) with 100 µl of the sensitizer solution to give final PDZ concentrations of 25, 50 or 100 mg l^{-1}. Then, the plate was irradiated with red LED light (25 J cm^{-2}). For aPDT mediated by RB (aPDT/RB groups), suspensions of *C. albicans* were incubated for 30 min with 100 µl of the sensitizer solution to give final RB concentration of 1, 5 and 10 µM. Then, the samples were irradiated with white LED light (25 J cm^{-2}).

For both treatments (SDT and aPDT), additional samples were treated with sensitizer only (PDZ and RB groups), US only (US group), LED light alone (White and Red light groups) or no treatment (Control group). To determine the cell viability after each treatment, the CFU test was performed as described previously. The treatments were performed in duplicate on three separate occasions.

Treatment against biofilms

For biofilm formation, the yeast suspension was prepared and the concentration adjusted as described previously (10^7 CFU ml^{-1}). An aliquot of 100 µl of the cell suspension was added to the wells of a flat-bottom 96-well polystyrene plate and the culture plate was incubated at 37°C in a shaker incubator (75 rpm) for 90 min (adhesion phase). After 90 min, the wells were washed twice with phosphate-buffered saline (PBS) to remove non-adhered cells. Then, 150 µl of RPMI 1640 buffered with morpholine propane sulfonic acid (MOPS) (Sigma-Aldrich) at pH 7 were added to each well. After incubation for 48 h in an orbital shaker (75 rpm) for biofilm formation, the suspension of each well was removed and the biofilm was washed twice with PBS. The biofilms were then treated with either (1) SDT using PDZ or RB, (2) PDT using PDZ or RB and (3) combined PDT/SDT using PDT or RB. Two concentrations of PDZ (175 and 200 mg l^{-1}) and RB (100 or 200 µM) were assessed with 100 µl of sensitizer added to the biofilm and incubated in the dark for 30 min. Where appropriate, the wells were then treated with light (using a red or white LED at a dose of 50 or 113 J cm^{-2}, (PDZ and RB groups respectively) or US (frequency of 1 MHz, a power density of 2.5 W cm^{-2}, 50% of duty cycle and pulse frequency of 100 Hz for 5 min). For combined aPDT/SDT treatments both light and US were administered simultaneously using the same parameters as described above. After treatment, the biofilm was detached by rubbing the pipette tip for 30 s in all directions (horizontal, vertical and circular) on the bottom of the well. To determine cell survival in the biofilms, the CFU ml^{-1} assay was performed in the same way as for the planktonic cultures. The total biomass of biofilm was quantified using crystal violet (CV) staining (Stepanovic et al. 2000; Quishida et al. 2015). After treatments, biofilms were washed with PBS and then fixed with 200 µl of methanol for 15 min. The methanol was removed and the plates were kept at 37°C for 20 min to dry. Subsequently, 200 µl of CV (1% v v^{-1}) were added and maintained for 5 min. The wells were washed with ultrapure water, and after this, 33% acetic acid was added to remove the dye. The absorbance of the resulting solution at 570 nm was determined using a microplate. Each evaluation was performed in duplicate on three different occasions.

The assessment of biofilm morphology and architecture were performed using light and fluorescence microscopy. After treatment, biofilms were washed twice with 0.89% sterile NaCl. Next, the biofilms were incubated with Trypan Blue solution (TB) (Gibco by Life Technologies, Carlsbad, CA, USA). The stock solution of TB (0.4%) was diluted in PBS in the proportion of 1:2, respectively. Then, biofilms were incubated with TB for 15 min, at 37°C in the dark. TB was then removed and samples were washed with 0.89% sterile NaCl and the fluorophore Concanavalin Alexa Fluor 488 conjugate (Con-A) (Molecular Probes, Inc., Eugene, OR, USA) at a concentration of 100 μg ml^{-1} was added (Chandra et al. 2008). Samples were incubated with Con-A for 30 min at 37°C in the dark and biofilms were then washed with 0.89% sterile NaCl. The TB solution stains the nucleus of dead cells and the Con-A (excitation wavelength: 488 nm and emission: 505 nm long-pass filter) binds to the polysaccharide cell wall with green fluorescence. The TB dye was examined using light microscopy (Leica, London) and the fluorophore Con-A was observed using fluorescent microscopy (Leica), both with a 20 × objective lens. Images were acquired in each microscope and merged using Adobe Photoshop CS6 software (Adobe Systems, San Jose, CA, USA). The thickness of the biofilms was determined using confocal laser scanning microscopy (CLSM) (Zeiss LSM 700 Confocal, Zeiss).

Statistical analysis

The CFU ml^{-1} values were transformed into $\log_{10}$ and the homogeneity of variance and normality of the data were verified by the Levene and Shapiro–Wilk tests, respectively. The results were analyzed statistically by means of one-way analysis of variance (one-way ANOVA) and, for multiple comparisons, the *post hoc* Tukey test was applied. The level of significance adopted was 5% ($\alpha = 0.05$). These analyses were performed using a SPSS software package (IBM® SPSS® Statistics, version 20, Chicago, IL, USA).

Results

Planktonic culture treatments

First, the effect of exposing planktonic cultures to US alone was evaluated. The impact of a range of duty cycles, time exposures and power densities were assessed. It was found that exposure to US alone was capable of completely eradicating the *C. albicans* cultures using a duty cycle higher than 50% at a power density of 3 W cm^{-2}, when the US was applied for more than 5 min (data not shown). Therefore, subsequent tests were performed using the US for 5 min, with 50% of the duty cycle at an US power density of 2.5 W cm^{-2}.

Figure 1A shows the results of treatment with SDT mediated by PDZ (25, 50 or 100 mg l^{-1}) or RB (1, 5, 10 μM), and the control groups (only US, only sensitizer, and control). As shown in Figure 1A, SDT mediated by PDZ 50 (SDT/PDZ 50) or PDZ 100 (SDT/PDZ 100) resulted in eradication of the microorganism. In addition, a significant reduction of 4.35 $\log_{10}$ in the SDT/PDZ 25 group was observed ($p = 0.001$). Treatment with US or PDZ separately did not have any significant impact on the viability of *C. albicans* and values were similar ($p \geq 0.984$) to the control group (6.38 $\log_{10}$). Treatment with SDT mediated by RB 5 (SDT/RB 5) or RB 10 (SDT/RB 10) resulted in the eradication of the microorganism. In addition, it a significant reduction ($p = 0.001$) of 5.01 $\log_{10}$ was observed in the group treated with SDT mediated by RB 1 (SDT/RB 1) when compared with the untreated control group (Figure 1B). The results also demonstrated that when cells were treated with RB alone at concentrations of 5 and 10 μM the viability of planktonic cultures decreased significantly ($p \leq 0.028$) (Figure 1B).

The aPDT mediated by PDZ 100 (aPDT/PDZ 100) resulted in the eradication of the microorganism. A significant reduction ($p \leq 0.001$) in cell viability was also observed in the aPDT/PDZ 25 and aPDT/PDZ 50 treatment groups equivalent to 5.23 and 5.87 $\log_{10}$, respectively, compared with the control group. Treatment with red LED light or PDZ alone had no effect on the viability of *C. albicans* and the results were similar to the control group ($p >= 0.989$) (Figure 1C).

The aPDT mediated by RB 10 (aPDT/RB 10) resulted in the eradication of *C. albicans*. In addition, compared with the control group, a significant reduction ($p = 0.001$) in viability of the groups treated with RB 1 (aPDT/RB 1) and RB 5 (aPDT/RB 5) of 5.24 and 5.39 $\log_{10}$, respectively, was achieved. The use of light alone did not affect the microorganism and it was similar to the control group ($p = 0.999$) (Figure 1D).

Biofilm treatments

The effect of US treatment alone on biofilms was also evaluated, testing a range of treatment times (5, 6, 7, 8 and 10 min) and US power densities (2.5 and 3 W cm^{-2}). It was observed that US in the absence of a sensitizer reduced the viability of *C. albicans* biofilms after application for 6 min at power densities of 2.5 or 3 W cm^{-2} (data not shown). For this reason, the subsequent tests were performed using the US for 5 min, with 50% of duty cycle at 2.5 W cm^{-2}.

The association of aPDT+SDT mediated by PDZ at the concentrations of 175 or 200 mg l^{-1} resulted in significant ($p \leq 0.001$) reductions in viability of 2.08 and 3.39 $\log_{10}$, respectively (Figure 2A). Moreover, the combination of

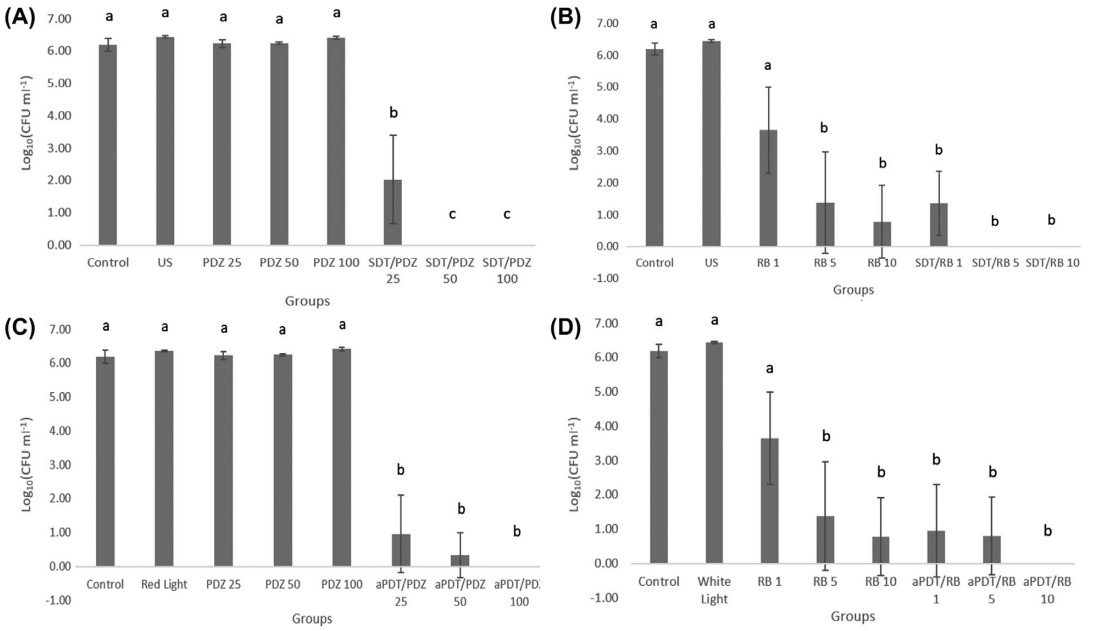


Figure 1. (A, B) Mean values and SD of Log_{10} (CFU ml^{-1}) of planktonic cultures of *C. albicans* treated with SDT mediated by PDZ (SDT/PDZ 25, SDT/PDZ 50, SDT/PDZ 100 groups) or RB (SDT/RB 1, SDT/RB 5, and SDT/RB 10 groups), and control groups: control, only US (US group) and only sensitizer (PDZ 25, PDZ 50, PDZ 100, RB 1, RB 5 and RB 10 groups). US: 5 min, 50% of duty cycle, 2.5 W cm^{-2}. (C, D) Mean values and SD of Log_{10}(CFU ml^{-1}) of planktonic cultures of *C. albicans* treated with aPDT mediated by PDZ (aPDT/PDZ 25, aPDT/PDZ 50 and aPDT/PDZ 100 groups) or RB (aPDT/RB 1, aPDT/RB 5, and aPDT/RB 10 groups), and control groups: control, only light (Red or White light groups) and only sensitizer (PDZ 25, PDZ 50, PDZ 100, RB 1, RB 5 and RB 10 groups). Red light: LED 660 nm, 25 J cm^{-2}. White light: white LED, 25 J cm^{-2}. Equal letters denote statistical similarity (p>0.05).

aPDT+SDT mediated by RB at concentrations of 100 or 200 μM resulted in significant ($p \leq 0.001$) reductions in viability equivalent to 1.45 and 1.91 log_{10}, respectively (Figure 2B). The treatment with only aPDT or SDT did not reduce the viability *of C. albicans* and the results were similar to the control group ($p = 1.000$) (Figure 2A and B). The viability of the microorganism after treatment with PDZ, RB or Light+US separately was also similar to the control group ($p \geq 0.999$) (Figure 2A and B).

The CV assay demonstrated that the combined treatment aPDT+SDT resulted in a significant reduction in the total biomass. The aPDT+SDT mediated by PDZ at 175 or 200 mg l^{-1} resulted in a significant reduction ($p \leq 0.001$) of 75.5 and 71.2%, respectively, compared to the control group (Figure 2C). The treatment with aPDT+SDT mediated by RB at 100 or 200 μM was able to significantly reduce ($p \leq 0.001$) the total biomass by 62.1 and 73.0%, respectively (Figure 2D). On the other hand, only the application of aPDT mediated by PDZ 200 (aPDT/PDZ 200) significantly reduced the total biomass by ~ 30.9% ($p = 0.025$) (Figure 2C). The aPDT mediated by RB at 100 and 200 (aPDT/RB 100 and aPDT/RB 200 groups) was able to significantly ($p \leq 0.012$) reduce the total biomass by 34.8 and 35.2%, respectively (Figure 2D). The total biomass of the biofilms treated with SDT mediated by PDZ was similar to the control group ($p \geq 0.823$) (Figure 2C). On the other hand, the RB-mediated SDT significantly ($p \leq 0.005$) reduced the total biomass of the biofilms by 36.6 and 53.4% when compared to the control group (Figure 2D).

The assessment of biofilm morphology and architecture was performed using light and fluorescence microscopy (Figure 3). The image captured in the control group shows a denser biofilm, a high concentration of live cells (blastopore and hypha) and a thickness equivalent to 88.54 μm when measured by CLSM. The biofilms treated with aPDT+SDT mediated by 175 or 200 mg l^{-1} of PDZ showed a reduction in biofilm density with an equivalent thickness of 45.3 and 44.6 μm, respectively, a smaller number of cells, a reduction in the filamentous form and most of the cell nuclei were stained with TB, indicating cell death. The images obtained in the groups treated with aPDT+SDT mediated by 100 or 200 mg l^{-1} of RB demonstrated a reduced density (with a thickness equivalent 42.07 and 49.84 μm, respectively), a reduction in hyphae and most of the cell nuclei had stained with TB. The results visualized by microscopy are in accordance with the results obtained in the CFU and total biomass

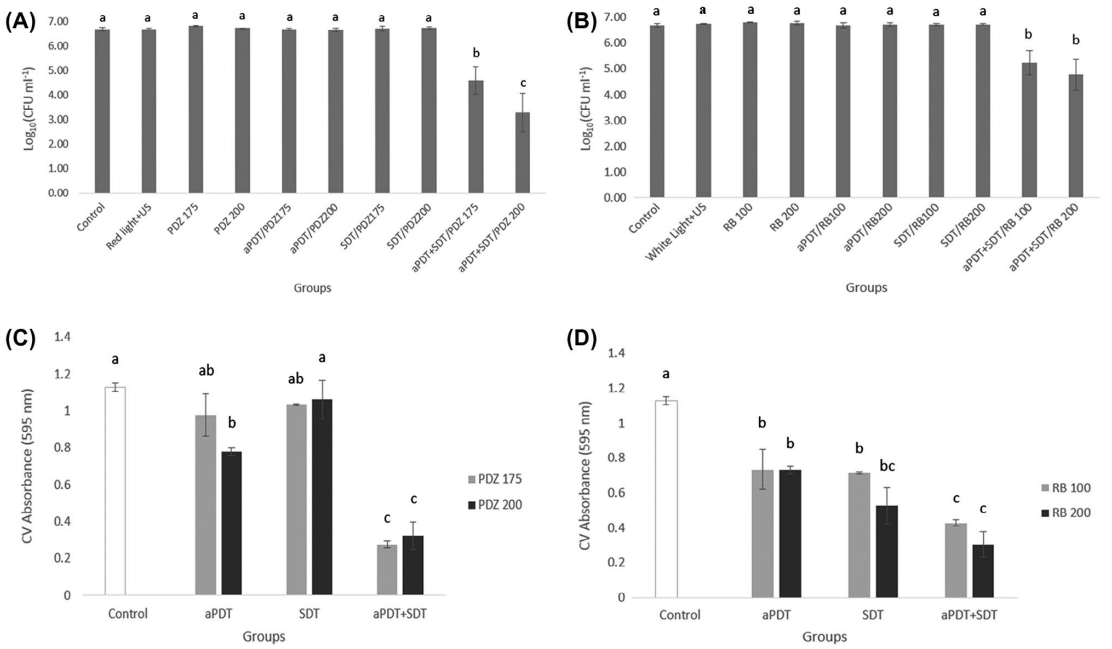


Figure 2. (A, B) Mean values and SD of Log_{10}(CFU ml^{-1}) of *C. albicans* biofilms treated with aPDT, SDT, aPDT+SDT mediated by PDZ (175 and 200 mg l^{-1}) or RB (100 or 200 μM of RB) and control groups (Control, Red light+US, White light+US, PDZ 175, PDZ 200, RB 100 and RB 200 groups). Red light: LED 660 nm, 50 J cm^{-2}. White light: 113 J cm^{-2}. US: 5 min, 50% of duty cycle, 2.5 W cm^{-2}. (C, D) Mean values and SD of crystal violet absorbance of *C. albicans* biofilms treated with aPDT, SDT and aPDT+SDT mediated by PDZ (175 or 200 mg l^{-1}) or RB (100 or 200 μM). Red light: 50 J cm^{-2}. White light: 113 J cm^{-2}. US: 5 min, 50% of duty cycle, 2.5 W cm^{-2}. Equal letters denote statistical similarity (p>0.05).

assays, where the combined treatment of SDT and aPDT reduced significantly the viability of *C. albicans*.

Discussion

To overcome the problems associated with antifungal resistance, studies have been performed to search for alternative therapies to treat infections. aPDT (Dovigo, Pavarina, Carmello et al. 2011; Dovigo et al. 2013; Pereira et al. 2011; Costa et al. 2012) and SDT (Ma et al. 2009; Wang et al. 2014; Zhuang et al. 2014; Costley et al. 2015; Serpe and Giuntini 2015) have been suggested as promising therapies for the inactivation of microorganisms. According to the data, it was observed that the application of aPDT, mediated by PDZ at 100 mg l^{-1} or RB 10 μM, eradicated planktonic cultures of *C. albicans*. These results agree with those found by Dovigo et al. (2013) and Freire et al. (2014) who observed complete killing of *C. albicans* suspensions, when aPDT was mediated by PDZ (50 and 75 mg l^{-1}) and RB (12.5 μM), respectively. On the other hand, other studies assessing RB as PS to mediate aPDT obtained different results. Costa et al. (2012) observed that RB at 40 μM against clinical isolates of *C. albicans* resulted in a reduction equivalent to 1.97 log_{10}. In another investigation, using RB at 200 μmol l^{-1} for 20 min, reductions of 4 log_{10} and 6 log_{10} were observed for cellular densities of 10^7 and 10^6 cells ml^{-1}, respectively (Demidova and Hamblin 2005). The divergent results obtained may be attributed to the different aPDT parameters and type of strains (clinical isolates × reference strains) used.

With respect to the SDT results in planktonic cultures, this treatment was also able to eradicate the microorganism. To the best of the authors' knowledge, this is the first study that aimed to assess SDT for the inactivation of *C. albicans*. The effectiveness of this treatment has been demonstrated against pathogenic bacterial species (Kremkau et al. 1976; Nakonechny et al. 2013; Wang et al. 2014; Zhuang et al. 2014; Costley et al. 2015). The results of these studies and those found in the present investigation demonstrate that SDT is able to inactivate pathogenic microbial species, including *C. albicans*, when cultivated in suspensions.

The extracellular matrix of the biofilm that surrounds the microbial cells can act as a physical barrier (Ramage et al. 2009). For this reason, the organization of *C. albicans* as a biofilm is a significant challenge associated with the

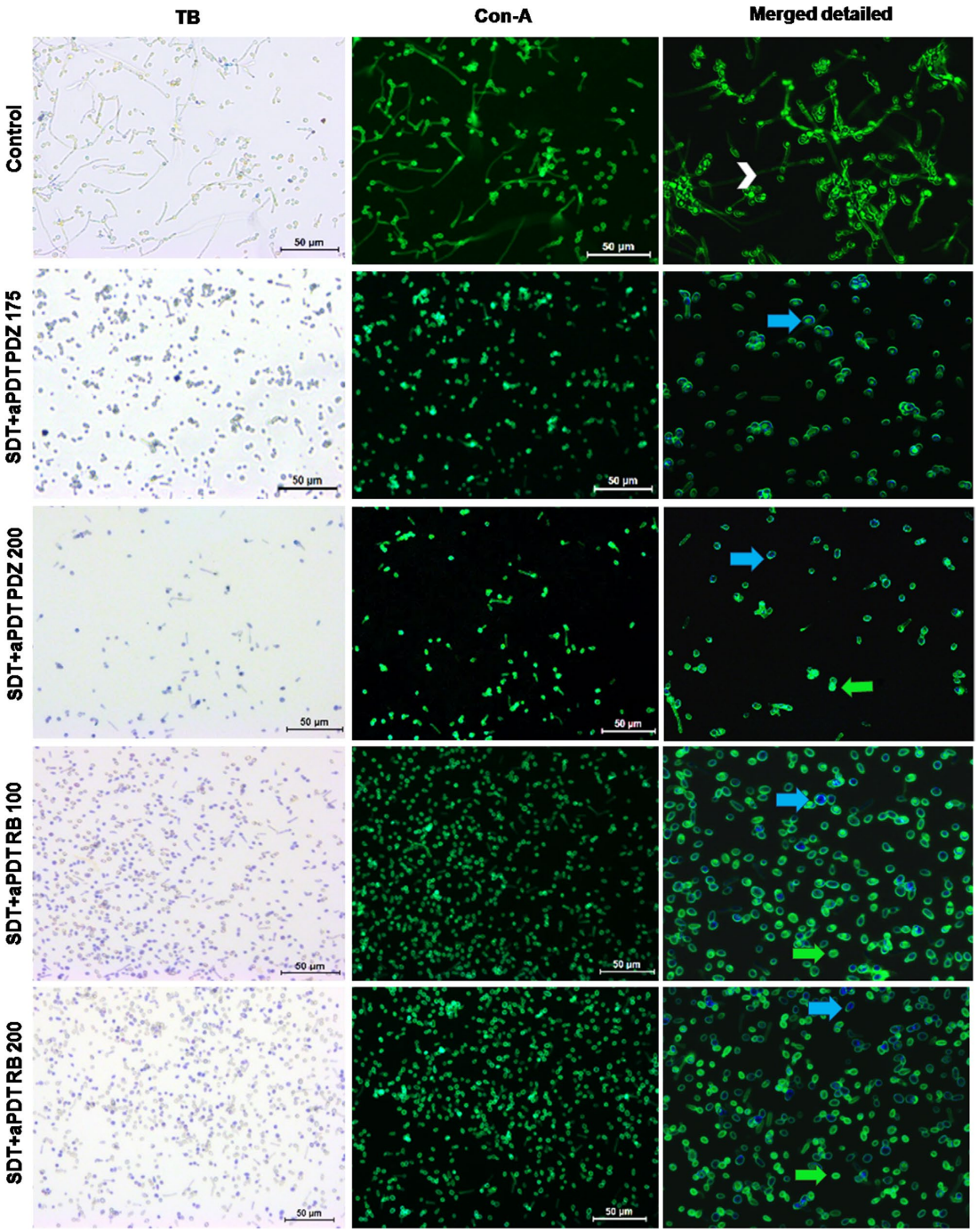


Figure 3. Light and fluorescence microscope images of the Control group and biofilms treated with aPDT+SDT. Samples were stained with Trypan Blue and Con-A. The TB solution stained the nuclei of dead cells (blue arrow) and the Con-A bound to the polysaccharide cell wall with green fluorescence (green arrow). The TB dye was examined under a light microscope ('TB' column) and Con-A was observed under a fluorescent microscope ('Con-A' column) (magnification 20×). The 'Merged detailed' column shows in detail the images that were captured in the light and fluorescent microscope and, then, merged. Arrow head: hyphae cell.

uptake of the sensitizer. In the present investigation, it was found that the simultaneous application of aPDT+SDT produced an enhanced effect compared to each treatment alone (SDT or aPDT). Significant reductions of 3.39 and 1.91 $\log_{10}$ were observed when the highest concentration of PDZ and RB were used, respectively. Some authors hypothesize that this increase may be a result of a synergistic aPDT and SDT effect due to US-induced diffusion of the sensitizers. Costley et al. (2015) proved that the pre-treatment of *Pseudomonas aeruginosa* biofilm with US for 5 min before the addition of RB produced a 2.6-fold increase in sensitizer diffusion through the biofilm compared with the untreated biofilm control. According to the authors, the US facilitated dispersion of sensitizers through the biofilms, thereby improving efficacy of the treatment (Costley et al. 2015). It has also been suggested that US increases the uptake of molecules through transient pores formed in the membrane (Bao et al. 1997; Miller 2000; Rosenthal et al. 2004), a process known as sonoporation. During this process, exogenous molecules, such as sensitizers, can enter into the cells through these pores, which can reseal after the uptake (Bao et al. 1997; Miller 2000; Rosenthal et al. 2004). Another possibility is that the physical agitation of the solution from the applied US causes circulation of the microorganism in the wells and increases exposure to the light source. Possibly one treatment must be sensitizing the fungal cells making the other more effective. However, to gain a more comprehensive understanding of the mechanisms involved and possible effects further study is required.

Regarding the application of aPDT or SDT separately, it was observed that these treatments were not effective in reducing the viability of *C. albicans* biofilm. It has been demonstrated that *Candida* biofilms are less susceptible to aPDT when compared with their planktonic counterparts (Dovigo, Pavarina, Mima et al. 2011; Dovigo et al. 2013; Costa et al. 2012) and in the present investigation it was also observed for the aPDT and SDT treatments. Previous studies have shown that aPDT mediated by PDZ or RB reduced the viability of *C. albicans* biofilm cells by <1 $\log_{10}$ l (Dovigo, Pavarina, Mima et al. 2011, Dovigo et al. 2013; Costa et al. 2012). The aPDT mediated by PDZ (125 mg l^{-1}) and LED light (37.5 J cm^{-2}) resulted in a reduction in *C. albicans* viability by 0.9 $\log_{10}$ in biofilms (clinical isolates) (Dovigo et al. 2013). The aPDT mediated by RB (40 μmol l^{-1}) promoted a reduction in viability of 0.12 $\log_{10}$ in clinical isolates of *C. albicans* grown as biofilms (Costa et al. 2012). In another study, aPDT using 200 μmol l^{-1} of RB reduced viability by 0.22 $\log_{10}$ in *C. albicans* biofilm (Freire et al. 2014). As this was the first study that aimed to assess SDT for the inactivation of fungal biofilms, it is not possible to directly compare the results found in this investigation.

The treatments employed here were also evaluated through quantification of total biomass by CV staining. The treatments performed simultaneously (aPDT+SDT) showed enhanced results in the CV assay. The highest concentrations of the sensitizers were able to reduce the total biomass of the biofilm by 71.2 and 73.0% when PDZ and RB were used, respectively. It is important to emphasize that the CV stains the matrix as well as both living and dead cells within the biofilm (Peeters et al. 2008). It is possible to hypothesize that the combination of both treatments was able to disrupt the biofilm, enabling penetration of the sensitizer more deeply into the biofilm. In addition, as mentioned previously, US can increase the uptake of the sensitizer *via* sonoporation (Bao et al. 1997; Miller 2000). Once the sensitizer penetrates more deeply into the biofilm and is taken up by the microorganisms, the light and US will then activate the sensitizer, resulting in cell death. For this reason, it is suggested that the possible ability of the combined treatment to disrupt the biofilm is important for the dispersion, uptake and activation of the sensitizer and consequently, for the effectiveness of the treatment.

When aPDT was mediated by RB, a significant reduction in the total biomass by up to 35.2% was observed, depending on the concentration of the sensitizer. The application of aPDT mediated by PDZ at 200 mg l^{-1} reduced the biomass of the biofilm by 30.9%. These results are in agreement with those found in the literature which observed that the combination of 150 mg l^{-1} of PDZ associated with LED light produced reductions on total biomass equivalent to 24.4, 39.2 and 43.7% for *C. albicans*, *Candida tropicalis* and *C. glabrata*, respectively (Carmello et al. 2017). The total biomass of the biofilms treated with SDT mediated by PDZ was similar to the control group. On the other hand, the RB-mediated SDT significantly reduced the total biomass of the biofilms. As stated above, this is the first study that aimed to assess the effect of SDT against biofilms and therefore it is not possible to compare directly the CV results found in the present investigation.

The biofilm morphology and architecture after the application of the combined treatment (aPDT+SDT) was assessed using light and fluorescence microscopy. The images revealed that the biofilms treated with aPDT+SDT, mediated by PDZ and RB, showed a thinner thickness, a smaller number of cells, a reduction in the filamentous form and increased cell death. These results show that this new approach reduced the viability, disrupted the integrity of the biofilm and eliminated most of the filamentous cells. The fact that this treatment is able to reduce the filamentous form is a relevant finding. The ability of *C. albicans* to switch from unicellular yeast into filamentous form is thought to be important for *Candida*

virulence (Thompson et al. 2011). This type of morphology can invade layers of epithelial cells, to exert mechanical force, promote penetration and growth between the epithelial cells (Thompson et al. 2011). Thus, the filamentous form facilitates the invasion of the host tissue. The study conducted by Quishida et al. (2015) evaluated the architecture of mixed biofilms formed by *C. albicans*, *C. glabrata* and *Streptococcus mutans* that were submitted to aPDT mediated by PDZ using CLSM. According to the authors, a visual increase in dead cells was observed in the biofilms incubated with PDZ at 175 mg ml^{-1} and irradiated with 37.5 J cm^{-2}. However, this treatment did not reduce the numbers of cells, the thickness of the treated biofilm was similar to the control group and there was no change in cell morphology (Quishida et al. 2015).

The US power density (intensity), frequency, and exposure time have been shown to be important parameters for SDT antimicrobial effects (Nakonechny et al. 2013; Wang et al. 2014; Zhuang et al. 2014; Costley et al. 2015) and this was also observed in the present investigation. This study showed that US, when applied in the absence of sensitizer, was able to reduce *Candida* survival in planktonic cultures and biofilms when delivered at power densities >2.5 W cm^{-2}, 50% of DC and exposure for 5 min. The killing of *C. albicans* may be attributed to an US-induced increase in temperature (Kremkau et al. 1976; Harrison and Balcer-Kubiczek 1991). Thermal effects produced by US have been used for other therapeutic applications. The US-induced tissue hyperthermia, which transiently increases the tissue temperature to 40–45°C, has been studied for clinical benefits such as inflammation relief, physical therapy and enhancement of cancer chemotherapy. For thermal ablation, US can be used to increase tissue temperature to 60–85°C and has been used for non-invasive surgery in the treatment of solid tumors, sealing of blood vessels and correction of cardiac arrhythmias (Rosenthal et al. 2004). It is important to emphasize that, exposure to the US for 5 min, with 50% of duty cycle at an US power density of 2.5 W cm^{-2} did not affect the viability of *C. albicans* (suspension and biofilm). Therefore, subsequent tests evaluating the effectiveness of SDT and aPDT+SDT were performed using these parameters. For this reason, it is concluded that the effect of aPDT+SDT against *C. albicans* was a result of the treatment and not to the increase in temperature. Therefore, the determination of appropriate US parameters is crucial for using the US for antimicrobial proposes.

In addition, it was observed that the treatment with RB sensitizer in the absence of US or light reduced *C. albicans* survival in suspension. The study conducted by Maliszewska et al. (2017) verified that RB at concentrations>25 mg l^{-1} was able to significantly reduce planktonic cultures of *C. albicans* (ATCC 10231, 10^5 cells ml^{-1}). On the other hand, Freire et al. (2014) observed that RB in concentrations ranging from 0.78 to 200 μM had no effect on *C. albicans* suspensions. However, these authors evaluated another reference strain of *C. albicans* (ATCC 18804), the inoculum was cultured in different medium (Sabouraud dextrose broth) and the *C. albicans* suspension was incubated for only 5 min with RB. In contrast, when PDZ was applied in the absence of light or US, this PS was not able to reduce the suspension viability of *C. albicans*. The non-toxicity of PDZ has been reported in the literature (Dovigo et al. 2013; Carmello et al. 2017). Therefore, the effect of the sensitizers on the *C. albicans* viability depends on the type of the PS evaluated.

The present investigation also demonstrated that the treatments mediated by the sensitizer PDZ were more effective on both planktonic and biofilm phase growths in comparison with the RB treatments. These results obtained may be attributed to the different characteristics of each sensitizer. The sensitizer PDZ, classified as a second-generation PS, is obtained from the cyanobacterium *Spirulina platensis* as a noncovalent complex of N-methyl-D-glucosamine chlorine e6 salt on basis of chlorophyll *a* derivatives. PDZ has an absorption peak in the red region of the spectrum (660 nm) and it is known to produce a high amount of singlet oxygen (Ferreira et al. 2008). On the other hand, the xanthene dye RB is an anionic water-soluble synthetic fluorescein derivative, which has an absorption peak in the green region of the spectrum (450–600 nm) and a low rate of photodegradation (Spagnul et al. 2015). This PS is capable of photo-catalytic conversion of an oxygen molecule to singlet oxygen under 532 nm light irradiation, with a singlet oxygen quantum yield of ~76% (Encinas et al. 2009). Moreover, the higher efficacy of the aPDT treatment mediated by PDZ in comparison with RB may also be attributed to the wavelength of the LED device used. PDZ was excited by a LED device with the appropriated wavelength for this sensitizer (660 nm) and RB was not, and this may influence the efficacy of the treatment.

In conclusion, the results described above demonstrate the potential of combined aPDT/aSDT treatment as an alternative approach for the eradication of fungal biofilms. A powerful synergy was observed when the biofilms were treated with both aPDT and aSDT compared to either treatment alone. The reason for this synergy remains unknown but may result from SDT sensitizing the biofilm to PDT treatment. As mentioned previously, US is known to facilitate the dispersion of drugs through impermeable tissue as a result of cavitation induced effects. Therefore, SDT treatment may facilitate the generation of transient pores in the biofilm matrix enabling a greater diffusion of both the sensitizer and light. The authors are currently exploring this hypothesis in greater detail. In addition, they

are also interested in exploring the effects of the treatment on biofilms *in vivo* and its effect on the host-tissue. Given the issues associated with multi-drug resistant infections it is crucial that new approaches to treat such conditions are developed soon. It is believed that combined aPDT/SDT treatment could be one such approach for the targeted and efficacious control of localized fungal infection.

Acknowledgements

We thank Paula Aboud Barbugli and Bridgeen Callan for the help with the microscopy images.

Disclosure statement

The authors declare that they have no conflict of interest.

Funding

This work was supported by the São Paulo Research Foundation (FAPESP) [grant numbers 2016/00190-2, 2014/01262-1, 2013/ 07276-1] and PROPG-UNESP [grant 03/2016].

ORCID

Ana Cláudia Pavarina http://orcid.org/0000-0002-9231-1994

References

Banting DW, Greenhorn PA, McMinn JG. 1995. Effectiveness of a topical antifungal regimen for the treatment of oral candidiasis in older, chronically ill, institutionalized, adults. J Can Dent Assoc. 61:199–200, 203–205.

Bao S, Thrall BD, Miller DL. 1997. Transfection of a reporter plasmid into cultured cells by sonoporation *in vitro*. Ultrasound Med Biol. 23:953–959.. doi:10.1016/S0301-5629(97)00025-2

Barchiesi F, Arzeni D, Del Prete MS, Sinicco A, Falconi Di Francesco L, Pasticci MB, Lamura L, Nuzzo MM, Burzacchini F, Coppola S, et al. 1998. Fluconazole susceptibility and strain variation of *Candida albicans* isolates from HIV-infected patients with oropharyngeal candidosis. J Antimicrob Chemother. 41:541–548. Erratum in: J Antimicrob Chemother 1998; 42:413. doi:10.1093/jac/41.5.541

Bliss JM, Bigelow CE, Foster TH, Haidaris CG. 2004. Susceptibility of *Candida* species to photodynamic effects of Photofrin. Antimicrob Agents Chemother. 48:2000–2006. doi:10.1128/AAC.48.6.2000-2006.2004

Bonnett R, Martínez G. 2001. Photobleaching of sensitisers used in photodynamic therapy. Tetrahedron. 57:9513–9547. doi:10.1016/S0040-4020(01)00952-8

Carmello JC, Alves F, Mima EG, Jorge JH, Bagnato VS, Pavarina AC. 2017. Photoinactivation of single and mixed biofilms of *Candida albicans* and non-*albicans Candida* species using Phorodithazine®. Photodiagnosis Photodyn Ther. 17:194–199. Erratum in: Photodiagnosis Photodyn Ther. 2017; 20:288. doi:10.1016/j.pdpdt.2016.11.013

Chandra J, Mukherjee PK, Ghannoum MA. 2008. *In vitro* growth and analysis of *Candida* biofilms. Nat Protoc. 3:1909–1924. doi:10.1038/nprot.2008.192

Costa AC, Rasteiro VM, Pereira CA, Rossoni RD, Junqueira JC, Jorge AO. 2012. The effects of rose bengal- and erythrosine-mediated photodynamic therapy on *Candida albicans*. Mycoses. 55:56–63. doi:10.1111/myc.2011.55.issue-1

Costerton JW, Stewart PS, Greenberg EP. 1999. Bacterial biofilms: a common cause of persistent infections. Science. 284:1318–1322. doi:10.1126/science.284.5418.1318

Costley D, Mc Ewan C, Fowley C, McHale AP, Atchison J, Nomikou N, Callan JF. 2015. Treating cancer with sonodynamic therapy: a review. Int J Hyperthermia. 31:107–117. doi:10.3109/02656736.2014.992484

Costley D, Nesbitt H, Ternan N, Dooley J, Huang YY, Hamblin MR, McHale AP, Callan JF. 2017. Sonodynamic inactivation of Gram-positive and Gram-negative bacteria using a Rose Bengal-antimicrobial peptide conjugate. Int J Antimicrob Agents. 49:31–36. doi:10.1016/j.ijantimicag.2016.09.034

Demidova TN, Hamblin MR. 2005. Effect of cell-photosensitiser binding and cell density on microbial photoinactivation. Antimicrob Agents Chemother. 49:2329–2335. doi:10.1128/AAC.49.6.2329-2335.2005

Donnelly RF, McCarron PA, Tunney MM. 2008. Antifungal photodynamic therapy. Microbiol Res. 163:1–12. doi:10.1016/j.micres.2007.08.001

Dovigo LN, Carmello JC, Carvalho MT, Mima EG, Vergani CE, Bagnato VS, Pavarina AC. 2013. Photodynamic inactivation of clinical isolates of *Candida* using Photodithazine®. Biofouling. 29:1057–1067. doi:10.1080/08927014.2013.827668

Dovigo LN, Pavarina AC, Carmello JC, Machado AL, Brunetti IL, Bagnato VS. 2011. Susceptibility of clinical isolates of *Candida* to photodynamic effects of curcumin. Lasers Surg Med. 43:927–934. doi:10.1002/lsm.v43.9

Dovigo LN, Pavarina AC, Mima EGO, Giampaolo ET, Vergani CE, Bagnato VS. 2011. Fungicidal effect of photodynamic therapy against fluconazole-resistant *Candida albicans* and *Candida glabrata*. Mycoses. 54:123–130. doi:10.1111/myc.2011.54.issue-2

Ellepola AN, Samaranayake LP. 2000. Antimycotic agents in oral candidosis: an overview: 2. Treatment of oral candidosis. Dent Update. 27:165–170, 172–174. doi:10.12968/denu.2000.27.4.165

Encinas MC, Rufs AM, Bertolotti SG, Previtali CM. 2009. Xanthene dyes/amine as photoinitiators of radical polymerization: a comparative and photochemical study in aqueous medium. Polymer. 50:2762–2767. doi:10.1016/j.polymer.2009.04.024

Ferreira J, Menezes PFC, Kurachi C, Sibata C, Allison RR, Bagnato VS. 2008. Photostability of different chlorine photossensitisers. Laser Phys Lett. 5:156–161. doi:10.1002/lapl.200710099

Flemming HC, Wingender J. 2010. The biofilm matrix. Nat Rev Microbiol. 8:623–633. doi:10.1038/nrmicro2415

Freire F, Costa AC, Pereira CA, Beltrame Junior M, Junqueira JC, Jorge AO. 2014. Comparison of the effect of rose bengal- and eosin Y-mediated photodynamic inactivation on planktonic cells and biofilms of *Candida albicans*. Lasers Med Sci. 29:949–955. doi:10.1007/s10103-013-1435-x

Goldman GH, da Silva Ferreira ME, dos Reis Marques Everaldo, Savoldi M, Perlin D, Park S, Godoy Martinez PC, Goldman MH, Colombo AL. 2004. Evaluation of fluconazole resistance mechanisms in *Candida albicans*

clinical isolates from HIV-infected patients in Brazil. Diagn Microbiol Infect Dis. 50:25–32. doi:10.1016/j.diagmicrobio.2004.04.009

Harrison GH, Balcer-Kubiczek EK. 1991. Pulsed ultrasound and neoplastic transformation *in vitro*. Ultrasound Med Biol. 17:627–632. doi:10.1016/0301-5629(91)90033-S

Hiraoka W, Honda H, Feril LB Jr, Kudo N, Kondo T. 2006. Comparison between sonodynamic effect and photodynamic effect with photosensitisers on free radical formation and cell killing. Ultrason Sonochem. 13:535–542. doi:10.1016/j.ultsonch.2005.10.001

Hunter KD, Gibson J, Lockhart P, Pithie A, Bagg J. 1998. Fluconazole-resistant *Candida* species in the oral flora of fluconazole-exposed HIV-positive patients. Oral Surg Oral Med Oral Pathol Oral Radiol Endod. 85:558–564. doi:10.1016/S1079-2104(98)90291-8

Kremkau FW, Kaufmann JS, Walker MM, Burch PG, Spurr CL. 1976. Ultrasonic enhancement of nitrogen mustard cytotoxicity in mouse leukemia. Cancer. 37:1643–1647. doi:10.1002/(ISSN)1097-0142

Kulak Y, Arikan A, Delibalta N. 1994. Comparison of three different treatment methods for generalized denture stomatitis. J Prosthet Dent. 72:283–288. doi:10.1016/0022-3913(94)90341-7

Lombardi T, Budtz-Jorgensen E. 1993. Treatment of denture induced stomatitis: a review. Eur J Prosthodont Restor Dent. 2:17–22.

Ma X, Pan H, Wu G, Yang Z, Yi J. 2009. Ultrasound may be exploited for the treatment of microbial diseases. Med Hypotheses. 73:18–19. doi:10.1016/j.mehy.2009.01.033

Maliszewska I, Lisiak B, Popko K, Matczyszyn K. 2017. Enhancement of the efficacy of photodynamic inactivation of *Candida albicans* with the use of biogenic gold nanoparticles. Photochem Photobiol. 93:1081–1090. doi:10.1111/php.2017.93.issue-4

Miller MW. 2000. Gene transfection and drug delivery. Ultrasound Med Biol. 26:S59–62. doi:10.1016/S0301-5629(00)00166-6

Mima EG, Pavarina AC, Dovigo LN, Vergani CE, Costa CAS, Kurashi C, Bagnato VS. 2012. Susceptibility of *Candida albicans* to photodynamic therapy in a murine modelo of oral candidosis. Oral Surg Oral Med Oral Pathol Oral Radiol Endod. 109:392–401.

Nakonechny F, Nisnevitch M, Nitzan Y, Nisnevitch M. 2013. Sonodynamic excitation of Rose Bengal for eradication of gram-positive and gram-negative bacteria. Biomed Res Int. 2013:684930.

Paardekopper M, van de Broek PJ, de Bruijne AW, Elferink JG, Dubbelman TM, Van Steveninck J. 1992. Photodynamic treatment of yeast cells with the dye toluidine blue: all-or-none loss of plasma membrane barrier properties. Biochim Biophys Acta. 1108:86–90. doi:10.1016/0005-2736(92)90117-5

Park JH, Moon YH, Bang IS, Kim YC, Kim SA, Ahn SG, Yoon JH. 2010. Antimicrobial effect of photodynamic therapy using a highly pure chlorine e6. Laser Med Sci. 25:705–710. doi:10.1007/s10103-010-0781-1

Peeters E, Nelis HJ, Coenye T. 2008. Comparison of multiple methods for quantification of microbial biofilms grown in microtiter plates. J Microbiol Methods. 72:157–165. doi:10.1016/j.mimet.2007.11.010

Pereira CA, Romeiro RL, Costa AC, Machado AK, Junqueira JC, Jorge AO. 2011. Susceptibility of *Candida albicans*, *Staphylococcus aureus*, and *Streptococcus mutans* biofilms to photodynamic inactivation: an *in vitro* study. Lasers Med Sci. 26:341–348. doi:10.1007/s10103-010-0852-3

Peres-Bota D, Rodriguez-Villalobos H, Dimopoulos G, Melot C, Vincent JL. 2004. Potential risk factors for infection with *Candida* spp. in critically ill patients. Clin Microbiol Infect. 10:550–555. doi:10.1111/j.1469-0691.2004.00873.x

Pfaller MA, Diekema DJ. 2007. Epidemiology of invasive candidiasis: a persistent public health problem. J Clin Microbiol Rev. 20:133–163. doi:10.1128/CMR.00029-06

Quishida CC, Carmello JC, Mima EG, Bagnato VS, Machado AL, Pavarina AC. 2015. Susceptibility of multispecies biofilm to photodynamic therapy using Photodithazine®. Lasers Med Sci. 30:685–694. doi:10.1007/s10103-013-1397-z

Ramage G, Mowat E, Jones B, Williams C, Lopez-Ribot J. 2009. Our current understanding of fungal biofilms. Crit Rev Microbiol. 35:340–355. doi:10.3109/10408410903241436

Rosenthal I, Sostaric JZ, Riesz P. 2004. Sonodynamic therapy-a review of the synergistic effects of drugs and ultrasound. Ultrason Sonochem. 11:349-363.

Samaranayake LP, MacFarlane TW. 1981. A retrospective study of patients with recurrent chronic atrophic candidosis. Oral Surg Oral Med Oral Pathol. 52:150–153. doi:10.1016/0030-4220(81)90312-1

Serpe L, Giuntini F. 2015. Sonodynamic antimicrobial chemotherapy: first steps towards a sound approach for microbe inactivation. J Photochem Photobiol B. 150:44–49. doi:10.1016/j.jphotobiol.2015.05.012

Spagnul C, Turner LC, Boyle RW. 2015. Immobilized photosensitisers for antimicrobial applications. J Photochem Photobiol B. 150:11–30. doi:10.1016/j.jphotobiol.2015.04.021

Stepanovic S, Vukovic D, Dakic I, Savic B, Svabic-Vlahovic M. 2000. A modified microtiter-plate test for quantification of staphylococcal biofilm formation. J Microbiol Methods. 40:175–179. doi:10.1016/S0167-7012(00)00122-6

Strakhovskaia MG, Belenikina NS, Ivanova EV, Chemeris IK, Stranadko EF. 2002. The photodynamic inactivation of *Candida guilliermondii* in the presence of photodithazine. Mikrobiologiia. 71:349–353.

Sudbery PE. 2011. Growth of *Candida albicans* hyphae. Nat Rev Microbiol. 9:737–748. doi:10.1038/nrmicro2636

Thompson DS, Carlisle PL, Kadosh D. 2011. Coevolution of morphology and virulence in *Candida* species. Eukaryot Cell. 10:1173–1182. doi:10.1128/EC.05085-11

Umemura S, Yumita N, Umemura K, Nishigaki R. 1999. Sonodynamically induced effect of rose bengal on isolated sarcoma 180 cells. Cancer Chemother Pharmacol. 43:389–393. doi:10.1007/s002800050912

Wang X, Ip M, Leung AW, Xu C. 2014. Sonodynamic inactivation of methicillin-resistant *Staphylococcus aureus* in planktonic condition by curcumin under ultrasound sonication. Ultrasonics. 54:2109–2114. doi:10.1016/j.ultras.2014.06.017

White TC, Marr KA, Bowden RA. 1998. Clinical, cellular, and molecular factors that contribute to antifungal drug resistance. Clin Microbiol Rev. 11:382–402.

Zhuang D, Hou C, Bi L, Han J, Hao Y, Cao W, Zhou Q. 2014. Sonodynamic effects of hematoporphyrin monomethyl ether on *Staphylococcus aureus in vitro*. FEMS Microbiol Lett. 361:174–180. doi:10.1111/fml.2014.361.issue-2

3.6 Publicação 6·

microorganisms

MDPI

Article

Fungistatic Action of N-Acetylcysteine on *Candida albicans* Biofilms and Its Interaction with Antifungal Agents

Thaís Soares Bezerra Santos Nunes, Leticia Matheus Rosa, Yuliana Vega-Chacón and Ewerton Garcia de Oliveira Mima *

Laboratory of Applied Microbiology, Department of Dental Materials and Prosthodontics, School of Dentistry, São Paulo State University (UNESP), Araraquara 14801-903, SP, Brazil; thais.soaresbsn@gmail.com (T.S.B.S.N.); lemrosa@hotmail.com (L.M.R.); yuliana.v.chacon@gmail.com (Y.V.-C.)

* Correspondence: ewerton.mima@unesp.br; Tel.: +55-16-3301-6557

Received: 10 June 2020; Accepted: 23 June 2020; Published: 30 June 2020

check for updates

Abstract: Therapies targeted to fungal biofilms, mainly against the matrix, and therapies that do not induce microbial resistance are relevant. N-acetylcysteine (NAC), a mucolytic agent, has shown antimicrobial action. This study evaluated the effect of NAC against fluconazole-susceptible (CaS) and -resistant (CaR) *Candida albicans*. The susceptibility of planktonic cultures to NAC, the effect of NAC on biofilms and their matrix, the interaction of NAC with antifungal agents, and confocal microscopy were evaluated. Data were analyzed descriptively and by the ANOVA/Welch and Tukey/Gomes–Howell tests. The minimum inhibitory concentration (MIC) of NAC was 25 mg/mL for both strains. NAC significantly reduced the viability of both fungal strains. Concentrations higher than the MIC (100 and 50 mg/mL) reduced the viability and the biomass. NAC at 12.5 mg/mL increased the fungal viability. NAC also reduced the soluble components of the biofilm matrix, and showed synergism with caspofungin against planktonic cultures of CaS, but not against biofilms. Confocal images demonstrated that NAC reduced the biofilm thickness and the fluorescence intensity of most fluorochromes used. High concentrations of NAC had similar fungistatic effects against both strains, while a low concentration showed the opposite result. The antibiofilm action of NAC was due to its fungistatic action.

Keywords: acetylcysteine; biofilms; extracellular matrix; *Candida albicans*; drug resistance; antifungal agents

1. Introduction

Candida albicans is an opportunistic fungal pathogen found on human mucosae, such as those of the oral, gastrointestinal, and genitourinary tracts [1]. *C. albicans* exhibits the ability to adhere to surfaces and form biofilms, which are complex communities of microorganisms attached to biotic or abiotic surfaces and surrounded by a self-produced matrix [2]. Under specific host conditions, especially immunodeficiency, *C. albicans* causes a local infection known as candidiasis, which may spread systemically and result in candidemia, a nosocomial infection with high mortality rates [3]. Furthermore, *C. albicans* possess the ability to undergo morphological transition from commensal yeast to filamentous forms (pseudohyphae and hyphae), in a process known as polymorphism [4]. In the hyphal form, *C. albicans* is pathogenic, with the ability to invade host tissue [5]. Therefore, polymorphism is a significant virulence factor of this opportunistic fungal species [4,6].

C. albicans also grows as biofilms on biomedical devices, such as catheters and dental prostheses [7]. Oral candidiasis associated with denture use, known as denture stomatitis, is an oral infection prevalent

·Artigo nas normas do periódico *Microorganisms*.

in up to 70% of denture users, with larger proportions of females affected than males. Despite the multifactorial etiology of denture stomatitis, biofilm formation by *Candida* spp. on the denture surface is considered the main etiological factor [8]. Moreover, candidal biofilms formed in indwelling catheters act as a source of infection in candidemia, whose treatment requires both antifungal administration and timely removal of the catheter [9].

The biofilm matrix protects microbial cells growing within the biofilm from external agents, and acts as a barrier to antimicrobials and the host's immune cells. Thus, in a biofilm, microbial cells exhibit higher tolerance to antimicrobials [10]. The matrix is also responsible for the three-dimensional architecture and mechanical properties of biofilms, such as their adhesive strength, cohesion, and stiffness, which enables co-aggregation of microorganisms and facilitates formation of microcolonies. The environment of biofilm modulates gene expression, metabolism, and cell signaling by molecules, influencing microbial behavior (quorum sensing) [11]. The biofilm matrix of *C. albicans* is composed of carbohydrates, such as β-glucans and mannan, as well as proteins, lipids, and extracellular DNA (eDNA) [12], and hexosamines, uronic acid, and phosphorus [13]. The *Candida albicans* biofilm matrix, especially the polysaccharides, contributes to co-aggregation of bacteria and protects bacterial cells against antibacterial agents [14–17]. *Candida albicans* biofilms also produce extracellular vesicles, whose cargo (polysaccharides and proteins) forms the biofilm matrix and confers drug tolerance [18].

Antifungal agents used to treat infections caused by *Candida* spp. are divided into the following three main classes: polyenes, azoles (imidazoles and triazoles), and echinocandins [19]. Nystatin is a topical polyene used to treat palatal mucosa affected by denture stomatitis [20,21]; fluconazole (triazole) and caspofungin (echinocandin) are used for the treatment of invasive candidiasis [9]. However, *C. albicans* cells growing within biofilms have been shown to exhibit 4 to 128 times lower antifungal susceptibility than their planktonic counterparts [22]. In addition to the inherent microbial tolerance of biofilms, the widespread use and misuse of antifungals have led to the development of antifungal resistance [6]. Such resistance leads to treatment failure with commercially available antifungal agents, and persistent infection. As a result, antimicrobial resistance remains a global threat to public health [23]. Therefore, the development of treatments aimed at overcoming antifungal resistance and disrupting biofilm matrix on medical devices is critical.

N-acetylcysteine (NAC) is a mucolytic and thiol compound used to reduce the viscosity of pulmonary mucous in patients with chronic respiratory diseases, such as bronchitis [24] and cystic fibrosis [25], as well as being used to treat paracetamol (acetominophen) overdose [26]. The sulfhydryl component of the NAC molecule breaks the disulfide bonds in mucous [27], and also acts as a precursor for glutathione synthesis and as a reactive oxygen species (ROS) scavenger, conferring an antioxidant effect to NAC [28]. Other studies have demonstrated antimicrobial and antibiofilm properties of NAC against pathogenic bacteria, such as *Mycobacterium tuberculosis* [29], *Klebsiella pneumoniae*, *Escherichia coli*, *Pseudomonas aeruginosa* [30,31], methicillin-resistant *Staphylococcus aureus* and *Staphylococcus epidermidis* [32], *Prevotella intermedia* [33], *Actinomyces naeslundii*, *Lactobacillus salivarius*, *Streptococcus mutans*, and *Enterococcus faecalis* [34,35]. Studies have also shown synergism between NAC and antibiotics [31–33,36,37]. There have also been reports that NAC disrupts mature bacterial biofilms and reduces the matrix polysaccharides [31,38]. In this context, investigating new applications of existing drugs (drug repurposing) has the advantage of reducing the time and cost spent in the development of new medications, such as by negating the need for clinical safety trials [39].

The antifungal and antibiofilm action of NAC alone or in association with antifungal agents (fluconazole, ketoconazole, and amphotericin B) against *C. albicans* has also been reported [37,40,41]. However, the antifungal effects of NAC against resistant strains and its effects on the components of the *C. albicans* biofilm matrix, to the best of our knowledge, are still unknown. Therefore, the aim of this study was to evaluate the effect of NAC on biofilms of fluconazole-resistant (CaR) and -susceptible *C. albicans* (CaS). Aside from the fungal viability and biomass, we focused on the effects of NAC on the components of the biofilm matrix: polysaccharides, proteins, lipids, and eDNA. We also evaluated the interaction of NAC with agents belonging to the following three classes of antifungals: polyenes

(nystatin), azole (fluconazole), and echinocandin (caspofungin). Additionally, we analyzed biofilms treated with NAC using confocal scanning laser microscopy.

2. Materials and Methods

2.1. Strains and Culture Conditions

Standard strains of CaS (SC5314) and CaR (ATCC 96901—American Type Culture Collection, Rockville, MD, USA) were stored at −80 °C in yeast nitrogen broth (YNB; Difco, Detroit, MI, USA) with glycerol 50%; they were thawed and reactivated in Sabouraud dextrose agar with 0.05 mg/mL of chloramphenicol (SDA; Acumedia Manufacturers Inc., Lansing, MI, USA) at 37 °C for 48 h. Five colonies of each strain were transferred to YNB with 100 mM of glucose (YNBg) and incubated overnight at 37 °C. Each fungal suspension was diluted 1:10 in fresh YNBg and incubated at 37 °C until the optical density at 540 nm (OD_{540}) reached the mid-log phase of growth (mean ± standard deviation, SD, of OD_{540}: 0.424 ± 0.042 and 0.460 ± 0.030 arbitrary units, au, for CaS and CaR, respectively), corresponding to $6.64 \times 10^6 \pm 2.72 \times 10^6$ and $6.32 \times 10^6 \pm 1.49 \times 10^6$ colony forming units per milliliter (CFU/mL) for CaS and CaR, respectively. Then, each fungal suspension was centrifuged (10,000× *g* for 10 min at 4 °C) and resuspended in Roswell Park Memorial Institute (RPMI) 1640 medium—bicarbonate free (Sigma-Aldrich, St. Louis, MO, USA, product code R6504-10X1L), buffered with morpholinepropanesulfonic acid (MOPS; Sigma-Aldrich), and supplemented with 2% D-glucose (Synth, São Paulo, Brazil), pH 7.0 (RPMId). Then, the OD_{540} for each strain was measured (0.585 ± 0.167 and 0.498 ± 0.005 au for CaS and CaR, respectively).

2.2. Antifungal Evaluation of NAC

NAC (Sigma-Aldrich) was diluted in RPMId at 100 mg/mL, according to the manufacturer's instructions, for use in antifungal evaluation. The minimum inhibitory concentration (MIC) and minimum fungicidal concentration (MFC) were evaluated by the microdilution method, according to the recommendations of the Clinical and Laboratory Standards Institute (CLSI) [42] and the European Committee for Antimicrobial Susceptibility Testing (EUCAST) [43], with some modifications. Aliquots (100 µL) of twofold serial dilutions of NAC (final concentrations of 50 to 12.5 mg/mL) in RPMId were incubated with 100 µL of each fungal suspension individually for 24 h at 37 °C in 96-well, U-bottom microtiter plates (TPP, Trasadingen, Switzerland). A temperature of 37 °C was chosen, instead of 35 °C as recommended by the CLSI, for consistency with human body temperature and the temperature used for in vitro biofilm formation [44]. Aliquots (200 µL) of each fungal suspension with RPMId and of RPMId alone were used as controls (without NAC). For the test samples, each fungal suspension was diluted in RPMId with NAC to give a final concentration of $0.5–2.5 \times 10^3$ CFU/mL. After incubation, the OD_{540} was measured in a spectrophotometer (FLUOstar Omega microplate reader; BMG Labtech GmbH, Offenburg, Germany), to obtain quantitative values and avoid any bias that might arise from visual inspection. The lowest concentration whose OD_{540} value was similar to that observed for RPMId alone was defined as the MIC. In addition, samples were plated on SDA and incubated at 37 °C for 48 h. After incubation, the colonies were counted (CFU/mL) and the lowest NAC concentration that inhibited colony growth was defined as the MFC.

2.3. Time-Kill Curves

Time-kill curves were performed using the same protocol as for the MIC analysis above. Both strains were grown until mid-log phase, as described in Section 2.1. Aliquots of 100 µL of NAC were added to each fungal suspension (100 µL) to achieve final NAC concentrations of 50 to 0.09 mg/mL for CaS, and of 50 to 12.5 mg/mL for CaR, using a 96-well, U-bottom microtiter plate. RPMId alone (without NAC) with the fungal inocula were used as negative controls. The final concentration of fungal suspension was $0.5–2.5 \times 10^3$ CFU/mL. The absorbances of the samples in the plates were measured with a spectrophotometer (at 540 nm) during 24 h of incubation at 37 °C, with readings taken every 2 h.

2.4. Evaluation of NAC Activity on Biofilm Formation

Aliquots (200 µL) of each fungal suspension were transferred to 96-well, flat-bottom microtiter plates (Kasvi, São José dos Pinhais, Brazil) and incubated at 37 °C for 90 min (adhesion phase). Then, the medium from each well was aspirated, and each well was washed twice with 200 µL of sterile phosphate-buffered saline (PBS—0.136 M NaCl, 1 mM KH_2PO_4, 2 mM KCl, 10 mM Na_2HPO_4, pH 7.4) to remove non-adherent cells. NAC at 100, 50, 25, and 12.5 mg/mL in RPMId was added to each well (200 µL) and the plates incubated at 37 °C for 48 h to allow biofilm formation [44]. Control samples received only RPMId without NAC.

After 48 h, the biofilms were washed twice with 200 µL of PBS, and biofilm viability (CFU/mL) and total biomass (using the crystal violet assay) [45] were assessed. For viability analysis, 200 µL of PBS was added into each well, biofilms were individually scraped using a pipette tip, and tenfold serial dilutions in PBS were plated in duplicate on SDA, which was incubated at 37 °C for 48 h for colony counting. For biofilm total biomass analysis, 200 µL of 80% methanol was added to each well. After 15 min, the methanol was removed; then, 200 µL of 1% crystal violet was added to each well. After 5 min, samples were washed five times with PBS, and 200 µL of 33% acetic acid was added to remove the stain. This solution was transferred to another 96-well microtiter plate, and the absorbance at 570 nm was measured [45].

2.5. Effect of the Incubation Time with NAC on Biofilm Formation

The effect of NAC on biofilm formation was evaluated as described above, but the incubation period was reduced. The samples were evaluated for biofilm viability and total biomass after 6, 12, and 24 h of biofilm formation, with and without (control) NAC.

2.6. Evaluation of the Effect of NAC on Pre-Formed Biofilms

Biofilms of each strain were grown as described above, without NAC, for 48 h. After the first 24 h of incubation, 100 µL of each well sample was removed and 100 µL of fresh RPMId was added. After 48 h, the biofilms were washed twice with PBS, and NAC at 100, 50, 25, and 12.5 mg/mL in RPMId was added to the wells (200 µL) and incubated at 37 °C for 24 h. Controls received only RPMId without NAC. After incubation, the biofilm viability (CFU/mL) and total biomass were evaluated as described above.

2.7. Effect of NAC on the Composition of the Biofilm Matrix

In order to evaluate the effect of NAC on the composition of the biofilm matrix, biofilms of each fungal strain were grown in triplicate in 24-well microtiter plates (Kasvi) using 2.5 mL of individual fungal suspension in each well. NAC was added after the adhesion phase (50 and 12.5 mg/mL for biofilm formation experiments) or after 48 h of biofilm growth (100 mg/mL for pre-formed biofilm experiments, followed by incubation for 24 h), as described above. Biofilms were washed twice with sterile 0.89% NaCl, and after the addition of 2.5 mL of 0.89% NaCl they were scraped using a pipette tip for 1 min. The content of triplicate wells (7.5 mL) was transferred to a single Falcon tube (Kasvi): 100 µL was used for tenfold serial dilutions and plating on SDA (CFU/mL), and 100 µL was used for biofilm dry weight assessment. The remainder volume (7.3 mL) was centrifuged (5500× *g*; 10 min; 4 °C), and washed three times with 2 mL of sterile milliQ water. The supernatants were pooled (13.3 mL) and the pellet was resuspended in 2 mL of milliQ water. Aliquots of the supernatant were used to quantify the proteins (1.1 mL), water-soluble polysaccharides (WSPs, 3 mL), and eDNA (650 µL). The pellet suspension was used to quantify the insoluble dry weight (500 µL), proteins (550 µL), alkali-soluble polysaccharides (ASPs, 750 µL), and lipids (200 µL).

2.7.1. Biofilm Dry Weight

Aliquots (100 µL) of the biofilm scraped were transferred to microtubes that had been previously weighed. Samples were centrifuged (12,000 rpm; 15 min; 4 °C), the supernatant was discarded, and 300 µL of 99% ethanol was added. Then, samples were vortexed and kept at −80 °C for 18 h. Afterwards, the samples were centrifuged (12,000 rpm; 10 min; 4 °C), the supernatants were discarded, and the pellets were washed three times with 70% ethanol and air dried at room temperature. The microtubes were weighed again, and the difference between the weights was the biofilm dry weight [46,47]. To weight the samples, a precision weighing balance, with five decimal places (AUW 220D, Shimadzu, Tokyo, Japan), was used.

2.7.2. Insoluble Dry Weight

A 500 µL aliquot of the pellet suspension was transferred to a previously weighed piece of aluminum foil. Each sample was dried at 100 °C, and then weighed again. The difference between the weights was the insoluble dry weight.

2.7.3. Quantification of Soluble Proteins

A standard curve was prepared using bovine serum albumin (BSA; Sigma-Aldrich) at 0.0, 0.5, 1.0, 2.0, 4.0, 6.0, and 8.0 µg/mL in order to correlate protein concentrations with absorbance values (Figure S1A). Aliquots of 500 µL from the biofilm supernatants and from each standard curve sample were individually mixed with 500 µL of Bradford reagent (Sigma-Aldrich) [48] in duplicate. After 20 min mixing at 70 rpm, absorbance was measured at 595 nm.

2.7.4. Quantification of Insoluble Proteins

A 550 µL aliquot of the biofilm pellet suspension was heated at 100 °C for 90 min with mixing at 1,000 rpm, in order to extract its protein content. Then, 5 µL of the sample was added to 250 µL of Bradford reagent (Sigma-Aldrich) [48] in duplicate. Standard curves of BSA at 0.0, 0.5, 1.0, 2.0, 4.0, 6.0, and 8.0 µg/mL and at 0.0, 0.1, 0.2, 0.4, 0.6, 0.8, 1.0, and 1.2 mg/mL were also prepared. After 20 min mixing at 70 rpm, the absorbances of the test and standard curve samples were measured at 595 nm.

2.7.5. Quantification of WSPs

A 3 mL aliquot of the biofilm supernatant was mixed with 7.5 mL of 99% ethanol. Samples were vortexed and kept at −80 °C for 18 h to precipitate the polysaccharides. Then, samples were vortexed, centrifuged (9500× *g*; 20 min; 4 °C), washed three times with 70% ethanol, and air dried at room temperature. The pellets were individually resuspended in 1 mL of water, and the total carbohydrate was quantified by the phenol-sulfuric acid method [49]. A standard curve using glucose at 0.00, 3.75, 6.25, 12.50, 25.00, 50.00, 75.00, 100.00, and 125.00 µg/mL was created (Figure S1B). Aliquots of 200 µL of samples in triplicate and of each standard curve sample in duplicate were individually mixed with 200 µL of 5% phenol. Then, 1 mL of sulfuric acid was added to each sample. After 20 min, absorbance was measured at 490 nm.

2.7.6. Quantification of ASPs

A 750 µL aliquot of the biofilm pellet suspension was transferred to a previously weighed microtube. Samples were then centrifuged (13,000× *g*; 10 min; 4 °C), the supernatants were discarded, and the pellets were dried in a sample concentrator (RVC 2-18C D, Martin Christ Gefriertrocknungsanlagen GmbH, Osterode, Germany) for 4.5 h and weighed. For ASP extraction, 300 µL of 1 N NaOH was added for each 1 mg of the sample's dry weight. After 2 h of incubation, samples were centrifuged (13,000× *g*; 10 min), and the supernatants were individually collected. Another volume of 300 µL of 1 N NaOH/(mg of dry weight) was added to the pellets, vortexed, and incubated for 2 h. After centrifugation, the supernatant was collected and pooled with the previous supernatant. The same steps described

were repeated with the pellet for a third time, but instead of being incubated for 2 h, samples were vortexed and centrifuged. The last supernatant was pooled with the previous supernatants and the pellet was discarded. Thereafter, three volumes of 99% ethanol were added to each sample, which was incubated at −20 °C for 18 h for ASP precipitation. After this time, samples were centrifuged (13,000× *g*; 20 min; 4 °C), the supernatants were discarded, and the pellets were washed three times with 70% ethanol as described for WSPs. The air-dried pellets were resuspended in the same volume of 1 N NaOH and used for quantification of total carbohydrate by the phenol-sulfuric acid method [49], as described for WSPs. A standard curve with 1 N NaOH and glucose at final concentrations of 0.00, 3.75, 6.25, 12.50, 25.00, 50.00, 75.00, 100.00, and 125.00 μg/mL was prepared (Figure S1C).

2.7.7. Quantification of eDNA

To extract eDNA from the samples, 650 μL of phenol:chloroform:isoamilic acid (25:24:1) was added to an aliquot of 650 μL of each biofilm supernatant [50]. Then, the samples were centrifuged (10,000 rpm; 5 min; 4 °C), and the supernatants were treated with chloroform:isoamilic acid (24:1). After centrifugation, the supernatants were transferred to another tube, and three volumes of 99% ethanol and 1/10 volume of 3 M sodium acetate were added. Samples were incubated at −20 °C for 18 h for DNA precipitation. The samples were then centrifuged (13,000× *g*; 20 min; 4 °C), and the pellets were washed three times with 70% ethanol, air-dried, and resuspended in Tris-EDTA (TE) buffer. The DNA concentration was measured in a nanospectrophotometer at 260 nm [50].

2.7.8. Quantification of Lipids

A 200 μL aliquot of the biofilm pellet suspension was centrifuged (13,000× *g*; 10 min; 4 °C), the supernatant was removed, and the pellet was resuspended in 100 μL of 99% ethanol. Then, samples were vortexed, and the lipids were quantified by sulfo-phospho-vanillin reaction [51]. A standard curve using olive oil diluted in 99% ethanol at 0, 0.375, 0.750, 1.125, 2.250, 4.500, 7.500, and 9.750 mg/mL was prepared (Figure S1D). Aliquots of 20 μL of each standard curve sample in duplicate were evaporated by incubation at 70 °C for 15 min. Then, 200 μL of sulfuric acid was added to each experimental sample and to each standard curve sample and vortexed. The test tubes were placed in boiling water for 10 min, and cooled in cold water for 5 min. Afterwards, 10 mL of the phospho-vanillin reagent was added to each tube, which was vortexed and incubated in boiling water for 15 min. The samples were cooled, and after 30 min absorbance was measured at 540 nm.

2.8. Interaction of NAC with Antifungal Agents

The checkerboard microdilution method was used to evaluate the interaction of NAC with the antifungal agents nystatin (polyene), fluconazole (azole), and caspofungin (echinocandin) against planktonic cultures. Antifungal agents were purchased from Sigma-Aldrich and diluted (stock solutions) in dimethylsulfoxide (DMSO; for fluconazole and nystatin) or RPMId (caspofungin). Each drug solution was diluted 40× in the culture medium (RPMId) (work solution), so the final DMSO concentration was 2.5%. Twofold serial dilutions of NAC (50 μL) (in RPMId) and antifungal agents (50 μL) were distributed along the rows and columns, respectively, of a 96-well, U-bottom microtiter plate (Kasvi). The final concentrations of the drugs for both strains are shown in Table 1. Aliquots of 100 μL of CaS or CaR were added at the final concentration of 0.5–2.5×10^3 CFU/mL. The control consisted of fungal inoculum with no drug (only the vehicle solution). After 24 h of incubation at 37 °C, the OD_{540} was measured; the control and samples whose OD_{540} values were lower than the control were diluted and plated on SDA for colony counting. The fractional inhibitory concentration index (FICI) was determined by the sum of the FICI of each agent (FICI = $FICI_{NAC}$ + $FICI_{antifungal\ agent}$). The FICI of each agent was calculated by dividing the MIC of the agent in combination by the MIC of the agent alone ($FICI_A$ = $MIC_{A\ in\ the\ presence\ of\ B}$/ $MIC_{A\ alone}$). The interpretation of the FICI value was as follows: FICI < 0.5, synergism; 0.5 ≤ FICI ≤ 4.0, no interaction; and FICI > 4.0, antagonism [52]. Due to shortcomings of the FICI method [53], Bliss independence analysis [53–55] was performed, which is

based on the idea that each drug acts independently following the probability of independent events. This model is described by the equation: $E_{IND} = E_A + E_B - E_A \times E_B$ for a combination of drug A at concentration *a* with drug B at concentration *b*. E_A is the percentage of growth inhibition observed for drug A alone at concentration *a*, E_B is the percentage of growth inhibition observed for drug B alone at concentration *b*, and E_{IND} is the expected percentage of growth inhibition of a non-interactive association of drug A at *a* with drug B at *b*. The difference ($\Delta E = E_{OBS} - E_{IND}$) between the observed percentage of growth inhibition (E_{OBS}) and the expected one (E_{IND}) defined the interaction of drugs for each concentration as follows: Bliss synergism, when ΔE and its 95% confidence interval (CI) were > 0; Bliss antagonism, when ΔE and its 95% CI were < 0; and Bliss independence, when 95% CI of ΔE overlapped 0 [53–55]. The experiments were performed in three independent occasions, FICI and Bliss independence analyses were performed for each combination of drugs for each occasion with the OD_{540} values, and mean values of ΔE were used to produce a three-dimensional, interaction surface plot, where peaks above the 0 correspond to synergism and valleys below the 0 correspond to antagonism, while the 0 plane itself indicates no statistically significant interaction.

Table 1. Concentrations of drugs used in the checkerboard assay.

Drug	CaS	CaR
NAC (mg/mL)	25, 12.5, 6.25, 3.125, 1.562, 0.781, 0	25, 12.5, 6.25, 3.125, 1.562, 0.781, 0
Nystatin (μg/mL)	8, 4, 2, 1, 0.5, 0.25, 0.125, 0.062, 0.031, 0.015, 0.007, 0	8, 4, 2, 1, 0.5, 0.25, 0.125, 0.062, 0.031, 0.015, 0.007, 0
Fluconazole (μg/mL)	2, 1, 0.5, 0.25, 0.125, 0	125, 62.5, 31.25, 15.62, 7.81, 3.9, 1.95, 0.97, 0.48, 0
Caspofungin (μg/mL)	0.5, 0.25, 0.125, 0.062, 0.031, 0.015, 0.0075, 0.0038, 0	0.5, 0.25, 0.125, 0.062, 0.031, 0.015, 0.0075, 0.0038, 0

CaS: *Candida albicans* susceptible, and CaR: *Candida albicans* resistant.

Interaction of NAC with Caspofungin against Biofilms

Biofilms from each strain were cultured for 48 h, as described before (Section 2.6), then the checkerboard assay was performed as described above. Only caspofungin was evaluated, since it was the only antifungal agent that showed synergism with NAC against planktonic cultures (see Results section). For both strains, the final concentrations of NAC (100 μL) were 50, 25, 12.5, and 0 mg/mL, and of caspofungin (100 μL) were 2, 1, 0.5, 0.25, 0.13, 0.06, 0.03, 0.02, 0.01, and 0 μg/mL. Controls received only the drug vehicle solution. After incubation at 37 °C for 24 h, samples were washed twice with PBS and the metabolic activity was evaluated by the 2,3-bis (2-methoxy-4-nitro-5-sulfophenyl)-5-[(phenylamino) carbonyl]-2H-tetrazolium hydroxide (XTT; Sigma-Aldrich) colorimetric assay. The XTT was prepared using ultrapure water at a concentration of 1 mg/mL and kept at −70 °C until needed. A menadione solution (Sigma-Aldrich) was prepared in acetone at 0.007 g/mL just prior to each experiment. The XTT solution prepared in all experiments consisted of PBS with 200 mM of glucose, XTT, and the menadione solution in the following proportions: 158 μL, 40 μL, and 2 μL, respectively. An aliquot of 200 μL of the XTT solution was added into each well with the biofilms, and incubated at 37 °C for 3 h. After this time, aliquots of 100 μL of the XTT solution degradation product (supernatant) were transferred to the wells of another 96-well, flat-bottom plate and absorbance was measured at 492 nm. Bliss independence analysis was performed as described above and illustrated using interaction surface plots.

2.9. Confocal Laser Scanning Microscopy (CLSM)

Biofilm viability and matrix composition were also analyzed with a confocal laser microscope (LSM 800 with Airyscan; Carl Zeiss, Germany). Biofilms were grown in duplicate in 24-well, flat-bottom microtiter plates (Kasvi), as described above for pre-formed biofilms, treated with or without (control) NAC at 100 mg/mL for 24 h, washed twice with PBS, stained according to the manufacturers' instructions for each fluorochrome, and then samples were washed once with PBS before being observed by confocal laser scanning microscopy (CLSM).

For viability analysis, samples were stained with the Live/Dead BacLight Bacterial Viability kit (Molecular Probes, Invitrogen Corp., Carlsbad, CA, USA). Syto9 and propidium iodide (excitation/emission

at 488/488–550 nm and 488/656–700 nm, respectively) were diluted 1:1000 and incubated with the biofilm for 45 min in the dark. For polysaccharides (α-D-mannosyl and α-D-glucosyl) [56], concanavalin A-Alexa Fluor 594 (Molecular Probes) (561/600–700 nm) at 75 µg/mL was incubated with the biofilms for 30 min. For β-glucans [57], Calcofluor White (Sigma-Aldrich) (405/450 nm) at 0.5 g/L in 10% KOH was incubated with the biofilms for 10 min. For proteins [58], biofilms were incubated with FilmTracer Sypro Ruby (Molecular Probes) (488/576–700 nm) in the dark for 30 min. For lipids [59], Nile Red (Sigma-Aldrich) at 50 µg/mL prepared with 10 mL of 25% DMSO/H_2O was incubated with the biofilm for 10 min (488/563 nm for neutral lipids and 561/613–700 nm for polar lipids). In order to distinguish the red fluorescence of Nile Red from the polar lipids, the green color was chosen for neutral lipids as an alternative to orange color.

For each image, biofilm thickness was determined with *z*-stack readings at 1 µm. Quantification of each matrix component was estimated by the fluorescence intensity generated by each fluorochrome. For each biofilm sample (n = 2), 5 random fields were measured, totaling 10 fields for both duplicates.

2.10. Statistical Analysis

The MIC/MFC and biofilm assays were performed in quadruplicate on three different occasions (n = 12 for each group). The values of CFU/mL were $\log_{10}$ transformed and outliers were removed. For the matrix composition of biofilms, the sample size (α = 5%, power = 80%) was calculated using MedCalc software (version 19.1; MedCalc Software, Mariakerke, Belgium), resulting in n = 6. For each assay, data obtained were rated according to their original volume (biofilm supernatant or biofilm pellet suspension). Biofilm dry weight was used to normalize the data from WSPs, soluble proteins, and eDNA, while insoluble dry weight was used to normalize the data from ASPs, lipids, and insoluble proteins. Normal distribution and homoscedasticity of data were evaluated by Shapiro–Wilk and Levene tests, respectively. Data were analyzed by two-way ANOVA (with strain and treatment as independent variables). For homoscedastic data, a post-hoc Tukey test was used. When data were heteroscedastic, they were evaluated by a post-hoc Games–Howell test. The level of significance was 5% and SPSS software (version 20.0; SPSS Inc., Chicago, IL, USA) was used. Data from the checkerboard assays and CLSM were analyzed as previously described.

3. Results

3.1. Antifungal Evaluation of NAC

The MIC of NAC was 25 mg/mL after 24 h and 48 h for both strains. After 24 h, a significant interaction ($p < 0.001$) was found between the strain and the treatment (Figure 1A), while after 48 h, no interaction ($p = 0.915$) was observed, but a significant effect ($p \leq 0.04$) was verified for both the treatment (Figure 1B) and the strain (mean ± SD of 0.98 ± 0.79 au, for CaS and 0.79 ± 0.74 au for CaR). No MFC was found, since no concentration of NAC inhibited the colony growth of the strains. However, significant reduction of fungal viability was observed. After 24 h, there was a significant interaction ($p = 0.008$) between the strain and the treatment. NAC at 50 and 25 mg/mL reduced ($p < 0.001$) the viability of CaS by 4.06 and 2.25 $\log_{10}$, respectively, and of CaR by 2.98 and 1.81 $\log_{10}$, respectively. Conversely, NAC at 12.5 mg/mL increased ($p \leq 0.041$) the fungal viability by 0.34 and 0.57 $\log_{10}$ for CaS and CaR, respectively (Figure 1C). After 48 h of incubation with NAC, two-way ANOVA demonstrated a significant interaction ($p = 0.001$) between the strain and the treatment. Only the concentration of 50 mg/mL reduced ($p < 0.001$) the viability of CaS by 2.26 $\log_{10}$ (Figure 1D), while NAC at 50 and 25 mg/mL reduced ($p < 0.001$) the colony growth of CaR by 3.26 and 0.46 $\log_{10}$, respectively.

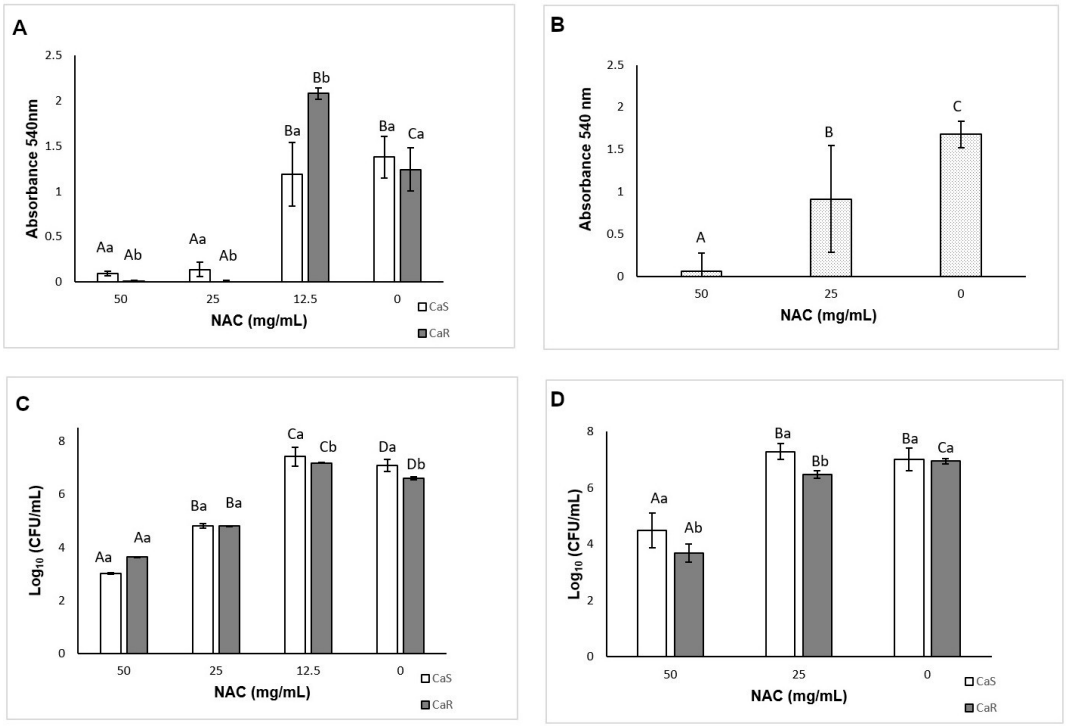


Figure 1. Mean optical density (OD) values obtained for (**A**) 24 h minimum inhibitory concentration (MIC) against *Candida albicans* susceptible (CaS) and *Candida albicans* resistant (CaR) and for (**B**) 48 h MIC against CaS and CaR; mean $\log_{10}$(CFU/mL) values for (**C**) 24 h CaS and CaR and (**D**) for 48 h CaS and CaR. Error bars: standard deviation (n = 12). Different capital letters (A, B, C) on the top of the bars denote a significant difference ($p < 0.05$) among the *N*-acetylcysteine (NAC) concentrations for the same strain, and different lowercase (a, b) letters denote a significant difference ($p < 0.05$) between the strains for the same NAC concentration. In the same way, similar capital letters on the top of the bars denote no significant difference ($p \geq 0.05$) among the groups for the same strain, and similar lowercase letters denote no significant difference ($p \geq 0.05$) between the strains for the same NAC concentration.

3.2. Time-Kill Curves

For both strains, OD_{540} values increased after 6 h (Figure 2) for control samples and those treated with NAC at concentrations lower than the MIC (subMIC). NAC at 25 and 50 mg/mL inhibited fungal growth during the 24 h incubation, but after 22 h the samples treated with 25 mg/mL NAC showed a slight increase in the OD_{540} values. Compared with the controls (no NAC), samples with NAC at subMIC demonstrated higher OD_{540} values, suggesting that these concentrations increased fungal growth.

3.3. Evaluation of the Effect of NAC on Biofilm Formation

The results of viability assessments demonstrated a significant interaction ($p < 0.001$) between the strain and the treatment. Compared with the controls, NAC at 100 and 50 mg/mL inhibited ($p \leq 0.005$) biofilm formation by 1.63 and 1.42 $\log_{10}$ for CaS, respectively, and by 2.77 and 1.52 $\log_{10}$ for CaR, respectively (Figure 3A). However, NAC at 12.5 mg/mL increased the biofilm formation of CaS by 0.73 $\log_{10}$ ($p = 0.01$).

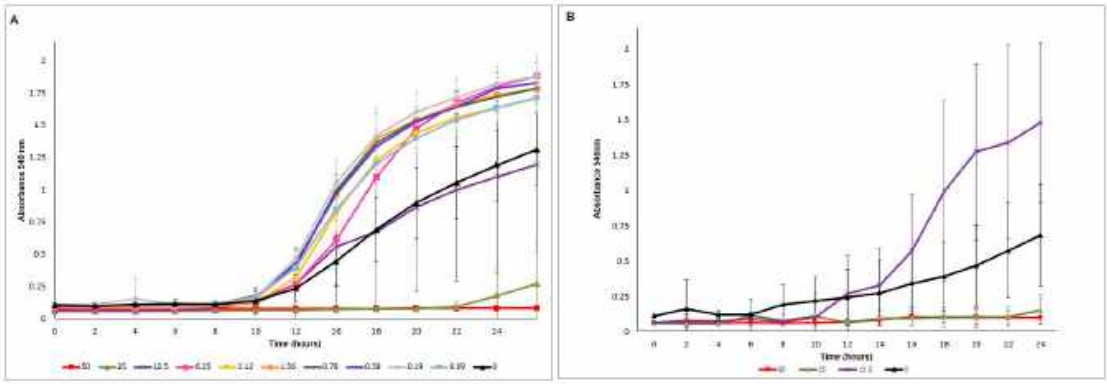


Figure 2. Time-kill curves, mean absorbance (OD_{540}) values obtained for CaS (**A**) and CaR (**B**) grown with NAC during 24 h. Error bars: standard deviation (n = 12).

When total biomass was evaluated, there was significant interaction ($p < 0.001$) between the strain and the treatment. NAC at 100, 50, and 25 mg/mL reduced ($p < 0.001$) the biofilm formation of CaS by 65.13, 88.70, 77.33%, respectively, compared with the control. For CaR, only NAC at 100 mg/mL reduced the total biomass of biofilms, by 63.62% ($p = 0.003$) (Figure 3B).

3.4. Effect of Incubation Time with NAC on Biofilm Formation

At the late stage (24 h) of biofilm formation in the presence of NAC, two-way ANOVA showed a significant interaction ($p = 0.001$) between the strain and the treatment. Only NAC at 100 mg/mL inhibited ($p < 0.001$) the CaS viability, by 1.98 $\log_{10}$, during biofilm formation (Figure 3C). For CaR, NAC at 100 and 50 mg/mL reduced ($p < 0.001$) the fungal viability by 1.71 and 1.09 $\log_{10}$, respectively (Figure 3C). For the total biomass, a significant interaction ($p = 0.015$) was found between the strain and the treatment. NAC at 100 and 50 mg/mL reduced the CaS total biomass by 85.62 and 58.79% ($p \leq 0.002$), respectively, and for CaR only NAC at 100 mg/mL reduced the total biomass, by 52.63% ($p = 0.041$) (Figure 3D).

When biofilm formation was evaluated during the middle stage (12 h), a significant interaction was observed between the strain and the treatment for viability ($p = 0.004$) and total biomass ($p = 0.014$). NAC at 100 and 50 mg/mL reduced the CaS viability by 0.87 and 0.62 $\log_{10}$ ($p \leq 0.001$), respectively, and the CaR viability by 0.94 and 1.42 $\log_{10}$ ($p \leq 0.008$), respectively (Figure 3E). These concentrations also reduced the total biomass of CaS biofilm by 67.13 and 69.42% ($p < 0.001$), respectively, and of CaR biofilm by 60.42 and 62.11% ($p \leq 0.003$), respectively (Figure 3F).

At the early stage (6 h) of biofilm formation, there was also a significant interaction between the strain and the treatment for viability ($p = 0.022$) and total biomass ($p < 0.001$). NAC at 100 and 50 mg/mL inhibited the CaS viability by 1.10 and 1.09 $\log_{10}$ ($p < 0.001$), respectively (Figure 3G), and the CaR viability by 1.34 and 1.56 $\log_{10}$ ($p < 0.001$), respectively. Moreover, NAC at 25 mg/mL also reduced ($p < 0.001$) the CaR viability by 0.70 $\log_{10}$ compared with the control (Figure 3G). For the total biomass after 6 h, NAC at 100, 50, and 25 mg/mL inhibited the biofilm formation by 77.37, 81.47, and 39.98%, respectively, for CaS ($p \leq 0.006$), and by 86.28, 87.35, and 79.77%, respectively, for CaR ($p < 0.001$) (Figure 3H).

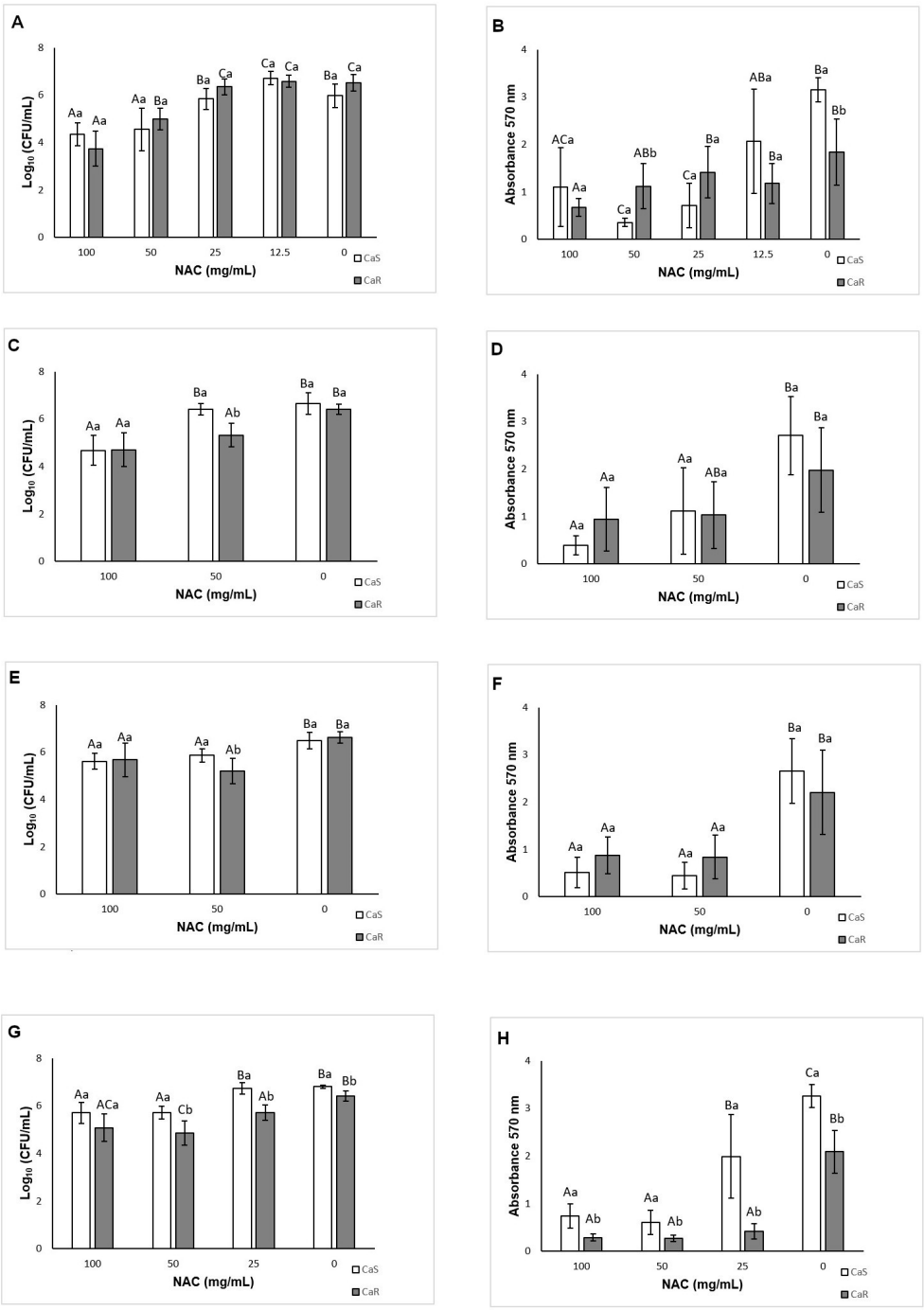


Figure 3. Mean $\log_{10}$(CFU/mL) and absorbance (total biomass) values for CaS and CaR obtained during biofilm formation in the presence of NAC at 48 h (**A**,**B**), 24 h (**C**,**D**), 12 h (**E**,**F**), and 6 h (**G**,**H**). Error bars: standard deviation (n = 12). Different capital letters (A, B, C) on the top of the bars denote a significant difference ($p < 0.05$) among the NAC concentrations for the same strain, and different lowercase (a, b) letters denote a significant difference ($p < 0.05$) between the strains for the same NAC concentration. In the same way, similar capital letters on the top of the bars denote no significant difference ($p \geq 0.05$) among the groups for the same strain, and similar lowercase letters denote no significant difference ($p \geq 0.05$) between the strains for the same NAC concentration.

3.5. Evaluation of the Effect of NAC on Pre-Formed Biofilms

When viability was assessed, a significant interaction ($p < 0.001$) between the strain and the treatment was verified. Only NAC at 100 mg/mL decreased ($p < 0.001$) the CaS biofilm, by 1.14 $\log_{10}$, compared with the control (Figure 4A). For CaR, NAC at 100, 50, and 25 mg/mL reduced ($p \leq 0.025$) the CFU/mL values by 2.30, 1.26, and 0.64 $\log_{10}$, respectively (Figure 4A). Conversely, NAC at 12.5 mg/mL increased ($p < 0.001$) the viability of CaS biofilm by 0.26 $\log_{10}$. The findings of the biofilm total biomass evaluation also demonstrated a significant interaction ($p < 0.001$) between the strain and the treatment. Only NAC at 100 mg/mL decreased ($p < 0.001$) the CaS total biomass, by 73.69%. For CaR, NAC at 100, 50, and 25 mg/mL decreased ($p \leq 0.026$) its total biomass by 69.28, 63.54, and 47.53%, respectively (Figure 4B).

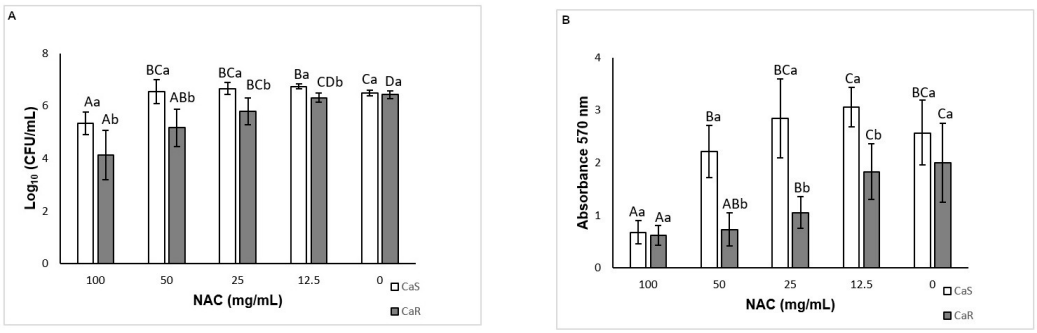


Figure 4. Mean $\log_{10}$(CFU/mL) (**A**) and absorbance (total biomass) values (**B**) for CaS and CaR obtained for pre-formed biofilm in the presence of NAC. Error bars: standard deviation ($n = 12$). Different capital letters (A, B, C) on the top of the bars denote a significant difference ($p < 0.05$) among the NAC concentrations for the same strain, and different lowercase (a, b) letters denote a significant difference ($p < 0.05$) between the strains for the same NAC concentration. In the same way, similar capital letters on the top of the bars denote no significant difference ($p \geq 0.05$) among the groups for the same strain, and similar lowercase letters denote no significant difference ($p \geq 0.05$) between the strains for the same NAC concentration.

3.6. Effect of NAC on the Composition of the Biofilm Matrix

When pre-formed biofilms of CaS and CaR were treated with NAC, two-way ANOVA demonstrated no significant interaction ($p = 0.837$) between the strain and the treatment for viability, and a significant effect was observed only for the treatment ($p < 0.001$). NAC at 100 mg/mL decreased ($p < 0.001$) the pre-formed biofilms by 0.60 $\log_{10}$ (Figure 5A). For biofilm formation in the presence of NAC, a significant interaction between the strain and the treatment was observed ($p < 0.001$) for viability. While NAC at 50 mg/mL reduced ($p \leq 0.01$) the fungal viability by 0.78 and 1.36 $\log_{10}$ for CaS and CaR, respectively (Figure 5B), NAC at 12.5 mg/mL increased ($p < 0.001$) the CaS viability by 0.33 $\log_{10}$.

3.6.1. Biofilm Dry Weight

For pre-formed biofilms, there was no significant interaction ($p = 0.803$) between the strain and the treatment, and a significant effect was found only for the treatment ($p = 0.004$). Biofilms treated with NAC at 100 mg/mL showed a significant ($p = 0.003$) reduction of dry weight by 6.38 mg (Figure 5C). For the biofilm formation analysis, no significant interaction ($p = 0.23$) was found between the strain and the treatment, but a significant effect ($p < 0.001$) was observed for both the strain and treatment. The biofilm dry weight of CaS (mean ± SD of 25.42 ± 19.42 mg) was higher ($p < 0.001$) than that of CaR (19.42 ± 9.79 mg). NAC at 50 mg/mL reduced ($p < 0.001$) the biofilm dry weight by 12.13 mg, while NAC at 12.5 mg/mL increased ($p < 0.001$) the biofilm dry weight by 11.13 mg (Figure 5D).

3.6.2. Insoluble Dry Weight

No interaction ($p = 0.428$) between the strain and the treatment was observed for pre-formed biofilms, and only treatment was a significant factor ($p = 0.034$). NAC at 100 mg/mL decreased the insoluble dry weight ($p = 0.037$) by 3.03 mg (Figure 5E). For the biofilm formation analysis, a significant interaction ($p < 0.001$) was verified between the strain and the treatment. NAC at 50 mg/mL decreased the insoluble dry weight only for CaR ($p = 0.004$), by 3.33 mg (Figure 5F), while 12.5 mg/mL NAC increased the insoluble dry weight during biofilm formation of CaS ($p = 0.001$) by 2.29 mg (Figure 5F).

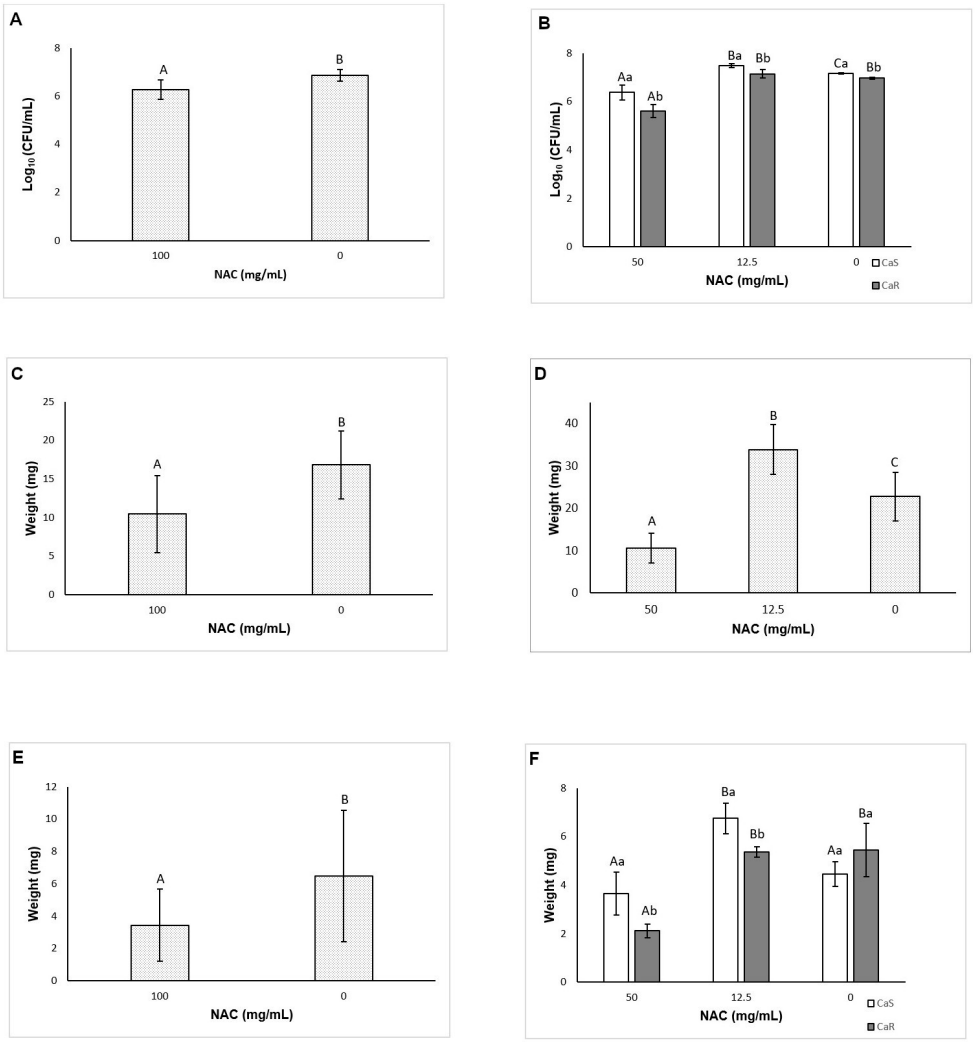


Figure 5. Mean $\log_{10}$(CFU/mL) values for pre-formed biofilm (**A**) and for biofilm formation (**B**). Mean values of biofilm dry weight of pre-formed biofilms (**C**) and for biofilm formation (**D**). Mean values of insoluble dry weight of pre-formed biofilm (**E**) and for biofilm formation (**F**). Error bars: standard deviation ($n = 6$). Different capital letters (A, B, C) on the top of the bars denote a significant difference ($p < 0.05$) among the NAC concentrations for the same strain, and different lowercase (a, b) letters denote a significant difference ($p < 0.05$) between the strains for the same NAC concentration. In the same way, similar capital letters on the top of the bars denote no significant difference ($p \geq 0.05$) among the groups for the same strain, and similar lowercase letters denote no significant difference ($p \geq 0.05$) between the strains for the same NAC concentration.

3.6.3. Quantification of Soluble Proteins

Two-way ANOVA showed a significant interaction (p = 0.045) between the strain and the treatment for pre-formed biofilms. NAC at 100 mg/mL decreased (p = 0.036) soluble proteins of CaS by 95.62 μg/mL, but not of CaR (p = 0.217) (Figure 6A). For the biofilm formation analysis, a significant interaction (p = 0.015) was found between the strain and the treatment. However, no significant difference ($p \geq 0.084$) between control and NAC at 50 and 12.5 mg/mL was observed for either strain (Figure 6B).

3.6.4. Quantification of Insoluble Proteins

In this assay, some samples treated with 100 and 50 mg/mL NAC for pre-formed biofilms and biofilm formation, respectively, showed OD_{595} values below the lowest point on the standard curve. However, the samples' concentrations were calculated based on the standard curve, which was used to calculate the original sample volume. However, the data showed a wide variation, and a statistical inference could not be made (Figure S2).

3.6.5. Quantification of WSPs

For pre-formed biofilm, there was a significant interaction between the strain and the treatment (p = 0.003). NAC at 100 mg/mL decreased WSPs ($p \leq 0.017$) by 2696.19 and 798.15 μg/mL for CaS and CaR, respectively (Figure 6C). For the biofilm formation analysis, no significant interaction (p = 0.056) was found between the strain and the treatment, but a significant effect was verified for the strain (p = 0.001) and for the treatment (p = 0.015). The level of WSPs for CaS biofilms (mean ± SD of 1468.16 ± 1471.80 μg/mL) was higher than that for CaR biofilms (325.25 ± 169.63 μg/mL). No significant difference ($p \geq 0.097$) was observed between biofilms treated with NAC and the control (Figure 6D).

3.6.6. Quantification of ASPs

For pre-formed biofilm, no significant interaction was observed between the strain and the treatment (p = 0.858), and neither of the main factors showed a significant effect ($p \geq 0.106$, mean ± SD of 1099.57 ± 103.15 and 1677.94 ± 461.99 μg/mL for CaS and CaR, respectively, treated with 100 mg/mL NAC; and 1401.34 ± 968.14 and 2117.98 ± 1571.12 μg/mL for controls CaS and CaR, respectively). However, for the biofilm formation analysis, a significant interaction was found between the strain and the treatment (p = 0.024). NAC at 50 mg/mL reduced (p = 0.035) ASPs by 1538.16 μg/mL only for CaR (Figure 6E).

3.6.7. Quantification of eDNA

Two-way ANOVA demonstrated no significant interaction between the strain and the treatment (p = 0.152) for pre-formed biofilm, and only the treatment was a significant factor (p = 0.021). NAC at 100 mg/mL reduced the eDNA (p = 0.028) in 1008.73 ηg/μL (Figure 6F). For the biofilm formation analysis, there was no significant interaction between the strain and the treatment (p = 0.269), and only the strain was a significant factor (p = 0.01). CaS showed higher (p = 0.017) values of eDNA (mean ± SD of 2915.18 ± 1718.37 ηg/μL) than CaR (1354.24 ± 529.91 ηg/μL).

3.6.8. Quantification of Lipids

For pre-formed biofilms, no significant interaction between the strain and the treatment (p = 0.245) was verified, and neither of the main factors demonstrated a significant effect ($p \geq 0.661$, mean ± SD of 33.62 ± 6.23 and 37.24 ± 8.12 mg/mL for CaS and CaR, respectively, treated with 100 mg/mL NAC; and 36.98 ± 14.51 and 29.92 ± 12.72 mg/mL for controls CaS and CaR, respectively). For biofilm formation analysis, no significant interaction was observed between the strain and the treatment (p = 0.051), but both main factors showed a significant effect ($p \leq 0.036$). CaR showed higher (p = 0.036)

values of lipids (mean ± SD of 36.27 ± 29.03 mg/mL) than CaS (23.33 ± 12.33 mg/mL). NAC at 50 mg/mL showed higher ($p < 0.001$) values of lipids than 12.5 mg/mL NAC and the control (Figure 6G).

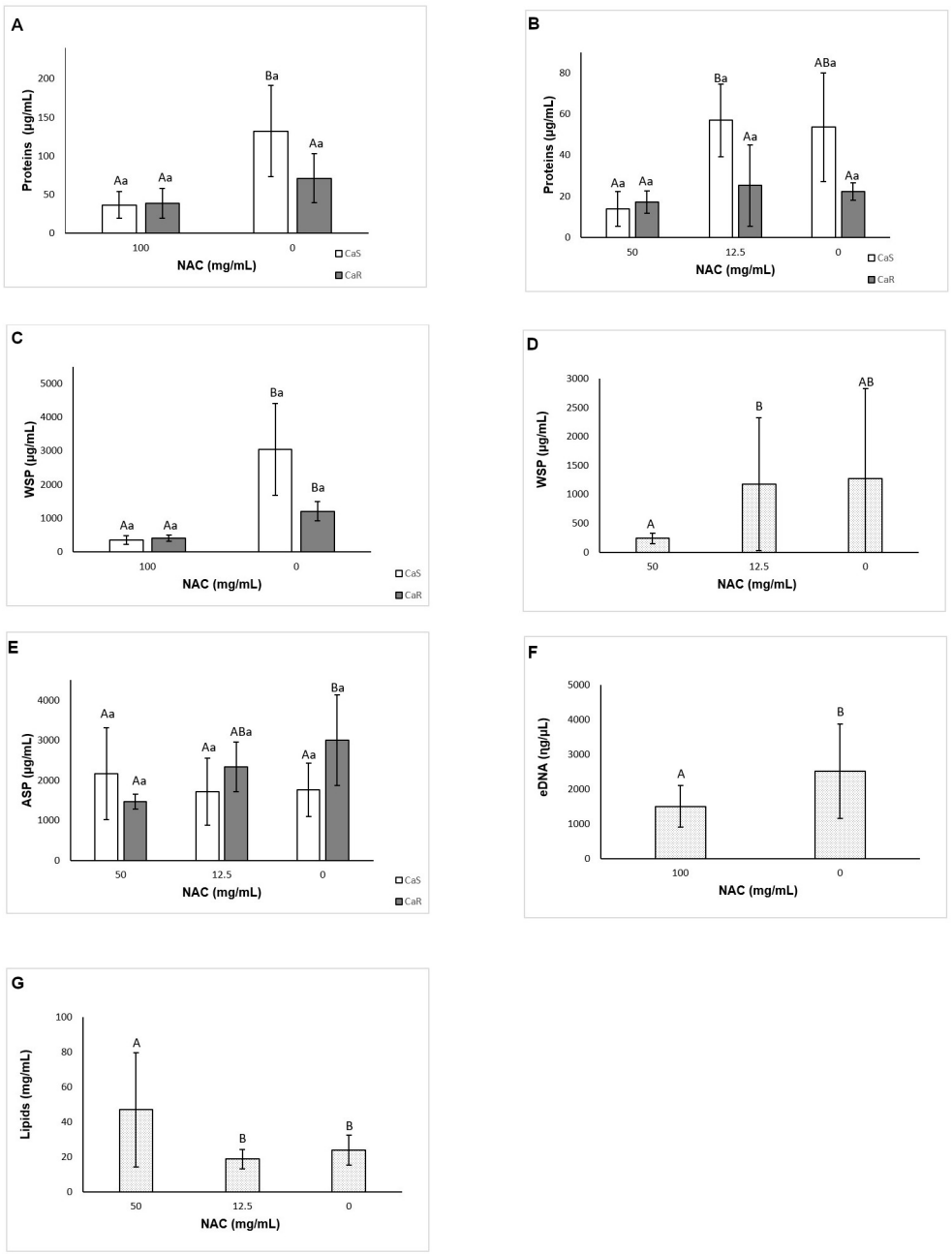


Figure 6. Mean values of soluble protein concentration of pre-formed biofilm (**A**) and biofilm formation (**B**); water-soluble polysaccharides (WSPs) of pre-formed biofilm (**C**) and biofilm formation (**D**); alkali-soluble polysaccharides (ASPs) from biofilm formation (**E**); eDNA of pre-formed biofilm (**F**) and lipids from biofilm formation (**G**). Error bars: standard deviation ($n = 6$). Different capital letters (A, B) on the top of the bars denote a significant difference ($p < 0.05$) among the NAC concentrations for the same strain, and different lowercase (a) letters denote a significant difference ($p < 0.05$) between the strains for the same NAC concentration. In the same way, similar capital letters on the top of the bars denote no significant difference ($p \geq 0.05$) among the groups for the same strain, and similar lowercase letters denote no significant difference ($p \geq 0.05$) between the strains for the same NAC concentration.

3.7. Interaction of NAC with Antifungal Agents

The MICs of nystatin, fluconazole, and caspofungin for CaS were 2, 0.5, and 0.25 µg/mL, respectively, and for CaR were 2, 125, and 0.5 µg/mL, respectively. The FICI method showed synergism of NAC only with caspofungin for CaS, with FICI values of 0.245 (3.125 mg/mL NAC with 0.015 µg/mL caspofungin) and 0.373 (3.125 mg/mL NAC with 0.031 µg/mL caspofungin), and reductions of viability from 1.15 to 1.28 $\log_{10}$, respectively (Figure S3). However, the Bliss independence analysis demonstrated antagonism of NAC with nystatin for CaS (Figure 7A, CI from −0.6803–−0.0003 to −1.6437–−1.0301 for NAC at all concentrations with 2 µg/mL nystatin) and CaR (Figure 7B, CI from −0.2059–−0.0398 to −1.2331–−0.5081 for NAC at 25 and 6.25 mg/mL, respectively, with 2 µg/mL nystatin). For CaS, synergism was observed for NAC at 1.56 mg/mL with fluconazole at 0.125 µg/mL (Figure 7C, CI 0.0084–0.1115). For CaR, synergism was observed with NAC at 0.78 mg/mL with fluconazole at 15.62, 7.81, 0.97, and 0.48 µg/mL (Figure 7D, CI from 0.0684–0.1808 to 0.0720–0.3834), but antagonism was also observed for NAC at 6.25 mg/mL with fluconazole at 1.95 µg/mL (CI −0.2277–−0.0340). Synergism with higher values of mean ΔE was observed for CaS when NAC at 6.25 and 3.125 mg/mL was associated with caspofungin from 0.062 to 0.015 µg/mL (Figure 7E, CI from 0.0141–0.1560 to 0.0892–2.2102). For CaR, synergism was also verified with NAC at 3.125 and 1.56 mg/mL associated with 0.25 µg/mL caspofungin (Figure 7F, CI from 0.0035–0.1328 to 0.6138–0.6496). Bliss independence analysis was not performed for CFU/mL data, because only samples with OD_{540} values lower than the control were plated (Figure S3).

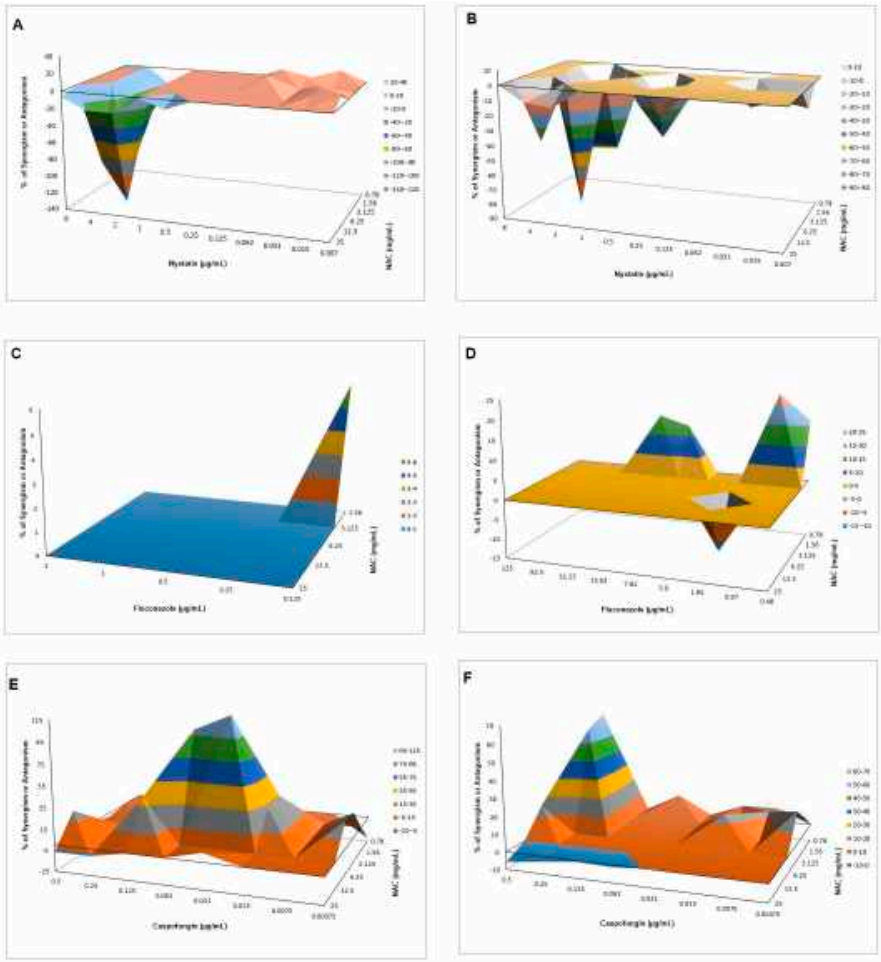


Figure 7. Interaction surface plot obtained from the Bliss independence analysis of the combination of NAC with nystatin (**A**,**B**), fluconazole (**C**,**D**), and caspofungin (**E**,**F**) against CaS (**A**,**C**,**E**) and CaR (**B**,**D**,**F**).

Peaks above the 0 correspond to synergism and valleys below the 0 correspond to antagonism, while the 0 plane itself indicates no statistically significant interaction. Each experiment was performed in three independent occasions.

Interaction of NAC with Caspofungin against Biofilms

All concentrations of caspofungin alone (with NAC at 0 mg/mL) resulted in the highest values of metabolic activity for biofilms of both strains. Therefore, FICI was not calculated. NAC alone at 50 and 25 mg/mL (with caspofungin at 0 µg/mL) reduced the metabolic activity of CaS biofilms by 37.37% and 24.44%, respectively, and of CaR biofilms by 59.29% and 57.69%, respectively. NAC at 12.5 mg/mL with caspofungin at 0.03 µg/mL reduced the metabolic activity of CaS and CaR biofilms by 85.05% and 49.45%, respectively. The Bliss independence analysis showed antagonism for CaS (Figure 8A, CI from −0.1421–−0.1391 to −1.1360–−0.8701), but synergism for CaR (Figure 8B, CI from 0.0257–0.0408 to 0.1698–0.4252).

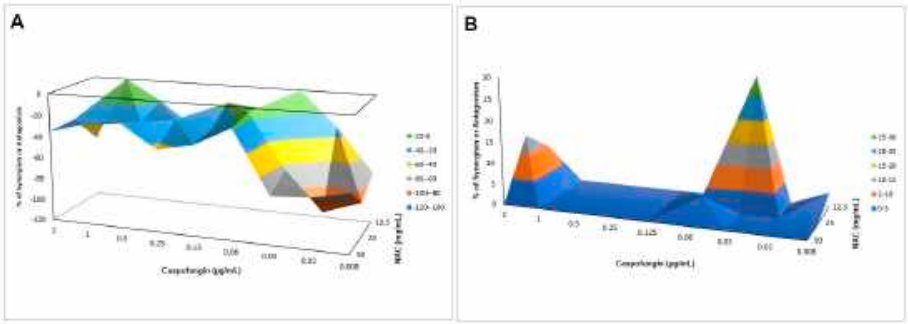


Figure 8. Interaction surface plot obtained from the Bliss independence analysis through the combination of NAC with caspofungin against biofilms of CaS (**A**) and CaR (**B**). Peaks above the 0 correspond to synergism and valleys below the 0 correspond to antagonism, while the 0 plane itself indicates no statistically significant interaction. Each experiment was performed in three independent occasions.

3.8. CLSM

CLSM images (Figures 9 and 10) showed that biofilms treated with NAC were thinner than those of the controls for viability, polysaccharide, lipid, and protein experiments for both strains, with the exception of CaS viability (Table 2). When fluorescence intensity was quantified (Table 2), control biofilms showed higher values compared with biofilms treated with NAC for living cells, polysaccharides (α-D-mannosyl and α-D-glucosyl), and polar lipids for both strains; it also demonstrated a higher intensity of dead cells when biofilms were treated with NAC. Conversely, for polysaccharides (β-glucans), proteins, and neutral lipids, the fluorescence intensities of control biofilms were lower than those treated with NAC for CaS, while CaR showed lower values for the biofilms treated with NAC.

Table 2. Thickness values and fluorescence quantification (mean ± standard deviation) determined from CLSM of CaS and CaR biofilms labeled with different fluorochromes.

Fluorochromes	Thickness (µm)				Fluorescence Intensity			
	CaS		CaR		CaS		CaR	
	Contr.	NAC	Contr.	NAC	Contr.	NAC	Contr.	NAC
S9	24.00	24.00	24.00	20.00	77.68 ± 18.47	45.86 ± 5.16	74.74 ± 9.96	38.85 ± 15.64
PI					13.22 ± 5.65	28.64 ± 6.06	6.04 ± 1.03	55.06 ± 18.52
Conc	36.00	30.00	18.00	12.00	105.99 ± 15.09	89.22 ± 11.86	78.82 ± 21.11	40.83 ± 14.44
CalcW	34.38	23.04	34.38	30.56	100.33 ± 30.68	125.12 ± 27.71	178.29 ± 9.86	23.34 ± 6.91
SR	51.92	23.60	47.2	23.60	25.70 ± 7.33	49.16 ± 10.36	70.42 ± 14.40	56.25 ± 19.30
NRp	40.00	28.00	37.76	28.32	44.85 ± 15.70	37.01 ± 11.12	148.14 ± 12.66	16.51 ± 4.29
NRn					69.62 ± 21.39	74.75± 21.50	107.62 ± 8.00	15.59 ± 2.51

Fluorochrome abbreviations and respective definitions: Syto 9 (S9) for live cells; Propidium Iodide (PI) for dead cells; Concanavalin (Conc) for α-D-mannosyl and α-D-glucosyl; Calcofluor White (CalcW) for β-glucans; Sypro Ruby (SR) for proteins; Nile Red for polar lipids (NRp) and Nile Red for neutral lipids (NRn). Contr.: Control (no NAC).

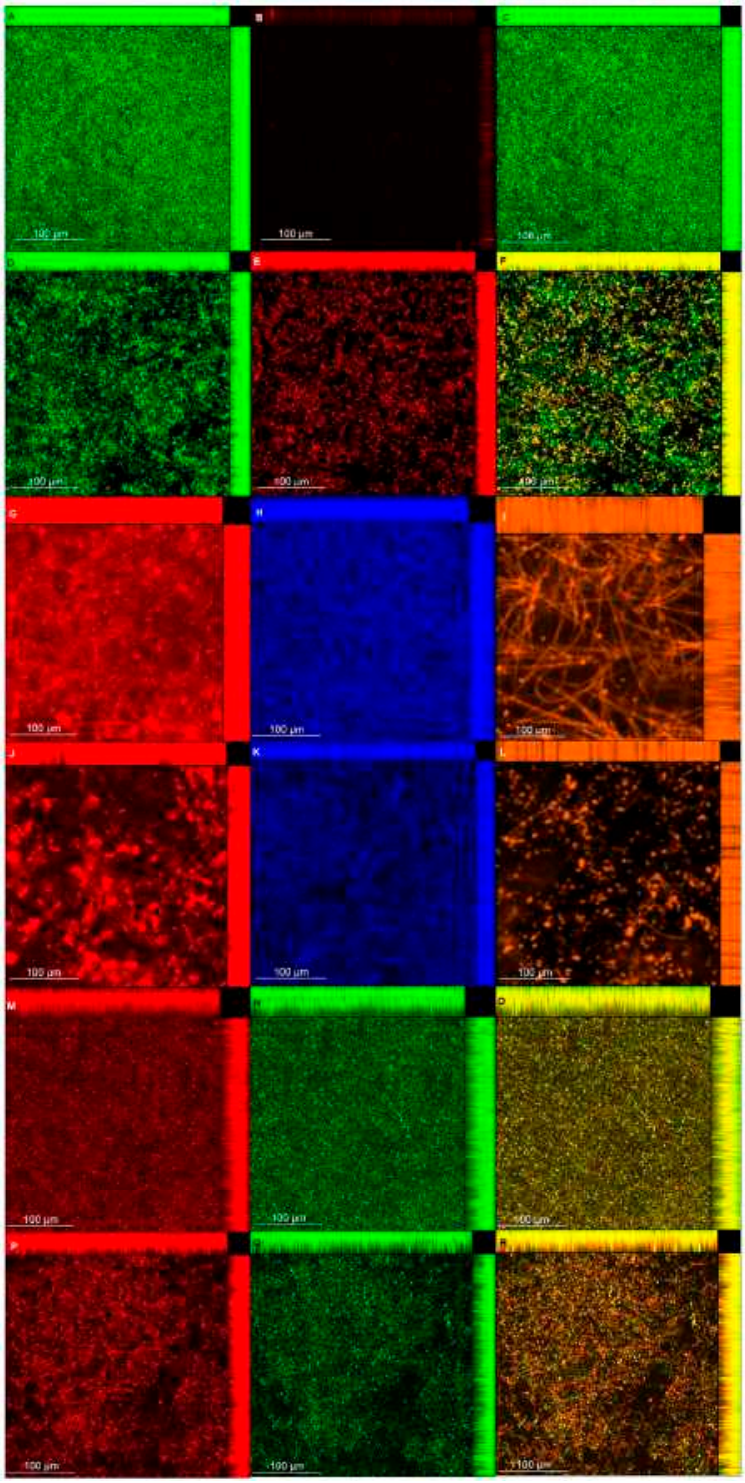


Figure 9. Confocal laser scanning microscopy (CLSM) images obtained for pre-formed CaS biofilm labeled with Syto9 (**A**,**D**, living cells) and propidium iodide (**B**,**E**, dead cells) for viability (**C**,**F**, overlap), without (A–C) and with NAC (**D**–**F**); concanavalin A-Alexa Fluor 594 (**G**,**J**, α-D-mannosyl and -glucosyl polysaccharides), Calcofluor White (H and K, β-glucans polysaccharide), and Sypro Ruby (**I**,**L**, proteins), without (**G**–**I**) and with NAC (**J**–**L**); and Nile Red (**M**–**R**, lipids) without (**M**–**O**) and with NAC (**P**–**R**) (**O**,**R**, overlap).

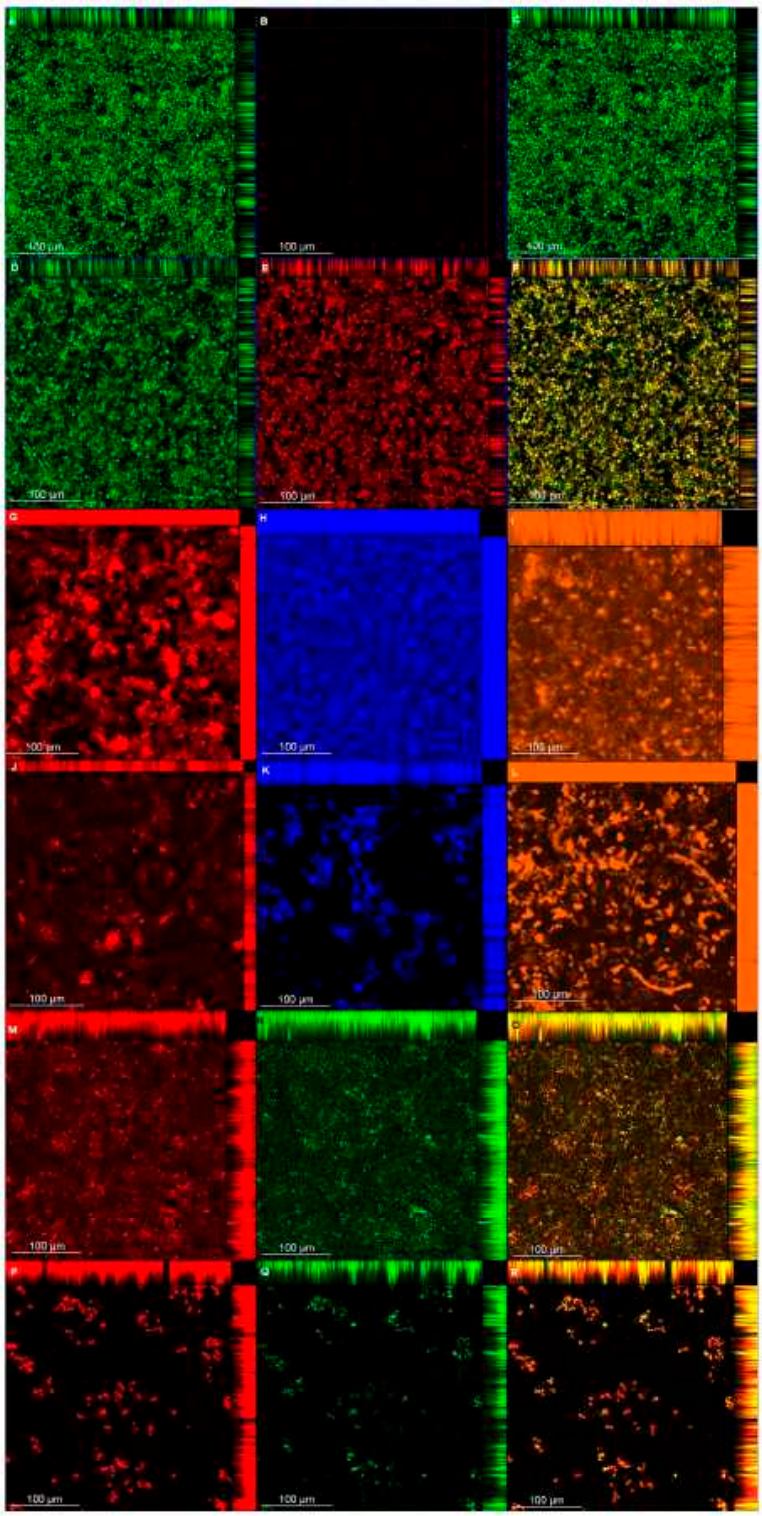


Figure 10. CLSM images obtained for pre-formed CaR biofilm labeled with Syto9 (**A** and **D**, living cells) and propidium iodide (**B**,**E**, dead cells) for viability (**C**,**F**, overlap), without (**A**–**C**) and with NAC (**D**–**F**); concanavalin A-Alexa Fluor 594 (**G**,**J**, α-D-mannosyl and -glucosyl polysaccharides), Calcofluor White (**H** and **K**, β-glucans polysaccharide), and Sypro Ruby (**I**,**L**, proteins), without (**G**–**I**) and with NAC (**J**–**L**); and Nile Red (**M**–**R**, lipids) without (**M**–**O**) and with NAC (**P**–**R**) (**O**,**R**, overlap).

4. Discussion

Our investigation demonstrated that NAC showed the same MIC (25 mg/mL) for CaS and CaR, an important finding in the current battle against antimicrobial resistance. Although we did not evaluate the target of NAC in the fungal cell to explain its fungicidal action, one of the limitations of our study, we suggest that NAC may act on the polysaccharides of the fungal cell wall, which is composed of mannan, glucan and chitin [4]. Such hypothesis is supported by our findings from the matrix components assays (reduction of soluble polysaccharides) and may also explain the same susceptibility of both fluconazole-resistant and -susceptible strains to NAC. Although other studies have shown an antifungal effect of NAC against *C. albicans*, only clinical isolates were used [37,40,41] and only one study reported that the strains were susceptible to ketoconazole [41]. Therefore, the present investigation may be the first to report the antifungal effect of NAC on a resistant strain of *C. albicans*. Moreover, this investigation evaluated reference strains since, as was observed by Alnuaimi et al. (2013) [60], reference strains have higher biofilm growth activity than clinical isolates, which is important for an in vitro evaluation before an in vivo evaluation. The studies mentioned above showed NAC MIC values of 40, 20, and 16.5 mg/mL against clinical isolates of *C. albicans* using the macrodilution and agar dilution methods [40,41]. The differences between the results of our investigation and those of the mentioned studies [35,36] may be ascribed to the different stock concentrations of NAC and the strains used. In all these investigations, the MIC values were close to the NAC stock concentrations used, which demonstrates that high concentrations are needed for a fungistatic effect. However, a fungicidal effect (MFC) was not observed in our investigation, since none of the concentrations of NAC inhibited colony growth. Another study showed that NAC at 160 mg/mL inhibited 99.9% of fungal growth [41]. However, inhibition of microbial growth should be evaluated by logarithm, since only 1 log of reduction is the same as a 99% decrease. According to the American Society for Microbiology, an agent is considered as antimicrobial when it reduces the microbial growth by at least 3 log [61]. In the present investigation, significant reductions from 1.81 to 4.06 log were observed. Therefore, although an MFC was not found, NAC was effective in reducing the fungal viability of both strains.

The time-kill curves showed that NAC at the MIC or higher concentrations reduced the fungal growth after 24 h; this was more evident after 6–10 h. Another study also verified that NAC at 80 mg/mL decreased *C. albicans* viability after 24 h, while lower concentrations resulted in an increase of fungal viability after 2–4 h [40]. The present investigation also found an increase of fungal growth when NAC was used at subMIC levels. NAC is a precursor of glutathione, an essential metabolite for *C. albicans*; at low concentrations NAC may provide glutathione to *C. albicans*, which is metabolized via γ-glutamylcysteine synthetase—GCS1 [62]. Thus, the results suggest that NAC at subMIC levels may stimulate fungal growth, but this in vitro finding cannot be extrapolated to the clinical scenario.

As a preventive strategy to control biofilm development, NAC was added during biofilm formation. NAC at concentrations higher than the MIC inhibited biofilm formation for both strains tested, reducing both the viability and the biomass of the biofilms. This result was not surprising, since the MIC assay demonstrated that these concentrations were fungistatic. Another study showed a reduction of biofilm formation in clinical *C. albicans* isolates using NAC at subMIC [41]. However, in this study, NAC at subMIC (12.5 mg/mL) showed a similar result to the control biofilm (without NAC) for CaR, while NAC at 12.5 mg/mL increased biofilm viability for CaS. These findings confirm that NAC at low concentrations may have an opposite effect to an antimicrobial agent. When the incubation time was evaluated, NAC at the MIC (25 mg/mL) reduced biofilm formation of CaR at the early stage (6 h), while NAC at concentrations higher than the MIC decreased the biofilm formation at all stages (6, 12, and 24 h) of both strains, except for the viability of CaS biofilms incubated with 50 mg/mL NAC for 24 h. Although NAC at the MIC was not evaluated for the intermediate–late stages (12 and 24 h), the findings observed in the incubation time assay corroborated those found for 48 h biofilm formation, in which only NAC at 100 and 50 mg/mL reduced biofilm formation.

As NAC is a mucolytic agent, it was tested against pre-formed biofilms as a therapeutic strategy for disrupting biofilms. Only NAC at 100 mg/mL reduced the viability and biomass of CaS biofilm, while other concentrations (50, and 25 mg/mL, as well as 100 mg/mL) could also decrease the viability and biomass of CaR biofilm. Therefore, NAC was more effective for pre-formed biofilms of CaR. Other studies also have observed a reduction of the viability and biomass of pre-formed biofilms after treatment with NAC [37,41]. However, these studies did not evaluate resistant strains. The present investigation also demonstrated a significant increase in the biofilm viability when NAC was used at 12.5 mg/mL. However, clinical isolates may have a different susceptibility response. Therefore, since we did not evaluate clinical isolates, it may be a limitation of our study.

A novel aspect of this investigation is the evaluation of the effect of NAC on the matrix composition of fungal biofilms. Before the quantification of the matrix components, the viability of biofilms treated (pre-formed biofilms) and grown with NAC (biofilm formation in the presence of NAC) was evaluated. The reductions observed for pre-formed biofilms treated with NAC at 100 mg/mL was lower than those observed in the previous assay using 96-well microtiter plate (see Section 3.5). Probably the larger area of 24-well microtiter plate and volume of fungal inoculum used in the matrix assays could have improved the biofilm grown and reduced its susceptibility to NAC. On the other hand, for biofilm formation, the reductions observed in the presence of NAC at 50 mg/mL and the increase of CaS with NAC at 12.5 mg/mL agreed with those found the previous assay (see Section 3.3). The results also showed that NAC reduced the soluble components of the biofilm matrix (soluble proteins for CaS, and WSPs and eDNA for both strains) for pre-formed biofilms, but not for biofilm formation. Other investigations have evaluated the effect of NAC only on the extracellular polysaccharides of the biofilm supernatant (WSPs) of bacterial strains [31,38]. In those studies, NAC inhibited WSP production at lower concentrations (0.5 and 1 mg/mL) than those needed for viability inhibition [31,38]. In this study, only concentrations of NAC higher than the MIC were used to evaluate the matrix components, since NAC at subMIC did not reduce biofilm formation and pre-formed biofilms in the previous assays. Thus, NAC at subMIC would be effective in reducing the WSPs only for bacterial biofilms. Although NAC reduced the viability, the biofilm dry weight, and the insoluble dry weight of both pre-formed biofilms and of biofilms during their formation in the present investigation, it was able to reduce the soluble components of the matrix only for pre-formed biofilm. NAC had no effect on the soluble components during biofilm formation. This result suggests that NAC is able to disrupt pre-formed biofilms by acting on their soluble components, but does not interfere in the synthesis of the matrix components during biofilm formation.

NAC was ineffective in reducing most water-insoluble components (ASPs and lipids), with the exception of the ASPs of CaR during biofilm formation. A previous study evaluated the effect of an antifungal agent (fluconazole) on the biofilm matrix of the same resistant strain used in the present investigation. Using the same methodology to quantify the matrix compounds, the authors observed reduction of WSPs and biomass (total dry weight) for all strains evaluated, and reduction of ASPs only for CaS [63]. Another investigation demonstrated higher values of ASPs than WSPs from biofilms of CaS treated with fluconazole and nystatin [64]. All these findings demonstrate that the insoluble components of the biofilm matrix may be less susceptible to antibiofilm approaches.

The CLSM analysis corroborated, in part, the biochemical quantification assays of the matrix components. Biofilms treated with NAC showed a lower thickness than the control biofilms, except for those of CaS stained with Live/Dead (for viability analysis). This unexpected result may be ascribed to the dense cells observed for biofilms of CaS (Figure 9) compared with those of CaR (Figure 10), which may hinder the penetration of NAC into the CaS biofilm. Moreover, the fluorescence intensity results for biofilms treated with NAC also showed lower values than for the control biofilms, except for polysaccharides (β-glucans), proteins, and neutral lipids of CaS biofilms. These exceptions may be justified by the insolubility of these components in water, as observed in the matrix-component quantification assays. However, beyond the lower thickness of samples treated with NAC, the images clearly show more "black spaces" in the samples treated with NAC compared with controls. In addition,

hyphae were observed only in biofilms stained with Sypro Ruby (proteins). Since the biofilms were grown with an RPMI-based medium, it was expected that we would observe a predominance of hyphae in the samples. It is likely that the supplementation of the medium with glucose and the staining procedure used for the other chromophores may have influenced the yeast morphology of *C. albicans*. Another study also used Calcofluor White and Sypro Ruby to evaluate, respectively, the architecture and the permeability of the biofilms of two types of *C. albicans*: a heterozygous strain of the mating type locus (MTL; a/α cells) and an MTL-homozygous strain (a/a cells). Although biofilms formed by both kind of cells showed similar architecture, a/α biofilms showed pathogenic traits of impermeability, impenetrability by human phagocytic leukocytes, and fluconazole-resistance, while a/a biofilms did not show these traits [65].

According to Nett et al. (2007) [66] and Zarnowski et al. (2014) [12], the WSP comprises the α-mannans, and the ASP comprises 1,6-β-glucan and 1,3-β-glucan. Mannan is indicated as the most abundant polysaccharide in the fungal biofilm matrix, comprising approximately 87% of the polysaccharide, followed by 1,6-β-glucan at 13%, and a tiny percentage of 1,3-β-glucan, which together give rise to the mannan-glucan complex (MGC) [12]. Another investigation suggested that the stability of each matrix polysaccharide (α-mannans, 1,6-β-glucan, and 1,3-β-glucan) is responsible for maintaining the MGC, which is crucial for biofilm resistance [67]. Moreover, the 1,3-β-glucan in the biofilm is also responsible for drug sequestration and fluconazole resistance [66,68]. Consequently, a reduction in any polysaccharide of the matrix may increase the susceptibility of the biofilm to antifungal agents. When the enzyme 1,3-β-glucanase was used against *C. albicans*, a reduction in the viability of the biofilm but not the planktonic culture was observed [66]. Moreover, other enzymes promoted detachment of *C. albicans* biofilms from a polystyrene surface, such as proteinase K, chitinase, DNAse I, β-*N*-acetylglucosaminidase, and lyticase, while lipase type II, phospholipase A2, and protease type XIV did not [13]. Lyticase, which also hydrolases 1,3-β-glucan, caused the greatest reduction of the biofilms [13].

When associated with antifungal agents, NAC showed greater synergism with caspofungin for planktonic cultures, which may be explained by the similar mechanism of action of the two drugs. Since caspofungin inhibits 1,3-β-D-glucan synthase, an enzyme necessary for the synthesis of an important fungal cell-wall polysaccharide [69], and NAC is reported to reduce the polysaccharides of biofilm matrix [31,38], as observed in the quantification of WSPs of pre-formed biofilms in the present investigation, the association of both drugs may have potentiated the antifungal effect. However, this association showed antagonism for CaS biofilms, which suggests that the biofilm alters the action of this combination of drugs, although higher decrease of metabolic activity of CaS was observed when the drugs were associated than that observed with NAC alone. Moreover, antagonism was also observed for NAC associated with nystatin, suggesting that the mechanism of action of one or both drugs may be hindered when the drugs are combined. Although the combination of NAC with fluconazole showed synergism at some concentrations, this result should be viewed with caution, since low mean values of ΔE (percentage growth inhibition) were observed (only 6% for CaS and 12% to 23% for CaR), which may be not enough to properly treat an infection caused by *C. albicans*.

In another study [37], NAC had a synergistic effect with amphotericin B and fluconazole against biofilms of *C. albicans*. However, the authors did not evaluate planktonic cultures and the synergism was evaluated by the median effect, which employs equations to calculate the combination indices. Furthermore, NAC and fluconazole did not show synergism when the combination ratio was 1000:1, evaluated by an inhibitory effect of 90% [37]. In the present investigation, we did not evaluate the interaction of NAC with another polyene (nystatin) and fluconazole in biofilms, because the FICI showed no synergism of these drugs in the planktonic assays. Another study demonstrated that the association of NAC with ketoconazole promoted higher inhibition of biofilm adherence and pre-formed biofilms than the drugs alone [41]. Synergism was also observed when fluconazole and amphotericin B were associated with the enzyme 1,3-β-glucanase against *C. albicans* biofilm [66]. However, the mentioned studies did not use the Bliss independence method for synergism evaluation.

It is important to note that NAC is a drug commercially available for clinical use, especially for respiratory illnesses, and, therefore, it is safe. A report reviewing the multiple clinical applications of NAC pointed out that even doses up to 1200 mg are well tolerated and have unusual side effects [70]. This information gave us confidence regarding the use of NAC in our research, because the highest concentration tested was 100 mg/mL. For this reason, we did not evaluate the cytotoxic effect of NAC, which is another limitation of our study. However, as already mentioned, the clinical use of NAC is well established, and consequently it does not show side effects when properly used.

In conclusion, NAC showed a fungistatic effect against CaS and CaR. However, a subMIC level (12.5 mg/mL) resulted in the opposite effect (an increase of fungal growth). The antibiofilm effect of NAC was due to its fungistatic action, since only concentrations greater than the MIC reduced biofilm formation, pre-formed biofilms, biofilm thickness, and the matrix composition, especially the water-soluble components of pre-formed biofilms. NAC also showed synergism with caspofungin for planktonic cultures, but not for biofilms of CaS. However, clinical isolates were not used in this investigation, which may have different virulence factors and susceptibility to NAC. Therefore, our in vitro findings cannot be extrapolated to the clinical scenario. Future studies are needed to elucidate the fungistatic mechanism of action of NAC against *C. albicans*, and to evaluate the efficacy of NAC against other non-*albicans Candida* species and the infections caused by them.

Supplementary Materials: The following are available online at http://www.mdpi.com/2076-2607/8/7/980/s1. Figure S1: Standard curve of soluble proteins (A), WSP (B), ASP (C) and lipids (D). Figure S2: Insoluble protein values obtained for CaS and CaR for pre-formed biofilms (A) and biofilm formation (B). Dash: median; top box: 3rd quartile; bottom box: 1st quartile; whiskers: maximum and minimum values. Figure S3: Mean values of viability of planktonic cultures obtained from the interaction of NAC with Nystatin for CaS (A) and CaR (B); NAC with Fluconazole for CaS (C) and CaR (D); and NAC with Caspofungin for CaS (E) and CaR (F).

Author Contributions: Conceptualization, E.G.d.O.M.; methodology T.S.B.S.N., L.M.R., and Y.V.-C.; validation, T.S.B.S.N. and E.G.d.O.M.; formal analysis T.S.B.S.N., E.G.d.O.M.; investigation, T.S.B.S.N., L.M.R., and Y.V.-C.; resources, E.G.d.O.M.; data curation, T.S.B.S.N.; writing—original draft preparation, T.S.B.S.N., Y.V.-C., and E.G.d.O.M.; writing—review and editing, T.S.B.S.N., Y.V.-C., E.G.d.O.M.; visualization, T.S.B.S.N. and E.G.d.O.M.; supervision, E.G.d.O.M.; project administration, E.G.d.O.M.; funding acquisition, E.G.d.O.M. All authors have read and agreed to the published version of the manuscript.

Funding: This research was funded by São Paulo Research Foundation (FAPESP), grant number #2018/02513-9; by the Coordination for the Improvement of Higher Education Personnel (CAPES), grant number 001; and the Programa Institucional de Bolsas de Iniciação Científica e Tecnológica UNESP (PIBIC).

Acknowledgments: The authors thank Midian Clara Castillo Pedraza and Marlise Inêz Klein for providing details of the biofilm matrix methodology, Paula Aboud Barbugli for the methodology and support with the CLSM, and Ana Cláudia Siqueira for technical support with the microbiological assays.

Conflicts of Interest: The authors declare no conflict of interest. The funders had no role in the design of the study; in the collection, analyses, or interpretation of data; in the writing of the manuscript, or in the decision to publish the results.

Abbreviations

ASP, alkali-soluble polysaccharide; au, arbitrary units; BSA, bovine serum albumin; CaR, fluconazole-resistant *C. albicans*; CaS, fluconazole-susceptible *C. albicans*; CFU, colony forming unit; CI, confidence interval; CLSM, confocal laser scanning microscopy; DMSO, dimethylsulfoxide; eDNA, extracellular DNA; FICI, fractional inhibitory concentration index; MFC, minimum fungicidal concentration; MIC, minimum inhibitory concentration; NAC, N-acetylcysteine; PBS, phosphate-buffered saline; subMIC, concentrations lower than the MIC; WSP, water-soluble polysaccharide; XTT, 2,3-bis (2-methoxy-4-nitro-5-sulfophenyl)-5-[(phenylamino) carbonyl]-2H-tetrazolium hydroxide.

References

1. Telles, D.R.; Karki, N.; Marshall, M.W. Oral fungal infections: Diagnosis and management. *Dent. Clin. N. Am.* **2017**, *61*, 319–349. [CrossRef]
2. Mukherjee, P.K.; Zhou, G.; Munyon, R.; Ghannoum, M.A. *Candida* biofilm: A well-designed protected environment. *Med. Mycol.* **2005**, *43*, 191–208. [CrossRef] [PubMed]

3. Pfaller, M.A.; Castanheira, M. Nosocomial candidiasis: Antifungal stewardship and the importance of rapid diagnosis. *Med. Mycol.* **2016**, *54*, 1–22. [CrossRef]
4. Gow, N.A.; van de Veerdonk, F.L.; Brown, A.J.; Netea, M.G. *Candida albicans* morphogenesis and host defence: Discriminating invasion from colonization. *Nat. Rev. Microbiol.* **2011**, *10*, 112–122. [CrossRef]
5. Sudbery, P.E. Growth of *Candida albicans* hyphae. *Nat. Rev. Microbiol.* **2011**, *9*, 737–748. [CrossRef]
6. Shapiro, R.S.; Robbins, N.; Cowen, L.E. Regulatory circuitry governing fungal development, drug resistance, and disease. *Microbiol. Mol. Biol. Rev.* **2011**, *75*, 213–267. [CrossRef]
7. Kim, J.; Sudbery, P. *Candida albicans*, a major human fungal pathogen. *J. Microbiol.* **2011**, *49*, 171–177. [CrossRef] [PubMed]
8. Gendreau, L.; Loewy, Z.G. Epidemiology and etiology of denture stomatitis. *J. Prosthodont.* **2011**, *20*, 251–260. [CrossRef]
9. Ben-Ami, R. Treatment of invasive candidiasis: A narrative review. *J. Fungi* **2018**, *4*, 97. [CrossRef] [PubMed]
10. Rautemaa, R.; Ramage, G. Oral candidosis—Clinical challenges of a biofilm disease. *Crit. Rev. Microbiol.* **2011**, *37*, 328–336. [CrossRef]
11. Koo, H.; Yamada, K.M. Dynamic cell–matrix interactions modulate microbial biofilm and tissue 3D microenvironments. *Curr. Opin. Cell. Biol.* **2016**, *42*, 102–112. [CrossRef]
12. Zarnowski, R.; Westler, W.M.; Lacmbouh, G.A.; Marita, J.M.; Bothe, J.R.; Bernhardt, J.; Lounes-Hadj Sahraoui, A.; Fontaine, J.; Sanchez, H.; Hatfield, R.D.; et al. Novel entries in a fungal biofilm matrix encyclopedia. *mBio* **2014**, *5*, e01333-14. [CrossRef]
13. Al-Fattani, M.A.; Douglas, L.J. Biofilm matrix of *Candida albicans* and *Candida tropicalis*: Chemical composition and role in drug resistance. *J. Med. Microbiol.* **2006**, *55*, 999–1008. [CrossRef]
14. Pierce, C.G.; Vila, T.; Romo, J.A.; Montelongo-Jauregui, D.; Wall, G.; Ramasubramanian, A.; Lopez-Ribot, J.L. The *Candida albicans* biofilm matrix: Composition, structure and function. *J. Fungi (Basel)* **2017**, *3*, 14. [CrossRef]
15. Kong, E.F.; Tsui, C.; Kucharíková, S.; Andes, D.; Van Dijck, P.; Jabra-Rizk, M.A. Commensal protection of *Staphylococcus aureus* against antimicrobials by *Candida albicans* biofilm matrix. *mBio* **2016**, *7*, e01365-16. [CrossRef]
16. Montelongo-Jauregui, D.; Saville, S.P.; Lopez-Ribot, J.L. Contributions of *Candida albicans* dimorphism, adhesive interactions, and extracellular matrix to the formation of dual-species biofilms with *Streptococcus gordonii*. *mBio* **2019**, *10*, e01179-19. [CrossRef]
17. Khoury, Z.H.; Vila, T.; Puthran, T.R.; Sultan, A.S.; Montelongo-Jauregui, D.; Melo, M.A.S.; Jabra-Rizk, M.A. The role of *Candida albicans* secreted polysaccharides in augmenting *Streptococcus mutans* adherence and mixed biofilm formation: In vitro and in vivo studies. *Front. Microbiol.* **2020**, *11*, 307. [CrossRef]
18. Zarnowski, R.; Sanchez, H.; Covelli, A.S.; Dominguez, E.; Jaromin, A.; Bernhardt, J.; Mitchell, K.F.; Heiss, C.; Azadi, P.; Mitchell, A.; et al. *Candida albicans* biofilm-induced vesicles confer drug resistance through matrix biogenesis. *PLoS Biol* **2018**, *16*, e2006872. [CrossRef]
19. Nett, J.E.; Andes, D.R. Antifungal agents: Spectrum of activity, pharmacology, and clinical indications. *Infect. Dis. Clin. N. Am.* **2016**, *30*, 51–83. [CrossRef]
20. Bergendal, T.; Isacsson, G. Effect of nystatin in the treatment of denture stomatitis. *Scand. J. Dent. Res.* **1980**, *88*, 446–454. [CrossRef]
21. Hilgert, J.B.; Giordani, J.M.; de Souza, R.F.; Wendland, E.M.; D'Avila, O.P.; Hugo, F.N. Interventions for the management of denture stomatitis: A systematic review and meta-analysis. *J. Am. Geriatr. Soc.* **2016**, *64*, 2539–2545. [CrossRef] [PubMed]
22. Chandra, J.; Kuhn, D.M.; Mukherjee, P.K.; Hoyer, L.L.; McCormick, T.; Ghannoum, M.A. Biofilm formation by the fungal pathogen *Candida albicans*: Development, architecture, and drug resistance. *J. Bacteriol.* **2001**, *183*, 5385–5394. [CrossRef] [PubMed]
23. Roca, I.; Akova, M.; Baquero, F.; Carlet, J.; Cavaleri, M.; Coenen, S.; Cohen, J.; Findlay, D.; Gyssens, I.; Heuer, O.E.; et al. The global threat of antimicrobial resistance: Science for intervention. *New Microbes New Infect.* **2015**, *6*, 22–29. [CrossRef] [PubMed]
24. Stey, C.; Steurer, J.; Bachmann, S.; Medici, T.C.; Tramer, M.R. The effect of oral N-acetylcysteine in chronic bronchitis: A quantitative systematic review. *Eur. Respir. J.* **2000**, *16*, 253–262. [CrossRef] [PubMed]
25. Henke, M.O.; Ratjen, F. Mucolytics in cystic fibrosis. *Paediatr. Respir. Rev.* **2007**, *8*, 24–29. [CrossRef]
26. Heard, K.J. Acetylcysteine for acetaminophen poisoning. *N. Engl. J. Med.* **2008**, *359*, 285–292. [CrossRef]

27. Sheffner, A.L. The reduction in vitro in viscosity of mucoprotein solutions by a new mucolytic agent, N-acetyl-L-cysteine. *Ann. N. Y. Acad. Sci.* **1963**, *106*, 298–310. [CrossRef]
28. Sadowska, A.M.; Manuel-Y-Keenoy, B.; De Backer, W.A. Antioxidant and anti-inflammatory efficacy of NAC in the treatment of COPD: Discordant in vitro and in vivo dose-effects: A review. *Pulm. Pharmacol. Ther.* **2007**, *20*, 9–22. [CrossRef]
29. Amaral, E.P.; Conceição, E.L.; Costa, D.L.; Rocha, M.S.; Marinho, J.M.; Cordeiro-Santos, M.; D'Império-Lima, M.R.; Barbosa, T.; Sher, A.; Andrade, B.B. N-acetyl-cysteine exhibits potent anti-mycobacterial activity in addition to its known anti-oxidative functions. *BMC Microbiol.* **2016**, *16*, 251. [CrossRef]
30. Ferris, R.A.; McCue, P.M.; Borlee, G.I.; Loncar, K.D.; Hennet, M.L.; Borlee, B.R. In vitro efficacy of nonantibiotic treatments on biofilm disruption of Gram-negative pathogens and an in vivo model of infectious endometritis utilizing isolates from the equine uterus. *J. Clin. Microbiol.* **2016**, *54*, 631–639. [CrossRef]
31. Zhao, T.; Liu, Y. N-acetylcysteine inhibit biofilms produced by *Pseudomonas aeruginosa*. *BMC Microbiol.* **2010**, *10*, 140. [CrossRef] [PubMed]
32. Aslam, S.; Darouiche, R.O. Role of antibiofilm-antimicrobial agents in controlling device-related infections. *Int. J. Artif. Organs.* **2011**, *34*, 752–758. [CrossRef]
33. Moon, J.H.; Jang, E.Y.; Shim, K.S.; Lee, J.Y. In vitro effects of N-acetyl cysteine alone and in combination with antibiotics on *Prevotella intermedia*. *J. Microbiol.* **2015**, *53*, 321–329. [CrossRef]
34. Moon, J.H.; Choi, Y.S.; Lee, H.W.; Heo, J.S.; Chang, S.W.; Lee, J.Y. Antibacterial effects of N-acetylcysteine against endodontic pathogens. *J. Microbiol.* **2016**, *54*, 322–329. [CrossRef] [PubMed]
35. Quah, S.Y.; Wu, S.; Lui, J.N.; Sum, C.P.; Tan, K.S. N-acetylcysteine inhibits growth and eradicates biofilm of *Enterococcus faecalis*. *J. Endod.* **2012**, *38*, 81–85. [CrossRef] [PubMed]
36. Parry, M.F.; Neu, H.C. Effect of N-acetylcysteine on antibiotic activity and bacterial growth In vitro. *J. Clin. Microbiol.* **1977**, *5*, 58–61.
37. Venkatesh, M.; Rong, L.; Raad, I.; Versalovic, J. Novel synergistic antibiofilm combinations for salvage of infected catheters. *J. Med. Microbiol.* **2009**, *58*, 936–944. [CrossRef]
38. Olofsson, A.C.; Hermansson, M.; Elwing, H. N-acetyl-L-cysteine affects growth, extracellular polysaccharide production, and bacterial biofilm formation on solid surfaces. *Appl. Environ. Microbiol.* **2003**, *69*, 4814–4822. [CrossRef]
39. Corsello, S.M.; Bittker, J.A.; Liu, Z.; Gould, J.; McCarren, P.; Hirschman, J.E.; Johnston, S.E.; Vrcic, A.; Wong, B.; Khan, M.; et al. The drug repurposing hub: A next-generation drug library and information resource. *Nat. Med.* **2017**, *23*, 405–408. [CrossRef]
40. Aslam, S.; Trautner, B.W.; Ramanathan, V.; Darouiche, R.O. Combination of tigecycline and N-acetylcysteine reduces biofilm-embedded bacteria on vascular catheters. *Antimicrob. Agents Chemother.* **2007**, *51*, 1556–1558. [CrossRef]
41. El-Baky, R.M.A.; Dalia, M.M.A.; Gamal, F.M.G. N-acetylcysteine inhibits and eradicates *Candida albicans* biofilms. *Am. J. Infect. Dis. Microbiol.* **2014**, *2*, 122–130. [CrossRef]
42. CLSI. *Reference Method for Broth Dilution Antifungal Susceptibility Testing of Yeasts: Approved Standard—Third Edition*; CLSI document M27-A3; Clinical and Laboratory Standards Institute: Wayne, PA, USA, 2008.
43. Arendrup, M.C.; Meletiadis, J.; Mouton, J.W.; Lagrou, K.; Hamal, P.; Guinea, J.; The Subcommittee on Antifungal Susceptibility Testing (AFST) of the ESCMID European Committee for Antimicrobial Susceptibility Testing (EUCAST). *Method for the Determination of Broth Dilution Minimum Inhibitory Concentrations of Antifungal Agents for Yeasts*; EUCAST Definitive Document E.DEF 7.3; EUCAST: Basel, Switzerland, 2017.
44. Chandra, J.; Mukherjee, P.K.; Ghannoum, M.A. In vitro growth and analysis of *Candida* biofilms. *Nat. Protoc.* **2008**, *3*, 1909–1924. [CrossRef]
45. Stepanovic, S.; Vukovic, D.; Dakic, I.; Savic, B.; Svabic-Vlahovic, M. A modified microtiter-plate test for quantification of staphylococcal biofilm formation. *J. Microbiol. Methods.* **2000**, *40*, 175–179. [CrossRef]
46. Panariello, B.H.D.; Klein, M.I.; Pavarina, A.C.; Duarte, S. Inactivation of genes TEC1 and EFG1 in *Candida albicans* influences extracellular matrix composition and biofilm morphology. *J. Oral. Microbiol* **2017**, *9*, 1385372. [CrossRef] [PubMed]
47. Castillo Pedraza, M.C.; Novais, T.F.; Faustoferri, R.C.; Quivey, R.G., Jr.; Terekhov, A.; Hamaker, B.R.; Klein, M.I. Extracellular DNA and lipoteicoic acids interact with exopolysaccharides in the extracellular matrix of *Streptococcus mutans* biofilms. *Biofouling.* **2017**, *33*, 722–740. [CrossRef] [PubMed]

48. Bradford, M.M. Rapid and sensitive method for the quantitation of microgram quantities of protein utilizing the principle of protein-dye binding. *Anal. Biochem.* **1976**, *72*, 248–254. [CrossRef]
49. Dubois, M.; Gilles, K.A.; Hamilton, J.K.; Rebers, P.A.; Smith, F. Colorimetric method for determination of sugars and related substances. *Anal. Chem.* **1956**, *28*, 350–356. [CrossRef]
50. Rice, K.C.; Mann, E.E.; Endres, J.L.; Weiss, E.C.; Cassat, J.E.; Smeltzer, M.S.; Smeltzer, M.S.; Bayles, K.W. The cidA murein hydrolase regulator contributes to DNA release and biofilm development in *Staphylococcus aureus*. *Proc. Natl. Acad. Sci. USA* **2007**, *104*, 8113–8118. [CrossRef]
51. Frings, C.S.; Fendley, T.W.; Dunn, R.T.; Queen, C.A. Improved determination of total serum lipids by the sulfo-phospho-vanillin reaction. *Clin. Chem.* **1972**, *18*, 673–674. [CrossRef]
52. Odds, F.C. Synergy, antagonism, and what the chequerboard puts between them. *J. Antimicrob. Chemother.* **2003**, *52*, 1. [CrossRef]
53. Meletiadis, J.; Verweij, P.E.; TeDorsthorst, D.T.; Meis, J.F.; Mouton, J.W. Assessing In vitro combinations of antifungal drugs against yeasts and filamentous fungi: Comparison of different drug interaction models. *Med. Mycol.* **2005**, *43*, 133–152. [CrossRef]
54. Petraitis, V.; Petraitiene, R.; Hope, W.W.; Meletiadis, J.; Mickiene, D.; Hughes, J.E.; Cotton, M.P.; Stergiopoulou, T.; Kasai, M.; Francesconi, A.; et al. Combination therapy in treatment of experimental pulmonary aspergillosis: In vitro and in vivo correlations of the concentration- and dose-dependent interactions between anidulafungin and voriconazole by Bliss independence drug interaction analysis. *Antimicrob. Agents Chemother.* **2009**, *53*, 2382–2391. [CrossRef]
55. Roell, K.R.; Reif, D.M.; Motsinger-Reif, A.A. An introduction to terminology and methodology of chemical synergy-perspectives from across disciplines. *Front. Pharmacol.* **2017**, *8*, 158. [CrossRef]
56. Kiernan, J.A. Localization of alpha-D-glucosyl and alpha-D-mannosyl groups of mucosubstances with concanavalin A and horseradish peroxidase. *Histochemistry* **1975**, *44*, 39–45. [CrossRef]
57. Nicholas, R.O.; Williams, D.W.; Hunter, P.A. Investigation of the value of β-glucan-specific fluorochromes for predicting the β-glucan content of the cell walls of zoopathogenic fungi. *Mycol. Res.* **1994**, *98*, 694–698. [CrossRef]
58. Vila, T.; Ishida, K.; Seabra, S.H.; Rozental, S. Miltefosine inhibits *Candida albicans* and non-*albicans Candida* spp. biofilms and impairs the dispersion of infectious cells. *Int. J. Antimicrob. Agents.* **2016**, *48*, 512–520. [CrossRef]
59. Kimura, K.; Yamaoka, M.; Kamisaka, Y. Rapid estimation of lipids in oleaginous fungi and yeasts using Nile red fluorescence. *J. Microbiol. Methods.* **2004**, *56*, 331–338. [CrossRef]
60. Alnuaimi, A.D.; O'Brien-Simpson, N.M.; Reynolds, E.C.; McCullough, M.J. Clinical isolates and laboratory reference *Candida* species and strains have varying abilities to form biofilms. *FEMS Yeast Res.* **2013**, *13*, 689–699. [CrossRef]
61. Cieplik, F.; Tabenski, L.; Buchalla, W.; Maisch, T. Antimicrobial photodynamic therapy for inactivation of biofilms formed by oral key pathogens. *Front. Microbiol.* **2014**, *5*, 405. [CrossRef]
62. Baek, Y.U.; Kim, Y.R.; Yim, H.S.; Kang, S.O. Disruption of gamma-glutamylcysteine synthetase results in absolute glutathione auxotrophy and apoptosis in *Candida albicans*. *FEBS Lett.* **2004**, *556*, 47–52. [CrossRef]
63. Panariello, B.H.D.; Klein, M.I.; Mima, E.G.O.; Pavarina, A.C. Fluconazole impacts the extracellular matrix of fluconazole-susceptible and -resistant *Candida albicans* and *Candida glabrata* biofilms. *J. Oral. Microbiol.* **2018**, *10*, 1476644. [CrossRef]
64. Da Silva, W.J.; Gonçalves, L.M.; Seneviratne, J.; Parahitiyawa, N.; Samaranayake, L.P.; Del Bel Cury, A.A. Exopolysaccharide matrix of developed *Candida albicans* biofilms after exposure to antifungal agents. *Braz. Dent. J.* **2012**, *23*, 716–722. [CrossRef]
65. Srikantha, T.; Daniels, K.J.; Pujol, C.; Kim, E.; Soll, D.R. Identification of genes upregulated by the transcription factor Bcr1 that are involved in impermeability, impenetrability, and drug resistance of *Candida albicans* a/α biofilms. *Eukaryot. Cell.* **2013**, *12*, 875–888. [CrossRef]
66. Nett, J.; Lincoln, L.; Marchillo, K.; Massey, R.; Holoyda, K.; Hoff, B.; VanHandel, M.; Andes, D. Putative role of beta-1,3 glucans in *Candida albicans* biofilm resistance. *Antimicrob. Agents Chemother.* **2007**, *51*, 510–520. [CrossRef]
67. Mitchell, K.F.; Zarnowski, R.; Sanchez, H.; Edward, J.A.; Reinicke, E.L.; Nett, J.E.; Mitchell, A.P.; Andes, D.R. Community participation in biofilm matrix assembly and function. *Proc. Natl. Acad. Sci. USA* **2015**, *112*, 4092–4097. [CrossRef]

68. Nett, J.E.; Sanchez, H.; Cain, M.; Andes, D.R. Genetic basis of *Candida* biofilm resistance due to drug-sequestering matrix glucan. *J. Infect. Dis.* **2010**, *202*, 171–175. [CrossRef]
69. Sucher, A.J.; Chahine, E.B.; Balcer, H.E. Echinocandins: The newest class of antifungals. *Ann. Pharmacother.* **2009**, *43*, 1647–1657. [CrossRef]
70. Millea, P.J. N-acetylcysteine: Multiple clinical applications. *Am. Fam. Physician* **2009**, *80*, 265–269.



© 2020 by the authors. Licensee MDPI, Basel, Switzerland. This article is an open access article distributed under the terms and conditions of the Creative Commons Attribution (CC BY) license (http://creativecommons.org/licenses/by/4.0/).

4 DISCUSSÃO

Esta obra apresenta os trabalhos desenvolvidos pelo grupo de pesquisa do candidato que tiveram como objetivo a inativação de biofilmes patogênicos responsáveis por infecções médico-odontológicas, incluindo biofilmes formados por cepas resistentes, as quais têm sido um grande desafio atual para a área de saúde. Assim, métodos alternativos aos agentes antimicrobianos atuais, cujo uso indiscriminado tem resultado no desenvolvimento de resistência antimicrobiana, foram avaliados nesses estudos.

No primeiro artigo científico[81], nanopartículas de TiO_2:Ag foram sintetizadas e avaliadas in vitro contra micro-organismos patogênicos, com o intuito de serem utilizadas posteriormente como revestimento (*coating*) de materiais e superfícies empregadas na área de saúde. Assim, buscamos a associação de um material inerte, estável, não tóxico e de baixo custo como o TiO_2 com o potencial antimicrobiano da Ag para essa finalidade. Para a síntese dessas nanopartículas, o método de tratamento hidrotermal assistido por irradiação de micro-ondas foi utilizado, uma vez que esse método é considerado seguro, ecológico e reproduzível para a síntese de nanomateriais[120]. Antes da avaliação antimicrobiana, a caracterização das nanopartículas é uma etapa fundamental para a confirmação das propriedades e características do sistema, para que este possa ser utilizado aos fins a que se destina. Os microcristais obtidos demonstraram sinais de difração em raio-X referentes à fase anatásio do TiO_2 com estrutura tetragonal e Ag metálica. Com relação à sua propriedade fotocatalítica, o espectro de absorção de luz ultravioleta-visível juntamente com a equação descrita por Wood e Tauc[121] demonstraram que o TiO_2:Ag apresentou intervalo de banda de energia óptica de 1,52 eV, menor que 3,03 eV verificado para o TiO_2, em virtude da presença da Ag que modifica a estrutura cristalina molecular do TiO_2. Quando observadas em microscopia eletrônica de varredura por emissão de campo, as nanopartículas apresentaram morfologia esférica e homogênea, com aglomerações e tamanho médio de 112 nm. As imagens de microscopia eletrônica de transmissão de alta resolução permitiram visualizar as nanopartículas de Ag na superfície do TiO_2, com diâmetros menores que 10 nm e distância interplanar de 2,37 Å, correspondente ao padrão observado na difração de raio-X. O espectro Raman do TiO_2:Ag demonstrou um deslocamento dos sinais máximos observados para o TiO_2, característicos de anatásio, além da presença de dois outros sinais semelhantes à fase bruquita do TiO_2. Essas alterações no perfil Raman foram atribuídas à desordem local e ao estresse compressivo resultante da presença de Ag.

No teste de susceptibilidade de SARM e das espécies de *Candida* ao TiO_2:Ag, foram verificados valores de concentração inibitória mínima de 62,5; 15,0; 31,25 e 500 mg/L para *C. albicans*, *C. glabrata*, *C. tropicalis* e SARM, respectivamente, o que demonstrou que *C. glabrata* foi a espécie mais susceptível ao TiO_2:Ag, ao passa que SARM foi a espécie avaliada menos susceptível (*C. glabrata* < *C. tropicalis* < *C. albicans* < SARM). Já as concentrações fungicida/bactericida mínima observadas para o TiO_2:Ag foram de 250 e 1000 mg/L para *C. glabrata* e SARM, respectivamente, enquanto que concentrações fungicidas não foram observados para *C. albicans* e *C. tropicalis*, somente reduções significativas de viabilidade. Para os biofilmes, somente a concentração de 1000 mg/L de TiO_2:Ag promoveu reduções significativas de viabilidade (1,54 a 2,11 log_{10}) e biomassa total (19,51 a 35,66%) para *Candida* spp., enquanto que as concentrações de 500 e 1000 mg/L diminuíram a viabilidade de SARM em 2,33 e 1,81 log_{10}, respectivamente, e somente 1000 mg/L reduziu a biomassa total (11,91%). Finalmente, para explicar o mecanismo antimicrobiano do TiO_2:Ag, modelos e cálculos teóricos foram utilizados para demonstrar a interação eletroquímica entre o metal (Ag) e o semicondutor (TiO_2), interação essa que envolve troca de elétrons entre ambos e resulta na formação de espécies reativas oxidativas.

Nos capítulos seguintes, uma outra estratégia antimicrobiana, a aPDT, foi utilizada contra biofilmes formados por micro-organismos patogênicos. Nos capítulos 2[101] e 3[103], a CUR foi utilizada como FS e, para melhorar sua solubilidade para permitir sua utilização in vivo, a CUR foi encapsulada em nanopartículas poliméricas. Para a síntese das nanopartículas, foram utilizados o ácido polilático, que é um polímero biodegradável, biocompatível e que gera produtos não tóxicos aos tecidos[122], e a dextrana, com o intuito de atuar como uma fonte atrativa aos micro-organismos. O processo de síntese utilizado foi o método da nanoprecipitação, considerado simples, rápido, reproduzível, econômico e de fácil aplicação em escala industrial[123]. No estudo referente ao segundo capítulo[101], que também resultou num depósito de patente (INPI, processo BR 10 2016 015631 9, "Processo de Obtenção de Nanopartículas Poliméricas Aniônicas e Catiônicas de Curcumina, Nanopartículas obtidas e Seus Usos", Anexo A), objetivamos padronizar o método de síntese de nanopartículas aniônicas e catiônicas, caracterizar as nanopartículas obtidas e avaliar in vitro sua ação fotodinâmica antimicrobiana. A concentração máxima de CUR encapsulada foi 260 μM, pois concentrações maiores acarretavam em agregação da CUR. Na análise das propriedades físico-químicas por espalhamento dinâmico de luz, foi verificado que o tamanho, a polidispersão e a carga (potencial zeta) das nanopartículas alteravam-se com o tempo (40 dias) após a síntese. Assim, as nanopartículas foram utilizadas sempre 24 h

imediatamente após a sua completa síntese. Com o encapsulamento, foi verificado que a que o espectro de absorção da luz das nanopartículas, tanto aniônicas como catiônicas, não era modificado em relação ao da CUR livre (não encapsulada, dissolvida em 10% de DMSO), com sinal máximo de absorção no espectro de luz azul (425 a 429 nm), e a fotodegradação de todas as formas de CUR (livre e encapsulada) foi maior que 71% após 43.2 J/cm^2 (20 minutos) de luz azul (455 nm). A eficiência de encapsulamento da CUR foi de 64% e 67% para as nanopartículas catiônicas e aniônicas, respectivamente, o que demonstrou que nem toda CUR empregada durante a síntese foi encapsulada. Além disso, a liberação da CUR das nanopartículas foi gradual ao longo do tempo, com 96% da CUR liberada das nanopartículas em 48 h.

Na avaliação fotodinâmica antimicrobiana, tanto a CUR livre como a CUR em nanopartícula catiônica utilizadas como FS mostraram completa inativação de culturas planctônicas de *S. mutans*, *C. albicans* e SARM, enquanto que a CUR em nanopartícula aniônica associada à luz azul resultou em reduções significativas de 6,54; 0,78 e 6,47 $\log_{10}$ para essas espécies, respectivamente. Entretanto, as nanopartículas catiônicas, com ou sem CUR, na ausência de luz também demonstraram erradicação das culturas planctônicas das três espécies avaliadas, indicando provável citotoxicidade celular, uma vez que o FS deve ser inerte na ausência de luz. Já quando cultivadas na forma de biofilmes simples, essas espécies mostraram menores valores de redução. Para a aPDT mediada pela CUR livre, reduções médias de 1,24; 2,26 e 2,47 $\log_{10}$ foram observados para SARM, *C. albicans* e *S. mutans*. Por outro lado, quando as nanopartículas aniônicas de CUR foram avaliadas como FS, não foram verificadas reduções nos biofilmes de *C. albicans* e SARM, somente no de *S. mutans* (1,70 $\log_{10}$). Já a aPDT mediada pela CUR em nanopartículas catiônicas promoveu reduções significativas somente para *C. albicans* e *S. mutans*, mas não para SARM. Apesar desses valores de reduções sugerirem maior eficácia da aPDT mediada pela CUR livre contra os biofilmes, é importante ressaltar que a concentração da CUR livre utilizada (1200 μM) foi 4,6 vezes maior que a CUR em nanopartículas, uma vez que concentrações menores de CUR livre não demonstraram ação fotodinâmica antimicrobiana no estudo piloto prévio. Além disso, a ausência de ação antimicrobiana fotodinâmica das nanopartículas aniônicas pode ser atribuída a sua carga negativa semelhante a da matrix do biofilme, o que geraria repulsão entre as nanopartículas e seu alvo, reduzindo sua interação com o biofilme e eficácia, além da lenta liberação da CUR das nanopartículas.

Nos biofilmes mistos formados por duas espécies (*C. albicans* + *S. mutans*, *C. albicans* + SARM e *S. mutans* + SARM), a aPDT mediada pela CUR livre demonstrou

reduções de até 2,86 log_{10} (*S. mutans* quando associado a SARM), sendo que o biofilme *C. albicans* + MRSA foi mais susceptível (reduções de 1,39 e 2,06 log_{10}, respectivamente) do que os demais, os quais não mostraram redução de *S. mutans* (para *C. albicans* + *S. mutans*) e nem de SARM (para *S. mutans* e SARM). Quando a aPDT foi realizada com nanopartículas de CUR aniônicas, reduções de até 1,37 log_{10} foram observadas (*C. albicans* quando associada a SARM) e o biofilme bacteriano apresentou menor susceptibilidade (ausência de redução para ambas espécies) enquanto que o biofilme de *S. mutans* + *C. albicans* mostrou maior susceptibilidade (redução de ambas espécies). Já quando a CUR em nanopartículas catiônicas foi utilizada como FS, reduções de até 4,11 log_{10} foram observadas (para *S. mutans* quando cultivado com SARM), sendo que o biofilme bacteriano foi mais susceptível e o biofilme de *C. albicans* + SARM foi menos susceptível (ausência de redução significativa para SARM).

Nos biofilmes formados pelas três espécies, a aPDT mediada pela CUR livre demonstrou reduções de 1,05; 2,41 e 0,90 log_{10} para *S. mutans*, *C. albicans* e SARM, respectivamente. Por outro lado, a CUR em nanopartícula aniônica associada a luz azul não resultou em redução de viabilidade das espécies avaliadas quando comparada com o grupo controle. Já para as nanopartículas catiônicas, reduções significativas de até 5,05 log_{10} foram observadas tanto para a aPDT como para os grupos tratados somente com as nanopartículas catiônicas com ou sem CUR na ausência de luz, indicando citotoxicidade dessas nanopartículas como verificado para as culturas planctônicas. Adicionalmente, a lavagem dos FSs previamente a aplicação da luz reduziu a viabilidade do biofilme em 1 a 2 log_{10} em relação ao biofilme não lavado. As imagens de microscopia confocal também mostraram visualmente menor intensidade de fluorescência para as amostras lavadas, porém sem redução da espessura dos biofilmes, sugerindo que a lavagem reduz a captura do FS pelo biofilme. Por fim, o teste de citotoxicidade confirmou a toxicidade das nanopartículas catiônicas, atribuída a presença de CTAB nessas amostras, assim como a do DMSO utilizado para solubilizar a CUR livre. Porém, as nanopartículas aniônicas não foram tóxicas às células de queratinócitos orais, o que demonstrou que o encapsulamento da CUR nas nanopartículas aniônicas eliminou a citotoxicidade do solvente orgânico utilizado para solubilizar a CUR.

Em continuidade a esses achados, o artigo apresentado no terceiro capítulo[103] avaliou a ação fotodinâmica antimicrobiana das nanopartículas de CUR em um modelo de candidíase bucal em camundongos. Esse modelo animal, primeiramente descrito por Takakura et al. em 2003[124], mimetiza a candidíase pseudomembranosa de humanos, com lesões brancas nas língua dos camundongos, e requer a imunossupressão dos animais e administração de

antibiótico durante todo o período experimental, além da inoculação de *C. albicans*. Posteriormente, esse protocolo de infecção foi estendido[104] para aumentar o período de infecção e realizar aplicações consecutivas da aPDT. Os resultados obtidos com a síntese e a caracterização das nanopartículas de CUR foram similares aos adquiridos no estudo anterior[101], o que demonstrou que a obtenção das nanopartículas foi reproduzível. Após cinco administrações da aPDT realizada em dias consecutivos, a aPDT mediada pela CUR livre e pela CUR em nanopartículas catiônicas reduziu a recuperação de *C. albicans* da língua dos animais em 1,11 e 0,74 log_{10}, ao passo que a aPDT mediada pela CUR em nanopartículas aniônicas não promoveu redução fúngica. Entretanto, as maiores reduções foram verificadas no grupos de animais tratados com nistatina uma vez (com anestesia, semelhante à aPDT) e quatro vezes ao dia (sem anestesia, simulando uso clínico) também por 5 dias consecutivos, equivalentes a 2,57 e 1,58 log_{10}. A anestesia do animal permite que o antifúngico permaneça mais tempo em contato com o tecido infectado, o que pode aumentar a ação antimicrobiana. Não foi verificada diferença significativa entre os grupos de animais tratados com a aPDT mediada pela CUR livre e com a nistatina quatro vezes ao dia, o que sugere um grande potencial promissor da aPDT, uma vez que esta foi realizada somente uma vez ao dia e sua ação antimicrobiana ocorre somente durante a irradiação, uma vez que as espécies reativas de oxigênio têm um curto período de vida de microsegundos[89]. Semelhante ao observado no estudo anterior, as nanopartículas catiônicas de CUR na ausência de luz também promoveram redução fúngica (0,44 log_{10}).

Os resultados da análise histopatológica demonstraram alteração das papilas filiformes, presença da forma filamentosa de *C. albicans* na camada de queratina com invasão no epitélio e poucas células inflamatórias na lamina própria da mucosa lingual. A quantidade de células fúngicas foi visualmente menor nos grupos de animais tratados com nistatina e aPDT com CUR livre. Esses achados foram semelhantes tanto para os animais eutanasiados 24 h após o término dos tratamentos como para os eutanasiados sete dias após os tratamentos, o que sugere que a condição de imunossupressão dos animais não permitiu melhora da condição patológica após o fim dos tratamentos.

Um outro aspecto original desse estudo foi a avaliação da imunoexpressão de citoqueratinas. A indução de candidíase bucal nos animais aumentou a imunomarcação das citoqueratinas 13 e 14 do epitélio, o que pode ser considerada uma resposta do epitélio frente a infecção fúngica. Um achado interessante foi a menor imunomarcação observada para os animais tratados com a aPDT mediada pela CUR livre, mais próxima aos animais controle sem infecção. Isso sugere que, além da ação antimicrobiana, a aPDT pode ter contribuído para

regular a expressão dessas citoqueratinas. Surpreendentemente, nos animais submetidos à nistatina, apesar desses terem apresentado maior redução de *C. albicans*, a expressão de citoqueratinas 13 e 14 foi semelhante aos demais animais com a infecção bucal, o que sugere que o antifúngico não foi efetivo para reoganizar o citoesqueleto epitelial. De maneira semelhante, o tratamento com CUR em nanopartículas catiônicas, apesar de ter reduzido a recuperação fúngica, resultou em imunoexpressão de citoqueratinas semelhante aos demais animais com candidíase bucal, o que pode ser atribuído a ação citotóxica do CTAB verificado no estudo in vitro prévio[101].

Para avaliar a segurança das aplicações consecutivas da aPDT, o método de marcação fluorescente de "*nicks*" por 2´-deoxiuridina,5´-trifosfato (dUTP) e deoxinucleotidil terminal transferase (TUNEL) foi realizado para verificar possíveis danos ao DNA das células do hospedeiro. Não foram observados danos ao DNA 24 h após os tratamentos, porém houve aumento de células com dano ao DNA após 7 dias nos grupos com maior quantidade de fungos no tecido, o que sugere que tal injúria é consequência da presença de *C. albicans*.

No quarto capítulo desta obra[106], foi explorado o potencial da aPDT na inativação de patógenos bucais num biofilme polimicrobiano. Um outro FS, ftalocianina de cloro e alumínio (FcClAl), em outro sistema de liberação de fármacos, nanoemulsão catiônica (cNE), foi combinado com luz vermelha (~660 nm) para a aPDT contra um biofilme misto in vitro formado por *C. albicans*, *C. glabrata* e *S. mutans*. Além das espécies de *Candida*, que são o principal fator etiológico da candidíase bucal, como a estomatite protética[28], espécies bacterianas orais também colonizam as próteses desses pacientes, como *S. mutans*[40,41], que, quando associado com *C. albicans*, apresenta maior virulência, como maior biomassa, aumento da expressão de quorum sensing[125] e maior severidade de lesões de cárie[126]. Foi verificado que a aPDT, mediada pela cNE-FcClAl a 31,8 μM e LED vermelho a 39,3 J/cm^2, resultou em redução da viabilidade do biofilme, com maior inativação de *S. mutans* (2,24 $\log_{10}$), seguido de *C. glabrata* (1,39 $\log_{10}$) e *C. albicans* (1,30 $\log_{10}$) e redução da atividade metabólica do biofilme de 53,7%.

Porém, os resultados dessa investigação também demonstraram que a biomassa do biofilme não foi afetada, sugerindo ausência de ação da aPDT na estrutura física do biofilme, apesar da redução de viabilidade e da captura do FS pelas células do biofilme, conforme observado em microscopia confocal. Essa ausência de efeito da aPDT na estrutura do biofilme seria justificada pela maior biomassa e matriz extracelular sintetizada pelos micro-organismos em biofilmes polimicrobianos em relação aos biofilmes monoespécies[125,126]. Além disso, os resultados desse estudo também mostraram que diferentes concentrações do FS e maior dose

de luz não promoveram maior fotoinativação, de maneira que uma relação dose-dependente de inativação não foi verificada, possivelmente devido ao uso de uma concentração muito baixa do FS (16 μM), incapaz de fotosensibilizar as células do biofilme, e de uma concentração muito elevada (68,8 μM), que poderia promover agregação do FS e redução da eficácia fotodinâmica[127], mesmo associada a uma maior dose de luz (78,63 J/cm^2) que, apesar do longo tempo de irradiação (1 hora), por si só, não demonstrou efeito antimicrobiano.

Os resultados com a aPDT demonstram que, apesar de haver inativação das células microbianas, a susceptibilidade do biofilme à aPDT é bem menor quando comparada com a das culturas planctônicas. A barreira formada pela matriz do biofilme protege as células microbianas em seu interior, de maneira que agentes e/ou abordagens antimicrobianas, como a aPDT, acabam por apresentar uma ação superficial, sem atingir as células das camadas mais profundas do biofilme[128,129]. Portanto, no quinto capítulo desta obra[112], a SDT foi avaliada contra biofilme de *C. albicans* com o intuito de se atingir as camadas mais internas do biofilme com o uso do ultrassom e, assim, potencializar a inativação microbiana. Inicialmente, foram selecionados parâmetros do ultrassom (50% de ciclo de trabalho e densidade de potência de 2,5 W/cm^2, equivalente a 5 min) que não promovessem inativação microbiana na ausência do SS. Para as culturas planctônicas, quando o PDZ foi associado ao ultrassom, foram observadas reduções de 4,35 $\log_{10}$ até completa inativação fúngica. A SDT mediada pela rosa bengala resultou em redução fúngica de 5,01 $\log_{10}$ até completa inativação. Já a aPDT mediada pelo PDZ e pela rosa bengala demonstrou reduções de 5,23 e 5,24 $\log_{10}$, respectivamente, até completa inativação.

Quando biofilmes foram avaliados, a aplicação isolada da aPDT e SDT não promoveu diminuição de viabilidade fúngica, somente da biomassa total. A aPDT mediada pelo PDZ e pela rosa bengala reduziu a biomassa total do biofilme em até 30,9% e 35,2%, respectivamente, enquanto que a SDT reduziu a biomassa em até 53,4% somente quando a rosa bengala foi utilizada como SS. A inativação da viabilidade do biofilme foi verificada somente quando a SDT foi aplicada simultaneamente com a aPDT (aplicação de luz e ultrassom simultânea após incubação com o SS), com reduções de até 3,39 e 1,91 $\log_{10}$ com a utilização do PDZ e rosa bengala, respectivamente. A combinação da SDT e da aPDT também promoveu maior redução de biomassa total do biofilme quando comparada com as terapias isoladas, de até 75,5% e 73% com o PDZ e rosa bengala, respectivamente. Imagens de microscopias óptica e de fluorescência mostraram que a associação de SDT e aPDT, tanto para o PDZ quando para a rosa bengala, diminuiu a espessura do biofilme, a presença de formas filamentosas e aumentou o número de células mortas (marcadas pelo azul de Tripan).

A maior eficácia das terapias combinadas foi atribuída a um possível sinergismo entre elas, com maior difusão do SS no biofilme e sensibilização das células por ação do ultrassom (sonoporação) e maior exposição à luz com a circulação de micro-organismos promovida pelo ultrassom. Adicionalmente, os resultados mais efetivos obtidos com o PDZ quando comparado com a rosa bengala foram atribuídos às diferenças entre os SSs e a utilização de um fonte de luz com comprimento de onda mais específico para o PDZ.

Como a matriz do biofilme atua como uma barreira protetora às células microbianas, abordagens que visam desestruturar e/ou atuar nos componentes da matriz podem ser uma estratégia promissora no tratamento de infecções causadas por biofilmes. Assim, no sexto capítulo desta obra[119], o efeito da NAC em biofilmes de *C. albicans* susceptível e resistente a fluconazol foi avaliado. A concentração inibitória mínima da NAC encontrada (25 mg/mL) foi igual para ambas as cepas, um achado importante na atual era de resistência microbiana. Concentrações maiores e/ou iguais à CIM inibiram a formação de biofilme em até 2,77 $\log_{10}$ para viabilidade e em até 88,7% da biomassa e reduziram biofilmes maduros em até 2,30 $\log_{10}$ para viabilidade e em até 73,69% da biomassa. Entretanto, concentração da NAC menor que a CIM aumentou a viabilidade fúngica no biofilme em até 0,73 $\log_{10}$, resultado esse que sugere cautela no uso da NAC devido à possibilidade de se ter um resultado oposto ao efeito antimicrobiano esperado. Esse efeito oposto pode ser justificado pela NAC ser precursora da glutationa, um metabólito essencial para *C. albicans*[130]. Logo, em baixa concentração, a NAC poderia prover glutationa para *C. albicans*.

A ação da NAC na matriz dos biofilmes foi marcadamente nos componentes solúveis da matriz, com redução de até 2.696,15 μg/mL dos polissacarídeo e de até 1.008,73 ηg/μL do eDNA de ambas as cepas, além de diminuir as proteínas solúveis do biofilme da cepa susceptível em até 95.62 μg/mL. Esses resultados bioquímicos foram confirmados também pela microscopia confocal, a qual mostrou redução da espessura e da intensidade de fluorescência dos biofilmes tratados com NAC para a maioria dos fluorocromos avaliados. Esses resultados confirmam que os componentes insolúveis da matriz são menos susceptíveis a abordagens antibiofilmes. Adicionalmente, foi observado sinergismo entre a NAC e a caspofungina em culturas planctônicas de ambas as cepas, o que pode ser justificado pela semelhança do mecanismo de ação dos dois medicamentos, uma vez que ambos atuam nos polissacarídeos da parede fúngica. Entretanto, esse sinergismo não foi observado em biofilme, o que demonstra que a organização de *C. albicans* em biofilme altera a ação dos medicamentos associados.

Os resutados dos trabalhos apresentados nesta obra mostram que mais esforços precisam ser dispensados no desenvolvimento de abordagens antibiofilmes e no combate da resitência antimicrobiana, uma vez que esses estudos mostraram menor eficácia dessas modalidades terapêuticas em biofilmes (reduções menores que 3 log_{10}, com excessão da combinação da SDT com aPDT) do que em culturas planctônicas. Segundo a Sociedade de Microbiologia Americana, um método somente pode ser considerado antimicrobiano quando ele promove redução do crescimento microbiano maior que 3 log_{10}[131]. Portanto, apesar desses métodos mostrarem ação antibiofilme, a eficácia dessas abordagens precisa ser melhorada antes de avaliações clínicas em humanos serem realizadas. A combinação de terapias com alvos tanto na célula microbiana como na matriz do biofilme, o uso de nanosistemas de liberação de fármacos ativados por estímulos externos (como luz, pH, temperatura, etc.) e a utilização de modelos animais de estomatite protética mais semelhantes às condições clínicas em humanos podem ajudar a estabeler protocolos terapêuticos mais eficazes para serem posteriormente avaliados em ensaios clínicos.

5 CONCLUSÃO

Os trabalhos que compõem esta obra demonstraram que métodos alternativos aos tratamentos antimicrobianos convencionais, como nanopartículas de TiO_2:Ag, aPDT mediada por FS veiculados em nanosistemas de liberação de fármacos, SDT e NAC apresentaram efeito antibacteriano e/ou antifúngico maior em culturas planctônicas do que em biofilmes de micro-organismos patogênicos, inclusive de cepas resistentes. A avaliação in vivo da aPDT demonstrou segurança em sua utilização, devido ausência de efeitos adversos no tecido do hospedeiro. Somente a combinação da SDT com aPDT foi eficaz na redução da viabilidade do biofilme fúngico. A NAC mostrou ação fungistática, inibiu a formação de biofilmes, reduziu biofilmes maduros e os componentes solúves da matriz e mostrou sinergismo com a caspofungina em culturas planctônicas. Esses estudos direcionam rumos para o desenvolvimento de tratamentos mais efetivos contra infecções causadas por biofilmes e por cepas resistentes aos antimicrobianos convencionais.

REFERÊNCIAS·

1. Colombo APV, Tanner ACR. The Role of Bacterial Biofilms in Dental Caries and Periodontal and Peri-implant Diseases: A Historical Perspective. J Dent Res. 2019; 98(4): 373-85. doi: 10.1177/0022034519830686.

2. Costerton JW, Cheng KJ, Geesey GG, Ladd TI, Nickel NC, Dasgupta M, et al. Bacterial biofilms in nature and disease. Ann Rev Microbiol. 1987; 41: 435-64.

3. Hall-Stoodley L, Costerton JW, Stoodley P. Bacterial biofilms: from the natural environment to infectious diseases. Nat Rev Microbiol. 2004; 2(2): 95-108.

4. Socransky SS, Haffajee AD. Dental biofilms: difficult therapeutic targets. Periodontol 2000. 2002; 28: 12-55.

5. Rosebury T. The nature and significance of infection in periodontal disease. Oral Surg Oral Med Oral Pathol. 1947; 33(9): 658-65.

6. Loesche WJ. Clinical and microbiological aspects of chemotherapeutic agents used according to the specific plaque hypothesis. J Dent Res. 1979; 58(12): 2404-12.

7. Marsh PD. Microbial ecology of dental plaque and its significance in health and disease. Adv Dent Res. 1994; 8: 263-71.

8. Marsh PD. Dental plaque: biological significance of a biofilm and community life-style. J Clin Periodontol. 2005; 32(6): 7S-15S.

9. Paster BJ, Boches SK, Galvin JL, Ericson RE, Lau CN, Levanos VA, et al. Bacterial diversity in human subgingival plaque. J Bacteriol. 2001; 183(12): 3770-83.

10. Dewhirst FE, Chen T, Izard J, Paster BJ, Tanner AC, Yu WH, Lakshmanan A, et al. The human oral microbiome. Bacteriol. 2010; 192(19): 5002-17. doi: 10.1128/JB.00542-10.

11. Griffen AL, Beall CJ, Campbell JH, Firestone ND, Kumar PS, Yang ZK, et al. Distinct and complex bacterial profiles in human periodontitis and health revealed by 16S pyrosequencing. ISME J. 2012; 6(6):1176-85. doi: 10.1038/ismej.2011.191.

12. Simón-Soro A, Belda-Ferre P, Cabrera-Rubio R, Alcaraz LD, Mira A. A tissue-dependent hypothesis of dental caries. Caries Res. 2013; 47(6): 591-600. doi: 10.1159/000351663.

13. Negrini TC, Koo H, Arthur RA. *Candida*-Bacterial Biofilms and Host-Microbe Interactions in Oral Diseases. Adv Exp Med Biol. 2019; 1197: 119-41. doi:10.1007/978-3-030-28524-1_10.

14. O'Donnell LE, Millhouse E, Sherry L, Kean R, Malcolm J, Nile CJ, et al. Polymicrobial *Candida* biofilms: friends and foe in the oral cavity. FEMS Yeast Res. 2015; 15(7). pii: fov077. doi: 10.1093/femsyr/fov077.

· De acordo com o Guia de Trabalhos Acadêmicos da FOAr, adaptado das Normas Vancouver. Disponível no site da Biblioteca: http://www.foar.unesp.br/Home/Biblioteca/guia-de-normalizacao-atualizado.pdf

15. Ghannoum MA, Jurevic RJ, Mukherjee PK, Cui F, Sikaroodi M, Naqvi A, Gillevet PM. Characterization of the oral fungal microbiome (mycobiome) in healthy individuals. PLoS Pathog. 2010; 6(1): e1000713. doi: 10.1371/journal.ppat.1000713.

16. Darwazeh AM, Hammad MM, Al-Jamaei AA. The relationship between oral hygiene and oral colonization with *Candida* species in healthy adult subjects. Int J Dent Hygiene. 2010; 8: 128-33.

17. Dağistan S, Aktas AE, Caglayan F, Ayyildiz A, Bilge M. Differential diagnosis of denture-induced stomatitis, *Candida*, and their variations in patients using complete denture: a clinical and mycological study. Mycoses. 2009; 52(3): 266-71. doi: 10.1111/j.1439-0507.2008.01592.x.

18. Krasse B. The relationship between lactobacilli, *Candida* and streptococci and dental caries; examination of saliva and plaque material collected on the same occasion. Odontol Revy. 1954; 5: 241-61.

19. Koo H, Bowen WH. *Candida albicans* and *Streptococcus mutans*: a potential synergistic alliance to cause virulent tooth decay in children. Future Microbiol. 2014; 9: 1295-7. doi: 10.2217/fmb.14.92.

20. Canabarro A, Valle C, Farias MR, Santos FB, Lazera M, Wanke B. Association of subgingival colonization of *Candida albicans* and other yeasts with severity of chronic periodontitis. J Periodontal Res 2013; 48: 428-32. doi: 10.1111/jre.12022.

21. Sardi JC, Duque C, Mariano FS, Marques MR, Höfling JF, Gonçalves RB. Adhesion and invasion of *Candida albicans* from periodontal pockets of patients with chronic periodontitis and diabetes to gingival human fibroblasts. Med Mycol. 2012; 50: 43-9. doi: 10.3109/13693786.2011.586133.

22. Hammad MM, Darwazeh AM, Idrees MM. The effect of glycemic control on *Candida* colonization of the tongue and the subgingival plaque in patients with type II diabetes and periodontitis. Oral Surg Oral Med O 2013; 116: 321-6. doi: 10.1016/j.oooo.2013.05.013.

23. Mombelli A, Décaillet F. The characteristics of biofilms in peri-implant disease. J Clin Periodontol. 2011 Mar; 11: 203-13. doi: 10.1111/j.1600-051X.2010.01666.x.

24. Siqueira JF, Jr, Sen BH. Fungi in endodontic infections. Oral Surg Oral Med Oral Pathol Oral Radiol Endod. 2004; 97: 632-41.

25. Baumgartner JC, Watts CM, Xia T. Occurrence of *Candida albicans* in infections of endodontic origin. J Endod. 2000; 26: 695-8.

26. Peciuliene V, Reynaud AH, Balciuniene I, et al. Isolation of yeasts and enteric bacteria in root-filled teeth with chronic apical periodontitis. Int Endod J. 2001; 34: 429-34.

27. Budtz-Jørgensen E. Ecology of *Candida*-associated denture stomatitis. Microbial Ecology in Health and Disease. 2000; 12: 170-85. doi: 10.1080/089106000750051846

28. Coco BJ, Bagg J, Cross LJ, Jose A, Cross J, Ramage G. Mixed *Candida albicans* and *Candida glabrata* populations associated with the pathogenesis of denture stomatitis. Oral Microbiol Immunol. 2008; 23(5): 377-83. doi: 10.1111/j.1399-302X.2008.00439.x.

29. Sanitá PV, Pavarina AC, Giampaolo ET, Silva MM, Mima EG, Ribeiro DG, Vergani CE. *Candida* spp. prevalence in well controlled type 2 diabetic patients with denture stomatitis. Oral Surg Oral Med Oral Pathol Oral Radiol Endod. 2011; 111(6): 726-33. doi: 10.1016/j.tripleo.2011.02.033.

30. Hoffmann C, Dollive S, Grunberg S, Chen J, Li H, Wu GD, et al. Archaea and fungi of the human gut microbiome: correlations with diet and bacterial residents. PLoS One. 2013; 8(6): e66019. doi: 10.1371/journal.pone.0066019.

31. Findley K, Oh J, Yang J, Conlan S, Deming C, Meyer JA, et al. Topographic diversity of fungal and bacterial communities in human skin. Nature. 2013; 498(7454): 367-70. doi: 10.1038/nature12171.

32. Merenstein D, Hu H, Wang C, Hamilton P, Blackmon M, Chen H, et al. Colonization by *Candida* species of the oral and vaginal mucosa in HIV-infected and noninfected women. AIDS Res Hum Retroviruses. 2013; 29(1): 30-4. doi: 10.1089/AID.2012.0269.

33. Sudbery PE. Growth of *Candida albicans* hyphae. Nat Rev Microbiol. 2011; 9(10): 737-48. doi: 10.1038/nrmicro2636.

34. Moyes DL, Richardson JP, Naglik JR. *Candida albicans*-epithelial interactions and pathogenicity mechanisms: scratching the surface. Virulence. 2015; 6(4): 338-46. doi: 10.1080/21505594.2015.1012981.

35. Noble SM, Gianetti BA, Witchley JN. *Candida albicans* cell-type switching and functional plasticity in the mammalian host. Nat Rev Microbiol. 2017; 15(2): 96-108. doi: 10.1038/nrmicro.2016.157.

36. Newton AV. Denture sore mouth. A possible etiology. British Dent J. 1962; 112, 357-60.

37. Gendreau L, Loewy ZG. Epidemiology and etiology of denture stomatitis. J Prosthodont. 2011; 20(4): 251-60. https://doi. org/10.1111/j.1532-849X.2011.00698.x.

38. Soysa NS, Samaranayake LP, Ellepola AN. Diabetes mellitus as a contributory factor in oral candidosis. Diabet Med. 2006; 23(5): 455-9.

39. Samaranayake LP, Keung Leung W, Jin L. Oral mucosal fungal infections. Periodontol 2000. 2009; 49: 39-59. 10.1111/j.1600-0757.2008.00291.x.

40. Ribeiro DG, Pavarina AC, Dovigo LN, Machado AL, Giampaolo ET, Vergani CE. Prevalence of *Candida* spp. associated with bacteria species on complete dentures. Gerodontology. 2012; 29(3): 203-8. doi:10.1111/j.1741-2358.2011.00578.x.

41. Shi B, Wu T, McLean J, Edlund A, Young Y, He X, et al. The Denture-Associated Oral Microbiome in Health and Stomatitis. mSphere. 2016; 1(6): e00215-16. doi:10.1128/mSphere.00215-16

42. Campos MS, Marchini L, Bernardes LA, Paulino LC, Nobrega FG. Biofilm microbial communities of denture stomatitis. Oral Microbiol Immunol. 2008; 23(5): 419-24. doi: 10.1111/j.1399-302X.2008.00445.x.

43. Koopmans AS, Kippuw N, de Graaff J. Bacterial involvement in denture-induced stomatitis. J Dent Res. 1988; 67(9): 1246-50.

44. Kulak Y, Arikan A, Kazazoglu E. Existence of *Candida albicans* and microorganisms in denture stomatitis patients. J Oral Rehabil. 1997; 24(10): 788-90.

45. Worthington HV, Clarkson JE, Khalid T, Meyer S, McCabe M. Interventions for treating oral candidiasis for patients with cancer receiving treatment. Cochrane Database Syst Rev [Internet]. 2010 [acesso 2020 Abr 15]. Disponível em: https://www.cochranelibrary.com/cdsr/doi/10.1002/14651858.CD001972.pub4/full

46. Institute of Medicine (US) Forum on Microbial Threats. Fungal Diseases: An Emerging Threat to Human, Animal, and Plant Health: Workshop Summary. Washington (DC): National Academies Press (US); 2011. Workshop Overview. Disponível em: https://www.ncbi.nlm.nih.gov/sites/books/NBK83178/

47. Patuwo C, Young K, Lin M, Pardi V, Murata RM. The changing role of HIV-associated oral candidiasis in the era of HAART. J Calif Dent Assoc. 2015; 43(2): 87-92.

48. Thompson GR 3rd, Patel PK, Kirkpatrick WR, Westbrook SD, Berg D, Erlandsen J, et al. Oropharyngeal candidiasis in the era of antiretroviral therapy. Oral Surg Oral Med Oral Pathol Oral Radiol Endod. 2010; 109(4): 488-95. doi: 10.1016/j.tripleo.2009.11.026.

49. Ben-Ami R. Treatment of Invasive Candidiasis: A Narrative Review. J Fungi (Basel). 2018; 4(3). pii: E97. doi: 10.3390/jof4030097.

50. Nett JE, Andes DR. Antifungal Agents: Spectrum of Activity, Pharmacology, and Clinical Indications. Infect Dis Clin North Am. 2016; 30(1): 51-83. doi: 10.1016/j.idc.2015.10.012.

51. Vergani CE, Sanitá PV, Mima EG, Pavarina AC, Machado AL. Oral candidiasis: conventional and alternative treatment options. In: Contreras F, Fluentes P. Candidiasis: epidemiology, symptoms and treatment options. 1st ed. Hauppaugs: Nova Science Publishers; 2013. p. 85-116.

52. Maertens JA. History of the development of azole derivatives. Clin Microbiol Infect. 2004;10 Suppl 1:1-10.

53. Kontoyiannis DP. Antifungal Resistance: An Emerging Reality and A Global Challenge. J Infect Dis. 2017; 216 Suppl 3: S431-5. doi: 10.1093/infdis/jix179.

54. Theuretzbacher U, Outterson K, Engel A, Karlén A. The global preclinical antibacterial pipeline. Nat Rev Microbiol. 2019. doi: 10.1038/s41579-019-0288-0.

55. McEwen SA, Collignon PJ. Antimicrobial Resistance: a One Health Perspective. Microbiol Spectr. 2018; 6(2). doi: 10.1128/microbiolspec.ARBA-0009-2017.

56. White TC, Marr KA, Bowden RA. Clinical, cellular, and molecular factors that contribute to antifungal drug resistance. Clin Microbiol Rev. 1998; 11(2): 382-402.

57. Shapiro RS, Robbins N, Cowen LE. Regulatory circuitry governing fungal development, drug resistance, and disease. Microbiol Mol Biol Rev. 2011; 75(2): 213-67. doi: 10.1128/MMBR.00045-10.

58. Perlin DS, Rautemaa-Richardson R, Alastruey-Izquierdo A. The global problem of antifungal resistance: prevalence, mechanisms, and management. Lancet Infect Dis. 2017; 17(12): e383-92. doi: 10.1016/S1473-3099(17)30316-X.

59. Sanglard D. Emerging Threats in Antifungal-Resistant Fungal Pathogens. Front Med (Lausanne). 2016; 3: 11. doi: 10.3389/fmed.2016.00011.

60. Hachem R, Hanna H, Kontoyiannis D, Jiang Y, Raad I. The changing epidemiology of invasive candidiasis: *Candida glabrata* and *Candida krusei* as the leading causes of candidemia in hematologic malignancy. Cancer. 2008; 112(11): 2493-9. doi: 10.1002/cncr.23466.

61. Whaley SG, Berkow EL, Rybak JM, Nishimoto AT, Barker KS, Rogers PD. Azole Antifungal Resistance in *Candida albicans* and Emerging Non-*albicans Candida* Species. Front Microbiol. 2017; 7: 2173. doi: 10.3389/fmicb.2016.02173.

62. Friedman DZP, Schwartz IS. Emerging Fungal Infections: New Patients, New Patterns, and New Pathogens. J Fungi (Basel). 2019; 5(3). pii: E67. doi: 10.3390/jof5030067.

63. Satoh K, Makimura K, Hasumi Y, Nishiyama Y, Uchida K, Yamaguchi H. *Candida auris* sp. nov., a novel ascomycetous yeast isolated from the external ear canal of an inpatient in a Japanese hospital. Microbiol Immunol. 2009; 53(1): 41-4. doi: 10.1111/j.1348-0421.2008.00083.x. Erratum in: Microbiol Immunol. 201; 62(3): 205.

64. Brauner A, Fridman O, Gefen O, Balaban NQ. Distinguishing between resistance, tolerance and persistence to antibiotic treatment. Nat Rev Microbiol. 2016; 14(5): 320-30. doi: 10.1038/nrmicro.2016.34.

65. Finkel JS, Mitchell AP. Genetic control of *Candida albicans* biofilm development. Nat Rev Microbiol. 2011; 9(2): 109-18. doi: 10.1038/nrmicro2475.

66. Koo H, Allan RN, Howlin RP, Stoodley P, Hall-Stoodley L. Targeting microbial biofilms: current and prospective therapeutic strategies. Nat Rev Microbiol. 2017; 15(12): 740-55. doi: 10.1038/nrmicro.2017.99.

67. Zarnowski R, Westler WM, Lacmbouh GA, Marita JM, Bothe JR, Bernhardt J, et al. Novel entries in a fungal biofilm encyclopedia. mBio. 2014; 5(4): e01333-14. doi: 10.1128/mBio.01333-14.

68. Al-Fattani MA, Douglas LJ. Biofilm matrix of *Candida albicans* and *Candida tropicalis*: chemical composition and role in drug resistance. J Med Microbiol. 2006; 55(Pt 8): 999-1008.

69. Nett J, Lincoln L, Marchillo K, Massey R, Holoyda K, Hoff B, et al. Putative role of beta-1,3 glucans in *Candida albicans* biofilm resistance. Antimicrob Agents Chemother. 2007; 51(2): 510-20.

70. Mitchell KF, Zarnowski R, Sanchez H, Edward JA, Reinicke EL, Nett JE, et al. Community participation in biofilm matrix assembly and function. Proc Natl Acad Sci U S A. 2015; 112(13): 4092-7. doi: 10.1073/pnas.1421437112.

71. Song W, Ge S. Application of Antimicrobial Nanoparticles in Dentistry. Molecules. 2019; 24(6). pii: E1033. doi: 10.3390/molecules24061033.

72. Khezerlou A, Alizadeh-Sani M, Azizi-Lalabadi M, Ehsani A. Nanoparticles and their antimicrobial properties against pathogens including bacteria, fungi, parasites and viruses. Microb Pathog. 2018; 123: 505-26. doi: 10.1016/j.micpath.2018.08.008.

73. Chen CH, Lu TK. Development and Challenges of Antimicrobial Peptides for Therapeutic Applications. Antibiotics (Basel). 2020; 9(1). pii: E24. doi: 10.3390/antibiotics9010024.

74. Sierra JM, Fusté E, Rabanal F, Vinuesa T, Viñas M. An overview of antimicrobial peptides and the latest advances in their development. Expert Opin Biol Ther. 2017; 17(6): 663-76. doi: 10.1080/14712598.2017.1315402.

75. Sadgrove NJ, Jones GL. From Petri Dish to Patient: Bioavailability Estimation and Mechanism of Action for Antimicrobial and Immunomodulatory Natural Products. Front Microbiol. 2019; 10: 2470. doi: 10.3389/fmicb.2019.02470.

76. Kumar A, Khan F, Saikia D. Exploration of Medicinal Plants as Sources of Novel Anticandidal Drugs. Curr Top Med Chem. 2019; 19(28): 2579-92. doi: 10.2174/1568026619666191025155856.

77. Hu X, Huang YY, Wang Y, Wang X, Hamblin MR. Antimicrobial Photodynamic Therapy to Control Clinically Relevant Biofilm Infections. Front Microbiol. 2018; 9: 1299. doi: 10.3389/fmicb.2018.01299.

78. Qi M, Chi M, Sun X, Xie X, Weir MD, Oates TW, et al. Novel nanomaterial-based antibacterial photodynamic therapies to combat oral bacterial biofilms and infectious diseases. Int J Nanomedicine. 2019; 14: 6937-56. doi: 10.2147/IJN.S212807.

79. Shi X, Zhang CY, Gao J, Wang Z. Recent advances in photodynamic therapy for cancer and infectious diseases. Wiley Interdiscip Rev Nanomed Nanobiotechnol. 2019; 11(5): e1560. doi: 10.1002/wnan.1560.

80. Eleraky NE, Allam A, Hassan SB, Omar MM. Nanomedicine Fight against Antibacterial Resistance: An Overview of the Recent Pharmaceutical Innovations. Pharmaceutics. 2020; 12(2). pii: E142. doi: 10.3390/pharmaceutics12020142.

81. André RS, Zamperini CA, Mima EG, Longo VM, Albuquerque AR, Sambrano JR, et al. Antimicrobial activity of TiO_2:Ag nanocrystalline heterostructures: Experimental and theoretical insights. Chemical Physics. 2015; 459: 87-95. http://dx.doi.org/10.1016/j.chemphys.2015.07.020

82. Liqiang J, Xiaojun S, Weimin C, Zili X, Yaoguo D, Honggang F. The preparation and characterization of nanoparticle TiO_2/Ti films and their photocatalytic activity. Journal of Physics and Chemistry of Solids. 2003; 64(4): 615-23. https://doi.org/10.1016/S0022-3697(02)00362-1

83. Nakata K, Fujishima A. TiO_2 photocatalysis: Design and applications. J Photochem Photobiol C: Photochem Reviews. 2012; 13(3): 169-89. https://doi.org/10.1016/j.jphotochemrev.2012.06.001.

84. Kim JS, Kuk E, Yu KN, Kim JH, Park SJ, Lee HJ, et al. Antimicrobial effects of silver nanoparticles. Nanomedicine. 2007; 3(1): 95-101. Erratum in: Nanomedicine. 2014; 10(5): e1119.

85. Mima EG, Pavarina AC, Dovigo LN, Vergani CE, Costa CA, Kurachi C, et al. Susceptibility of *Candida albicans* to photodynamic therapy in a murine model of oral candidosis. Oral Surg Oral Med Oral Pathol Oral Radiol Endod. 2010; 109(3): 392-401. doi: 10.1016/j.tripleo.2009.10.006.

86. Mima EG, Pavarina AC, Silva MM, Ribeiro DG, Vergani CE, Kurachi C, et al. Denture stomatitis treated with photodynamic therapy: five cases. Oral Surg Oral Med Oral Pathol Oral Radiol Endod. 2011; 112(5): 602-8. doi: 10.1016/j.tripleo.2011.05.019.

87. Mima EG, Vergani CE, Machado AL, Massucato EM, Colombo AL, Bagnato VS, et al. Comparison of Photodynamic Therapy versus conventional antifungal therapy for the treatment of denture stomatitis: a randomized clinical trial. Clin Microbiol Infect. 2012; 18(10): E380-8. doi: 10.1111/j.1469-0691.2012.03933.x.

88. Agostinis P, Berg K, Cengel KA, Foster TH, Girotti AW, Gollnick SO, et al. Photodynamic therapy of cancer: an update. CA Cancer J Clin. 2011; 61(4): 250-81. doi: 10.3322/caac.20114.

89. Soukos NS, Goodson JM. Photodynamic therapy in the control of oral biofilms. Periodontol 2000. 2011; 55(1): 143-66. doi: 10.1111/j.1600-0757.2010.00346.x.

90. Fleming A. On the Antibacterial Action of Cultures of a Penicillium, with Special Reference to their Use in the Isolation of B. Influenzæ. Br J Exp Pathol. 1929; 10(3): 226-36.

91. Hamblin MR, Abrahamse H. Oxygen-Independent Antimicrobial Photoinactivation: Type III Photochemical Mechanism? Antibiotics (Basel). 2020; 9(2). pii: E53. doi: 10.3390/antibiotics9020053.

92. Abrahamse H, Hamblin MR. New photosensitizers for photodynamic therapy. Biochem J. 2016; 473(4): 347-64. doi: 10.1042/BJ20150942

93. Hussain Z, Thu HE, Amjad MW, Hussain F, Ahmed TA, Khan S. Exploring recent developments to improve antioxidant, anti-inflammatory and antimicrobial efficacy of curcumin: A review of new trends and future perspectives. Mater Sci Eng C Mater Biol Appl. 2017; 77: 1316-26. doi: 10.1016/j.msec.2017.03.226.

94. Dovigo LN, Pavarina AC, Ribeiro AP, Brunetti IL, Costa CA, Jacomassi DP, et al. Investigation of the photodynamic effects of curcumin against *Candida albicans*. Photochem Photobiol. 2011; 87(4): 895-903. doi: 10.1111/j.1751-1097.2011.00937.x.

95. Dovigo LN, Pavarina AC, Carmello JC, Machado AL, Brunetti IL, Bagnato VS. Susceptibility of clinical isolates of *Candida* to photodynamic effects of curcumin. Lasers Surg Med. 2011; 43(9): 927-34. doi: 10.1002/lsm.21110.

96. Ribeiro AP, Pavarina AC, Dovigo LN, Brunetti IL, Bagnato VS, Vergani CE, et al. Phototoxic effect of curcumin on methicillin-resistant *Staphylococcus aureus* and L929 fibroblasts. Lasers Med Sci. 2013; 28(2): 391-8. doi: 10.1007/s10103-012-1064-9.

97. Quishida CC, De Oliveira Mima EG, Jorge JH, Vergani CE, Bagnato VS, Pavarina AC. Photodynamic inactivation of a multispecies biofilm using curcumin and LED light. Lasers Med Sci. 2016; 31(5): 997-1009. doi: 10.1007/s10103-016-1942-7.

98. Dovigo LN, Carmello JC, de Souza Costa CA, Vergani CE, Brunetti IL, Bagnato VS, et al. Curcumin-mediated photodynamic inactivation of *Candida albicans* in a murine model of oral candidiasis. Med Mycol. 2013; 51(3): 243-51. doi: 10.3109/13693786.2012.714081.

99. Flora G, Gupta D, Tiwari A. Nanocurcumin: a promising therapeutic advancement over native curcumin. Crit Rev Ther Drug Carrier Syst. 2013; 30(4): 331-68.

100. Hussain Z, Thu HE, Ng SF, Khan S, Katas H. Nanoencapsulation, an efficient and promising approach to maximize wound healing efficacy of curcumin: A review of new trends and state-of-the-art. Colloids Surf B Biointerfaces. 2017; 150: 223-41. doi: 10.1016/j.colsurfb.2016.11.036. Epub 2016 Nov 30.

101. Trigo Gutierrez JK, Zanatta GC, Ortega ALM, Balastegui MIC, Sanitá PV, Pavarina AC, et al. Encapsulation of curcumin in polymeric nanoparticles for antimicrobial Photodynamic Therapy. PLoS One. 2017; 12(11): e0187418. doi: 10.1371/journal.pone.0187418.

102. Gaumet M, Vargas A, Gurny R, Delie F. Nanoparticles for drug delivery: the need for precision in reporting particle size parameters. Eur J Pharm Biopharm. 2008; 69(1): 1-9.

103. Sakima VT, Barbugli PA, Cerri PS, Chorilli M, Carmello JC, Pavarina AC, et al. Antimicrobial Photodynamic Therapy Mediated by Curcumin-Loaded Polymeric Nanoparticles in a Murine Model of Oral Candidiasis. Molecules. 2018; 23(8). pii: E2075. doi: 10.3390/molecules23082075.

104. Carmello JC, Alves F, G Basso F, de Souza Costa CA, Bagnato VS, Mima EG, et al. Treatment of Oral Candidiasis Using Photodithazine®- Mediated Photodynamic Therapy In Vivo. PLoS One. 2016; 11(6): e0156947. doi: 10.1371/journal.pone.0156947.

105. Rao RS, Patil S, Ganavi BS. Oral cytokeratins in health and disease. J Contemp Dent Pract. 2014; 15(1): 127-36.

106. Trigo-Gutierrez JK, Sanitá PV, Tedesco AC, Pavarina AC, Mima EGO. Effect of Chloroaluminium phthalocyanine in cationic nanoemulsion on photoinactivation of multispecies biofilm. Photodiagnosis Photodyn Ther. 2018; 24: 212-9. doi: 10.1016/j.pdpdt.2018.10.005.

107. Jaiswal M, Dudhe R, Sharma PK. Nanoemulsion: an advanced mode of drug delivery system. 3 Biotech. 2015; 5(2): 123-7. doi: 10.1007/s13205-014-0214-0.

108. Ribeiro AP, Andrade MC, da Silva Jde F, Jorge JH, Primo FL, Tedesco AC, et al. Photodynamic inactivation of planktonic cultures and biofilms of *Candida albicans* mediated by aluminum-chloride-phthalocyanine entrapped in nanoemulsions. Photochem Photobiol. 2013; 89(1): 111-9. doi: 10.1111/j.1751-1097.2012.01198.x.

109. Ribeiro AP, Andrade MC, Bagnato VS, Vergani CE, Primo FL, Tedesco AC, et al. Antimicrobial photodynamic therapy against pathogenic bacterial suspensions and biofilms using chloro-aluminum phthalocyanine encapsulated in nanoemulsions. Lasers Med Sci. 2015; 30(2): 549-59. doi: 10.1007/s10103-013-1354-x.

110. Carmello JC, Alves F, Ribeiro A, Basso FG, de Souza Costa CA, Tedesco AC, et al. In vivo photodynamic inactivation of *Candida albicans* using chloro-aluminum phthalocyanine. Oral Dis. 2016; 22(5): 415-22. doi: 10.1111/odi.12466.

111. Cabrini Carmello J, Alves F, Basso FG, de Souza Costa CA, Tedesco AC, Lucas Primo F, et al. Antimicrobial photodynamic therapy reduces adhesion capacity and biofilm formation of *Candida albicans* from induced oral candidiasis in mice. Photodiagnosis Photodyn Ther. 2019; 27: 402-7. doi: 10.1016/j.pdpdt.2019.06.010.

112. Alves F, Pavarina AC, Mima EGO, McHale AP, Callan JF. Antimicrobial sonodynamic and photodynamic therapies against *Candida albicans.* Biofouling. 2018; 34(4): 357-67. doi: 10.1080/08927014.2018.1439935.

113. Costley D, Nesbitt H, Ternan N, Dooley J, Huang YY, Hamblin MR, et al. Sonodynamic inactivation of Gram-positive and Gram-negative bacteria using a Rose Bengal-antimicrobial peptide conjugate. Int J Antimicrob Agents. 2017; 49(1): 31-6. doi: 10.1016/j.ijantimicag.2016.09.034.

114. Serpe L, Giuntini F. Sonodynamic antimicrobial chemotherapy: First steps towards a sound approach for microbe inactivation. J Photochem Photobiol B. 2015; 150: 44-9. doi: 10.1016/j.jphotobiol.2015.05.012.

115. Corsello S.M, Bittker J.A., Liu Z., Gould J., McCarren P., Hirschman J.E., et al. The Drug Repurposing Hub: a next-generation drug library and information resource. Nat. Med. 2017; 23(4): 405-8. doi: 10.1038/nm.4306.

116. Stey C, Steurer J, Bachmann S, Medici TC, Tramer MR. The effect of oral N-acetylcysteine in chronic bronchitis: a quantitative systematic review. Eur. Respir. J. 2000; 16: 253-62. doi: 10.1034 / j.1399-3003.2000.16b12.x.

117. Olofsson A.C., Hermansson M., Elwing H. N-acetyl-L-cysteine affects growth, extracellular polysaccharide production, and bacterial biofilm formation on solid surfaces. Appl. Environ. Microbiol. 2003; 69(8), 4814-22. doi: 10.1128 / AEM.69.8.4814-4822.2003.

118. Zhao T., and Liu Y. N-acetylcysteine inhibit biofilms produced by *Pseudomonas aeruginosa*. BMC Microbiol. 2010; 10: 140. doi: 10.1186/1471-2180-10-140.

119. Nunes TSBS, Rosa LM, Chacón YPV, Mima EG. Fungistatic Action of *N*-acetylcysteine on *Candida albicans* biofilms and its interaction with antifungal agents. Microorganism. 2020; 8, 980. doi:10.3390/microorganisms8070980

120. Moreira ML, Paris EC, Nascimento GS, Longo VM, Sambrano JR, Mastelaro VR, et al. Structural and optical properties of $CaTiO_3$ perovskite-based materials obtained by microwave-assisted hydrothermal synthesis: An experimental and theoretical insight. Acta Materialia. 2009; 57: 5174-85.

121. Wood DL, Tauc J. Weak absorption tails in amorphous semiconductors. Physical Review B. 1972; 5(8): 3144-51.

122. Farah S, Anderson DG, Langer R. Physical and mechanical properties of PLA, and their functions in widespread applications—A comprehensive review. Adv Drug Deliv Rev. 2016; 107: 367-92. https:// doi.org/10.1016/j.addr.2016.06.012.

123. Vauthier C, Bouchemal K. Methods for the preparation and manufacture of polymeric nanoparticles. Pharm Res. 2009; 26: 1025-58. https://doi.org/10.1007/s11095-008-9800-3.

124. Takakura N, Sato Y, Ishibashi H, Oshima H, Uchida K, Yamaguchi H, et al. A novel murine model of oral candidiasis with local symptoms characteristic of oral thrush. Microbiol Immunol. 2003; 47(5): 321-6.

125. Sztajer H, Szafranski SP, Tomasch J, Reck M, Nimtz M, Rohde M, et al. Cross-feeding and interkingdom communication in dual-species biofilms of *Streptococcus mutans* and *Candida albicans*. ISME J. 2014; 8(11): 2256-71. doi: 10.1038/ismej.2014.73.

126. Falsetta ML, Klein MI, Colonne PM, Scott-Anne K, Gregoire S, Pai CH, et al. Symbiotic relationship between *Streptococcus mutans* and *Candida albicans* synergizes virulence of plaque biofilms in vivo. Infect Immun. 2014 May;82(5):1968-81. doi: 10.1128/IAI.00087-14.

127. Ghanadzadeh A, Zeini A, Kashef A, Moghadam M. Concentration effect on the absorption spectra of oxazine1 and methylene blue in aqueous and alcoholic solutions. J M Liq. 2008; 138(1-3): 100-6. https://doi.org/10.1016/j.molliq.2007.09.005

128. Andrade MC, Ribeiro AP, Dovigo LN, Brunetti IL, Giampaolo ET, Bagnato VS, et al. Effect of different pre-irradiation times on curcumin-mediated photodynamic therapy against planktonic cultures and biofilms of *Candida* spp. Arch Oral Biol. 2013; 58(2): 200-10. doi: 10.1016/j.archoralbio.2012.10.011.

129. Zanin IC, Gonçalves RB, Junior AB, Hope CK, Pratten J. Susceptibility of *Streptococcus mutans* biofilms to photodynamic therapy: an in vitro study. J Antimicrob Chemother. 2005; 56(2): 324-30.

130. Baek YU, Kim YR, Yim HS, Kang SO. Disruption of gamma-glutamylcysteine synthetase results in absolute glutathione auxotrophy and apoptosis in *Candida albicans*. FEBS Lett. 2004; 556: 47-52. doi: 10.1016 / S0014-5793 (03) 01363-2.

131. Cieplik F, Tabenski L, Buchalla W, Maisch T. Antimicrobial photodynamic therapy for inactivation of biofilms formed by oral key pathogens. Front Microbiol. 2014; 5: 405. doi: 10.3389/fmicb.2014.00405.

ANEXO A – PATENTE

Processo de Obtenção de Nanopartículas Poliméricas Aniônicas e Catiônicas de Curcumina, Nanopartículas obtidas e Seus Usos

INSTITUTO NACIONAL DA PROPRIEDADE INDUSTRIAL

04/07/2016 870160033565 15:47

00.000.2.2.16.0137284.6

Pedido nacional de Invenção, Modelo de Utilidade, Certificado de Adição de Invenção e entrada na fase nacional do PCT

Número do Processo: BR 10 2016 015631 9

Dados do Depositante (71)

Depositante 1 de 1

Nome ou Razão Social: UNIVERSIDADE ESTADUAL PAULISTA JULIO DE MESQUITA FILHO
Tipo de Pessoa: Pessoa Jurídica
CPF/CNPJ: 48031918000124
Nacionalidade: Brasileira
Qualificação Jurídica: Instituição de Ensino e Pesquisa
Endereço: Rua Quirino de Andrade, 215
Cidade: São Paulo
Estado: SP
CEP: 01049-010
País: Brasil
Telefone: 11 5084-5330
Fax: 115084-5334
Email: tinoco@tinoco.com.br

Dados do Pedido

Natureza Patente: 10 - Patente de Invenção (PI)

Título da Invenção ou Modelo de Utilidade (54): PROCESSO DE OBTENÇÃO DE NANOPARTÍCULAS POLIMÉRICAS ANIÔNICAS E CATIÔNICAS DE CURCUMINA, NANOPARTÍCULAS OBTIDAS E SEUS USOS

Resumo: A presente invenção refere-se a um processo de obtenção de nanopartículas poliméricas (CUR-NP) aniônicas e catiônicas de curcumina, as quais são sintetizadas utilizando-se polímero poliácido lático (PLA) e sulfato de dextrana (DEX). Adicionalmente, a invenção se refere às CUR-NPs aniônicas e catiônicas obtidas e ao seu uso para o preparo de uma composição para aplicação em terapia antimicrobiana, associadas ou não à luz, em culturas de S. mutans, SARM e C. albicans, preferencialmente para o preparo de um medicamento para tratar a candidose bucal.

Figura a publicar: 2

Dados do Procurador

Procurador:

Nome ou Razão Social: Fabíola de Moraes Spiandorello Bueno

Numero OAB: 244141SP

Numero API:

CPF/CNPJ: 13521027813

Endereço: Rua Faustina Barbosa Stackfleth, 149, Parque Centenário

Cidade: Jundiaí

Estado: SP

CEP: 13214-773

Telefone: (11) 992340347

Fax:

Email: spianfm@terra.com.br

Dados do Inventor (72)

Inventor 1 de 5

Nome: EWERTON GARCIA DE OLIVEIRA MIMA
CPF: 29023609832
Nacionalidade: Brasileira
Qualificação Física: Professor do ensino superior
Endereço: Avenida Humaitá, nº 1640, Centro
Cidade: Araraquara
Estado: SP
CEP: 14801-903
País: BRASIL
Telefone: (11) 339 37904
Fax:
Email: auin@unesp.br

Inventor 2 de 5

Nome: PAULA ABOUD BARBUGLI
CPF: 22165448840
Nacionalidade: Brasileira
Qualificação Física: Servidor das demais carreiras da administração pública direta, autárquica e fundacional
Endereço: Avenida Humaitá, nº 1640, Centro
Cidade: Araraquara
Estado: SP
CEP: 14801-903
País: BRASIL
Telefone: (11) 339 37904
Fax:
Email: auin@unesp.br

Inventor 3 de 5

Nome: JEFFERSSON KRISHAN TRIGO GUTIERREZ
CPF: 23706405881
Nacionalidade: Boliviana
Qualificação Física: Odontólogo
Endereço: Avenida Humaitá, nº 1640, Centro
Cidade: Araraquara
Estado: SP
CEP: 14801-903
País: BRASIL
Telefone: (11) 339 37904
Fax:
Email: auin@unesp.br

Inventor 4 de 5

Nome: ANA CLÁUDIA PAVARINA
CPF: 12237866848
Nacionalidade: Brasileira
Qualificação Física: Professor do ensino superior
Endereço: Avenida Humaitá, nº 1640, Centro
Cidade: Araraquara
Estado: SP
CEP: 14801-903
País: BRASIL
Telefone: (11) 339 37904
Fax:
Email: auin@unesp.br

Inventor 5 de 5

Nome: MARLUS CHORILLI
CPF: 21539386864
Nacionalidade: Brasileira
Qualificação Física: Professor do ensino superior
Endereço: Rodovia Araraquara – Jaú, km 1, Campus Ville
Cidade: Araraquara
Estado: SP
CEP: 14801-902
País: BRASIL
Telefone: (11) 339 37904
Fax:
Email: auin@unesp.br

Documentos anexados

Tipo Anexo	Nome
Comprovante de pagamento de GRU 200	16AUIN023 - CURCUMINA - GRU.pdf
Procuração	PROCURACAO UNESP LEOPOLDO-FABIOLA 2016.pdf
Documento de Cessão	16AUIN023 - NANO CURCUMINA - TERMO CESSAO ASSINADO.pdf
Relatório Descritivo	16AUIN023 - CURCUMINA - RELATORIO DESCRITIVO.pdf
Reivindicação	16AUIN023 - CURCUMINA - REIVINDICACOES.pdf
Desenho	16AUIN023 - CURCUMINA - DESENHOS.pdf
Resumo	16AUIN023 - CURCUMINA - RESUMO.pdf

Acesso ao Patrimônio Genético

☑ Declaração Negativa de Acesso - Declaro que o objeto do presente pedido de patente de invenção não foi obtido em decorrência de acesso à amostra de componente do Patrimônio Genético Brasileiro, o acesso foi realizado antes de 30 de junho de 2000, ou não se aplica.

Declaração de veracidade

☑ Declaro, sob as penas da lei, que todas as informações acima prestadas são completas e verdadeiras.

Obrigado por acessar o Peticionamento Eletrônico

PETICIONAMENTO ELETRÔNICO

Este pedido foi enviado pelo sistema Peticionamento Eletrônico em 04/07/2016 às 15:47

BANCO DO BRASIL | 001-9 | **RECIBO DO SACADO**

Local de Pagamento
Pagável em qualquer Banco

Vencimento
Contra-apresentação

Cedente
INPI - Instituto Nacional da Propriedade Industrial

Agência/Código Cedente
2234-9/333.028-1

Data do Documento	*Nº. documento*	*Espécie doc.*	*Aceite*	*Data Proces.*
24/02/2016	1601372846	RC	N	24/02/2016

Nosso Número
00.000.2.2.16.0137284.6

Uso Banco	*Carteira*	*Espécie*	*Quantidade*	*Valor*
	18/027	R$		

(=)Valor Documento
R$ 70,00

Número: *NN Complementar:* *Peticionamento: Eletrônico*

Natureza: 10 - Patente de

Cod *Serviço* *Petição Vinculada* *RPI* *Valor*

200 - Pedido nacional de Invenção, Modelo de Utilidade, Certificado de Adição de Invenção e entrada na fase nacional do PCT - - *R$ 70,00*

(-)Desconto/Abatimento

(-) Outras deduções

(+)Mora/Multa

(+)Outros Acréscimos

OAB: 235031SP *Procurador: Leopoldo Campos Zuaneti*

(=)Valor Cobrado
R$ 70,00

Governo Federal - Guia de Recolhimento da União. GRU - Cobrança

Sacado
UNIVERSIDADE ESTADUAL PAULISTA JULIO DE MESQUITA FILHO
Rua Quirino de Andrade, 215, São Paulo, BR/SP, 01049-010
Sacador/Avalista

Corte na linha pontilhada

Autenticação mecânica - Controle Cedente

BANCO DO BRASIL | 001-9 | **00199.53637 10000.022169 01372.846210 8 00000000007000**

Local de Pagamento
Pagável em qualquer Banco

Vencimento
Contra-apresentação

Cedente
INPI - Instituto Nacional da Propriedade Industrial

Agência/Código Cedente
2234-9/333.028-1

Data do Documento	*Nº. documento*	*Espécie doc.*	*Aceite*	*Data Proces.*
24/02/2016	1601372846	RC	N	24/02/2016

Nosso Número
00.000.2.2.16.0137284.6

Uso Banco	*Carteira*	*Espécie*	*Quantidade*	*Valor*
	18/027	R$		

(=)Valor Documento
R$ 70,00

Instruções:
1. Valores expressos em reais.
2. Pagamento em cheque, anotar no verso o 'Nosso Número'.
3. Pagamento via SIAFI(OB-FATURA): Identificar na 'ob' o 'Nosso Número'.
4. Vencimento contra apresentação.

(-)Desconto/Abatimento

(-) Outras deduções

(+)Mora/Multa

(+)Outros Acréscimos

OAB: 235031SP *Procurador: Leopoldo Campos Zuaneti*

(=)Valor Cobrado
R$ 70,00

Governo Federal - Guia de Recolhimento da União. GRU - Cobrança

Sacado
UNIVERSIDADE ESTADUAL PAULISTA JULIO DE MESQUITA FILHO
Rua Quirino de Andrade, 215, São Paulo, BR/SP, 01049-010
Sacador/Avalista

Autenticação mecânica - Ficha de Compensação

Corte na linha pontilhada

- GRU ÚNICA: a GRU apresentada ao INPI, como comprovante da retribuição, deve ser única. Não utilize cópias desta GRU para outro pagamento.- PAGAMENTO: o pagamento da GRU deve ser providenciado no PRAZO ADMINISTRATIVO, regulamentado em lei ou Ato Normativo próprio.

FUNDACAO PARA O DESENVOLVIMENTO DA UNESP **Agência:** 0239 **Conta Corrente:** 43-002320-8

DETALHE DO COMPROMISSO

Convênio:	0033-0239-004900019792	**Conta de Débito:**	0239-000130027340
Tipo do Documento:	CNPJ	**CPF/CNPJ do Fornecedor:**	
Nome do Fornecedor:	000009853INPI - INST. NACIONAL		
No. compromisso banco:	1022071000100004	**No. compromisso cliente:**	137284/DS1 1011
Tipo de Pagamento:	BLQ Outros		
Código de Barras:	00199536371000002216901372846210800000000007000		
Valor Nominal:	70,00		
Desc./Abat.:	0,00	**Juros:**	0,00
Data de Vencimento:	08/03/2016		
Data de Pagamento:	08/03/2016		
Situação:	Efetivado	**No. Protocolo:**	PGTFORNB08032016900110369
No. Lista de Débito:			
Autenticação:			
		Valor a Pagar:	**70,00**
Tipo de Serviço:	Pagamento Fornecedor		
Complemento do Tipo de Serviço:			
Emitir Aviso:	Não emitir		

Central de Atendimento Santander Empresarial 4004-2125 (Regiões Metropolitanas) 0800 726 2125 (Demais Localidades) **SAC** 0800 762 7777 **Ouvidoria** 0800 726 0322

retornar imprimir

UNIVERSIDADE ESTADUAL PAULISTA "JÚLIO DE MESQUITA FILHO"
GABINETE DO REITOR

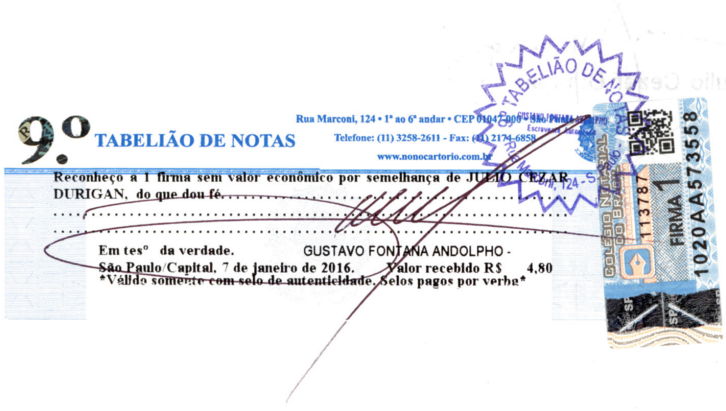
PROCURAÇÃO

Por este instrumento, a **UNIVERSIDADE ESTADUAL PAULISTA "JULIO DE MESQUITA FILHO"**, autarquia estadual de regime especial, criada pela Lei nº 952 de 30/01/1976, com sede na Rua Quirino de Andrade, nº 215, Centro, CEP 01049-010, São Paulo/SP, inscrita no CNPJ do MF sob o nº 48.031.918/0001-24, doravante designada simplesmente **UNESP**, neste ato representada por seu Magnífico Reitor, de acordo com o Art. 34 de seu Estatuto, Prof. Dr. **JÚLIO CEZAR DURIGAN**, brasileiro, casado, professor universitário, portador do RG nº 5.872.573-3 SSP/SP, inscrito no CPF/MF sob o nº 833.745.238-20, ou quem legalmente o substitua, nomeia e constitui seus procuradores, **1) LEOPOLDO CAMPOS ZUANETI**, brasileiro, advogado, devidamente inscrito na Ordem dos Advogados do Brasil Secção de São Paulo sob o número 235.031; e **2) FABÍOLA DE MORAES SPIANDORELLO**, brasileira, advogada, devidamente inscrita na Ordem dos Advogados do Brasil Secção de São Paulo, Subseção de Jundiaí sob o número 244.141, ambos lotados junto à Agência UNESP de Inovação, outorgando-lhes poderes para representá-la perante o Instituto Nacional da Propriedade Industrial – INPI, para o fim de requerer e processar direitos de propriedade intelectual, tais como patentes de invenção, de modelos de utilidade, desenhos industriais, registros de marcas de produto, de serviço, coletivas ou de certificação, de indicações geográficas, cultivares, direitos de autor, de programas de computador e mantê-los em vigor com amplos e ilimitados poderes para assinar petições, autorizações para cópia, termos de cessão de direitos, acordos de gestão e compartilhamento de propriedade intelectual, documentos diversos relacionados ao processo administrativo de proteção de direitos de propriedade industrial, incluindo, mas não se limitando, aos documentos já utilizados pelo INPI, bem como àqueles que vierem a ser adotados e utilizados para instrução processual de patentes, modelos de utilidades, marcas, desenhos industriais e programas de computador, pagar taxas, retribuições, impostos, fazer prova de uso das invenções patenteadas ou das marcas registradas, efetuar pagamentos e receber restituições, dando as respectivas quitações, apresentar oposições, recursos, réplicas, desistir, renunciar, anotar, averbar contratos de licença e transferências de tecnologia, elaborar notificações extrajudiciais, requerer prorrogação dos prazos de proteção, fazer declarações, opor, protestar, impugnar, recorrer, pedir reconsideração, manifestar-se sobre oposições e recursos, obter vista de processos, cumprir exigências, apresentar defesas escritas ou orais, desistir, replicar, transigir, receber, juntar e retirar documentos, requerer caducidade e contestar pedido de caducidade, requerer e contestar nulidade administrativa e licença compulsória, preencher qualquer tipo de formalidade, requerer anotação e averbação de cessão, alterações de nome e de sede, proceder à publicação de editais de chamamento para instruir, elaborar, firmar e acompanhar contratos de transferência de tecnologia e/ou licenciamento com exclusividade ou não, e praticar para o fim mencionado todos os atos necessários perante as autoridades administrativas competentes no Brasil em benefício da Outorgante.

Este instrumento é válido até 31 de janeiro de 2017.

São Paulo, 7 de janeiro de 2016.

Julio Cezar Durigan
Reitor


9.º TABELIÃO DE NOTAS
Rua Marconi, 124 • 1º ao 6º andar • CEP 01047-000 • São Paulo - SP
Telefone: (11) 3258-2611 - Fax: (11) 2174-6858
www.nonocartorio.com.br
Reconheço a 1 firma sem valor econômico por semelhança de JULIO CEZAR DURIGAN, do que dou fé.
Em tes° da verdade.
GUSTAVO FONTANA ANDOLPHO -
São Paulo/Capital, 7 de janeiro de 2016. Valor recebido R$ 4,80
Válido somente com selo de autenticidade. Selos pagos por verba
TABELIÃO DE NOTAS
COLÉGIO NOTARIAL DO BRASIL
113787
FIRMA 1
1020AA573558

UNIVERSIDADE ESTADUAL PAULISTA
"JÚLIO DE MESQUITA FILHO"
Reitoria

TERMO DE CESSÃO DE DIREITOS SOBRE PROPRIEDADE INTELECTUAL

Cedentes: 1. EWERTON GARCIA DE OLIVEIRA MIMA, brasileiro, solteiro, professor universitário, inscrito no CPF/MF sob o nº 290.236.098-32, portador do documento de identidade RG nº 30.611.169-X, SSP/SP, residente em Araraquara (SP), na Avenida Humaitá, 1640, Centro, CEP 14.801-903; **2. PAULA ABOUD BARBUGLI**, brasileira, casada, servidora pública, inscrita no CPF/MF sob o nº 221.654.488-40, portadora do documento de identidade RG nº 32.818.249-7, SSP/SP, residente em Araraquara (SP), na Avenida Humaitá, 1640, Centro, CEP 14.801-903; **3. JEFFERSSON KRISHAN TRIGO GUTIERREZ**, boliviano, solteiro, cirurgião dentista, inscrito no CPF/MF sob o nº 237.064.058-81, portador do documento de identidade RNE G018501-Q, CGPI/DIREX/DPF, residente em Araraquara (SP), Avenida Humaitá, 1640, Centro, CEP 14.801-903; **4. ANA CLÁUDIA PAVARINA**, brasileira, casada, professora universitária, inscrita no CPF/MF sob o nº 122.378.668-48, portadora do documento de identidade RG nº 19.599.025-0, SSP/SP, residente em Araraquara (SP), na Avenida Humaitá, 1640, Centro, CEP 14.801-903; **5. MARLUS CHORILLI**, brasileiro, casado, professor universitário, inscrito no CPF/MF sob o nº 215.393.868-64, portador do documento de identidade RG nº 28.837.112-4, SSP/SP, residente em Araraquara (SP), na Rodovia Araraquara – Jaú, km 1, Câmpus, CEP 14.801-902.

Cessionária: UNIVERSIDADE ESTADUAL PAULISTA "JÚLIO DE MESQUITA FILHO" - UNESP, autarquia estadual de regime especial, criada pela Lei n° 952 de 30.01.1976, devidamente inscrita no CNPJ/MF sob o nº 48.031.918/0001-24, com sede na Rua Quirino de Andrade, 215, Centro, São Paulo (SP), CEP 01.049-010.

Pelo presente instrumento, nesta e na melhor forma de direito, os Cedentes autorizam a Cessionária a depositar o pedido de patente intitulado **"PROCESSO DE OBTENÇÃO DE NANOPARTÍCULAS POLIMÉRICAS ANIÔNICAS E CATIÔNICAS DE CURCUMINA, NANOPARTÍCULAS OBTIDAS E SEUS USOS"** junto ao Instituto Nacional da Propriedade Industrial, cedendo todos os direitos patrimoniais a ele relativos na forma e para os fins do disposto na Lei 9.279 de 14.05.1996 e Lei 8.666 de 21.06.1993, Artigo 111, a título gratuito, sem qualquer restrição quanto à forma, tempo ou lugar, desde já ficando autorizadas quaisquer alterações que venham a ser consubstanciadas em futuras atualizações, modificações ou derivações tecnológicas.

Por ser a expressão da verdade, este documento é firmado na presença de duas testemunhas que também o assinam.

Araraquara, 20 de junho de 2016.

Cedentes:

EWERTON GARCIA DE OLIVEIRA MIMA

PAULA ABOUD BARBUGLI

JEFFERSSON KRISHAN TRIGO GUTIERREZ

ANA CLÁUDIA PAVARINA

MARLUS CHORILLI

Cessionária:

UNIVERSIDADE ESTADUAL PAULISTA "JÚLIO DE MESQUITA FILHO" – UNESP
LEOPOLDO C. ZUANETI
Assessor Jurídico
Agência Unesp de Inovação

Testemunhas:

1. Keyla Santos Bento
CPF/MF: 323.669.268-55

2. Fabíola de Moraes Spiandorello
CPF/MF: 135.210.278-13

Agência UNESP de Inovação
Rua Dr. Bento Teobaldo Ferraz, 271 - Bloco II - Barra Funda
CEP. 01.140-070, São Paulo - Estado de São Paulo - Brasil
Fone: +55 11 3393-7901 / 7903 /7904 - E-mail: auin@unesp.br

PROCESSO DE OBTENÇÃO DE NANOPARTÍCULAS POLIMÉRICAS ANIÔNICAS E CATIÔNICAS DE CURCUMINA, NANOPARTÍCULAS OBTIDAS E SEUS USOS

Campo da invenção:

[001] A presente invenção se aplica no campo da ciência médica e odontológica, de forma mais específica na área farmacêutica e faz referência a um processo de obtenção de nanopartículas poliméricas (CUR-NP) aniônicas e catiônicas de curcumina. Adicionalmente, a invenção se refere às CUR-NPs aniônicas e catiônicas obtidas e ao seu uso no preparo de uma composição para aplicação em terapia antimicrobiana, associadas ou não à luz, em culturas de *Streptococcus mutans*, *Staphylococcus aureus* resistente à meticilina (SARM) e *Candida albicans*, preferencialmente no preparo de um medicamento para tratar a candidose bucal.

Fundamentos da invenção:

[002] A candidose bucal é a infecção fúngica mais comum que acomete os humanos e cujo principal fator etiológico é o fungo do gênero *Candida*, sendo *C. albicans* a espécie mais prevalente e de maior virulência que vive como comensal em diversas regiões do organismo na maioria dos indivíduos saudáveis. No entanto, sob determinadas condições, esse microrganismo se transforma em um patógeno oportunista, podendo colonizar mucosas, invadir tecidos e causar infecções.

[003] Apesar das espécies fúngicas de *Candida* serem consideradas os principais patógenos no desenvolvimento da candidose bucal, as bactérias da microbiota também contribuem para a colonização e proliferação das espécies fúngicas na cavidade bucal.

[004] Ambos os microrganismos, bactérias e fungos, convivem em harmonia uns com os outros na cavidade bucal. Um dos colonizadores iniciais da cavidade bucal correspondem às espécies de *Streptococcus*, como *S. mutans* que é o principal agente etiológico da cárie dentária e apresenta reconhecidos fatores de virulência. Além das lesões de cáries, *S. mutans* tem sido associado a doenças sistêmicas como endocardite infecciosa aguda.

[005] O uso indiscriminado dos agentes antimicrobianos (antibióticos e antifúngicos) tem propiciado o desenvolvimento de cepas resistentes. Nesse contexto, a bactéria *S. aureus* é considerada um dos patógenos humanos de maior patogenicidade, e algumas cepas desse microrganismo, devido a alterações em sua parede celular, desenvolveram resistência a vários agentes antibacterianos, sendo denominadas cepas de *S. aureus* resistentes à meticilina (SARM).

[006] Considerado uma das principais causas de infecção hospitalar, o SARM tem sido apontado como um problema mundial de saúde pública. Aproximadamente 52% das infecções hospitalares em pacientes em unidades de terapia intensiva (UTI) são causadas por esse microrganismo.

[007] Devido às deficiências verificadas nos tratamentos atualmente disponíveis, alternativas antimicrobianas têm sido pesquisadas. Uma modalidade terapêutica promissora para a inativação de microrganismos é a Terapia Fotodinâmica Antimicrobiana (do inglês "*Antimicrobial Photodynamic Therapy*", ou aPDT), que utiliza a associação de um agente fotossensibilizador (FS) a uma fonte de luz de comprimento de onda adequado.

[008] A interação entre o FS e a luz na presença do oxigênio resulta na produção de espécies reativas tóxicas, principalmente o oxigênio singleto e radicais livres que promovem dano e morte celular. Todos esses produtos formados geram uma sequência de eventos oxidativos, os quais resultam na inativação de espécies microbianas bucais e não promove danos aos tecidos e às células do hospedeiro.

[009] Vários estudos *in vitro* demonstraram a eficácia da aPDT na inativação de diversos microrganismos, incluindo *S. mutans*, SARM e *C. albicans*. Entretanto, apesar desses resultados, alguns FS, como hematoporfirinas e corantes fenotiazínicos têm demonstrado baixa efetividade em promover inativação microbiana in vivo.

[010] A baixa efetividade da aPDT na inativação de *Candida* spp. pode ser justificada pelo fato de que as células fúngicas (eucariotas) são mais difíceis de serem fotoinativadas do que as bactérias (procariotas) devido ao seu maior tamanho celular, ao reduzido número de sítios de ação para o oxigênio singleto por unidade de volume de célula, além da presença de uma membrana nuclear nos fungos que atua como uma barreira adicional ao FS.

[011] Além disso, a presença da matriz polimérica extracelular que envolve as células organizadas em biofilme dificulta a penetração do FS. Ainda, para se alcançar a desinfecção de próteses dentárias colonizadas por *Candida* spp., além de elevadas concentrações de FS, são necessários longos tempos de pré-irradiação (incubação do microrganismos com o FS) e de iluminação. Portanto, mais estudos são necessários para se adequar esses parâmetros da

aPDT, com o intuito de tornar essa terapia mais viável clinicamente.

[012] Por essa razão, tendo em vista a necessidade de se aumentar a eficácia da aPDT, torna-se importante o desenvolvimento de pesquisas que avaliem FSs mais efetivos contra esses microrganismos.

[013] Neste contexto, a curcumina (CUR) tem mostrado um grande potencial de aplicação para fotoinativação microbiana, inclusive de biofilmes de *C. albicans* e culturas plactônicas de SARM.

[014] A CUR é um composto de baixo peso molecular isolado dos tubérculos da *Curcuma longa L.* e um dos componentes presentes no açafrão. Tem sido demonstrado que, isoladamente, a CUR já apresenta efeito antifúngico contra *C. albicans*, e estudos recentes verificaram que esse efeito é potencializado quando a CUR é utilizada como FS associada à luz.

[015] No entanto, a CUR não é hidrossolúvel, apresenta biodisponibilidade limitada e instabilidade (alta susceptibilidade à degradação fotolítica e hidrolítica).

[016] Adicionalmente, para veiculação da CUR tem sido utilizado solventes orgânicos, como dimetilsufóxido (DMSO), que apresentam toxicidade celular. Por isso, é importante a investigação de novos sistemas de veiculação com o intuito de aumentar a solubilidade e diminuir a degradação de FSs hidrofóbicos.

[017] Nanopartículas poliméricas são sistemas de liberação de fármacos muito estáveis e biocompatíveis, que incluem nanoesferas e nanocápsulas. Essas nanoestruturas, além de possibilitarem a estabilidade e a solubilização de

FSs hidrofóbicos em soluções aquosas, apresentam um potencial fotodinâmico para aplicação antimicrobiana. No entanto, os efeitos fotodinâmicos da CUR em nanoformulações contra culturas de *C. albicans* ainda não são conhecidos.

[018] Portanto, a presente invenção refere-se a um processo de obtenção de nanopartículas poliméricas (CUR-NP) aniônicas e catiônicas de curcumina para o preparo de uma composição para aplicação em terapia antimicrobiana, associadas ou não à luz, em culturas de *S. mutans*, SARM e *C. albicans*, preferencialmente no preparo de um medicamento para tratar a candidose bucal.

[019] Desse modo, o encapsulamento da curcumina elimina suas características desvantajosas, permitindo aplicação de suas propriedades terapêuticas na prática clínica. Além disso, o encapsulamento da curcumina em nanopartícula polimérica permite melhorar sua biodisponibilidade e soluciona os problemas de insolubilidade em água e degradação. Assim, é possível a utilização clínica da curcumina em seres vivos.

Estado da técnica:

[020] Alguns documentos do estado da técnica descrevem nanopartículas de curcumina.

[021] Em US2015283093 (A1) é descrito um processo de nanoencapsulamento de curcuminóides sintetizado utilizando PLLA. Nesse processo, metabólitos curcuminóides, e não a curcumina propriamente dita, é encapsulada em nanopartículas poliméricas.

[022] O documento CN103768012 (A) descreve um processo de obtenção de nanopartículas lipídicas de curcumina. Essa nanopartícula apresenta um componente

lipídico em sua estrutura e é obtida por um método de injeção para a mistura das fases lipídica e aquosa.

[023] Os documentos US2015258026 (A1), CN101548946 (A) e RU2009141499 (A) descrevem nanopartículas de curcumina, sintetizadas utilizando PLGA para aplicação no tratamento do câncer. No documento US2015258026 (A1), a estrutura da nanopartícula apresenta um núcleo polimérico de PLGA e uma superfície lipídica, sendo utilizada para tratamento de câncer. O documento CN101548946 (A) descreve uma formulação líquida nanolipídica obtida por injeção e emulsificação para tratamento de tumores. O documento RU2009141499 (A) menciona nanopartículas com agentes estabilizadores anfifílicos na superfície polimérica para encapsulamento de substâncias ativas diversas, incluindo medicação anticâncer.

[024] Diferentemente dos documentos mencionados, a presente invenção utiliza poliácido lático (PLA) e sulfato de dextrana (DEX) para a síntese de nanopartículas poliméricas, sem lipídeos. Durante a síntese das nanopartículas, curcumina é encapsulada como substância ativa através de um método de nanoprecipitação. A aplicação dessa formulação tem como finalidade a inativação de microrganismos patogênicos quando associada à luz (aPDT) ou não. A formulação traz como inovação, além do PLA, que é um biopolímero, o uso de DEX que é um polissacarídeo e pode atuar como um agente atrativo para os microrganismos aumentando a captação da formulação pelos patógenos.

[025] Portanto, nenhum dos documentos do estado da técnica descreve um processo de obtenção de nanopartículas poliméricas (CUR-NP) aniônicas e catiônicas de curcumina

para o preparo de uma composição para aplicação em terapia antimicrobiana tal como aqui proposto.

Breve descrição da invenção:

[026] A presente invenção refere-se a um processo de obtenção de nanopartículas de ácido polilático (PLA) aniônicas e catiônicas de curcumina para o preparo de uma composição para aplicação em terapia antimicrobiana.

[027] A tecnologia consiste no encapsulamento de curcumina na concentração que varia de 0,01 a 0,02% em nanopartículas de PLA na faixa de 0,1 a 0,25%. O ácido polilático é um polímero constituído por moléculas de ácido lático, biodegradável, facilmente degradado em água e carbono. A curcumina (CUR) é um pigmento natural encontrado no açafrão da Índia, isolada dos tubérculos da *Curcuma longa* L. e que apresenta propriedades terapêuticas antiinflamatória, antioxidante, antimicrobiana e anticâncer.

[028] Desse modo, a síntese da nanopartícula proposta é realizada de forma simples, rápida (em torno de 10 minutos), de baixo custo e não exige grandes e complexos equipamentos para sua produção, sendo um processo de síntese facilmente escalonável.

Breve descrição das figuras:

[029] Para obter uma total e completa visualização do objeto desta invenção, são apresentadas as figuras as quais se fazem referências, conforme se segue.

[030] As Figuras 1A-B são imagens microscopia eletrônica de varredura com canhão de emissão de campo (MEV-FEG), em que A é a morfologia das nanopartículas de PLA-DEX contendo CUR e B é o tamanho da nanopartícula

(ambos em magnificação de 100.000x).

[031] A Figura 2 representa graficamente os valores (porcentagem) de liberação de CUR das nanopartículas aniônica e catiônica ao longo do tempo.

[032] A Figura 3 representa graficamente os valores médios de log_{10}(UFC/mL) de *S. mutans* obtidos para cada grupo avaliado para as amostras de CUR e CUR-NP aniônica e catiônica, em que barras de erro equivalem ao desvio-padrão; L: luz; CUR: curcumina; NP: nanopartícula sem curcumina; CURNP: curcumina em nanopartícula; -: carga aniônica; +: carga catiônica; e n= 9 em cada grupo.

[033] A Figura 4 representa graficamente os valores médios de log_{10}(UFC/mL) de SARM obtidos para cada grupo avaliado para as amostras de CUR e CUR-NP aniônica e catiônica, em que barras de erro equivalem ao desvio-padrão; L: luz; CUR: curcumina; NP: nanopartícula sem curcumina; CURNP: curcumina em nanopartícula; -: carga aniônica; +: carga catiônica; e n= 9 em cada grupo.

[034] A Figura 5 representa graficamente os valores médios de log_{10}(UFC/mL) de *C. albicans* obtidos para cada grupo avaliado para as amostras de CUR e CUR-NP aniônica e catiônica, em que barras de erro equivalem ao desvio-padrão; L: luz; CUR: curcumina; NP: nanopartícula sem curcumina; CURNP: curcumina em nanopartícula; -: carga aniônica; +: carga catiônica; e n= 9 em cada grupo.

Descrição detalhada da invenção:

[035] A presente invenção refere-se a um processo de obtenção de nanopartículas poliméricas aniônicas e catiônicas de curcumina.

[036] A curcumina é encapsulada como substância

ativa através de um método de nanoprecipitação que compreende as seguintes etapas de:

a) Preparar a curcumina (CUR) em acetona;

b) Preparar a fase orgânica com poliácido láctico (PLA) em acetona;

c) Adicionar a CUR à fase orgânica;

d) Adicionar a fase aquosa composta por sulfato de dextrana (DEX) à fase orgânica com CUR e misturá-las; e

e) Evaporar o solvente.

[037] Na etapa "a" é preparada uma solução estoque de CUR em acetona na proporção de 0,4%.

[038] A fase orgânica, preparada na etapa "b", compreende concentração que varia de 0,1 a 0,5% de PLA em acetona, preferencialmente concentração inicial de 0,5%.

[039] Na etapa "c", a CUR é adicionada em temperatura ambiente à fase orgânica na proporção que varia de 0,02% a 0,03%.

[040] Quando as fases orgânica e aquosa são misturadas na etapa "d", a concentração inicial de PLA reduz (dilui). Com a evaporação do solvente, a concentração final de PLA fica entre 0,1 e 0,25%, enquanto que a concentração de DEX se mantém em 1%.

[041] Desse modo, na etapa "d" a fase aquosa composta por DEX a 1% em água ultra-pura estéril é adicionada por gotejamento na fase orgânica que contém PLA e CUR. A mistura da fase é feita sob agitação magnética que varia de 90 a 110 rpm em temperatura ambiente que varia de 22 a 25 °C, preferencialmente 25 °C, por 10 minutos.

[042] A DEX é utilizada para atuar como um agente atrativo para os microrganismos com intuito de aumentar a

captação da formulação pelos patógenos.

[043] Após este tempo, na etapa "e", a solução é deixada descansando em temperatura ambiente por 24 horas para total evaporação da acetona (solvente).

[044] Vale ressaltar que todos os procedimentos são realizados em fluxo laminar estéril.

[045] As nanopartículas obtidas conforme processo aqui descrito são aniônicas. Para a obtenção de nanopartículas catiônicas, uma solução de brometo de cetil-trimetil-amônio (CTAB) a 2% é preparada em água ultra-pura e NaCl 1,76%.

[046] Após a etapa "e", adiciona-se a solução preparada de CTAB à solução de nanopartícula aniônica numa proporção final de CTAB de 0,1 a 0,2% e NaCl de 0,08 a 0,09%.

[047] Adicionalmente, a presente invenção refere-se às nanopartículas poliméricas aniônicas e catiônicas obtidas conforme processo anteriormente descrito.

[048] As nanopartículas aniônicas possuem carga entre -40,1 e -4,5 mV, diâmetro de partícula entre 186,5 e 433,1 nm e índice de polidispersão entre 0,038 e 0,364, as quais compreendem as seguintes concentrações finais:

- de 0,01 a 0,02% de curcumina;
- de 0,1 a 0,25% de poliácido lático;
- 1% de sulfato de dextrana; e
- qsp de água ultra pura.

[049] Já as nanopartículas catiônicas possuem carga na faixa de +9,97 e +42 mV, diâmetro de partícula entre 179,4 e 341,7 nm e índice de polidispersão entre 0,06 e 0,347, as quais compreendem as seguintes concentrações

finais:

- de 0,01 a 0,02% de curcumina;
- de 0,1 a 0,25% de poliácido lático;
- 1% de sulfato de dextrana;
- de 0,1 a 0,2% de CTAB; e
- qsp de água ultra pura.

[050] É importante ressaltar que essas propriedades nanométricas de ambas as formulações (aniônica e catiônica), determinadas em aparelho *ZetaSizer*, foram mantidas por até 35 dias, indicando estabilidade de ambas formulações, com índice de polidispersão médio em torno de 0,104, o que confirma a estabilidade do sistema e a não agregação das nanopartículas.

[051] Em microscopia eletrônica de varredura com canhão de emissão de campo (MEV-FEG), as nanopartículas mostram-se esféricas, com tamanho compatível com as leituras realizadas em *ZetaSizer* (Figura 1).

[052] As formulações de curcumina em nanopartículas (CUR-NP) também foram caracterizadas quanto ao espectro de absorção, fotoestabilidade (fotodegradação), eficiência de encapsulamento e liberação de curcumina, os quais estão mais bem detalhados a seguir.

[053] Todas avaliações, exceto o Ensaio de Eficiência de Encapsulamento e o Teste de Liberação de Curcumina, foram realizadas empregando-se a curcumina livre a 260 µM (0,01%) preparada em solução de dimetilsulfóxido (DMSO) a 10% e água ultra-pura estéril.

- Espectros de absorção:

[054] Os espectros de absorção de luz UV-visível demonstraram valores de absorbância semelhantes para CUR e

CUR-NP aniônica e catiônica, com pico máximo entre 425 e 430 nm, e com valores de absorbância mais elevados para as amostras de CUR-NP (Tabela 1, tempo 0 de iluminação). Esse resultado demonstrou que o encapsulamento da CUR não alterou sua propriedade fotossensível.

Tabela 1 - Valores de absorbância obtidos para as amostras de CUR, CUR-NP aniônica e catiônica nos diferentes tempos de iluminação.

Tempo iluminação (minutos)	CUR 429 nm	CUR-NP aniônica 427 nm	CUR-NP catiônica 425 nm
0	1,644 (0%)	2,118 (0%)	2,425 (0%)
5	1,131 (20,26%)	0,837 (60,48%)	1,402 (42,19%)
10	0,720 (56,20%)	0,445 (78,99%)	1,020 (57,94%)
15	0,544 (66,90%)	0,302 (85,74%)	0,813 (66,47%)
20	0,410 (75,06%)	0,234 (88,95%)	0,687 (71,67%)

Os valores em porcentagem entre parênteses indicam a % de redução da absorção da amostra.

[055] Vale ressaltar que os valores de absorbância foram registrados para o comprimento de onda de absorção máximo de cada amostra (tempo 0 de iluminação).

- Ensaios de Fotodegradação:

[056] Para os ensaios de fotodegradação, as amostras de CUR e curcumina encapsulada em nanopartículas (CUR-NP aniônica e catiônica) na concentração de 130 µM foram iluminadas por um aparelho de LED de 455 nm (intensidade de luz de 33,58 mW/cm^2) durante diferentes

tempos de iluminação (5, 10, 15 e 20 minutos) e, em seguida, a absorbância das amostras foram lidas em um aparelho espectrofotômetro.

[057] Os resultados demonstraram redução do pico de absorção máximo das formulações proporcional ao tempo de iluminação, conforme observado na Tabela 1, com redução de 71% a 88% após 20 minutos de iluminação.

- Ensaios de eficiência de encapsulamento (EE):

[058] Para os ensaios de eficiência de encapsulamento (EE), as amostras de CUR-NP aniônica e catiônica a 52 µM foram centrifugadas a 6000 rpm por 10 minutos, e a porção sedimentada (nanopartículas) foi resuspendida em água ultra-pura.

[059] A absorbância das amostras foi determinada antes ($A_{inicial}$) e após (A_{final}) a centrifugação em espectrofotômetro UV-visível para os comprimentos de onda que apresentaram absorbância máxima, e a EE foi calculada utilizando-se a fórmula 1:

$$\% = A_{final} \times 100 / A_{inicial} \quad (1)$$

[060] Desse modo, verificou-se que a EE da CUR-NP aniônica foi de 69% e da CUR-NP catiônica foi de 67%.

- Teste de liberação de curcumina:

[061] Outro aspecto importante para caracterização das formulações é a liberação da CUR das nanopartículas.

[062] Para esse teste, as amostras de CUR-NP (aniônica e catiônica) foram diluídas em tampão de fosfato e salina (PBS) na concentração de 2 mg/mL e incubadas em estufa a 37 °C sob agitação a 100 rpm.

[063] A cada intervalo de 2 horas, as amostras foram centrifugadas a 6000 rpm por 10 minutos para separar

as nanopartículas da solução, e então as nanopartículas foram diluídas em acetona para solubilizar a CUR não liberada, cuja absorbância foi determinada em espectrofotômetro UV-visível.

[064] O total de CUR liberada foi calculada dividindo-se a absorbância lida em cada intervalo de tempo pela absorbância da CUR encapsulada estimada como máxima.

[065] Como pode ser observado na Figura 2, houve uma liberação gradativa de CUR ao longo do tempo, sendo que após 48 horas cerca de 96% da CUR havia sido liberada das nanopartículas, tanto para as amostras aniônicas como catiônicas.

[066] Adicionalmente, a presente invenção refere-se ao uso das nanopartículas (CUR-NP) aniônicas e catiônicas aqui descritas para o preparo de composições com ação antimicrobiana, tais como para descontaminação de águas, produtos hospitalares, entre outros.

[067] Além disso, a presente invenção refere-se ao uso das referidas nanopartículas (CUR-NP) aniônicas e catiônicas para o preparo de uma composição para aplicação em terapia antimicrobiana, associadas à luz (aPDT) ou não, em culturas de *Streptococcus mutans*, *Staphylococcus aureus* resistente à meticilina (SARM) e *Candida albicans*.

[068] Em uma modalidade preferida da presente invenção, as referidas nanopartículas aniônicas e catiônicas são utilizadas para o preparo de um medicamento para tratar a candidose bucal.

[069] Para tal, a seguir, são apresentados alguns testes realizados referentes à aplicação das nanopartículas.

Testes Realizados:

- Ação da Terapia Fotodinâmica antimicrobiana (aPDT):

[070] A ação da Terapia Fotodinâmica (aPDT) antimicrobiana das amostras de CUR-NP aniônica e catiônica foram avaliadas contra as bactérias *Streptococcus mutans*, principal agente etiológico da cárie dentária, *Staphylococcus aureus* resistente à meticilina (SARM), bactéria frequentemente isolada de infecções hospitalares com elevadas taxas de morbidade e mortalidade, e também contra o fungo *Candida albicans*, encontrado na cavidade bucal e o principal fungo infeccioso da espécie humana.

[071] A atividade fotodinâmica antimicrobiana das amostras de CUR-NP aniônica e catiônica foi comparada com a da CUR livre. Cada microrganismo foi cultivado em meio de cultura específico e padronizado nas concentrações de 10^7-10^8 (bactérias) e 10^6-10^7 (fungo).

[072] Em seguida, as culturas foram incubadas com uma das amostras de CUR ou CUR-NP (aniônica ou catiônica) na concentração final de 130 µM durante 40 minutos no escuro em temperatura ambiente.

[073] Em seguida as amostras foram iluminadas pelo mesmo aparelho de luz LED utilizados nos ensaios de Fotodegradação e Atividade Fotodinâmica (455 nm, intensidade de luz de 33,58 mW/cm^2) durante 20 minutos (dose de luz de 40 J/cm^2).

[074] Para efeito de comparação, amostras microbianas adicionais de cada espécie avaliada foram tratadas somente com luz na mesma dose avaliada, somente com CUR ou CUR-NP aniônica ou catiônica e não receberam nenhum tratamento (somente PBS em substituição à CUR, grupo

controle).

[075] Além disso, a ação das nanopartículas aniônica e catiônica sem curcumina contra cada espécie de microrganismo também foi avaliada.

[076] Em seguida cada amostra de cada grupo foi submetida a diluições seriadas decimais, as quais foram plaqueadas em meios de cultura ágares específicos para cada microrganismo para crescimento de colônias em estufa a 37 °C por 48 horas em estufa aeróbia.

[077] Somente os experimentos com *S. mutans* utilizaram estufa de CO_2 a 5%, uma vez que essa bactéria é de microaerofilia. Após 48 horas de incubação as colônias foram contadas para determinação dos valores de Unidades Formadoras de Colônias por Mililitros (CFU/mL), os quais foram transformados em logaritmo na base 10. Todos experimentos microbiológicos foram realizados em triplicatas em 3 ocasiões distintas.

[078] Para *S. mutans* (Figura 3), os resultados demonstraram que a aPDT mediada pela CUR resultou em completa inativação bacteriana, enquanto que a aPDT mediada pela CUR-NP aniônica promoveu uma drástica redução no crescimento de colônias, com a maioria das amostras sem crescimento de colônias e somente 2 amostras com crescimento de poucas colônias.

[079] Verificou-se também ausência de ação antibacteriana da luz, da CUR livre e CUR-NP aniônica na ausência de luz e da nanopartícula aniônica sem CUR, cujos valores foram próximos ou semelhantes ao do grupo controle.

[080] Entretanto, todos os grupos tratados com nanopartículas catiônicas com ou sem curcumina na ausência

ou presença de luz apresentaram valores nulos, indicando efeito tóxico dessas nanopartículas catiônicas possivelmente associado à presença de CTAB.

[081] Para SARM (Figura 4), os resultados demonstraram que a aPDT mediada pela CUR resultou em completa inativação bacteriana, enquanto que a aPDT mediada pela CUR-NP aniônica promoveu uma drástica redução no crescimento de colônias, com a maioria das amostras sem crescimento de colônias e somente 4 amostras com crescimento de poucas colônias.

[082] Verificou-se também ausência de ação antibacteriana da luz, da CUR livre e CUR-NP aniônica na ausência de luz e da nanopartícula aniônica sem CUR, cujos valores foram próximos ao do grupo controle.

[083] Entretanto, todos os grupos tratados com nanopartículas catiônicas com ou sem curcumina na ausência ou presença de luz apresentaram valores nulos, indicando também para SARM um efeito tóxico dessas nanopartículas catiônicas possivelmente associado à presença de CTAB.

[084] Para *C. albicans* (Figura 5), os resultados demonstraram que a aPDT mediada pela CUR resultou em completa inativação fúngica, enquanto que a aPDT mediada pela CUR-NP aniônica promoveu uma pequena redução no crescimento de colônias (cerca de 1 $\log_{10}$ apenas).

[085] Verificou-se também ausência de ação antifúngica da luz, da CUR-NP aniônica na ausência de luz e da nanopartícula aniônica sem CUR, cujos valores foram próximos ao do grupo controle.

[086] Ao contrário das amostras tratadas somente com CUR-NP aniônica, as amostras tratadas somente com CUR

livre apresentaram redução nos valores médios de log_{10}(UFC/mL) (cerca de 2 log_{10} em relação ao controle), indicando que a própria CUR livre já apresenta ação antifúngica na concentração avaliada, o que não ocorre quando essa mesma concentração de CUR é encapsulada em nanopartículas aniônicas.

[087] As nanopartículas catiônicas, assim como observado para as bactérias avaliadas, resultaram em completa inativação fúngica em todos os grupos avaliados (NP com ou sem curcumina na ausência ou presença de luz), confirmando o efeito tóxico dessas nanopartículas catiônicas também em *C. albicans* possivelmente atribuído à presença de CTAB.

[088] Portanto, as nanopartículas sintetizadas compreendendo curcumina apresentaram-se estáveis e homogêneas, sendo que as de carga negativa (aniônicas) demonstraram eficácia fotodinâmica (associadas à luz) antimicrobiana em culturas planctônicas dos microrganismos avaliados. Já as nanopartículas de carga positiva (catiônicas) apresentaram ação antimicrobiana nas culturas planctônicas dos microrganismos avaliados tanto na ausência como na presença de luz, demonstrando efeito tóxico.

[089] Os versados na arte valorizarão os conhecimentos aqui apresentados e poderão reproduzir a invenção nas modalidades apresentadas e em outras variantes, abrangidas no escopo das reivindicações anexas.

REIVINDICAÇÕES

1. Processo de obtenção de nanopartículas poliméricas aniônicas e catiônicas de curcumina **caracterizado** pelo fato de compreender as etapas de:

a) Preparar a curcumina (CUR) em acetona;

b) Preparar a fase orgânica com poliácido láctico (PLA) em acetona;

c) Adicionar a CUR à fase orgânica;

d) Adicionar a fase aquosa composta por sulfato de dextrana (DEX) à fase orgânica com CUR e misturá-las; e

e) Evaporar o solvente.

2. Processo, de acordo com a reivindicação 1, **caracterizado** pelo fato ser através de um método de nanoprecipitação.

3. Processo, de acordo com a reivindicação 1 ou 2, **caracterizado** pelo fato de, na etapa "a", a CUR ser preparada em acetona na proporção de 0,4%.

4. Processo, de acordo com a reivindicação 1 ou 2, **caracterizado** pelo fato de a fase orgânica preparada na etapa "b" compreender concentração que varia de 0,1 a 0,5% de PLA em acetona, preferencialmente concentração inicial de 0,5%.

5. Processo, de acordo com a reivindicação 1 ou 2, **caracterizado** pelo fato de, na etapa "c", a CUR ser adicionada em temperatura ambiente à fase orgânica na proporção que varia de 0,02% a 0,03%.

6. Processo, de acordo com a reivindicação 1 ou 2, **caracterizado** pelo fato de, na etapa "d", a fase aquosa composta por DEX a 1% em água ultra-pura estéril ser adicionada por gotejamento na fase orgânica que contém PLA

e CUR, em que a mistura da fase é feita sob agitação magnética que varia de 90 a 110 rpm em temperatura ambiente que varia de 22 a 25 °C, preferencialmente 25 °C, por 10 minutos.

7. Processo, de acordo com a reivindicação 1 ou 2, **caracterizado** pelo fato de, na etapa "e", a solução ser deixada em repouso em temperatura ambiente por 24 horas para total evaporação da acetona (solvente).

8. Processo, de acordo com a reivindicação 7, **caracterizado** pelo fato de, para a obtenção de nanopartículas catiônicas, após a etapa "e", prepara-se uma solução de brometo de cetil-trimetil-amônio (CTAB) a 2% em água ultra-pura e NaCl 1,76%, em que adiciona-se a solução preparada de CTAB à solução de nanopartícula aniônica obtida na etapa "e" numa proporção final de CTAB de 0,1 a 0,2% e NaCl de 0,08 a 0,09%.

9. Nanopartículas poliméricas aniônicas obtidas pelo processo, conforme definido em qualquer uma das reivindicações 1 a 7, **caracterizadas** pelo fato de possuírem carga entre -40,1 e -4,5 mV, serem esféricas com diâmetro de partícula entre 186,5 e 433,1 nm e índice de polidispersão entre 0,038 e 0,364, as quais compreendem concentrações finais:

- de 0,01 a 0,02% de curcumina;
- de 0,1 a 0,25% de poliácido lático;
- 1% de sulfato de dextrana; e
- qsp de água ultra pura.

10. Nanopartículas poliméricas catiônicas obtidas pelo processo, conforme definido em qualquer uma das reivindicações 1 a 8, **caracterizadas** pelo fato de possuírem

carga na faixa de +9,97 e +42 mV, serem esféricas com diâmetro de partícula entre 179,4 e 341,7 nm, e índice de polidispersão entre 0,06 e 0,347, as quais compreendem concentrações finais:

- de 0,01 a 0,02% de curcumina;
- de 0,1 a 0,25% de poliácido lático;
- 1% de sulfato de dextrana;
- de 0,1 a 0,2% de CTAB; e
- qsp de água ultra pura.

11. Uso das nanopartículas poliméricas aniônicas conforme definidas na reivindicação 9, **caracterizado** pelo fato de ser no preparo de uma composição com ação antimicrobiana.

12. Uso, de acordo com a reivindicação 11, **caracterizado** pelo fato de ser no preparo de uma composição para aplicação em terapia antimicrobiana, associadas à luz (aPDT) ou não, em culturas de *Streptococcus mutans*, *Staphylococcus aureus* resistente à meticilina (SARM) e *Candida albicans*.

13. Uso, de acordo com a reivindicação 12, **caracterizado** pelo fato de ser no preparo de um medicamento para tratar a candidose bucal.

14. Uso das nanopartículas poliméricas catiônicas conforme definidas na reivindicação 10, **caracterizado** pelo fato de ser no preparo de uma composição com ação antimicrobiana.

15. Uso, de acordo com a reivindicação 14, **caracterizado** pelo fato de ser no preparo de uma composição para aplicação em terapia antimicrobiana, associadas à luz (aPDT) ou não, em culturas de *Streptococcus mutans*, *Staphylococcus aureus*

resistente à meticilina (SARM) e *Candida albicans*.

16. Uso, de acordo com a reivindicação 15, **caracterizado** pelo fato de ser no preparo de um medicamento para tratar a candidose bucal.

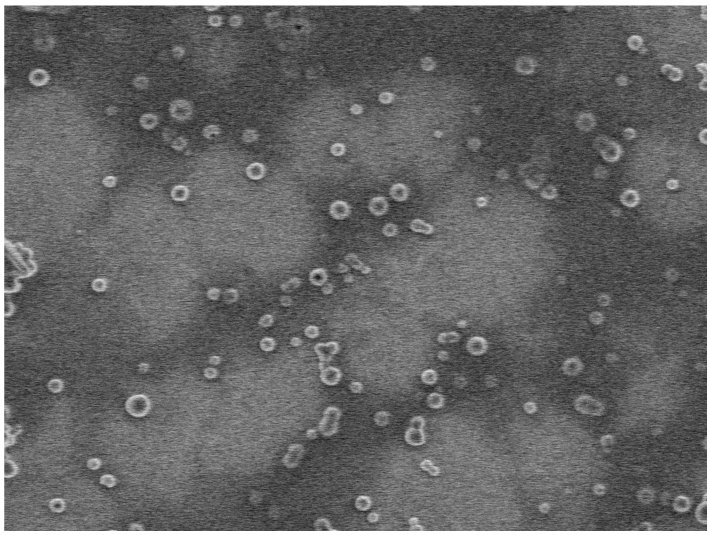


Figura 1A

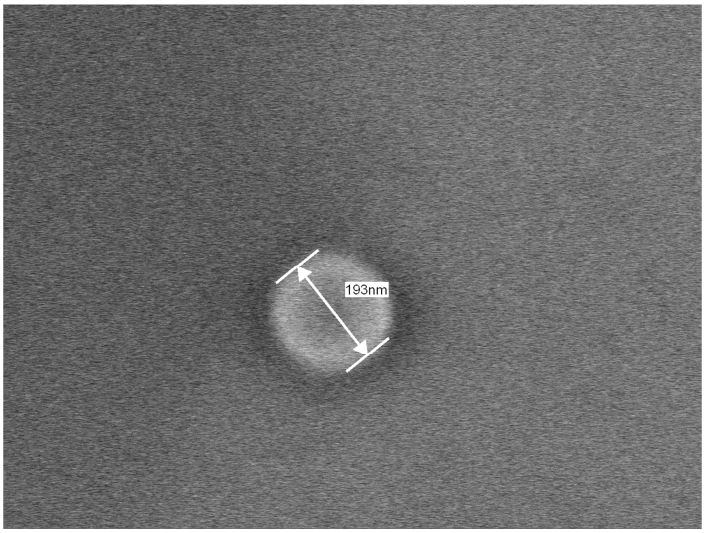


Figura 1B

2/3

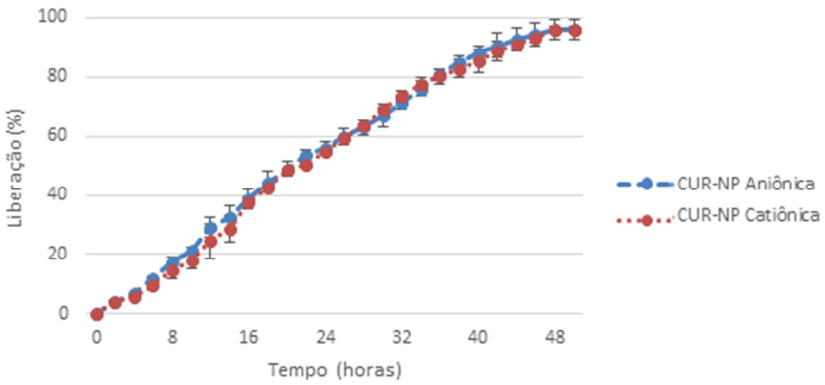


Figura 2

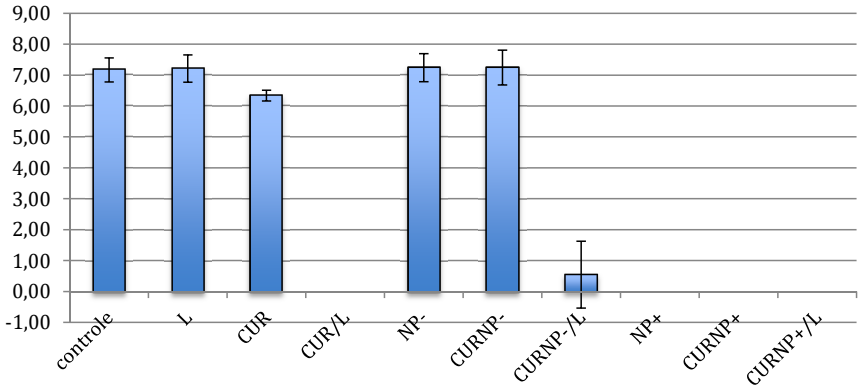


Figura 3

3/3

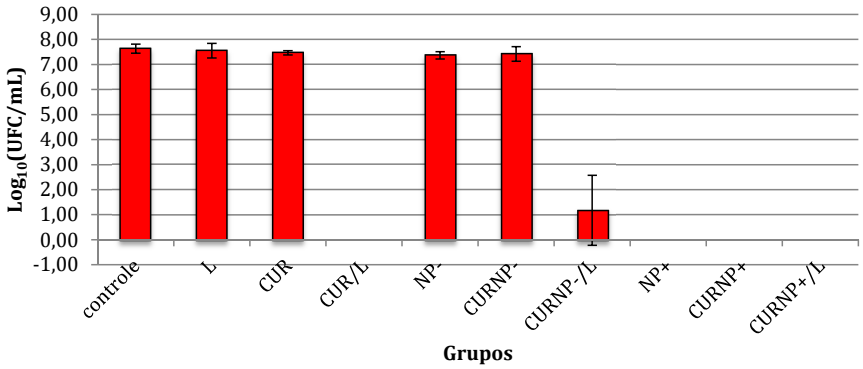


Figura 4

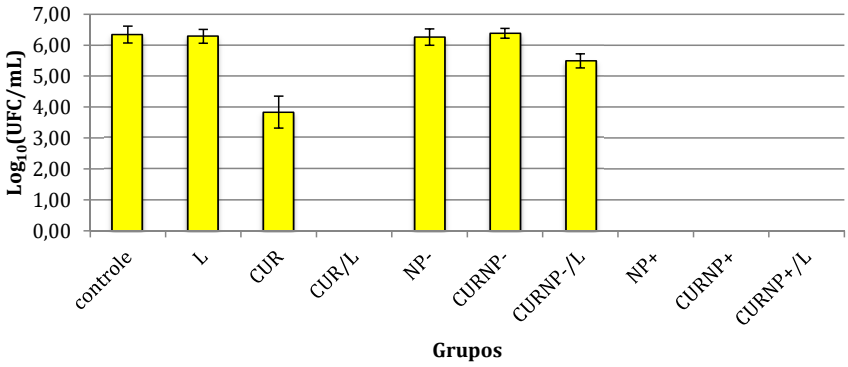


Figura 5

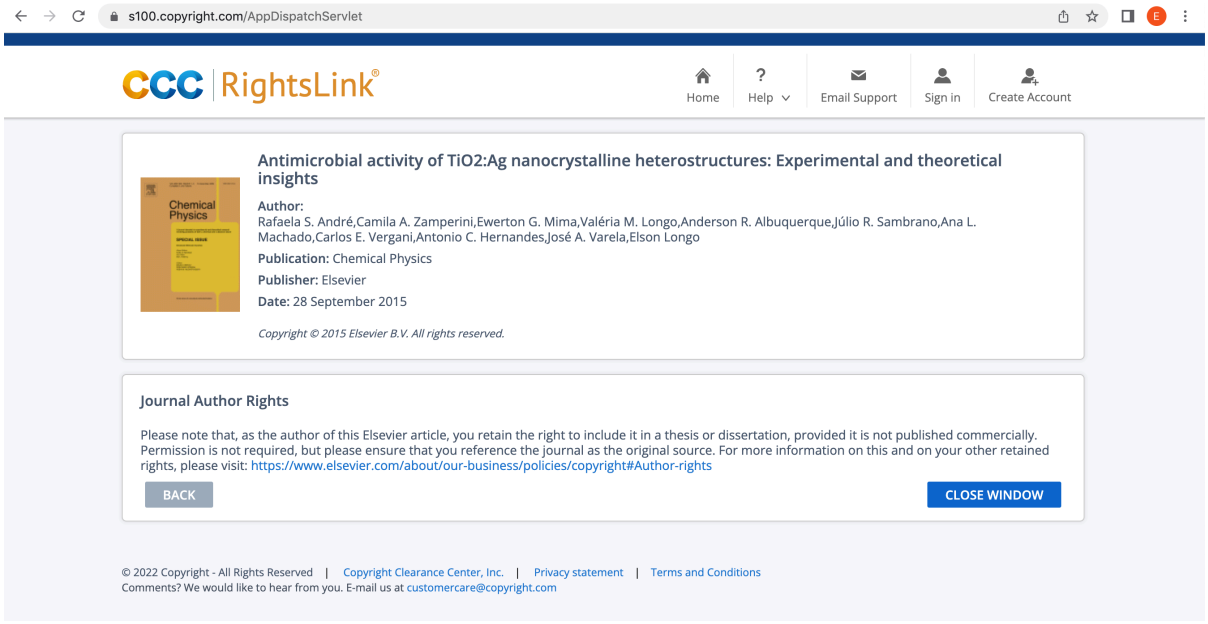
Resumo

PROCESSO DE OBTENÇÃO DE NANOPARTÍCULAS POLIMÉRICAS ANIÔNICAS E CATIÔNICAS DE CURCUMINA, NANOPARTÍCULAS OBTIDAS E SEUS USOS

A presente invenção refere-se a um processo de obtenção de nanopartículas poliméricas (CUR-NP) aniônicas e catiônicas de curcumina, as quais são sintetizadas utilizando-se polímero poliácido lático (PLA) e sulfato de dextrana (DEX). Adicionalmente, a invenção se refere às CUR-NPs aniônicas e catiônicas obtidas e ao seu uso para o preparo de uma composição para aplicação em terapia antimicrobiana, associadas ou não à luz, em culturas de *S. mutans*, SARM e *C. albicans*, preferencialmente para o preparo de um medicamento para tratar a candidose bucal.

ANEXO B – AUTORIZAÇÃO PARA PUBLICAÇÃO EM REPOSITÓRIO

Publicação 1: Chemical Physics



Publicação 2: PLoS One

Reuse of PLOS Article Content

Content Owned by Someone Else

Using Article Content Previously Published in Another Journal

Acceptable Licenses for Data Repositories

Removal of Content Used Without Clear Rights

Guidelines for Trademarks

Giving Proper Attribution for Use of Content

Licenses and Copyright

The following policy applies to all PLOS journals, unless otherwise noted.

Reuse of PLOS Article Content

PLOS applies the Creative Commons Attribution (CC BY) license to articles and other works we publish. If you submit your paper for publication by PLOS, you agree to have the CC BY license applied to your work. Under this Open Access license, you as the author agree that anyone can reuse your article in whole or part for any purpose, for free, even for commercial purposes. These permitted uses include but are not limited to self-archiving by authors of submitted, accepted and published versions of their papers in institutional repositories. Anyone may copy, distribute, or reuse the content as long as the author and original source are properly cited. This facilitates freedom in reuse and also ensures that PLOS content can be mined without barriers for the needs of research.

Content Owned by Someone Else

If your manuscript contains confidential information or content such as photos, images, figures, tables, audio files, videos, proprietary protocols, code, etc., that you or your co-authors do not own, we will require you to provide us with proof that the owner of that content (a) has given you written permission to use it, and (b) has approved of the publication of such information or content under the CC BY license. This form can be used to request permissions. Under no circumstances should your manuscript contain third party trade secret information.

If you do not have owner permission, we will ask you to remove that content and/or replace it with other content that you own or have such permission to use.

Don't assume that you can use any content you find on the Internet, or that the content is fair game just because it isn't clear who the owner is or what license applies. It's up to you to ascertain what rights you have—if any—to use that content.

Using Article Content Previously Published in Another Journal

Many authors assume that if they previously published a paper through another publisher, they own the rights to that content and they can freely use that content in their PLOS paper, but that's not necessarily the case – it depends on the license that covers the other paper. Some publishers allow free and unrestricted re-use of article content they own, such as under the CC BY license. Other publishers use licenses that allow re-use only if the same license is applied by the person or publisher re-using the content.

If the paper was published under a CC BY license or another license that allows free and unrestricted use, you may use the content in your PLOS paper provided that you give proper attribution, as explained above.

If the content was published under a more restrictive license, you must ascertain what rights you have under that license. At a minimum, review the license to make sure you can use the content. Contact that publisher if you have any questions about the license terms – PLOS staff cannot give you legal advice about your rights to use third-party content. If the license does not permit you to use the content in a paper that will be covered by an unrestricted license, you must obtain written permission from the publisher to use the content in your PLOS paper. Please do not include any content in your PLOS paper which you do not have rights to use, and always give proper attribution.

Acceptable Licenses for Data Repositories

If any relevant accompanying data is submitted to repositories with stated licensing policies, the policies should not be more restrictive than CC BY.

Removal of Content Used Without Clear Rights

PLOS reserves the right to remove any photos, captures, images, figures, tables, illustrations, audio and video files, or other confidential or proprietary content, from any article, whether before or after publication, if concerns are raised about copyright, license, or permissions and the authors are unable to provide documentation confirming that appropriate permissions were obtained for publication of the content in question under a CC BY license.

Guidelines for Trademarks

Publicação 3 e 6: Molecules e Microorganisms

Journals (/about/journals) Information (/authors) Author Services (/authors/english) Initiatives (/about/initiatives) About (/about)

Sign In / Sign Up (/user/login)

Submit (https://susy.mdpi.com/user/manuscripts/upload)

Search for Articles:

Title / Keyword

Author / Affiliation

All Journals

All Article Types

Search

Advanced Search

Information

For Authors (/authors)

For Reviewers (/reviewers)

For Editors (/editors)

For Librarians (/librarians)

For Publishers (/publishing_services)

For Societies (/societies)

For Conference Organizers (/conference_organizers)

Article Processing Charges (/apc)

Open Access Policy

- Permissions
- External Open Access Resources
- Open Access Explained!
- Meaning of Open Access
- Advantages of Open Access for Authors
- Links and Notes

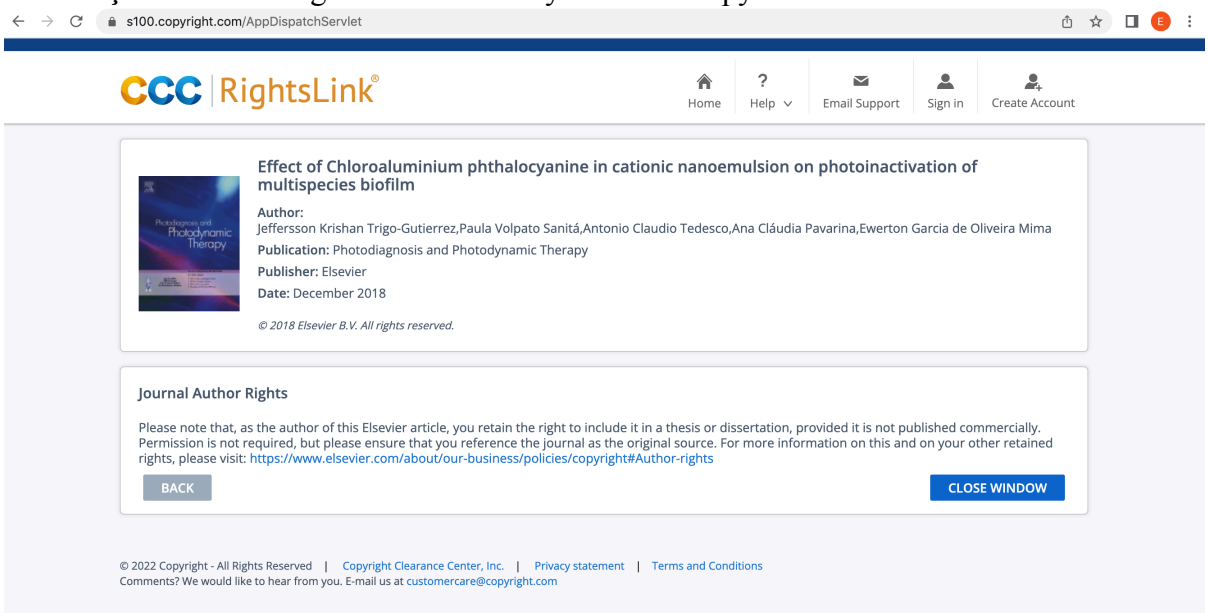
Institutional O.A. Program (/ioap)

Editorial Process (/editorial_process)

Awards (/awards)

Research and Publication Ethics (/ethics)

Publicação 4: Photodiagnosis and Photodynamic Therapy



Publicação 5: Biofouling

unesp

Ewerton Garcia de Oliveira Mima <ewerton.mima@unesp.br>

RE: gbif20:Antimicrobial sonodynamic and photodynamic therapies against Candida albicans

1 mensagem

Academic UK Non Rightslink <permissionrequest@tandf.co.uk> 7 de março de 2022 09:05
Para: Ewerton Garcia de Oliveira Mima <ewerton.mima@unesp.br>

Dear Author,

Thank you for your correspondence requesting permission to reproduce the above content from our Journal in your thesis to be posted on your University's repository.

We will be pleased to grant permission to reproduce your '**Accepted/Original Manuscript'** (please check the embargo: Open access cost finder - Author Services (taylorandfrancis.com) on the sole condition that you acknowledge the original source of publication.

This is an '**Accepted/Original Manuscript'** of an article published by Taylor & Francis Group in [JOURNAL TITLE] on [DATE], available online: https://wwww.tandfonline.com/[Article DOI]."

This permission does not cover any third party copyrighted work which may appear in the material requested. Please ensure you have checked all original source details for the rights holder.

Further permission will be required if your thesis is published. (Please see information for sharing your work https://authorservices.taylorandfrancis.com/sharing-your-work/)

Thank you for your interest in our Journal.

With best wishes,

Annabel

Annabel Fludel Permissions Administrator

Journals, Taylor & Francis Group

Permissions e-mail: permissionrequest@tandf.co.uk

Web: www.tandfonline.com

APÊNDICE A – DECLARAÇÃO

UNIVERSIDADE ESTADUAL PAULISTA
"JÚLIO DE MESQUITA FILHO"
Câmpus de Araraquara

DECLARAÇÃO

As cópias dos artigos já publicados e da patente de minha autoria e co-autoria e incluídos nesta obra acadêmica de produção científica intitulada "**Terapias alternativas para infecções causadas por biofilmes microbianos**" não infringem os dispostos da lei número 9.610/98 nem o direito autoral de qualquer editora.

Araraquara, 14 de abril de 2020

Prof. Dr. Ewerton Garcia de Oliveira Mima
R.G.: 30.611.169-X
Departamento de Materiais Odontológicos e Prótese
Faculdade de Odontologia, Araraquara – UNESP
email: ewerton.mima@unesp.br